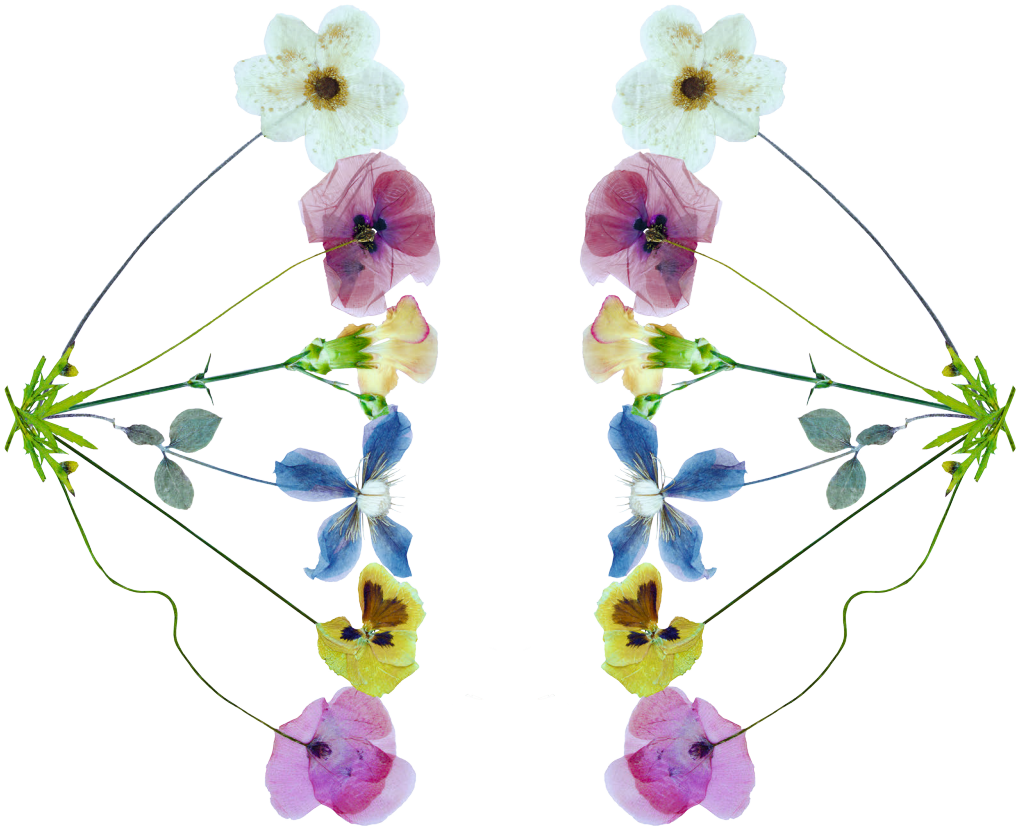


IDENTIFYING VULNERABILITIES OF CHROMOSOMAL INSTABILITY

= equal sharing is caring =



Louise Maria Elisabeth Janssen

IDENTIFYING VULNERABILITIES OF CHROMOSOMAL INSTABILITY

= equal sharing is caring =

Louise Maria Elisabeth Janssen

ISBN: 978-94-6458-344-1

Provided by thesis specialist Ridderprint, ridderprint.nl

Printing: Ridderprint

Layout and design: Jesse Haaksman, persoonlijkproefschrift.nl

Copyright © 2022 L.M.E. Janssen

About the cover: photograph of pressed flowers, arranged as a specific mitotic phase (anaphase), where the mitotic spindle separates sister chromatids to form two identical daughter cells.

Identifying vulnerabilities of chromosomal instability

Equal sharing is caring

De zwakke plekken van chromosomale instabiliteit identificeren

Eerlijk delen is zorgzaam

(met een samenvatting in het Nederlands)

Proefschrift

ter verkrijging van de graad van doctor aan de Universiteit Utrecht op gezag van de rector magnificus, prof.dr. H.R.B.M. Kummeling, ingevolge het besluit van het college voor promoties in het openbaar te verdedigen op donderdag 14 juli 2022 des ochtends te 10.15 uur

door

Louise Maria Elisabeth Janssen

geboren op 24 maart 1993
te Muscat, Oman

Promotor:

Prof. dr. R.H. Medema

Copromotor:

Dr. J.A. Raaijmakers

"I have never tried that before, so I think I should definitely be able to do that"

Pippi Longstocking, Astrid Lindgren



TABLE OF CONTENTS

Chapter 1	General introduction	9
Chapter 2	Loss of Kif18A results in spindle assembly checkpoint activation at microtubule attached kinetochores	27
Chapter 3	A haploid genetic screen in human cells to identify regulators of the replication stress response	59
Chapter 4	SRBD1: A novel factor in sister chromatid decatenation?	81
Chapter 5	Identifying vulnerabilities of chromosomally unstable cells using haploid genetic approaches	115
Chapter 6	General discussion	135
Addendum	References	153
	Nederlandse samenvatting	166
	Curriculum Vitae	169
	Publication list	170
	Acknowledgments	171



General introduction

Louise M.E. Janssen, René H. Medema, Jonne A. Raaijmakers



The cell cycle

Every human is built up from trillions of cells, that all originate from one fertilized oocyte. This cell number is reached by many rounds of cell division. During cell division, the genome (DNA), which contains all the information a cell needs to function properly, is duplicated and divided equally over two newly formed daughter cells. Cell divisions are not only needed for the development of an organism, but also throughout their life to maintain and regenerate tissues. The cell division cycle consists of four successive phases (Fig. 1). The first cell cycle stage is known as the Gap1 (G1) phase, where cells can stay for a couple of hours to prepare for duplication of their genome¹. Cell division starts when cells enter synthesis (S) phase, a phase in which the genetic information of all chromosomes is completely duplicated in the process of DNA replication^{2,3}. Upon completion of S-phase, cells enter the next Gap2 (G2) phase, where the cell prepares for the actual division of the duplicated DNA in the subsequent mitosis (M)^{1,2}.

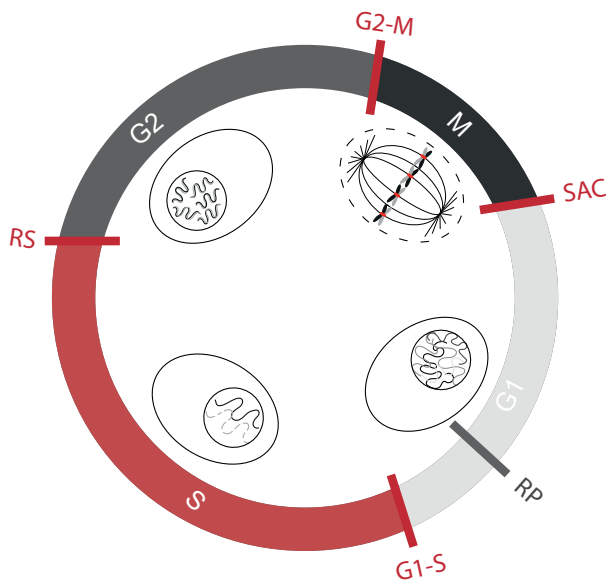


Figure 1: Cell cycle phases and checkpoints

Schematic representation of the four cell cycle phases. In short, cells in the G1 can commit to starting a round of cell division once the restriction point (RP, grey bar), and the G1-S checkpoint (red bar) controls are met. Cells then enter S-phase, where the DNA is replicated and two identical sister chromatids are formed. During S-phase, replication stress (replication fork stalling and reversal) can activate the replication stress response or DNA-damage response (RS, indicated in red throughout the whole S-phase) which can delay S-phase progression. After S-phase, cells enter G2 and prepare for separation of the sister chromatids in mitosis (M). Upon G2-M checkpoint satisfaction (red bar) cells enter mitosis where all the sister chromatids are pulled apart once the spindle-assembly checkpoint (SAC) (red bar) is silenced and the DNA is then equally divided over two newly formed daughter cells.

Cell division is highly controlled in order to maintain tissue homeostasis. Transition from one cell cycle phase to the next is tightly controlled through cell cycle checkpoints to ensure stability of the genome¹. For example, cell cycle checkpoints are in place to sense DNA damage, in order to promote a cell cycle arrest and DNA damage repair in case lesions are detected in the genome^{1,4}. Additionally, cell cycle checkpoints can induce cell death through apoptosis when the threats to genomic integrity are too severe¹. Together, these processes ensure healthy, genomically stable cells. When mutations occur in the processes that ensure the fidelity of cell division, cells can start to proliferate at a higher frequency and accumulate damage. This process can lead to the formation of cancer⁵; uncontrollable cell growth, that progressively becomes more aggressive. A well-known example of mutations in these control processes is the inactivation of the tumor suppressor gene TP53, a master regulator of the cell cycle arrest and/or apoptosis that is induced in response to DNA damage¹.

According to data collected by the world health organization (WHO), cancer is one of the leading causes of death worldwide. Cancer cells display genomic instability (GIN)⁵, probably due to their initial mutations in cell cycle control pathways. This GIN could be a targetable cancer-specific vulnerability⁶. Therefore, understanding how GIN is both a cause of and a threat to cancer is of high interest. In the next sections, several safeguarding mechanisms of genomic stability and their relation to cancer will be discussed.

Gap1 (G1)

In G1, cells prepare for a new round of cell division. For example, replication origins are licensed by the loading of MCM complexes on the DNA⁷. During G1, many signals have to be sensed and decisions made on whether or not the cell is ready to enter S-phase. Cells need to make sure the surrounding conditions are favorable for cell division. For example, there needs to be a sufficient supply of growth factors, and cues from neighboring cells that cell division is needed¹. Once conditions are satisfactory, G1 cells pass the restriction point and are committed to cell division². Besides this restriction point, cells should only enter S-phase when their DNA is intact. Here, the G1-S checkpoint plays a vital role¹. Faulty regulation of these control mechanisms leads to untimely cell proliferation, and can therefore be a cause of cancer formation¹.

DNA insults can cause mutations that potentially hamper cell homeostasis. Thus, ensuring genomic stability through the G1-S checkpoint is of utmost importance. The DNA can

be subjected to many types of insults, like base-modifications, DNA-adducts, single- or double-stranded DNA breaks⁸. Of these lesions, double-stranded breaks (DSBs) are the most toxic^{8,9}. Upon a DSB, the ATM (ataxia telangiectasia mutated) kinase is recruited to the DNA lesion, where it is subsequently activated to trigger checkpoint signaling via the checkpoint kinase CHK2^{10,11}. This in turn causes the stabilization of the transcription factor p53, which activates the transcription of several target genes, including *CDKN1A* which encodes for p21¹⁰. Subsequently, p21 binds to and thereby inhibits cyclin-dependent kinases (CDKs), which are normally needed for cell cycle progression^{11,12}. Together, these processes cause a cell cycle arrest^{10,11}. Additionally, ATM activation leads to the recruitment of repair factors¹¹. In G1 there is no sister chromatid in proximity to allow for homology-mediated repair. Therefore, the main repair pathway initiated in G1 is non-homologous end joining (NHEJ) (see **Box 1**). Upon completion of repair, several of the ATM targets are dephosphorylated and cells are able to resume their proliferation¹³.

Box 1. Canonical Non-Homologous End Joining (c-NHEJ)

Upon DSB detection, ATM and DNA-PK localize to the DSB¹²⁵. A cascade of events follows, including the phosphorylation of H2AX (γH2AX), which serves as a recruitment platform for other repair factors, such as the MRN complex (consisting of Mre11, Rad50, and Nbs1), 53BP1 and BRCA1¹²⁶. While 53BP1 acts to inhibit resection in favor of canonical non-homologous end joining (c-NHEJ), BRCA1 promotes homology-directed repair^{125,127} (HR: see box 2). What repair pathway a cell utilizes depends on both the structure of the break, and on the cell cycle phase the cell is in. c-NHEJ functions throughout interphase, and is initiated upon binding of the Ku70/80 heterodimer to the DSB¹²⁸. This leads to localization and activation of DNA-dependent protein kinase (DNA-PK). In turn, the catalytic subunit of DNA-PK (DNAPKcs) phosphorylates downstream effectors that are needed for end-ligation. Due to the re-ligation of the broken DNA ends, c-NHEJ can cause small insertions or deletions¹²⁹. Therefore, c-NHEJ is more error prone than HR. Even though c-NHEJ is error prone, it is an efficient and fast way to repair a DSB. Therefore, most DSBs are cleared through c-NHEJ, making it critical to limit genotoxicity^{129,130}. While loss of core c-NHEJ subunits has been shown to cause genomic instability, only a very small subset of cancers display mutations in the c-NHEJ pathway¹³¹.

Besides c-NHEJ and HR, alternative repair pathways are in place to repair a DSB. These pathways, such as microhomology-mediated end-joining (MMEJ) depend on end-resection and subsequent use of microhomology, and are highly error prone and can result in deletions and insertions¹³⁰.

G1/S checkpoint in cancer control

As one can imagine, improper G1-S checkpoint signaling causes uncontrolled cell cycle progression which can eventually lead to cancer formation. Besides loss of function of the G1-S checkpoint, mutations compromising restriction point functioning can also cause malignant transformation. For example, overexpression of the oncogene and transcription factor c-MYC and/or one of its downstream targets cyclin E1 (CCNE) can compromise the functions of both the restriction point and of the G1-S checkpoint¹⁴⁻¹⁶. This can lead to increased GIN, because genomic insults are less likely detected/repared before S-phase. That this loss of control can be highly tumorigenic is reflected by the fact that many cancers display mutations that amplify c-MYC or CCNE levels^{17,18}. Additionally, oncogene-induced cell cycle proliferation is hypothesized to cause a dysregulation of origin licensing in G1⁷. This could lead to cells entering S-phase with too few licensed origins, thereby causing replication stress, which can further promote malignant transformation⁷. Thus, proper functioning of both the G1-S checkpoint and the restriction point are important in preventing cancer development and progression.

S-phase (S)

During S-phase, the entire genome is duplicated by DNA replication (Fig. 2A). Replication is initiated by firing of licensed origins. Upon origin firing, the Mcm2-7 replicative helicase unwinds the double-stranded DNA¹⁹, creating a bi-directional replication fork. This creates a single-stranded DNA (ssDNA) template that serves as a substrate for DNA polymerases. DNA synthesis is initiated on both strands by DNA polymerase α , which provides RNA-DNA primers for DNA replication through its primase^{20,21}. Thereafter, polymerase ϵ and polymerase δ continue DNA synthesis by incorporating free deoxynucleoside triphosphates (dNTPs) in the leading and lagging strand, respectively²² (Fig. 2A). Upon completion of replication, every chromosome is present in the form of two identical sister chromatids. These sister chromatids are held together by DNA catenanes and cohesin rings^{23,24}. After replication, cells enter G2 where they prepare for separation of their sister chromatids in mitosis.

Replication stress

High fidelity of replication is important, because it is at the basis of preserving the genome, and thereby critical for healthy progeny. Besides the importance of error-free duplication of the genome, the integrity of the genome is in constant danger due to endogenous and exogenous genotoxic stresses. Several obstacles can be encountered that lead to the slowing down or stalling of the replication machinery and thus halt fork progression²⁵.

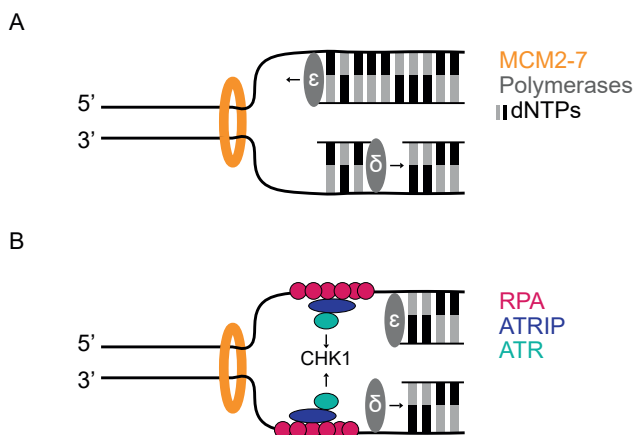


Figure 2: DNA replication and the replication stress response

(A) Schematic depiction of DNA replication. Upon origin firing, the Mcm2-7 helicase unwinds the DNA, creating a bi-directional replication fork. DNA polymerases bind to the ssDNA and incorporate free dNTPs, using the ssDNA strand as a template. On the leading strand (top), this happens in a continuous fashion, while on the lagging strand (bottom) DNA synthesis occurs in smaller steps. **(B)** Schematic depiction of the replication stress response. When the replication fork stalls, stretches of ssDNA are coated by RPA, which recruits a variety of checkpoint proteins. These include ATRIP and ATR, which signal to CHK1. In turn, CHK1 inhibits cell cycle progression and stabilizes the stalled fork. This will provide time for the cell to resolve the replication stress so that the stalled fork can progress.

For example, DNA damage, secondary DNA structures, transcription-replication conflicts and limited supply of the free dNTP pool can impair replication fork progression²⁵. Thus, cells need to ensure high fidelity of replication by continuously checking the DNA for under-replicated or damaged regions, and signaling for subsequent replication/repair. Any stress that causes stalling or slowing of the replication fork can lead to the activation of the replication stress (RS) response²⁵ (Fig. 2B). The stalling or slowing of replication produces long stretches of ssDNA, a typical feature of RS that serves as the platform of the RS-response. The ssDNA stretches are bound by replication protein A (RPA), which can recruit signaling proteins like the Ataxia-Telangiectasia and Rad3-related kinase (ATR) and its binding partner ATRIP^{26,27}. ATR is the main RS-response kinase^{28,29}, and inhibits cell cycle progression by phosphorylation and activation of CHK1³⁰ allowing time to resolve the stress (Fig. 2B). One way of resolving stalled replication forks is fork reversal³¹. This forms a four-way holiday junction that can be sensed as DNA-damage and repaired through homologous recombination (HR)-mediated repair (see **Box 2**). Additionally, replication stalling can be rescued by fork restart or via dormant origin firing^{30,32,33}. In this way, prolonged fork stalling is prevented, and replication can be completed. However, it can occur that a stalled fork is not able to restart. This can cause fork collapse, leaving

ssDNA gaps in the (partially replicated) DNA^{34,35}. These ssDNA gaps can be converted into a DSB either passively due to their less stable nature, or actively by endonuclease activity²⁵. Moreover, collapse of a reversed fork will also leave behind a DSB²⁵.

Since stalled, collapsed, and reversed forks can cause a DSB, they are a threat to genomic stability. Moreover, RS is shown to cause segregation errors in the subsequent mitosis^{36–40}, leading to (continuous) structural and numerical chromosome missegregations, also known as chromosomal instability (CIN). For example, DSBs that arise during S-phase can cause the fusion of two different chromatids³⁶. This creates a dicentric chromosome, which can cause a DNA bridge when the sister chromatids are pulled apart in mitosis. This will cause the DNA to break, and can create segregation errors through a breakage-fusion-bridge cycle (BFB)³⁶. Ongoing BFBs produce different karyotypes at each cell division, and therefore are a source of tumor heterogeneity³⁶. Moreover, it has been suggested that mild RS can cause premature centriole disengagement, resulting in multipolar spindles that cause lagging chromosomes and micronuclei³⁸. Interestingly, it has been shown that reducing RS by adding nucleosides could alleviate CIN and DNA-damage in CIN+ colorectal cancer cells³⁹. This further indicates that RS induces CIN and fuels tumor heterogeneity.

Besides DNA-damage and segregation errors, RS is shown to increase the occurrence of sister chromatid exchanges, translocations and deletions at fragile sites^{41,42}. These data further highlight that the consequences of RS affect genomic stability. Altogether, these studies show that RS is not only a threat to the genome in S-phase, but also in the following cell cycle stages.

DNA intertwining as a source of genomic instability

Another cause of GIN that can arise during replication/RS are DNA intertwinings. For example, during replication, the unwinding of the DNA through replicative helicases causes supercoiling of the DNA (Fig. 3A)³⁷. These supercoils pose a threat of DNA intertwining in the form of DNA catenane formation, and are termed pre-catenanes⁴³. In order to complete DNA replication, forks need to converge. During this process, pre-catenanes can form catenanes, which need to be decatenated by topoisomerases⁴³. Topoisomerases can relax supercoiling/decatenate the DNA by breaking and re-ligating the DNA (Fig. 3A), either in S-phase or during G2/M⁴⁴. Moreover, topoisomerase II activity itself has also been shown to induce catenane formation^{45,46}. While decatenation is important for proper sister chromatid separation in mitosis^{45–51}, it is thought that DNA catenanes generated during

replication, especially at the centromere, initially aid in keeping the sister chromatids together until anaphase^{52,53}.

Additionally, under-replicated regions that arise upon RS can cause DNA intertwinings (unlike DNA catenanes, these are single-stranded DNA interlinkages or hemicatenanes)³⁷. These DNA intertwinings have been shown to mainly arise at difficult to replicate regions (known as common fragile sites), and are characterized by FANCD2 foci (Fig. 3B)^{37,40}. Besides replication intermediates, HR intermediates, which can arise during the repair of a DNA lesion, can also cause single-stranded DNA intertwinings (Fig. 3C)³⁷.

If a DNA catenane/intertwine is not detected or repaired before anaphase onset, the pulling forces on the DNA during mitosis will cause the formation of ultra-fine bridges (UFBs)³⁷ (Fig. 3D. Resolution of UFBs depends on the localization of PICH and BLM helicases, in combination with topoisomerase II α ^{37,54}. The resolving of catenanes and UFBs includes the generation of DNA-damage (either single-stranded or double-stranded breaks,

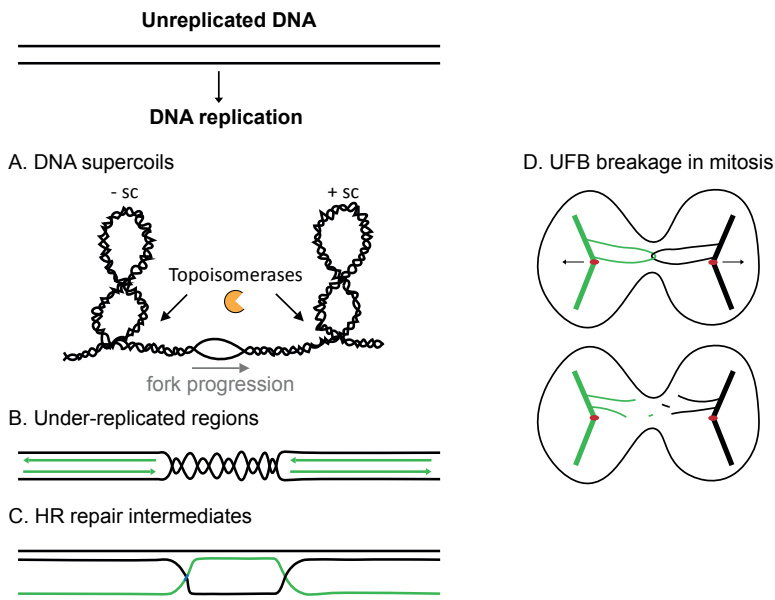


Figure 3: Replication intermediates and genomic instability

Upon replication, the intertwined DNA structure is opened up. However, this can lead to supercoiling upstream and downstream of the replication machinery (direction with the arrow). **(A)** Topoisomerases resolve these supercoils by cutting open and re-ligating the DNA. Additionally, under-replicated regions **(B)** and HR repair intermediates **(C)** can cause DNA intertwining structures. When not resolved, these structures can cause DNA bridges in mitosis **(D)**. Adapted from Fernández-Casañas et al. *Genes* 2018³⁷.

depending on the source of intertwiner) in order to resolve the interlinked DNA. Notably, incomplete resolution of catenanes and UFBs can also lead to DNA damage, as the DNA intertwiners will break when the chromatids are pulled apart in anaphase^{37,55}. As DSBs are the most cytotoxic type of DNA damage, prevention/repair of these lesions is highly important. Altogether, these studies show the importance of minimizing RS, and orchestrating the proper RS-response to prevent GIN.

Replication, genomic instability, and cancer

While cells use several mechanisms to limit RS, the most prominent inducer of GIN in cancer cells is RS^{30,56}. Above, we highlighted that various factors can contribute to RS. However, in cancer RS is most commonly caused by the activation of proto-oncogenes³⁰. As previously mentioned, amplification of cyclin E (CCNE) and MYC perturb the G1-S restriction point and can induce RS by dysregulated origin licensing in G1⁴⁻¹⁶. Moreover, both MYC and CCNE overexpression in cancer are thought to induce RS by increasing CDK2 activity, which regulates the firing of replication origins⁵⁷⁻⁵⁹. For example, it has been shown that CCNE amplification causes replication-transcription collisions due to increased replication initiation⁵⁹. Also, the increased rate of replication initiation causes depletion of free nucleotide pools^{56,59}, further feeding the occurrence of RS in CCNE-overexpressing cells.

RS that causes replication fork stalling and/or collapse will eventually lead to activation of the DNA damage response^{25,34,35}. Not surprisingly, cancer cells become partially refractory to RS through p53 inactivation⁶⁰. However, interfering with the DNA-damage checkpoint/RS-response also makes cells that experience RS more susceptible to GIN. For example, it was shown recently that cells displaying RS resulting from CCNE overexpression show mitotic defects, which are further increased upon p53 loss, or inhibition of ATR or WEE1⁶¹. These results create a window of opportunity; increasing GIN in cancer cells with RS could induce cancer-specific cell killing. For example, WEE1 inhibition will push cells through the G2/M checkpoint^{62,63}. Subsequently, when genomically unstable cancer cells enter mitosis with too much under-replicated/damaged DNA, they can be pushed into mitotic catastrophe^{62,63}. Following the idea of pushing cancer cells over their GIN-tolerance limit, ATR and Chk1 inhibitors entered clinical trials^{64,65}. This inhibition prevents activation of the RS checkpoint. Thereby, it could exacerbate the levels of RS-induced GIN in oncogene-driven tumors to levels that induce cell killing⁶⁵. Nonetheless, heterozygous loss of ATR or CHK1 results in an increased incidence of tumor formation in mouse models^{66,67}. This indicates that targeting ATR for tumor cell killing comes with a risk of inducing *de novo* tumor formation.

Taken together, it is difficult to tease apart whether RS is a driver of cancer formation, or a bystander of oncogenic gene activation. Nonetheless, it is clear that most cancer cells display levels of RS that could be exploited for future therapies.

Gap2 (G2), genomic instability, and cancer

During G2, cells prepare for division of their duplicated genome in the subsequent mitosis. Like G1, G2 ensures genomic stability, in this case by sensing DNA lesions/under-replicated DNA and halting progression into mitosis through a G2-M checkpoint⁶⁸. In G2, both ATM and ATR activity can induce a reversible cell cycle arrest, through the stabilization of p53 and the inhibition of CDKs¹¹. However, a big difference between G1 and G2, is that besides NHEJ, HR can be employed for DSB repair as a sister chromatid is now available to allow for homology-directed repair⁴ (HR, see **Box 2**). Like we mentioned in the previous section, under-replicated and unrepaired DNA pose threats to the genome, as their division in mitosis can cause DNA breakage. Once the G2-M checkpoint is satisfied, cells progress to the most astonishing cell cycle phase of all: mitosis.

Box 2. Homologous Recombination (HR)

Homologous recombination (HR) is known as an error-free repair mechanism of DSBs. It makes use of the sister chromatid as a repair template^{125,132}. Due to the need of this homologous template, HR is largely restricted to S and G2 phase¹³² (HR has been shown to take place in G1 in repetitive regions of the genome, such as rDNA^{125,133}). Upon DSB formation, the broken DNA ends are recognized by the MRN complex, consisting of Mre11, Rad50, and Nbs1, which recruits ATM¹³⁴. The ATM kinase in turn phosphorylates downstream effectors needed for the repair process. The main steps of HR involve DNA end resection, initiated by the Mre11 subunit of the MRN complex, followed by strand invasion and homology search through BRCA2 and Rad51¹³⁵. A D-loop structure is formed, and DNA polymerases can fill up the resected DNA using the homologous sister strand as a template¹²⁵. Once filled in, holiday junctions arise and need to be resolved by endonucleases like Mus81¹³⁶, which can result in sister chromatid exchanges (SCEs)¹³⁷. Deficiencies in HR are shown to result in impaired DSB repair, and drive tumorigenesis¹³⁸. Well known examples are mutations in the HR factors BRCA1 and BRCA2^{139,140}, mutations in which are associated with familial breast and cervical cancer. However, HR deficiency does give a window of opportunity for cancer treatment, as these cancer cells are more sensitive to anti-cancer drugs such as PARP inhibitors¹⁴¹.

Mitosis

During mitosis, the biggest morphological changes of the cell take place (Fig. 4). First, in prophase, the duplicated chromosomes (sister chromatids) start to condense, a process that is initiated by a ring-shaped protein complex known as condensin II, that compacts the DNA by forming loops⁶⁹. At the same time, the cohesin rings that hold sister chromatids together are removed from chromosome arms by Wapl, while cohesin at centromeres remains protected from Wapl-mediated removal by Shugoshin²³. Additionally, DNA catenanes that are present between sister chromatids are removed by topoisomerase II, following the pattern of cohesin removal²³. Condensation of the sister chromatids, together with retention of cohesion at the centromeres, leads to the typical X-shaped chromosomes. Moreover, in prophase the centrosomes are positioned at opposite sides of the nucleus⁷⁰. This creates the bi-polar mitotic spindle needed to separate the two sister chromatids from each other. After prophase, the nuclear envelope breaks down and prometaphase starts. Sister chromatids become exposed to condensin I, further condensing the chromosomes by forming nested loops within condensin II-generated loops⁶⁹. Microtubules (MTs) from the mitotic spindle attach to the centromeres through a protein structure known as the kinetochore (KT)⁷¹. Once all chromosomes are aligned at the middle of the mitotic spindle, the cell reaches a state called metaphase. Only when all chromosomes are correctly attached through a kinetochore-microtubule (KT-MT) interaction, cohesin is removed from the centromeres by proteolytic cleavage mediated by separase²³. Thereafter, the sister chromatids will be pulled apart by opposing pulling forces of the mitotic spindle during anaphase. After anaphase, the chromosomes decondense and a nuclear envelope is formed around the segregated chromosome packs during telophase. Finally, cytokinesis will divide the cytoplasm and the cell membrane, giving rise to two new daughter cells.

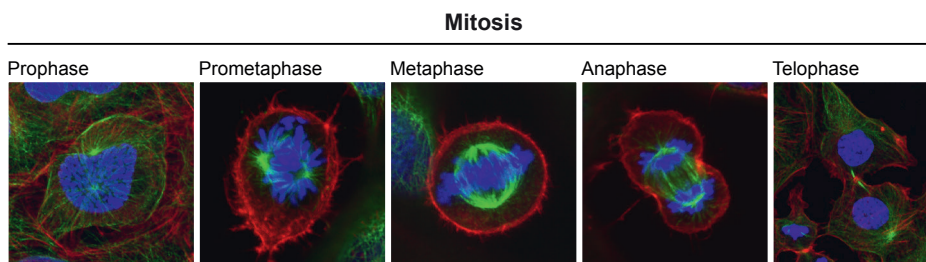


Figure 4: Stages of mitosis

Representative images of subsequent mitotic stages as described in the text. Images are acquired on a microscope; DNA is depicted in blue, spindle microtubules in green, and the cytoskeleton (actin) in red. Adapted from JA Raaijmakers⁴².

The spindle assembly checkpoint

Accurate segregation of chromosomes is ensured by a highly orchestrated and controlled checkpoint during mitosis, namely the spindle assembly checkpoint (SAC)^{72,73}. Faulty KT-MT attachments can lead to chromosome missegregations, for example by attachment of one KT by MTs from opposing spindle poles^{74,75}. Moreover, changes in MT dynamics also create faulty KT-MT attachments that can lead to chromosome segregation defects⁷⁶⁻⁷⁸. For example, increased KT-MT stability in cancer cells was found to cause persistent faulty KT-MT attachments, thereby leading to segregation errors⁷⁶. The SAC prevents missegregations by halting anaphase onset until all kinetochore pairs have established stable, bipolar attachments to the mitotic spindle (amphitelic attachment)^{72,73}. In order to do so, the SAC makes use of a sensing system that can detect the attachment status of each KT and the tension of each KT pair to the mitotic spindle (Fig. 5).

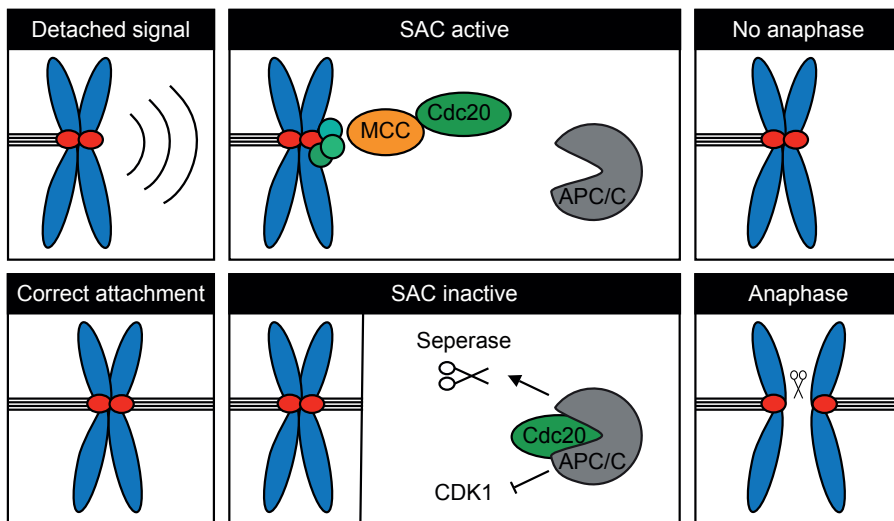


Figure 5: Spindle Assembly Checkpoint (SAC)

Schematic representation of the spindle assembly checkpoint. When a kinetochore (red) is detached, the SAC is activated. This creates a signal leading to the recruitment of checkpoint proteins to the kinetochore. These proteins ensure the formation of the mitotic checkpoint complex (MCC), which binds and sequesters Cdc20. This prevents Cdc20 from activating the anaphase promoting complex (APC/C), thereby prohibiting anaphase onset. Upon correct kinetochore-microtubule attachment, MCC formation is ceased, allowing Cdc20 to bind and activate the APC/C. In turn, the APC/C initiates ubiquitination events, that eventually leads to the inactivation of CDK1, and the activation of separase. This leads to anaphase onset, as separase cleaves the cohesin rings still present at the centromere of sister chromatids, and the pulling forces of the mitotic spindle pull the two sister chromatids to separate poles of the mitotic spindle.

It is well established that unattached kinetochores recruit a variety of checkpoint proteins, such as Mad1, Mad2, and the kinase Mps1^{79–81}. Together, these proteins ensure the formation of the mitotic checkpoint complex (MCC), which consists of Mad2, BubR1, Bub3, and Cdc20⁸². In this way, the MCC sequesters Cdc20⁸³ to ensure that Cdc20 is unable to activate the anaphase-promoting complex/cyclosome (APC/C) (Fig. 5, top panels). A correct KT-MT attachment displaces checkpoint proteins from the kinetochore, thereby reducing MCC production and inactivating the SAC^{84–87}. In the absence of the MCC, Cdc20 is able to activate the APC/C, which ubiquitinates cyclin B and securin for degradation^{72,73}. This leads to anaphase onset by inactivation of the mitotic kinase CDK1, and the activation of separase which cleaves the remaining cohesin rings at the centromeres that keep the sister chromatids together (Fig. 5, bottom panels)^{75,88,89}.

Besides sensing unattached kinetochores, the SAC also needs to act upon incorrect KT-MT attachment. Erroneous KT-MT attachments can arise when both sister KTs become attached by MTs originating from the same side of the mitotic spindle pole (syntelic attachment) or when one KT is bound by MTs from both sides of the mitotic spindle (merotelic attachment)⁹⁰. These incorrect attachments fail to produce sufficient tension across kinetochore pairs, and it is thought that this leaves kinetochore proteins in proximity of the protein kinase Aurora B⁹¹. Subsequently, Aurora B will phosphorylate outer kinetochore components, making the incorrect attachment unstable and converting it into an unattached KT. In this way, the MCC will be formed again, and APC/C activation is suppressed⁹¹. Upon correct KT-MT attachment and subsequent tension generation, Aurora B no longer de-stabilizes KT-MT attachments and SAC-activity is ceased, allowing anaphase onset. This way, the SAC ensures proper chromosome segregation and an equal division of the genome over the two newly formed daughter cells.

While the model where SAC is always activated by unattached KTs is the most favored one in the field, the direct role of tension defects in activation of the SAC have been difficult to study. In chapter 4 and 6 of this thesis we will shed more light on this ongoing discussion.

Mitosis, genomic instability, and cancer

As can be concluded from the paragraph above, many processes are in place to prevent chromosome missegregations during mitosis. Indeed, segregation errors occur at a very low rate in healthy tissues⁹², and a correct chromosome content is very important for normal development. Deviations to the normal chromosome content cause birth defects and are associated with aging^{93,94}. Paradoxically, chromosomal instability (CIN) and

aneuploidy are common traits in cancer^{95,96}. Where aneuploidy describes a steady state of karyotype imbalances, CIN refers to the ongoing missegregation of chromosomes. CIN leads to continuous karyotypic diversification, and this can create genetic heterogeneity in a tumor which can drive cancer evolution⁹⁶. Indeed, tumors with high CIN levels are associated with poor prognosis and increased therapy resistance⁹⁷⁻¹⁰⁰. However, CIN can also be seen as a specific cancer vulnerability, thus yielding potential clinical targets⁹¹.

Segregation errors can arise in various ways⁹⁶. As can be expected from the section above, faulty SAC functioning could cause segregation errors^{76,77,102-105}. Yet, SAC genes are rarely found mutated in cancer and actually are more often found to be overexpressed¹⁰⁶. This could be a coping mechanism of cancer cells to prevent severe CIN¹⁰⁷. However, overexpression of the SAC protein Mad2 was also shown to cause CIN and tumor formation in mice by delaying mitotic exit¹⁰⁸. Nonetheless, in human tumors the overexpression of single SAC-components has not been frequently observed, and the overexpression of SAC-proteins is thought to be a consequence of general upregulation of the cell division program¹⁰⁹.

If SAC-deficiency is not a common feature of cancer cells, then what could account for high CIN levels in tumors? Besides SAC-deficiency, missegregations can also occur due to RS (see section on **replication stress**). Additionally, cohesin defects and condensin defects have been shown to cause segregation errors, and mutations in core cohesin and condensin subunits have been identified in cancer¹¹⁰⁻¹¹². Both loss of cohesin and condensin are found to cause lagging chromosomes and lead to the formation of anaphase bridges^{111,113}. Other CIN-inducing features that are found in cancer cells include altered microtubule dynamics⁷⁷, and supernumerary centrosomes¹¹⁴. Additionally, DNA damage can result in acentric chromosome fragments¹¹⁵ or incorrect KT-MT attachments, and could thereby also contribute to missegregations during mitosis^{116,117}. Interestingly, aneuploidy itself is shown to drive CIN as well^{118,119}. An added layer of complexity is that different aneuploid states induce different levels of CIN^{120,121}. While this has been previously attributed to the deregulated gene expression of specific genes¹²², it was recently shown that the CIN levels correlate with the number of gained coding genes^{118,121}. How exactly aneuploidy drives CIN still needs to be determined. Nonetheless, the fact that CIN levels correlate to the overall increase in coding genes indicates that protein production and turnover might be involved in aneuploidy-induced CIN, a topic that is already highly debated^{121,123,124}. Altogether, even though the underlying causes and consequences of CIN vary enormously within experimental systems and in the different tumors in the clinic, CIN

is commonly found in cancer. Therefore, it is important to understand the vulnerabilities of CIN cells, as a means to define new ways to specifically tackle CIN cells as a treatment strategy.

Outline thesis

Cells have evolved several pathways to control correct chromosome replication and segregation, processes that are important to maintain genomic integrity. Genomic instability (GIN) poses a mayor threat to cell viability. Interestingly, the processes that are in place to ensure genomic integrity are often perturbed in cancer cells, resulting in chromosomal instability (CIN). As highlighted in the sections above, CIN can promote tumorigenesis and result in therapy resistance. However, CIN can also be seen as a cancer-specific vulnerability, as it compromises cancer cell viability when the instability becomes too severe. Here, we set out to uncover the vulnerabilities of CIN cells using haploid genetic screens. In every chapter of this thesis, we use a different way of inducing CIN, to investigate which genes are essential for viability in that specific setting. As a first approach we used HAPI cells lacking a functional mitotic checkpoint (SAC-deficiency) (**chapter 2**). Using this approach, we previously found genes involved in chromosome congression to become essential¹⁰⁵. For example, we found that loss of Bubl causes chromosome congression defects, which lead to segregation errors when the SAC is lost¹⁰⁵. In a second approach, we treated HAPI cells with low doses of RS-inducing drugs to induce CIN, and identify genes that become essential during the RS-response (**chapter 3**). Besides an enrichment of mitochondrial genes, we also identify other factors with a not yet identified role in the RS response. As a third approach (**chapter 4**), we use HAPI cells lacking condensin II, also shown to result in CIN. We followed up on an interesting synthetic viable interaction (see below). Finally, in **chapter 5**, we combine the SAC-deficient, RS and condensin II-deficient screens to look for shared therapeutic targets in CIN cancers. Using this approach, we identify condensin II and CENPO as common CIN vulnerabilities. Additionally, we find evidence that the most common weakness of CIN cells is interfering with their response to DNA-damage.

Even though all screens were set out to identify vulnerabilities of a variety of chromosomal instabilities, we also identified factors that become less essential than normal in a specific CIN setting. These interesting genetic interactions enabled us to identify the function of normally essential genes. Moreover, these genes turned out to have important roles in preventing GIN. More specifically, in **chapter 2** we show that Kif18A-depleted cells have SAC activity at microtubule-attached, but tensionless, kinetochores. These data resolve

a longstanding debate in the field, by providing proof that SAC-signaling can persist even when kinetochores seem correctly attached, but tension is lacking. In **chapter 4**, we show that the essential role of SRBD1 in chromosome segregation is lost upon depletion of condensin II. Depletion of SRBD1 alone gives a striking anaphase defect, where the DNA seems to be severely interlinked. This defect is rescued by loss of condensin II. We show that SRBD1 could play a role during decatenation in prophase and speculate that this is through an interplay with topoisomerase II. Together, these synthetic viable interactions helped us to identify new functions for Kif18A and SRBD1 as guardians of genomic stability.



Loss of Kif18A results
in spindle assembly
checkpoint activation at
microtubule-attached
kinetochores

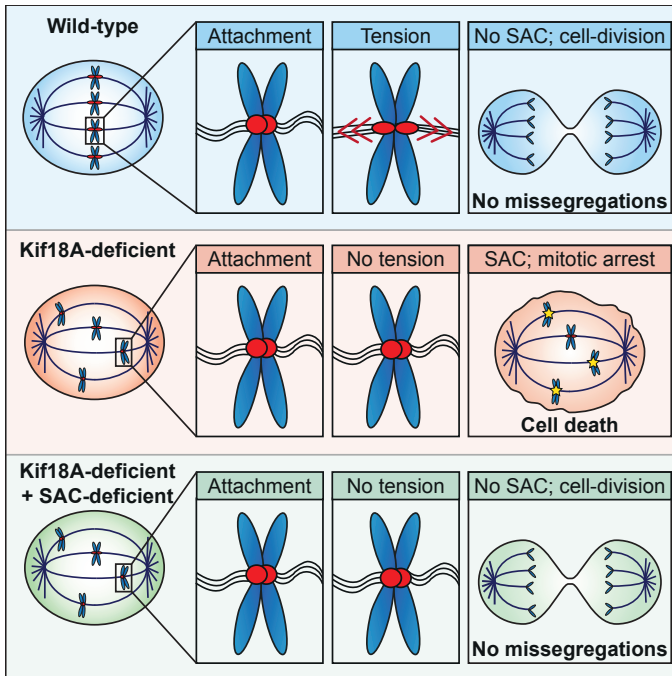


Louise M.E. Janssen, Tessa V. Averink, Vincent A. Blomen, Thijn R. Brummelkamp,
Rene H. Medema, Jonne A. Raaijmakers

Published in Current Biology

SUMMARY

The spindle assembly checkpoint (SAC) halts anaphase progression until all kinetochores have obtained bipolar, stable attachments to the mitotic spindle. Upon initial attachment, chromosomes undergo oscillatory movements to reach metaphase. Once a chromosome is correctly attached and positioned, these oscillatory movements are reduced by the motor protein Kif18A, and loss of Kif18A results in chromosome hyper-oscillations. By using a haploid genetic approach, we found that loss of Kif18A is lethal in wild-type human HAPI cells but not in SAC-deficient HAPI cells. Unexpectedly, we found that the hyper-oscillations after Kif18A loss are not associated with chromosome missegregations. Rather, we found that loss of Kif18A results in a loss of tension across a subset of kinetochores accompanying SAC activation. Strikingly, the SAC-active kinetochores appear to have established fully functional kinetochore-microtubule (k-Mt) attachments, allowing proper chromosome segregation. These findings shed new light on the role of Kif18A in chromosome segregation and demonstrate that the SAC can be activated at kinetochores that are occupied by fully functional k-Mts that lack tension.



Key-words: Mitosis, Mitotic Checkpoint, Spindle Assembly Checkpoint, Kinetochore, Chromosome Segregation, Kif18A, Astrin.

INTRODUCTION

Missegregation of chromosomes compromises cellular fitness and drives chromosomal instability, a major hallmark of cancer cells¹⁴³. To ensure proper chromosome segregation, the spindle assembly checkpoint (SAC) has evolved to delay anaphase onset until all paired sister chromatids are properly aligned at the metaphase plate¹⁴⁴. It is well established that SAC-activation can occur at unattached kinetochores^{75,144}, as unattached kinetochores recruit a variety of checkpoint proteins, such as Mad1 and Mad2, and the checkpoint kinases Mps1 and Bub1^{72,75,145}. These players act together to produce a soluble complex known as the mitotic checkpoint complex (MCC), that consists of Cdc20 bound to Mad2, BubR1 and Bub3^{146,147}. Cdc20 is an essential co-factor of the multi-subunit E3 ligase Anaphase Promoting Complex/Cyclosome (APC/C), and incorporation of Cdc20 in the MCC renders it incapable of activating the APC/C¹⁴⁸, thereby preventing premature chromatid separation¹⁴⁹. SAC inactivation occurs when correct kinetochore-microtubule (k-Mt) attachments displace the various checkpoint proteins from the kinetochore, so that MCC production will cease and Cdc20 can activate the APC/C^{73,75,150}, resulting in anaphase onset.

Thus, attached kinetochores silence the SAC. However, attachment of a microtubule to a kinetochore does not always produce a correct attachment. Erroneous k-Mt attachments can occur, for example, when both sister kinetochores become attached to the same pole, or a single kinetochore is attached to both poles of the mitotic spindle^{90,151,152}. Whether erroneously attached kinetochores can directly promote MCC production has been a long-standing debate. What has become clear is that, due to physical constraints, erroneously attached k-Mts fail to produce tension across sister-kinetochores¹⁵³. This lack of tension is sensed by the Aurora B kinase, which phosphorylates outer kinetochore components involved in microtubule attachment⁹¹. This is thought to make erroneous attachments unstable, and therefore they are easily converted back to unattached kinetochores⁹¹. Thus, it is clear that tension plays a critical role in accurate chromatid segregation, but whether the lack of tension itself can directly promote SAC activity remains an unresolved issue. The leading view is that the SAC is activated by unattached kinetochores, and that lack of tension causes SAC activation as it results in the displacement of attached microtubules through Aurora B-activity^{75,85,144,148,154-156}. Nonetheless, in some cases a tension defect is thought to play a direct role in SAC activation. For example, it has been suggested that tension defects delay anaphase onset in budding yeast by interfering with SAC silencing¹⁵⁷. Besides, there are multiple

additional studies that point towards a direct role for tension defects in SAC activity¹⁵⁸⁻¹⁶⁰. However, direct evidence for this model is still lacking.

We recently obtained full Mad1 and Mad2 (both essential proteins for SAC function) knockout cell lines in a human haploid cell line (HAP1) and used these SAC-deficient cells to perform synthetic lethality screens in order to identify factors that mediate chromosome congression in human cells^{161,162}. Interestingly, besides several synthetic lethal interactions with SAC deficiency, we also identified two synthetic viable interactions. This implies that two essential genes, *KIF18A* and *SPAG5* (from this point referred to as *ASTRIN*), become non-essential in a SAC-deficient setting. This surprising finding suggested an unknown link between these proteins and the SAC.

RESULTS

The requirement of Kif18A and Astrin for viability is rescued by SAC-deficiency

In order to identify novel genes with functions in chromosome congression, parallel screens were performed in Δ Mad1 and Δ Mad2 HAP1 cells to identify genes required for optimal fitness of cells lacking a functional SAC¹⁶². These screens use insertional mutagenesis by genome-wide integration of a gene trap in near-haploid HAP1 cells, which are derived from the KBM-7 cell-line¹⁶¹. Besides several synthetic lethal interactions¹⁶², two synthetic viable interactions were identified, *KIF18A* and *ASTRIN* (Figures 1 A,B), indicating that these genes become non-essential in a SAC-deficient background.

The strongest synthetic viable interactor was Kif18A, a plus-end directed microtubule motor protein that either directly depolymerizes microtubules or inhibits microtubule polymerization^{163,164}. As Kif18A showed the most prominent synthetic viable interaction, we first focused on establishing the interaction between Kif18A loss and SAC activity. Kif18A-depletion was previously linked to chromosome hyper-oscillations, alignment defects, segregation errors and elongated mitotic spindles^{163,165,166}. Given the proposed role for Kif18A in chromosome alignment, we were surprised to find Kif18A as non-essential in a SAC-deficient setting. If loss of Kif18A leads to alignment defects that compromise cell viability, we would expect viability to be even further compromised in SAC-deficient cells, as the percentage of missegregations would be expected to increase. Instead, we found the opposite interaction, suggesting that loss of Kif18A does not perturb correct chromosome segregation. Rather, loss of Kif18A somehow promotes the inhibition of cell

growth through an unknown interaction with the SAC. Therefore, we decided to investigate this unexpected result in more detail.

As a first confirmation of our screen, we demonstrated that siRNA-mediated depletion of Kif18A (Figure S1A) specifically perturbed colony outgrowth in wild-type (WT) HAP1 cells but not in Δ Mad2 HAP1 cells (Figure 1C). In line with these observations, the Kif18A-depleted cultures displayed an increased mitotic index (Figure S1C), consistent with previous results in other cell types^{163,165}.

Lethality of Kif18A loss is caused by a prolonged mitotic arrest

To understand the cause of the mitotic enrichment observed in Kif18A-depleted cells and the observed rescue of viability in the SAC-deficient cells, we performed live-cell imaging experiments. We observed that the siKif18A-depleted cells indeed displayed hyper-oscillations and spent an unusually long time in mitosis, often followed by cell death as observed by hyper-condensation and fragmentation of the DNA (Figures 2A,B). Interestingly, the behavior of siKif18A-depleted cells was rather heterogeneous; although a subset of siKif18A-depleted cells displayed near-normal timing in mitosis, there was also a notable population of siKif18A-depleted cells that displayed a prominent mitotic delay followed by slippage¹⁶⁷ and/or cell death (Figure 2A). Interestingly, the subpopulation of Kif18A-depleted cells that reached anaphase did not display an increase in missegregations when compared to WT HAP1 cells (Figures 2B,C, Video S1, S2), despite the fact that loss of Kif18A has previously been associated with chromosome segregation errors^{165,166}. Besides, as we found Kif18A loss to be non-lethal in a SAC-deficient background this would also hint that Kif18A loss does not cause segregation defects. To test the effect of SAC deficiency on the phenotype seen upon Kif18A loss in more detail, we generated double-knockouts for Kif18A and Mad2 (Figures 2D and S1B; single Kif18A knockouts could not be obtained as predicted by the screen results in Figure 1 and the mitotic arrest in Figure 2A). Importantly, the mitotic delay as well as mitotic cell death, but not the chromosome oscillations (Video S3), were completely rescued in two independent double-knockout clones for Kif18A and Mad2 (Δ Mad2 Δ Kif18A_A1 and _B1), and we observed a similar mitotic timing and doubling time compared to Δ Mad2 cells (Figures 2A,E). Moreover, the Δ Mad2 Δ Kif18A cells showed a mild increase in segregation errors as compared to the parental HAP1 cells, that was similar to the increased missegregations observed in the Δ Mad2 cells (Figure 2C). Therefore, this increase could be completely attributed to Mad2 loss. Importantly, as predicted by the screens, we could confirm these results in Δ Mad1 and Δ Mad1 Δ Kif18A cells (Figure S2). In order to rule out minor segregation

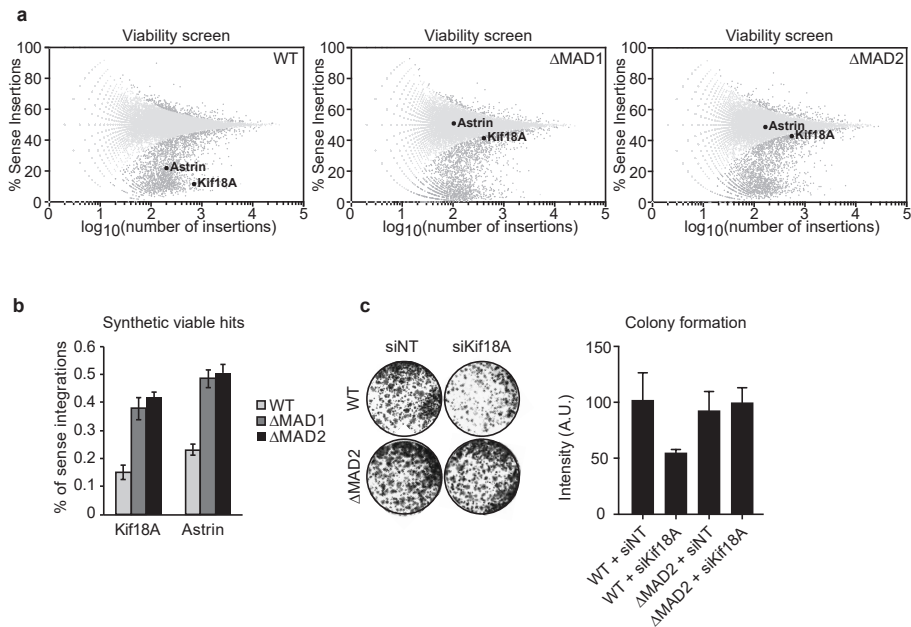


Figure 1: The identification of essential genes reveals *KIF18A* and *ASTRIN* as synthetic viable inter-actors with SAC deficiency.

(A) Representative plots of individual insertional mutagenesis screens in HAP1 WT, Δ Mad1 and Δ Mad2 cells. Each dot represents a single gene and the number of integrations per gene is plotted on the X-axis. On the Y-axis, the relative amount of sense integrations over the total amount of integrations is plotted. The synthetic viable hits *KIF18A* and *ASTRIN* are highlighted in red. **(B)** The average ratio of sense gene trap integrations over the total amount of integrations is plotted for both *KIF18A* and *ASTRIN*. The data is extracted from 4 individual WT, 2 individual Δ Mad1 and 2 individual Δ Mad2 insertional mutagenesis screens. Error bars represent standard deviation of two independent experiments. **(C)** Colony formation assay of WT and Mad2-deficient HAP1 cells treated with non-targeting siRNA (siNT) or siKif18A for 5 days, stained with crystal violet and quantified with Fiji. See also Figures S1 and S4.

defects in the Δ Mad2 Δ Kif18A cells, we quantified karyotypes with chromosome spreads. When karyotyping WT HAP1 cells, Δ Mad2 cells, and Δ Mad2 Δ Kif18A cells, no significant differences were found in chromosome gains or losses (Figure S1D). Thus, even in the absence of the SAC, the segregation errors do not increase upon Kif18A loss, implying that Kif18A is not required for normal chromosome segregation. This observation contradicts previous findings, where Kif18A-depletion resulted in increased chromosome segregation errors^{165,166}.

Moreover, our findings were surprising as Kif18A-depleted cells never seem to fully reach alignment due to chromosome hyper-oscillations. To rule out the possibility of knockout-adaptation leading to proper chromosome segregation in the Δ Mad2 Δ Kif18A double-

knockout cells, we sought to acutely reactivate the SAC in the Δ Mad2 Δ Kif18A cells. To this end, we generated a GFP-T2A-Mad2 cell line co-expressing GFP and Mad2 from the same vector, where we could induce the expression of Mad2 by the addition of doxycycline (DOX) (Figure 3A). Mad2-expressing cells were selected based on GFP-positivity, which were then used for the subsequent experiments. To test if the re-expression of Mad2 could completely rescue the SAC defect in the Δ Mad2 Δ Kif18A cells, we treated both WT HAP1 and Δ Mad2 Δ Kif18A cells expressing the DOX-inducible Mad2 with nocodazole. As expected, WT HAP1 cells treated with nocodazole arrested in mitosis, while the Δ Mad2 Δ Kif18A cells failed to do so (Figure 3B). Expression of GFP-T2A-Mad2 did not have any effect on the mitotic arrest observed in the WT HAP1 cells (Figure 3B, WT + DOX). Importantly, expression of GFP-T2A-Mad2 in the Δ Mad2 Δ Kif18A cells produced a nocodazole-induced mitotic arrest that was indistinguishable from the arrest observed in the WT HAP1 cells (Figure 3B). Thus, re-expression of Mad2 completely restored SAC-function in the Δ Mad2 Δ Kif18A cells.

We next examined the effect of Mad2 (re-)expression on cell division by live-cell imaging. The induced expression of GFP-T2A-Mad2 in WT cells slightly increased the average time spent in mitosis, whereas re-expression of Mad2 in the Δ Mad2 cells rescued the time spent in mitosis to the same extent as WT cells (Figure 3C). Most importantly, GFP-T2A-Mad2 re-expression in the Δ Mad2 Δ Kif18A cells caused a significant fraction of the cells to arrest in mitosis, eventually followed by mitotic cell death (Figure 3C). Besides the induction of a mitotic arrest, the re-expression of Mad2 in the Δ Mad2 Δ Kif18A cells also reduced the percentage of segregation errors seen in the Δ Mad2 background (Figure 3D), further confirming that the segregation errors observed in the Δ Mad2 Δ Kif18A cells are entirely due to loss of Mad2, not loss of Kif18A. Finally, to test whether the pleiotropic response to the acute restoration of SAC-function was sufficient to reduce cell viability, we measured the amount of GFP-T2A-Mad2-expressing (GFP-positive) cells over multiple days by fluorescence-activated cell sorting (FACS) (Figure 3E). We found that re-expression of Mad2 did not interfere with cell viability in WT or in the Δ Mad2 background but did progressively reduce viability of the Δ Mad2 Δ Kif18A cells (Figure 3E). This shows that, although Kif18A loss will only cause a subset of the mitotic cells to die, this is sufficient to reduce the long-term viability of the whole cell-population. Interestingly, the heterogeneity in the cellular response to loss of Kif18A by re-expressing Mad2 was very similar to what we observed in WT HAP1 cells depleted of Kif18A using siRNA (compare Figures 2A and 3C). This indicates that the heterogeneity is intrinsic to the loss of Kif18A and not due to an incomplete depletion of the protein in a subset of cells. Additionally, this means that the viability of the Δ Mad2 Δ Kif18A cells is not due to adaptation but reflects a real SAC-dependent essentiality.

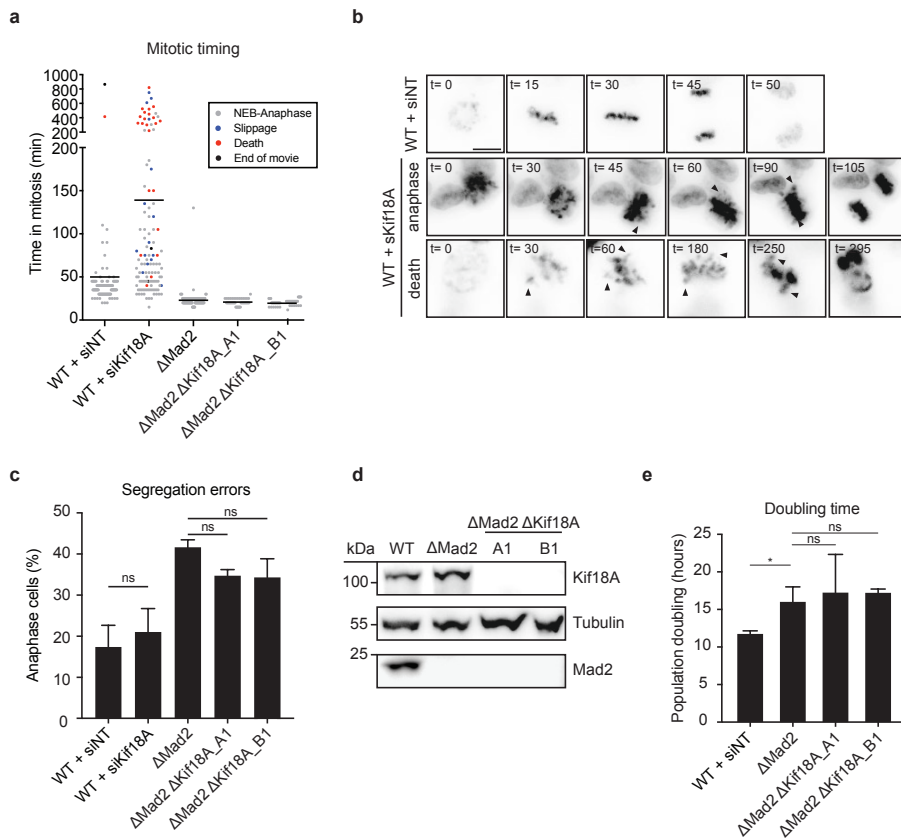


Figure 2: Depletion of Kif18A leads to a prolonged mitotic arrest and subsequent cell death.

(A) Mitotic timing and cell fate of individual cells followed by live-cell imaging of 3 independent experiments ($n \approx 90$ cells per condition). Each dot represents an individual cell. Cell fate was determined by either anaphase progression (NEB-Ana), start of NEB followed by interphase without anaphase (slippage), or DNA hypercondensation and fragmentation (cell death). Bars represent average time spent in mitosis. (B) Representative live-cell microscopy images of WT HAP1 cells treated with siNT or siKif18A for 48 hours. After siKif18A treatment, chromosome oscillations become visible (indicated with black arrow). One example is shown where cells progress into anaphase after a prolonged mitosis without segregation errors ($t = 105$) and one example is shown where prolonged mitosis results in cell death, indicated by DNA fragmentation at $t = 295$. Scale bar 10 μ m. (C) Quantification of chromosome segregation errors in WT HAP1 cells treated with siNT or siKif18A for 48 hours, Δ Mad2 and two different Δ Mad2 Δ Kif18A clones; cA1 and cB1. Segregation errors were scored during live-cell-imaging and consist of anaphase bridges and lagging chromosomes. Error bars represent standard deviation of 3 independent experiments ($n \approx 90$ per condition). An unpaired Student's t-test showed no significant difference between WT HAP1 cells and WT HAP1 cells treated with siKif18A, nor a difference between Δ Mad2 and the Δ Mad2 Δ Kif18A clones A1/B1. (D) Western blot analysis confirmed the successful generation of Kif18A and Mad2 double-knockout (Δ Mad2 Δ Kif18A) generation in HAP1 cells. Cell lysates were immunoblotted for Kif18A, Mad2 and α -Tubulin. (E) Doubling time as determined with a Lionheart microscope (1 independent experiment with samples plated in triplicate). An unpaired Student's t-test showed no significant difference in doubling time between Δ Mad2 and the Δ Mad2 Δ Kif18A clones A1/B1. See also Figures S1, S2, S3 and S4.

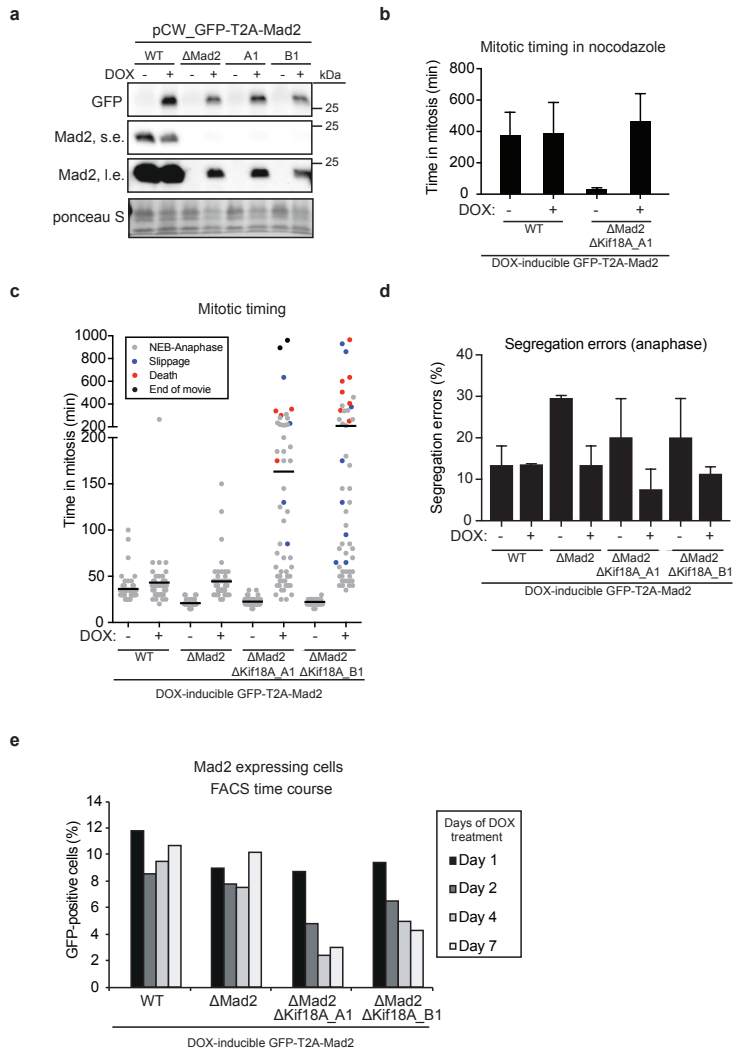


Figure 3: DOX-inducible Mad2 expression induces lethality in Δ Kif18A Δ Mad2 cells.

(A) Western blot analysis confirmed the doxycycline (DOX)-inducible GFP and Mad2 expression in WT, Δ Mad2, Δ Mad2 Δ Kif18A_A1, and Δ Mad2 Δ Kif18A_B1 cells. Cell lysates were immunoblotted for GFP and Mad2. S.e. indicates short exposure, l.e. indicates long exposure. **(B)** Mitotic timing of nocodazole-treated WT HAP1 and Δ Mad2 Δ Kif18A cells, treated with or without DOX to induce Mad2 expression ($n=15$ cells per condition, in 1 independent experiment). **(C)** Mitotic timing and cell fate of individual cells treated with or without DOX (8 hours prior to live-cell imaging) to induce Mad2 expression ($n=30$ cells per condition, in one independent experiment). Each dot represents an individual cell. **(D)** Quantification of segregation errors of cells shown in (C). **(E)** Percentage of GFP (and thus Mad2) expressing cells over time, determined by FACS over a period of 7 days.

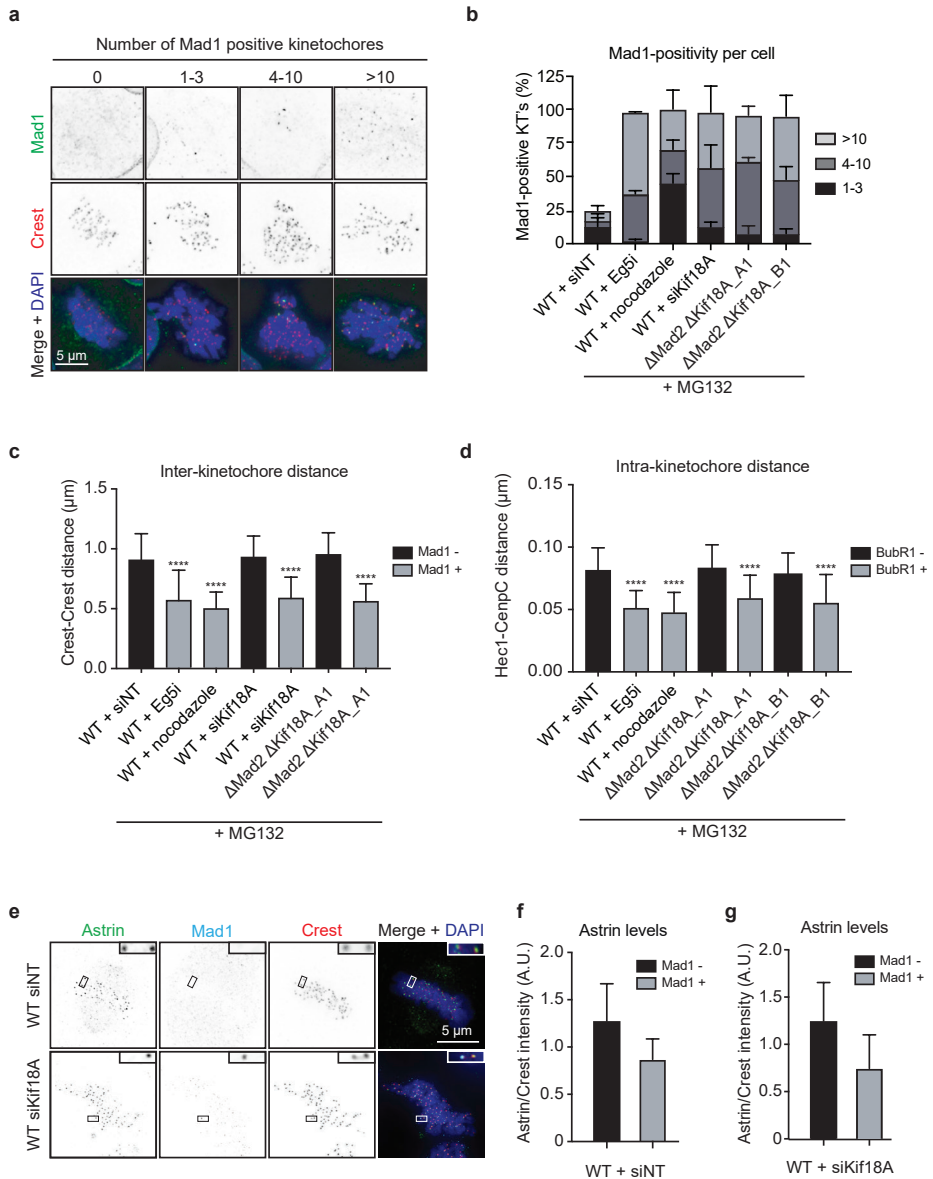
Taken together, we conclude that lethality of Kif18A loss is caused by a SAC-dependent mitotic delay (resulting in mitotic cell death or slippage) and not by an increase in chromosome segregation errors. This mitotic delay and the concurring cell death can be rescued by disabling SAC activity, in which case cells are viable with no apparent defects in chromosome segregation. Importantly, we could validate these findings in HeLa cells, the cell type used in previous Kif18A studies (Figures S3A,B)^{165,168}. It is interesting to note that loss of Kif18A results in SAC-activation, while without a functional SAC its loss does not lead to major problems in chromosome segregation. We therefore investigated the underlying cause for the observed SAC-activation in Kif18A-deficient cells.

Loss of Kif18A reduces tension at kinetochores

To investigate why loss of Kif18A results in SAC activation, we first investigated whether the SAC is activated at all, or only at a subset of kinetochores. To test this, we quantified the number of Mad1-positive kinetochores by immunofluorescence microscopy in WT HAP1 cells, siKif18A-depleted cells, and the Δ Kif18A- Δ Mad2 double-knockout clones. As WT HAP1 cells display limited checkpoint activity (Figure 4B), we activated the SAC in WT HAP1 cells as a control by treating them with a low dose of nocodazole to interfere directly with k-Mt stability, or an Eg5-inhibitor to interfere indirectly with k-Mt stability by creating a situation where tension cannot be established because the spindle poles are clustered. As anticipated, loss of Kif18A produced a clear increase in the number of Mad1-positive kinetochores in both siKif18A-depleted HAP1 cells and the Δ Kif18A- Δ Mad2 double-knockout clones (Figures 4A,B). Importantly, only a subset of kinetochores was Mad1-positive in the cells lacking Kif18A, suggesting that the SAC is only activated at specific kinetochores. The Mad1-positive kinetochores seen in the cells lacking Kif18A seemed to be mostly located outside of the main chromosome-pack, in line with previous observations¹⁶³.

Figure 4: Mad1-positive kinetochores of Kif18A-depleted cells display decreased tension.

(A) Representative images of the quantification of the number of Mad-positive kinetochores in Δ Mad2 Δ Kif18A_A1 cells. Scale bar 5 μ m. (B) Quantification of immunofluorescent staining of Mad1 at kinetochores in WT HAP1 cells treated with siNT (48 hours), Eg5-inhibitor STLC (10 μ M, 4 hours), Nocodazole (50 nM, 4 hours), siKif18A (48 hours) and Δ Mad2 Δ Kif18A_A1/B1 cells. All conditions were pre-treated for 1 hour with MG132 before fixation to arrest cells in mitosis. Error bars represent standard deviation of 4 independent experiments (n= ~15 cells and 100 kinetochores per condition). (C) Measurements of inter-kinetochore (KT) distance of WT HAP1 cells treated with siNT (48 hours), Eg5- inhibitor STLC (10 μ M, 4 hours), Nocodazole (50 nM, 4 hours), siKif18A (48 hours) and Δ Mad2 Δ Kif18A_A1. Measurements between Crest-pairs were separated in Mad1-positive and Mad1-negative kinetochores. Error bars represent standard deviation of minimally 15 kinetochore pairs per condition. P-values were determined by unpaired Student's t-test comparing all experimental conditions against WT + siNT. ****P<0.0001. (D) Measurements of intra-KT distance of WT HAP1 cells treated with siNT (48 hours), Eg5-inhibitor STLC (10 μ M, 4 hours), Nocodazole (50 nM, 4 hours), Δ Mad2 Δ Kif18A_A1 and Δ Mad2 Δ Kif18A_B1. Distance



measurements between Hec1 and CenpC were separated in BubR1-positive and BubR1-negative kinetochores. Error bars represent standard deviation of minimally 15 kinetochore pairs per condition. P-values were determined by unpaired Student's t-test comparing against WT + siNT. ****P<0.0001.

(E) Representative images of immunofluorescent staining of Astrin, Mad1 and Crest in WT HAP1 cells treated with siNT or siKif18A for 48 hours. Scale bar 5 μ m. **(F)** Quantification of Astrin levels on Mad1-positive and Mad1-negative kinetochores in WT HAP1 cells. Error bars represent standard deviation of 15 kinetochore pairs in 1 experiment. **(G)** Quantification of Astrin levels on Mad1-positive and Mad1-negative kinetochores in Δ Mad2 Δ Kif18A cells. Error bars represent standard deviation of 15 kinetochore pairs in 1 experiment.

Because previous studies showed that Kif18A-depletion could result in a loss of tension across sister kinetochores^{163,169}, we investigated if loss of Kif18A indeed leads to tension defects in our setting. For this analysis, we made a distinction between Mad1-negative and Mad1-positive kinetochores. The inter-kinetochore distance of Mad1-negative kinetochore pairs in Kif18A-depleted and Δ Mad2 Δ Kif18A cells was the same as the inter-kinetochore distance in control-depleted HAP1 cells (Figure 4C). This implies that these kinetochores are all properly attached to the mitotic spindle, or at least the spindle is able to generate the same amount of force on these attachments. In contrast, the Mad1-positive kinetochores in the control samples for checkpoint activation in WT HAP1 cells (Eg5-inhibitor or nocodazole treatment), siKif18A-depleted and Δ Mad2 Δ Kif18A cells displayed a clear decrease in inter-kinetochore distance compared to Mad1-negative kinetochores (Figure 4C). As previous work indicated that the intra-kinetochore stretch is more important for SAC inactivation than inter-kinetochore distance¹⁷⁰, we also measured the intra-kinetochore distance in the same conditions as Figure 4C, by performing immunofluorescent staining of the outer kinetochore component Hec1, the inner kinetochore component CENP-C, and BubR1 as a marker for checkpoint activation. Here, we find a similar trend where checkpoint-active (BubR1-positive) kinetochores display decreased intra-kinetochore distance (Figure 4D). As an independent measure of tension, we looked at the localization of Astrin, which is recruited to kinetochores once tension is established and Aurora B activity is reduced¹⁷¹. Both in WT HAP1 and siKif18A-depleted cells, there was a strong correlation between Mad1-positivity and Astrin-negativity (Figures 4,E-G), again indicating that checkpoint-active kinetochores in Kif18A-depleted cells are under low tension. In addition, the fact that we find Astrin on kinetochores in cells lacking Kif18A, indicates that Astrin is not recruited by Kif18A, as previously proposed¹⁶⁶. Together, our data confirm the previously observed tension defects upon loss of Kif18A^{163,169}.

Kinetochores of Kif18A-depleted cells show SAC activation in the presence of kinetochore-microtubule attachments

In summary, our data thus far show that loss of Kif18A results in chromosome oscillations and a loss of tension, resulting in SAC activation. However, when the SAC is inhibited, Kif18A cells do not display chromosome segregation errors. This is quite unexpected, as it suggests that, despite the recruitment of SAC proteins, kinetochores in Kif18A-depleted cells are correctly attached to the mitotic spindle. To investigate this in more detail, we visualized the kinetochore-attachment status by immunofluorescence microscopy. SAC-active kinetochores were selected based on Mad1-positivity. As expected, we observed that Mad1-negative kinetochores in WT HAP1 cells display a k-Mt attachment (Figure 5A).

In addition, checkpoint activation in WT HAP1 cells through Eg5 inhibition or nocodazole treatment, showed the expected result of Mad1-positivity at unattached kinetochores (Figures 5A,B). In striking contrast, the majority of Mad1-positive kinetochores in siKif18A-depleted and Δ Mad2 Δ Kif18A cells did display a k-Mt attachment (Figures 5A,B and S3C,D). Previous work has proposed that Mps1 and microtubules bind competitively to kinetochores^{84,172}, supporting the idea that only a lack of attachment is able to activate the SAC through Mps1 localization. However, other work has shown that Mps1 can be recruited to tension-less microtubule bound kinetochores¹⁷². As Mps1 is an upstream factor for Mad1 recruitment, we also visualized the attachment status of Mps1 positive kinetochores in control-depleted and Kif18A-depleted HAP1 cells (Figures S1E-G). Here, we again find that the majority of the checkpoint-signaling kinetochores in Kif18A-depleted cells harbor a microtubule attachment. This, together with our previous data, implies that the kinetochores that signal to the SAC in Kif18A-deficient cells are attached to the spindle despite the fact that they lack tension. Thus, this data implies that the SAC can be active even when a microtubule attachment is present.

But if there are still microtubule attachments present, how is the lack of tension translated into SAC-activation? One could argue that not all of the microtubule-binding sites present at the single kinetochore are occupied^{84,173}. Thus, the reduced tension could be both a cause and a consequence of a relative reduction in the total number of microtubules bound per kinetochore, resulting in a number of unoccupied microtubule-binding sites that could activate the SAC. In an effort to resolve this, we determined the quality of the microtubule attachments by measuring the width and intensity of the microtubule-bundles at Mad1-positive and Mad1-negative kinetochores in all previously described settings (Figure 5C). In untreated, Eg5-inhibitor-treated and low dose nocodazole-treated WT cells, very dense microtubule staining was exclusively observed adjacent to Mad1-negative kinetochores, suggesting they are attached by a k-fiber. Strikingly, in Kif18A-deficient cells, the Mad1-positive and Mad1-negative kinetochores displayed a similar intensity of microtubule staining, suggesting that the Mad1-positive kinetochores contain just as many microtubules as the Mad1-negative kinetochores (Figure 5C). This could explain why Δ Mad2 Δ Kif18A cells exhibit normal chromosome segregation. More importantly, these results imply that, under specific conditions, the SAC can be active in response to loss of tension, without any evident loss of attachment.

Loss of Astrin phenocopies loss of Kif18A

Besides Kif18A, we also found Astrin as a synthetic viable interactor with SAC-deficiency. Astrin is found to localize to kinetochores upon tension generation¹⁷¹ and is thought to be needed for stabilization of k-Mt attachments, which are needed to enable SAC silencing and proper chromosome segregation¹⁶⁶. As we found both Kif18A and Astrin to be synthetic viable with Mad1/Mad2 loss, both proteins might influence chromosomal movements and tension, possibly through the same pathway. Indeed, Astrin-depleted cells showed a mitotic arrest similar to Kif18A-depleted cells and displayed chromosomal oscillations (Figures S4A,B and Videos S4,5). No significant increase in segregation errors were found (Figure S4C and Video S4), and the Mad1-positive kinetochores were mostly attached by microtubules (Figures S4D-F). These Astrin phenotypes seemed to be a bit milder than the phenotypes seen after Kif18A depletion, but do indicate that Astrin loss, like Kif18A, results in SAC activity at kinetochores under low tension that are properly attached to the mitotic spindle.

DISCUSSION

Previous studies have shown that loss of Kif18A results in alignment problems, attributed to severe chromosome oscillations^{163,165,166,174,175}. These alignment problems are associated with a prolonged mitotic duration that is fully dependent on the SAC^{163,165}. Here, we show that loss of Kif18A is not compatible with cell viability in human HAPI cells. We find that lethality of Kif18A loss is rescued by deletion of Mad1 or Mad2, indicating that cell death in Kif18A-deficient cells is a consequence of (persistent) SAC activation. Indeed, we could show that loss of Mad2 prevents the mitotic cell death we see after Kif18A-depletion. Surprisingly, combined loss of Kif18A and Mad2 did not produce high rates of segregation errors. This was unexpected in light of the previous observations where loss of Kif18A caused problems in chromosome alignment. Since the missegregation rates in Δ Mad2 can be attributed to SAC-deficiency, and the loss of Kif18A leads to a mitotic arrest and not to increased missegregations, it is unlikely that the Mad2 deficient background influences the phenotype of Kif18A loss. Our findings indicate that loss of Kif18A in HAPI cells does not cause problems in attachment of kinetochores to the mitotic spindle, but nevertheless does lead to a persistent SAC-activation. In fact, we find that the k-Mt attachments that are established in Kif18A-deficient cells are functional enough to correctly separate sister-chromatids, and therefore, HAPI cells lacking Kif18A maintain a high fidelity of chromosome segregation. This has created a unique situation in which lack of tension is observed

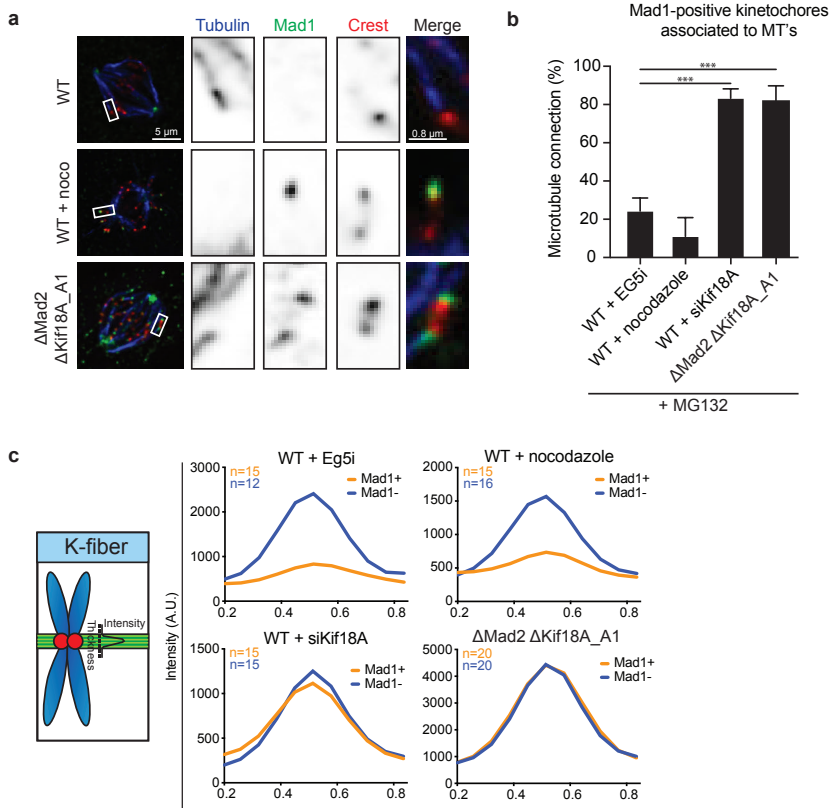


Figure 5: Kif18A loss results in recruitment of Mad1 in the presence of microtubule connections.

(A) Representative immunofluorescent images of WT HAPI, WT HAPI nocodazole treated (50 nM, 4 hours) and Δ Mad2 Δ Kif18A_A1 cells, stained for Tubulin, Mad1 and Crest. Scale bar 5 μ m in main figure and 0.8 μ m in inset. **(B)** Quantification of the amount of k-Mt attachments in Mad1-positive kinetochores of WT HAPI cells treated with Eg5-inhibitor STLC (10 μ M, 4 hours), nocodazole (50 nM, 4 hours), siKif18A (48 hours) and Δ Mad2 Δ Kif18A_A1 cells. All conditions were pre-treated with MG132 for 1 hour, after which cells were calcium treated and fixed before staining the cells for microtubules (α -tubulin), SAC-activity (Mad1) and centromeres (Crest). Error bars represent standard deviation of 3 independent experiments ($n = 20$ cells and 120 kinetochores per condition). P-values were determined by paired t-test, comparing Kif18A depleted cells against WT HAPI cells treated with Eg5-inhibitor STLC. *** $P < 0.001$. **(C)** Graphs showing measurements of k-fiber thickness and intensity ($n = 5$ cells and ~25 kinetochores per condition) in WT HAPI cells treated with siNT, Eg5-inhibitor STLC (10 μ M, 4 hours), nocodazole (50 nM, 4 hours), siKif18A (48 hours) and Δ Mad2 Δ Kif18A_A1 cells, all treated for 1 hour with MG132 before fixation. See also Figures S1, S3 and S4.

on kinetochores that are attached to microtubules that appear to be fully mature and functional.

The classic view is that in unperturbed conditions, the SAC senses loss of k-Mt attachments. Recently, it was shown that stabilizing k-Mt attachments with a non-phosphorylatable Hec1 mutant was sufficient to satisfy the SAC under conditions of low tension^{85,86}. Moreover, it was shown that Mps1 directly competes with microtubules for binding to Hec1, indicating that microtubule-attachment can directly displace an essential checkpoint component, consistent with a direct relation between attachment and SAC-silencing^{176,177}. These data suggest that SAC activation depends on a lack-of-attachment signal for its activation and implies that a lack-of-tension signal, due to erroneous attachments, cannot be sensed directly by the SAC. This potential caveat is fixed via an error-sensing mechanism that efficiently promotes detachment of misattached k-Mts, thus recreating an unattached kinetochore that can (re-)activate the SAC^{152,178}. However, another study shows that depleting Mklp2 leads to retention of Aurora B which in turn recruits different checkpoint proteins, such as Mps1, to the microtubule bound kinetochores in anaphase. In this setting, the recruitment of SAC proteins did not induce a mitotic delay, however it does implicate that Mps1 can be recruited to microtubule bound kinetochores¹⁷². In conclusion, many studies have confirmed a tight link between tension and attachment^{159,170,179}, and the general consensus is that SAC activation is due to a lack of k-Mt attachments^{75,180}. However, despite the evidence in favor of unattached kinetochores as the primary source of SAC activation, the role of tension in SAC-activation has never been fully resolved due to the intricate links between tension and attachment. Under normal circumstances, tension is needed to stabilize k-Mt attachments¹⁸¹, and besides, unattached kinetochores will never be under tension, making it challenging to obtain a setting where tension is normal, but attachments are lacking.

Several studies in budding yeast have suggested a direct role for tension in SAC-activation^{157,182,183}. There is only scant evidence for attachment-independent activation of the SAC in higher organisms. For example, PtK1 cells grown in hypothermic conditions are severely delayed in mitosis, despite the fact that their kinetochores acquire normal numbers of k-Mts¹⁶⁰. These kinetochores are not under full tension, and the mitotic delay can be rescued by inhibition of the SAC, indicating that loss-of-tension can directly activate the SAC under these conditions. However, there was no evidence of Mad2 recruitment to these kinetochores. Another study in PtK2 cells shows that Mad1 starts to be lost after end-on microtubule attachment and before a full k-fiber forms. This Mad1 loss is subsequently associated with force generation, leading to tension generation¹⁸⁴. This data implies a switch-like interplay between SAC-activity and tension.

Our current study provides a new set of data that need to be considered in this tension-versus-attachment debate. As mentioned above, tension and attachment are interlinked, making it difficult to experimentally dissect the two. Here, we provide a unique setting where a tension defect is established without (chemically) interfering with microtubule dynamics. We find that human HAP1 cells lacking Kif18A can establish fully functional k-Mt attachments that can facilitate proper chromosome segregation, but that the attached kinetochores experience defects in tension. Our intensity measurements of the k-Mts could not discern any reductions in the overall thickness or intensity of the staining of the k-Mts bound to kinetochores in Kif18A-deficient cells. However, the inter- and intra-kinetochore distance indicated a clear reduction in tension across checkpoint-signaling kinetochores, altogether suggesting that Mad1 is recruited to kinetochores that have functional k-Mt attachments. Of course, it is possible that minor differences in microtubule occupancy at kinetochores of Kif18A-deficient cells cannot be detected with these assays, but it should be noted that these cells are perfectly capable to drive proper chromosome segregation. Thus, this implies that either the SAC is activated by very minor defects in attachment, not detectable with our assays and not giving rise to segregation errors, or that the checkpoint is directly responsive to lack-of-tension, causing kinetochores to recruit Mad1. Based on our data, we conclude that the tension defects in Kif18A-depleted cells activate the SAC (Figure 6). In contrast, a direct role for Kif18A in SAC inactivation could also explain the observed SAC-dependent arrest in Kif18A-depleted cells. However, if Kif18A would be necessary for SAC inactivation, we would not expect to see Mad1 activity at only a subset of kinetochores, and we would not expect such a pleiotropic phenotype.

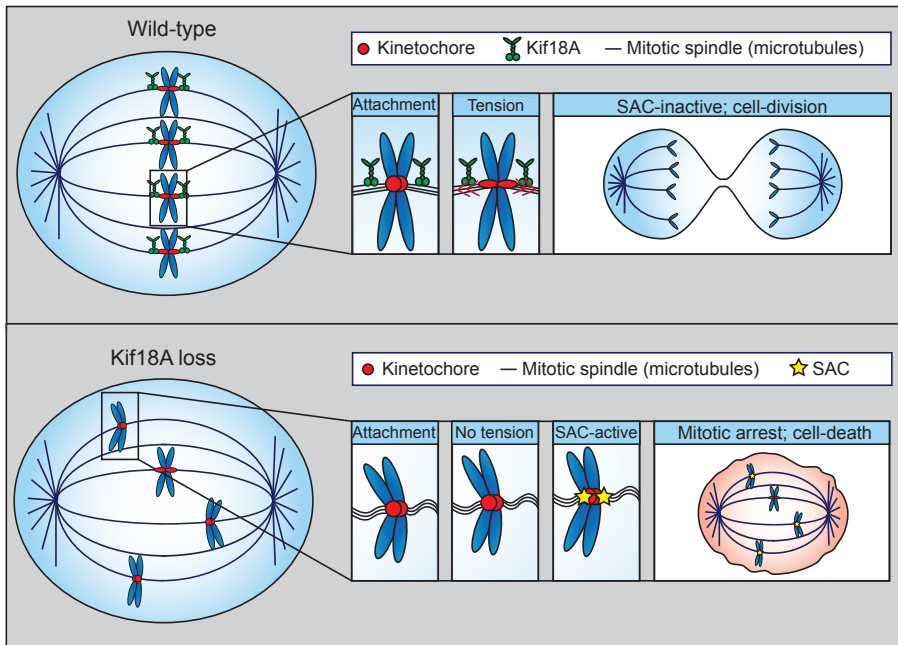


Figure 6: Loss of Kif18A results in SAC activation at microtubule-attached kinetochores.

Schematic overview of hypothetical model of Kif18A loss. In WT cells, Kif18A is recruited to the plus-ends of microtubules when chromosomes are properly aligned at the metaphase plate, leading to a reduction of chromosome oscillations, stabilization of k-Mt attachments and the generation of tension which silences the SAC and promotes anaphase onset. Upon loss of Kif18A, the oscillatory movements of chromosomes are no longer reduced, and tension defects are found at the checkpoint signaling kinetochores. Thus, the tension defect is able to activate or maintain the SAC, leading to a mitotic arrest and subsequent cell death, without destabilizing the k-Mt attachment.

We hypothesize that the tension defects upon Kif18A-depletion are linked to the hyper-oscillations of the chromosomes. Possibly, these extreme oscillations perturb the ability of the spindle microtubules to produce stable forces across sister kinetochores, especially when the chromosomes switch from poleward to anti-poleward movements and vice versa. These severe fluctuations in tension could then be translated into SAC activation. This hypothesis also fits with the fact that we mostly observe SAC activation on the kinetochores that reside outside the metaphase plate. Another possible explanation for the tension defects and hyper-oscillations observed in Kif18A-depleted cells could be that Kif18A is needed to directly stabilize the k-Mt attachment¹⁶⁵. When stabilization is impossible due to Kif18A loss, tension cannot be established across sister kinetochores. This lack of k-Mt stabilization could be the underlying cause of the chromosome hyper-oscillations seen after Kif18A loss. However, it needs to be noted that we observe that

the loss of tension in Kif18A-depleted cells occurs at kinetochores with apparent correct k-Mt attachment.

A remaining question is; if tension is lost, then why do we not see a loss of k-Mt attachments? We envision several explanations for this. First, it could be that the tension defect is very transient since chromosomes continuously move back and forth. This could provide insufficient time for Aurora B to destabilize the attached k-Mts yet provide enough time to recruit Mad1. Second, Kif18A has microtubule depolymerase activity, making it not unlikely that loss of Kif18A leads to hyper-stable k-Mts, leaving only room for SAC activation by tension defects. This transient state of tension loss, followed by SAC activation could also explain the pleiotropic mitotic phenotype observed upon loss of Kif18A; the stochasticity of SAC activation could result in a situation where there are no or an insufficient number of SAC-positive kinetochores to maintain the mitotic delay. This then results in anaphase onset and would explain why not all cells remain in mitosis persistently.

One other synthetic viable hit in our screen was Astrin, a protein that is known to bind to kinetochores upon generation of tension¹⁷¹. Astrin has previously been linked to stabilization of k-Mt attachments, chromosome alignment and SAC silencing¹⁶⁶. The fact that we find both Kif18A and Astrin to be synthetic viable with Mad1/Mad2 loss suggests that both proteins work in the same process, influencing chromosomal movements and thus tension. Indeed, Astrin-depleted cells behave similar to Kif18A-depleted cells. In contrast to another study¹⁶⁶, we observe Astrin localization in Kif18A-depleted cells. Thus, although Kif18A does not affect the recruitment of Astrin to kinetochores, it is likely that Kif18A and Astrin work in a similar pathway to suppress chromosome oscillations.

Taken together, our data show that loss of Kif18A (or Astrin) can induce SAC activation in the presence of fully functional k-Mt attachments. This not only allowed us to gain a better understanding of the function of Kif18A, but also provided us with a unique setting in which tension is lacking while attachments appear to be normal. Our observations suggest that the SAC can be activated, even when microtubules are bound, disputing a model where the SAC only senses unattached kinetochores. We cannot rule out that minor attachment defects that we fail to detect are the source of the checkpoint signal, but at least our data show that a lack-of-tension is enough to (re-)activate the SAC in a situation where the attachment is good enough to ensure proper segregation of the attached chromatid. It would therefore be interesting to look for other settings where the SAC is activated when fully functional k-Mt attachments are present, but most intriguingly,

it would be interesting to unravel how the lack-of-tension could promote Mps1 and Mad1 recruitment.

STAR Methods

Contact for Reagent and Resource Sharing

Further information and requests for resources and reagents should be directed to and will be fulfilled by the Lead Contact, Jonne Raaijmakers (j.raaijmakers@nki.nl).

Experimental Model and Subject Details

Cell Lines and Tissue Culture

Human derived near-haploid HAP1 cells were cultured in IMDM (Gibco) supplemented with 10% FCS, 1% GlutaMAX supplement (Gibco), 100 U/ml penicillin, and 100 µg/ml streptomycin. siRNA transfections were performed using RNAiMax (Invitrogen) according to the manufactures guidelines. The following siRNAs were used in this study: siNon-Targetable (Dharmacon), siKif18A (Dharmacon, custom: CCAACAACAGUGCCAUAUUU), siAstrin (Dharmacon OTP smartpool). All compounds (Nocodazole, MG132, Eg5-inhibitor STLC) were dissolved in DMSO and used at indicated concentrations.

Method Details

Insertional mutagenesis screens

Genes essential for fitness of WT and two Δ MAD1 and two Δ MAD2 cell lines were identified as previously described¹⁶¹. In brief, gene trap retrovirus was produced in HEK293T cells, as previously described¹⁶⁶. Retrovirus was harvested twice daily for a minimum of three days, and pelleted by centrifugation (2 hours, 21,000 rpm, 4 degrees Celsius using a SW28 rotor. Approximately 40 million Δ MAD1 and two Δ MAD2 HAP1 cells were mutagenized by transduction of the concentrated gene trap virus in the presence of 8 µg/ml protamine sulfate in a T175 flask for at least two consecutive days. The mutagenized cells were passaged for an additional 10-12 days after the last infection. After passaging, cells were collected by trypsin-EDTA followed by pelleting. Cells were fixed using fix buffer I (BD biosciences). To minimize confounding from diploid cells potentially harboring heterozygous mutations, fixed cells were stained with DAPI to allow sorting on G1 haploid DNA content using an Astrios Moflo. 30 million sorted cells were lysed overnight at 56 degrees Celsius to allow for de-crosslinking followed by genomic DNA isolation using a DNA mini kit (Qiagen).

Insertion site mapping

The gene trap insertion sites were amplified by LAM-PCR, followed by capture, ssDNA linker ligation, and an exponential amplification using primers containing illumina adapters prior to sequencing as described previously⁶¹. Mapping and analysis of insertions sites is described in detail by Raaijmakers *et al.*¹⁶². Briefly, following sequencing on a HiSeq 2000 or HiAeq 2500 (Illumina), insertion sites were mapped to the human genome (h19) allowing one mismatch⁶¹, and intersected with RefSeq coordinates to assign insertions sites to genes⁶⁷. Gene regions overlapping on opposite strands were not considered for analysis, while for genes overlapping on the same strand gene names were concatenated. For each replicate for both genotypes (*MAD1* and *MAD2*) gene essentiality was determined by binomial test. Synthetic lethality and viability was assessed by comparing the distribution of sense and antisense orientation integrations for each gene in the *MAD1/2* replicates with 4 wild type control datasets previously published¹⁶⁸ (NCBI SRA accession no. SRP058962) using Fisher's exact tests. A gene was considered a hit when it passed all Fisher's tests with a P-value cutoff of 0.05 and an effect size of at least 20%.

CRISPR-mediated generation of knockout cell-lines

Mad2 knockout cells were generated using CRISPR/Cas9 mediated genome editing. Guide sequences were designed using CRISPR design. Guides to generate knockout cell lines were targeted against exon 1-3 of the gene of interest, and subsequently cloned into the pX330 vector¹⁶⁹. pX330 and a donor vector containing a blasticidine resistance-cassette¹⁹⁰ were co-transfected in HAP1 cells and selected with 5 µg/ml blasticidin. Double-knockouts were generated by repeating the same procedure in *Mad2* knockout cells, using a donor vector containing a puromycin resistance-cassette. Individual clones were selected and knockouts were confirmed using both PCR to confirm integration of the blasticidin cassette at the correct locus and by western blot analysis. Guides used were: *Mad2* forward caccGATTTCGGCGCTCCCGCGCA, *Mad2* reverse aaacTGC GCGGGAGCGCCGAAATC, *Kif18A* clone A forward caccgAGTAGTAGTTCGTGTACGTC, *Kif18A* clone A reverse aaacGACGTACACGAACTACTACTc, *Kif18A* clone B forward caccgCTACTTTTCATATGGTGGCAC, *Kif18A* clone B reverse aaacGTGCCACCATATGAAAGTAGc, *Astrin* forward caccgTGCAGGGTAAGTTCACGGAG, and *Astrin* reverse aaacTCCGTGAACTTACCCTGCAC.

Plasmids and cell lines

The lentiviral plasmid pCW57.1 (Addgene #41393) was used as an all-in-one Tet responsive system. GFP-*Mad2* was inserted into the pCW57.1 plasmid by using the *NheI* and *AgeI* restriction sites. To insert the T2A sequence between GFP and *Mad2*, a synthetic block was

ordered (IDT) and inserted using EcoRI and PSTI restriction sites. To obtain a successfully cloned plasmid, the ligation product was transformed into StBL3 bacteria using heat shock and selected on LB ampicillin plates. Sequencing of plasmids confirmed successful insertion. Stable cell-lines were created by lentiviral production in HEK293T cells. For this, cloned plasmids were co-transfected with lentiviral packaging and viral envelope constructs. Virus was harvested 48 hours after HEK293T transfection and added into the cell culture medium of HAPI cells to achieve stable pCW_GFP_T2A_Mad2 integration into the genome.

Western blot

Cells were lysed using Laemmli buffer (120 mM Tris pH 6.8, 4% SDS, 20% glycerol). Equal amounts of protein were separated on a polyacrylamide gel followed by transfer to a nitrocellulose membrane. Membranes were blocked in a 5% Milk/TBS solution. Antibodies were incubated in 2,5% milk in TBS containing 0,1% Tween. The following antibodies were used in this study: rabbit anti-alpha-tubulin (Abcam, ab18251), rabbit anti-Mad2 (Bethyl, A300-300A), rabbit anti-Kif18A (Bethyl, A301-080A), rabbit anti-Astrin (Bethyl, A301-512A), rabbit-anti-HSP90 (Santa Cruz, sc7947). HRP-coupled secondary antibodies (DAKO) were incubated for 2h at room temperature in a 1:2500 dilution. The immunopositive bands were visualized using Immobilon Western HRP Substrate (Millipore) and a ChemiDoc MP System (Biorad).

Immunofluorescence

Cells were grown on 9mm glass coverslips and pre-extracted for 60 seconds in PEM buffer (100 mM PIPES, 10 mM EGTA, 1mM MgCl and 0.1% Triton X-100), followed by fixation for 10 minutes at room temperature in 4% formaldehyde in PEM buffer with 0.2% Triton X-100. The following antibodies were used: mouse anti-Mad1 (Santa Cruz, sc65494), human anti-Crest (Cortex Biochem, cs1058), rabbit anti-Kif18A (Bethyl, A301-080A) and rabbit anti-Astrin (Bethyl, A301-512A), rabbit anti-BubR1 (Bethyl, A300 386A), mouse anti-Hec1 (Genetex, 9G3.23), guinea pig anti-CENPC (PD030, MBL) and pH3Ser10 (Millipore, 06-570). All primary antibodies were incubated over night at 4°C. Secondary antibodies (Molecular probes, Invitrogen) and DAPI were incubated 2 hours at room temperature. Coverslips were mounted using ProLong Gold (Invitrogen). Images were acquired using a Deltavision deconvolution microscope (Applied Precision) with a 60x 1.40 NA oil objective. Softworx (Applied Precision), ImageJ, Adobe Photoshop and Illustrator CS6 were used to process acquired images.

For tubulin stainings, cells were grown on 9mm glass coverslips and treated with MG132 for 1 hour prior to fixing, to arrest cells in metaphase. Cells were then permeabilized/calcium

treated with calcium in PEM buffer (100 mM PIPES, 1mM MgCl₂, 0.1 mM CaCl₂ and 0.1% Triton X-100), followed by fixation for 10 minutes at room temperature in 4% formaldehyde (in (100 mM PIPES, 1mM MgCl₂, 0.1 mM CaCl₂ and 0.1% Triton X-100). The following antibodies were used: rabbit anti-alpha-tubulin (Abcam, ab18251), mouse anti-Mad1 (Santa Cruz, sc65494), human anti-Crest (Cortex Biochem, cs1058), rabbit anti-Kif18A (Bethyl, A301-080A) and rabbit anti-Astrin (Bethyl, A301-512A). All primary antibodies were incubated over night at 4°C. Secondary antibodies (Molecular probes, Invitrogen) and DAPI were incubated 2 hours at room temperature. Coverslips were mounted using ProLong Gold (Invitrogen). Images were acquired using a Deltavision deconvolution microscope (Applied Precision) with a 100x 1.40 NA oil objective. Softworx (Applied Precision), ImageJ, Adobe Photoshop and Illustrator CS6 were used to process acquired images.

For Mps1 stainings, cells were grown, fixed, stained and imaged as described for the tubulin stainings. However, before fixation, cells were pre-treated for half an hour with MG132, followed by one hour of Mps1 inhibition using 100nM Cpd-5⁹¹. The following primary antibodies were used: rabbit anti-alpha-tubulin (Abcam, ab18251), mouse anti-Mps1 (Millipore, NT, clone 3-472-1), human anti-Crest (Cortex Biochem, cs1058).

Live-Cell Microscopy

Cells were plated on 8-well glass-bottom dishes (LabTek) and cultured in L-15 CO₂ independent medium (Gibco). Cells were imaged using a Deltavision deconvolution microscope (Applied Precision) equipped with a heat chamber. For DNA visualization, 250nM SiR-DNA (Spirochrome) was added 2 hours before imaging. Images were acquired every five minutes using a 20x (0.25 NA) objective. Z-stacks were acquired with 2 μm intervals. Images were analyzed and processed using Softworx (Applied Precision) and ImageJ.

Chromosome spreads

Chromosome spreads were prepared from WT HAP1 cells treated with siNT for 48 hours, ΔMad2 cells, and ΔMad2ΔKif18A_A1/B1 cells. Cells were treated with Nocodazole for 1 hour prior to harvesting through shake-off. Cells were then incubated with 0.075M of KCl at 37°C for 10 minutes. Thereafter, a drop of fixative (methanol:acidic acid, in a 3:1 ratio made fresh) was added and the samples were centrifuged at 1500 rpm for 5 minutes. Supernatant was discarded and cells were fixed with 1 mL of fixative for 30 minutes. Fixative was then replaced by fixative + Dapi (1:1000). Subsequently, 15 μl of the cells suspension was dropped from 5 cm distance onto an ethanol cleaned coverslip. After the slides dried at room

temperature, chromosome spreads were mounted with ProLong Gold (Invitrogen). Images were acquired using a Deltavision deconvolution microscope (Applied Precision) with a 100x 1.40 NA oil objective. Softworx (Applied Precision), ImageJ, Adobe Photoshop and Illustrator CS6 were used to process acquired images.

FACS

Cells were harvested with trypsin and fixed in 70% ethanol. GFP-positivity was measured on a LSR Fortessa (BD Biosciences). Single cells were selected based on forward and side scatter diagrams, GFP-positive cells were identified by 488nm excited short pass (530 nm) versus long pass (710 nm) plots to exclude HAPI auto-fluorescence. 10.000 gated events were detected for each sample. Data were analyzed using FlowJo software (LLC).

Quantification and Statistical Analysis

Significant differences between cell-lines were calculated using a Student's t-test. The number of cells or kinetochores measured per individual experiment can be found in the corresponding figure legends. In all figures: *, p-value < 0.05; **, p-value < 0.01; ***, p-value < 0.001; ****, p-value < 0.0001.

Data and Software Availability

The data for each individual screen can be found under Database: NCBI SRA accession no. SRP119760.

Acknowledgments

We would like to thank the Medema and Rowland lab for helpful discussions. We would also like to thank Prof. S.M. Lens and Prof. G.J.P.L. Kops for sharing reagents. This study was supported by funds from the Dutch Cancer Society (KWF- NKI-2015-7832) granted to R.H.M. and J.A.R..

Author Contributions

R.H.M. and J.A.R. conceived the project. L.M.E.J, T.V.A. and J.A.R., performed and analyzed the experiments. V.A.B. performed data processing and data analysis. R.H.M. and T.R.B. provided resources and input on the project. L.M.E.J, J.A.R., R.H.M. wrote the paper.

Declaration of Interests

T.R.B. is co-founder and SAB member of Haplogen GmbH and co-founder and managing director of Scenic Biotech B.V.

SUPPLEMENTAL INFORMATION

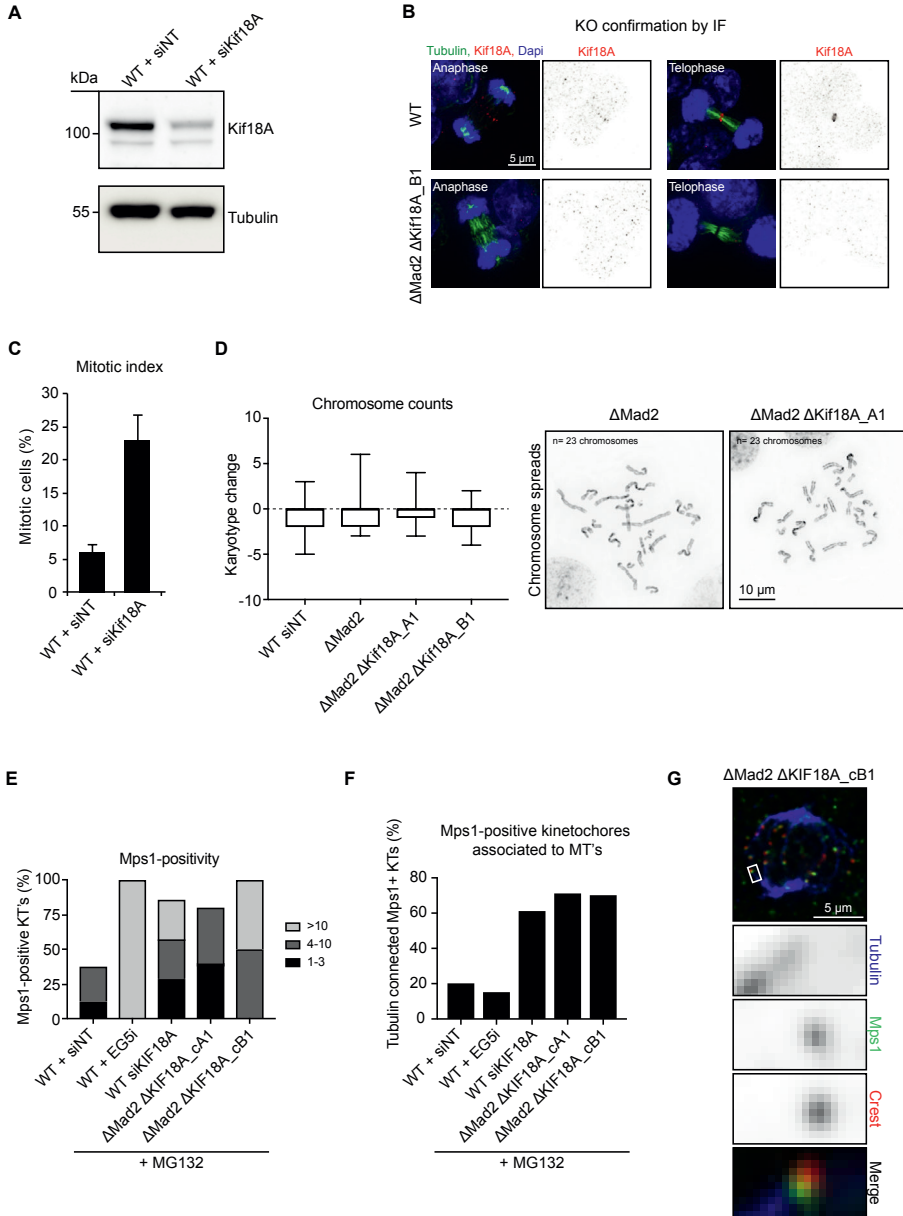


Figure S1: Validation of Δ Mad2 Δ Kif18A HAP1 cells. Related to Figures 1, 2 and 5.

(A) Western blot analysis of WT HAP1 cells treated with siNT or siKif18A for 48 hours. Cell lysates were immunoblotted for Kif18A and α -Tubulin. **(B)** Confirmation of knockout generation by immunofluorescent staining for Tubulin, Kif18A and DNA. **(C)** Mitotic index of Kif18A depleted HAP1 cells as determined by the number of pH3(Ser10)-positive cells over the total number of cells as determined by DAPI. An Image J macro was used to determine the mitotic index. **(D)** Plot showing the change in chromosome number from euploid chromosome number. An unpaired Student's t-test showed no significant difference between any of the displayed samples (n=15 chromosome spreads per condition, in an n=1 experiment). **(E)** Quantification of immunofluorescent staining of Mps1 at kinetochores in WT HAP1 cells treated with siNT (48 hours), Eg5-inhibitor STLC (10 μ M, 4 hours), siKif18A (48 hours) and Δ Mad2 Δ Kif18A_A1/B1 cells. All conditions were pre-treated for 30 minutes with MGI32 followed by 1 hour of MGI32 combined with 100nM of the Mps1 inhibitor Cpd-5 before fixation to arrest cells in metaphase. Data is shown of 1 independent experiment, n= 5 cells and minimally 30 kinetochores per condition. **(F)** Quantification of the amount of k-Mt attachments in Mps1-positive kinetochores (E) of WT HAP1 cells treated with Eg5-inhibitor STLC (10 μ M, 4 hours), siKif18A (48 hours) and Δ Mad2 Δ Kif18A_A1/B1 cells. All conditions were pre-treated for 30 minutes with MGI32 followed by 1 hour of MGI32 combined with 100nM of the Mps1 inhibitor Cpd-5, after which cells were calcium-treated and fixed before staining the cells for microtubules (α -tubulin), SAC-activity (Mps1) and centromeres (Crest). Data presented from 1 independent experiment, n= 5 cells and minimally 30 kinetochores per condition. **(G)** Representative immunofluorescent images of a Δ Mad2 Δ Kif18A_B1 cell, stained for Tubulin, Mps1 and Crest.

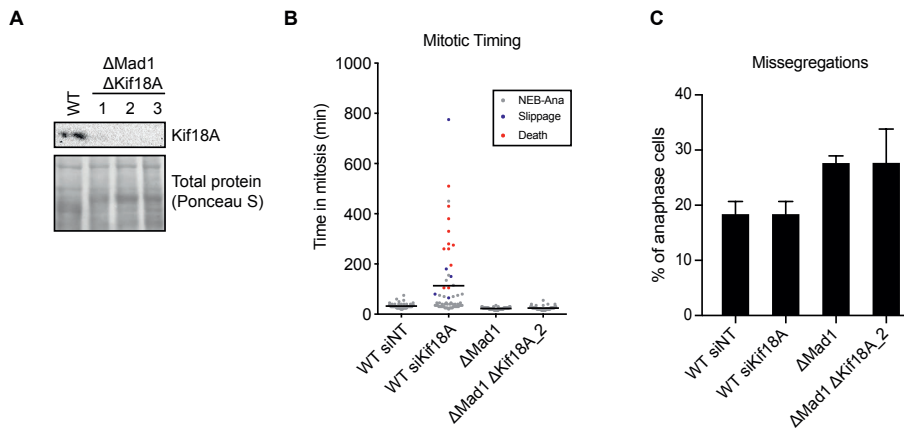


Figure S2: Δ Mad1 Δ Kif18A cells behave similar to Δ Mad2 Δ Kif18A cells. Related to Figure 2.

(A) Western blot analysis of WT HAPI cells and Δ Mad1 Δ Kif18A cells. Cell lysates were immunoblotted for Kif18A. Ponceau S staining served as a loading control. **(B)** Mitotic timing and cell fate of individual cells followed by live-cell-imaging of 2 independent experiments ($n \approx 60$ cells per condition). Each dot represents an individual cell. Cell fate was determined by either anaphase progression (NEB-Ana), start of NEB followed by interphase without anaphase (slippage), or DNA condensation and fragmentation (cell death). Bars represent average time spent in mitosis. **(C)** Quantification of chromosome segregation errors in WT HAPI cells treated with siNT or siKif18A for 48 hours, Δ Mad1 and Δ Mad1 Δ Kif18A_2. Segregation errors were scored during live-cell-imaging and consist of anaphase bridges and lagging chromosomes. Error bars represent standard deviation from 2 independent experiments ($n \approx 60$ per condition).

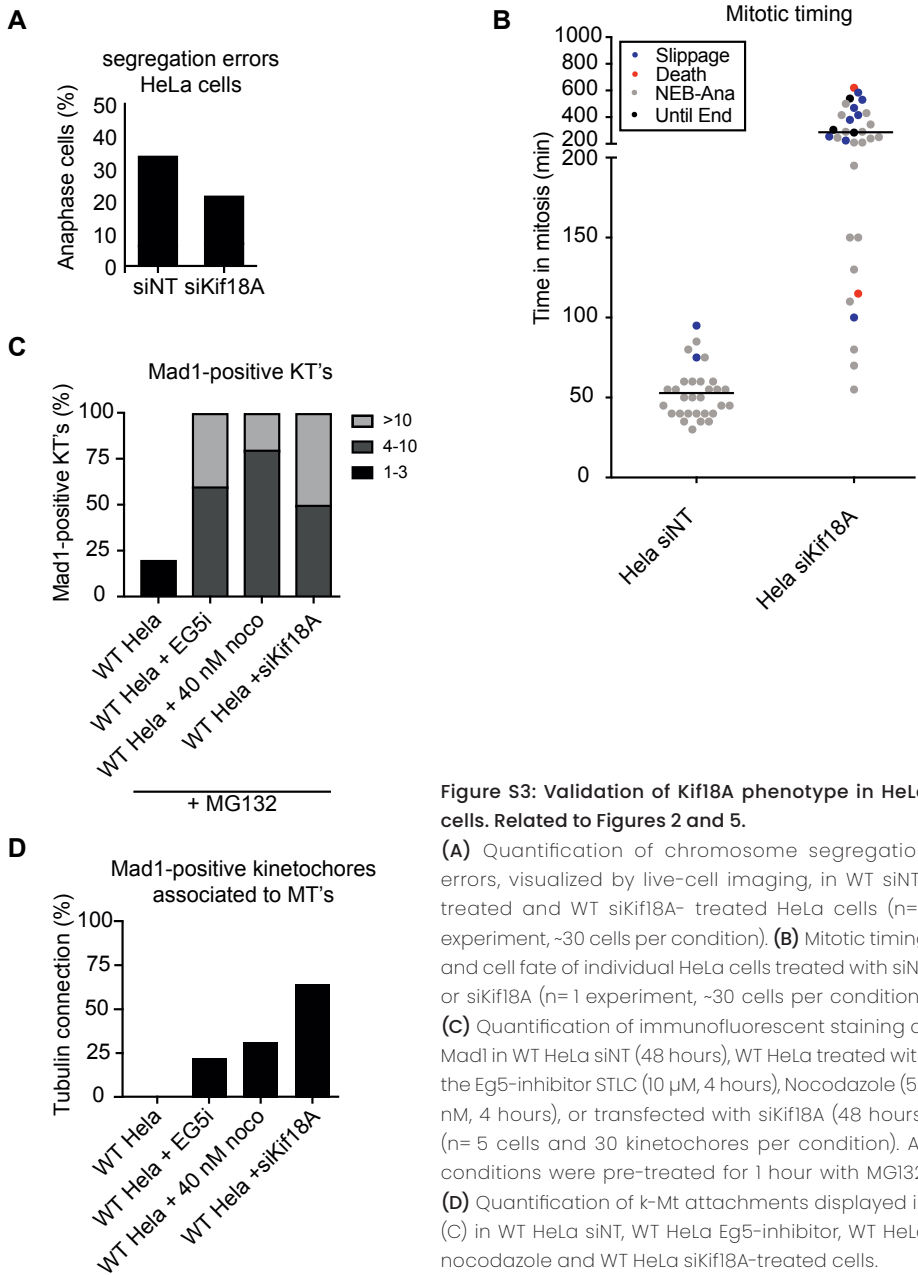


Figure S3: Validation of Kif18A phenotype in HeLa cells. Related to Figures 2 and 5.

(A) Quantification of chromosome segregation errors, visualized by live-cell imaging, in WT siNT-treated and WT siKif18A-treated HeLa cells ($n=1$ experiment, ~ 30 cells per condition). (B) Mitotic timing and cell fate of individual HeLa cells treated with siNT or siKif18A ($n=1$ experiment, ~ 30 cells per condition). (C) Quantification of immunofluorescent staining of Mad1 in WT HeLa siNT (48 hours), WT HeLa treated with the Eg5-inhibitor STLC ($10 \mu\text{M}$, 4 hours), Nocodazole (50 nM , 4 hours), or transfected with siKif18A (48 hours) ($n=5$ cells and 30 kinetochores per condition). All conditions were pre-treated for 1 hour with MG132. (D) Quantification of k-Mt attachments displayed in (C) in WT HeLa siNT, WT HeLa Eg5-inhibitor, WT HeLa nocodazole and WT HeLa siKif18A-treated cells.

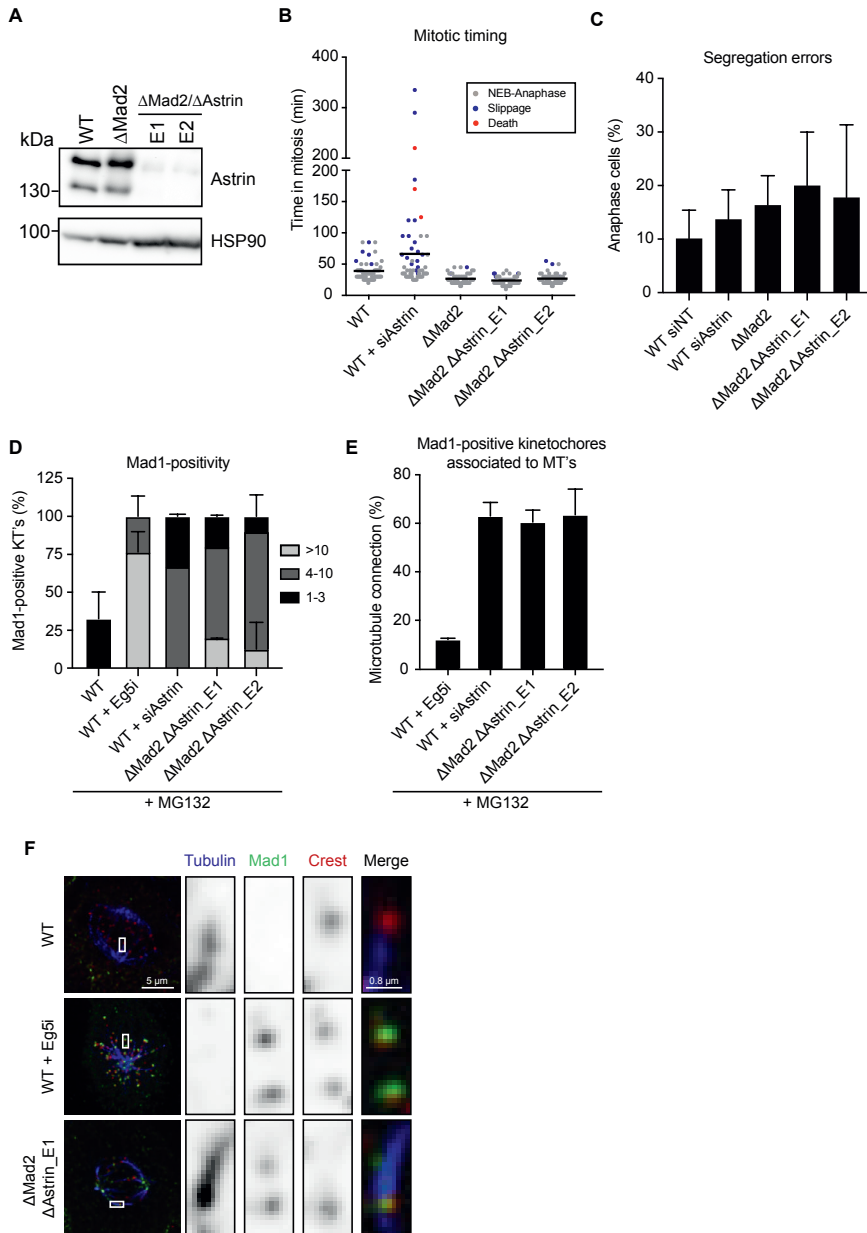


Figure S4: Depletion of Astrin leads to a prolonged mitotic arrest and checkpoint-activity at microtubule attached kinetochores, Related to Figures 1, 2 and 5.

(A) Western blot analysis confirmed the successful generation of Astrin and Mad2 double knockouts (Δ Mad2 Δ Astrin) in HAP1 cells. Cell lysates were immunoblotted for Astrin, and HSP90. The faint upper band of the Δ Mad2 Δ AstrinE1/E2 cells was unaffected by siAstrin treatment (data not shown). **(B)** Mitotic timing and cell fate of individual cells followed by live-cell- imaging of 2 independent experiments (n= \sim 60 cells per condition). Each dot represents an individual cell. Cell fate was determined by either anaphase progression (NEB-Ana), start of NEB followed by interphase without anaphase (slippage), or DNA condensation and fragmentation (cell death). Bars represent average time spent in mitosis. **(C)** Quantification of chromosome segregation errors in WT HAP1 cells treated with siNT or siAstrin for 48 hours, Δ Mad2 and two different Δ Mad2 Δ Astrin clones; E1 and E2. Segregation errors were scored during live-cell-imaging and consist of anaphase bridges and lagging chromosomes. Error bars represent standard deviation from 2 independent experiments (n= \sim 60 per condition). An unpaired Student's t-test showed no significant difference between WT HAP1 cells and WT HAP1 cells treated with siAstrin, nor a difference between Δ Mad2 and the Δ Mad2 Δ Astrin clones E1/E2. **(D)** Quantification of immunofluorescent staining of Mad1 at kinetochores in WT HAP1 cells treated with siNT (48 hours), Eg5-inhibitor STLC (10 μ M, 4 hours), siAstrin (48 hours) and Δ Mad2 Δ Astrin_E1/E2 cells. All conditions were pre-treated for 1 hour with MG132 before fixation. Error bars represent standard deviation of 2 independent experiments (n= \sim 10 cells per condition). **(E)** Quantification of the amount of k-Mt attachments in Mad1-positive kinetochores of WT HAP1 cells treated with Eg5-inhibitor STLC (10 μ M, 4 hours), siAstrin (48 hours) and Δ Mad2 Δ Astrin_E1/E2 cells. All conditions were pre-treated with MG132 for 1 hour, after which cells were calcium-treated and fixed before staining the cells for microtubules (α -tubulin), SAC-activity (Mad1) and centromeres (Crest). Error bars represent standard deviation of 2 independent experiments (n= 10 cells and 50 kinetochores per condition). **(F)** Representative immunofluorescent images of WT HAP1, WT HAP1 cells treated with Eg5-inhibitor and Δ Mad2 Δ Astrin_E1 cells, stained for Tubulin, Mad1 and Crest.



A haploid genetic
screen in human cells to
identify regulators of the
replication stress response



Louise M.E. Janssen, Empar Baltasar Perez, Matthijs Raaben, Elmar Stickel, Thijn R. Brummelkamp, René H. Medema, Jonne A. Raaijmakers

ABSTRACT

Many cancer cells show signs of replication stress, resulting in genomic instability. As a consequence, genomic diversification promotes tumor evolution, enhances adaptation of cancer cells, and aids in therapy resistance. However, besides promoting tumor progression, replication stress can also be a targetable cancer-specific vulnerability. In order to identify the vulnerabilities of cancer cells that experience replication stress, we performed a genetic screen to find (novel) genes that play a role in the replication stress response. Using HAP1 cells under the selective pressure of replication stress-inducing drugs, we identified several genes that seem to have no major effect on the proliferation of normal HAP1 cells, but only hamper cell survival when cells encounter replication stress. In addition to well-known players in DNA repair and the replication stress response, such as *RNASEH1*, *BRIP1*, and *MDC1*, we also found a large group of genes required for mitochondrial processes. Moreover, we found several genes with no prior described role in DNA replication/repair. Taken together, these data allow for the identification of several novel factors and pathways that are essential for cells experiencing replication stress. Further exploration of these factors is warranted to help us better understand this type of cancer-specific vulnerabilities.

INTRODUCTION

Proper DNA replication is a vital process for cell division, since the faithful duplication of the genome is a key step to ensure cell survival and to prevent malignant transformation. Therefore, it is not surprising that replication is a highly regulated process. Normally, DNA is replicated during S-phase, where licensed origins are fired. Upon origin firing, the Mcm2-7 replicative helicase unwinds the double-stranded DNA¹⁹, creating a replication fork, and leaving behind single-stranded DNA (ssDNA) that serves as a substrate for DNA polymerases. DNA synthesis is initiated on both ssDNA strands by DNA polymerase α , which provides RNA-DNA primers for DNA replication through its primase¹⁹². Thereafter, polymerase ϵ and polymerase δ continue DNA synthesis by incorporating free deoxynucleoside triphosphates (dNTPs) in the leading and lagging strand, respectively^{22,192}. Upon completion of replication, cells enter G2 and prepare for cell division in mitosis.

While replication is an orchestrated process, endogenous sources (such as limited dNTP supply, fragile sites, DNA damage) and exogenous sources (DNA damaging agents) can cause slowing down or stalling of the replication fork²⁵. This feature is also referred to as replication stress (RS)²⁵. Fork delay creates longer stretches of ssDNA, which can be bound by replication protein A (RPA)^{25,193}. Upon binding to ssDNA, RPA promotes the activation of the replication stress response via activation of ATR, which results in delayed S-phase progression, thereby providing time to resolve the stress^{25,26,194}.

However, in some cases the stress cannot be resolved (e.g. an unrepaired DNA lesion). In those cases, fork stalling can be overcome by firing dormant origins, enabling S-phase progression^{195,196}. While dormant origin firing can allow the replication machinery to bypass a DNA lesion, it also creates a ssDNA gap that needs to be dealt with^{25,193}. If ssDNA stretches persist and are not resolved properly before mitotic onset, they can give rise to chromosomal instability (CIN) through ultra-fine bridges (UFBs) and chromatin bridges^{39,40,52,197}. In order to prevent this type of genomic instability, the cell utilizes DNA damage tolerance (DDT) mechanisms such as translesion synthesis (TLS) or template switching (TS)¹⁹⁸ in order to replicate across the DNA lesion. However, DDT mechanisms can be error-prone, thereby also posing a threat to genomic stability. On the other hand, without replication progression, prolonged stalled forks will eventually collapse, creating another risk of genomic instability through the formation of single-strand and double-strand breaks (DSB)^{25,32}. Upon prolonged RS and the accompanying ss/dsDNA lesions, cells rely on the DNA damage response (DDR) to repair DNA lesions and resolve

UFBs^{25,40,199}. Altogether, there is a tight connection between the RS response and genomic instability; tolerating RS can prevent genomic instability through preventing fork collapse, but tolerating all RS will also threaten the stability of the genome by formation of UFBs and DNA lesions. This, together with the fact that replication fidelity is under constant threat of endogenous and exogenous sources, underlines the importance of tightly controlled S-phase progression by a tightly coordinated response to replication stress and DNA damage.

As stated above, RS can be a major cause of genomic instability and thereby threatens normal cell viability. Interestingly, oncogene activation in precancerous lesions is a known driver of replication stress^{25,56,59,200}. Amplified oncogenes such as *MYC* or *CCNE1* cause loss of cell cycle control, accompanied by replication stress-induced DNA damage²⁰⁰. This DNA damage creates selective pressure for loss of *TP53*, because persistent activation of the DDR would eventually lead to apoptosis through *TP53*^{200,201}. These findings link RS to the early stages of cancer formation. On top of that, cancer cells continue to display RS, a feature that is thought to promote cancer progression and tumor heterogeneity^{39,202,203}. The fact that RS is a cancer cell-specific hallmark creates a window of opportunity to find cancer-specific vulnerabilities²⁰⁴⁻²⁰⁶. Here, we aimed to identify these cancer-specific vulnerabilities using a genetic screen carried out in the presence of RS-inducing drugs. Using this unbiased approach, we found a large group of mitochondrial-related genes, with no known function in DNA replication or repair. In addition, we also found several genes with no established role in the replication stress response or in DNA damage repair, amongst which *HNRNPA2B1* and *GIGYF2*, to be specifically required in cells suffering from RS.

RESULTS

Induction of replication stress in human haploid cells

For our screens, we targeted two different enzymes to induce replication stress; either through selective inhibition of DNA polymerase- α activity using Aphidicolin (Aph)²⁰⁷, or via inhibition of ribonucleotide reductase by hydroxyurea (HU)²⁰⁸, thereby reducing the cellular dNTP pool. Both of these methods were shown to inhibit the replication machinery and result in delayed replication fork progression. To test their effect on cell viability, we performed growth assays in which we treated wild-type (WT) HAP1 cells with increasing doses of either Aph or HU (Fig. 1A) and calculated an IC₅₀ of 66 nM for Aph, and an IC₅₀ of 140 μ M for HU (Fig. 1B).

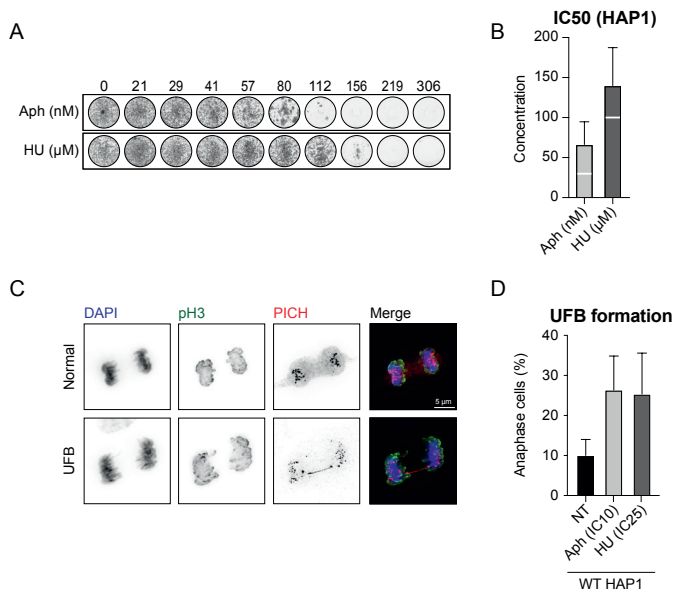


Figure 1: Induction of replication stress in HAP1 cells

(A) Representative growth assay of HAP1 cells subjected to increasing doses of Aph or HU for 5 days. **(B)** Average IC50 of 5 independent growth assays (IC50 for Aph 66 nM, for HU 140 μM). White line represents IC10 (Aph) or IC25 (HU). **(C)** Representative images of immunofluorescent staining of PICH fibers in anaphase HAP1 cells. **(D)** Quantification of PICH fibers in anaphase HAP1 cells treated with 27.5 nM Aph (IC10) or 100 μM HU (IC25) for 48 hours. Average of 4 independent experiments, mean + SD, differences just below significance.

Despite the fact that cells have sensing mechanisms for RS which induce a checkpoint response to halt cell cycle progression and ensure genomic stability^{28,209–213}, mild RS is shown to sometimes be tolerated²¹⁴. This causes cells to progress into mitosis with under-replicated DNA which can create genomically unstable structures like UFBs, ultimately leading to DNA damage^{39,40,52,197}. Since we were interested in inducing genomic instability through RS for multiple days, we aimed to find a drug concentration where cells experience mild RS, and show signs of RS-induced genomic instability, but proliferation was minimally affected. For this, we measured the occurrence of PICH fibers, a readout of UFBs^{40,215}, by immunofluorescence (Fig. 1C). Untreated WT HAP1 cells showed a baseline level of 10% anaphase cells with UFB's (Fig. 1D). When treating HAP1 cells with low doses of Aph or HU (using the IC10 of 27.5 nM, or the IC25 of 100 mM respectively) we were able to raise the percentage of the anaphase cells with UFBs to ~25% (Fig. 1D), yet cells were still able to proliferate over multiple days (Fig. 1A).

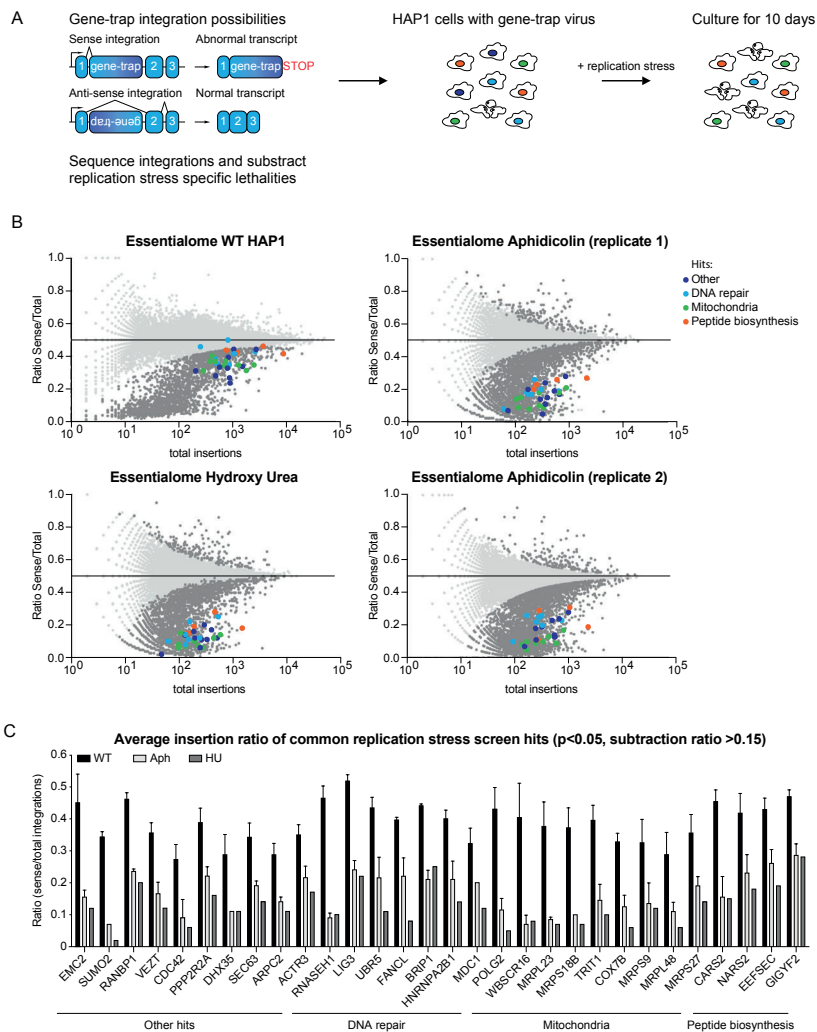


Figure 2: Identification of genes needed for survival upon replication stress using a haploid synthetic lethality screen.

(A) Schematic representation of screen set-up, and gene-trap virus integration possibilities. Sense integration will give rise to an abnormal transcript, equivalent to knock-out of the gene. Anti-sense integration will not disrupt gene transcription. By sequencing the ratio of sense and anti-sense genes, essential genes can be identified as having a bias towards anti-sense integrations. (B) Fishtail plots of gene-trap insertions in WT HAP1 cells, and HAP1 cells treated with low doses of either Aph or HU. Each dot in the plot represents a single gene, and the number of integrations per gene is plotted on the x axis. On the y axis, the relative amount of sense integrations over the total amount of integrations (sense+antisense) is plotted. The synthetic lethal hits are highlighted in color. (C) Graph of the average ratio of sense/total integrations in WT, and replication stressed HAP1 cells. The data are extracted from 4 individual WT, and the average of all replication stress induced insertional mutagenesis screens. Graph contains the top 30 hitlist, with $p < 0.05$, and a subtraction ratio (ratio WT – ratio replication stress) > 0.15 . Error bars represent SD of the 3 independent screens.

A synthetic lethality screen identifies genes required for survival during replication stress

Using Aph and HU to induce RS-dependent genomic instability, we set out to discover what genes are important for cell viability in cells that experience RS. We aimed to identify these genes by performing comparative genetic screens in HAP1 cells, grown with or without Aph or HU (Fig. 2A). These screens used genome-wide insertional mutagenesis of a gene-trap in near-haploid HAP1 cells¹⁶¹. The gene-trap was shown randomly insert into the genome, in either a sense (thereby inactivating the gene, equivalent to a knock-out of that gene due to the near haploid nature of this cell line) or antisense orientation (leaving gene expression intact)^{161,216} (Fig 2A, left part). Thus, cells with a sense integration in a gene that is essential for cell viability should drop out of the population. By comparing the sense/total integration ratio for each gene in untreated WT HAP1 cells (Fig. 2B, upper left panel) with the sense/total integration ratio in HAP1 cells treated continuously with Aph or HU for 10 days (Fig. 2B, other panels), we identified specific synthetic lethal interactions for cells enduring replication stress (Fig. 2C) (see **methods** for more details). Using this strategy, we expected to identify genes that have a potential role in the RS-response, the DNA damage response (DDR), and chromosomal instability^{38,201}. Indeed, we identified multiple genes previously shown to be involved in the RS-response/DNA damage repair, such as *RNASEH1*^{217,218}, *LIG3*^{219–221}, *UBR5*^{222–224}, *FANCL*^{225–227}, *BRIPI*^{227,228}, and *MDCT229* (Fig. 2B/C), indicating our screen setup was capable of picking up specific vulnerabilities of replication-stressed cells.

Loss of mitochondrial genes makes cells vulnerable to replication stress

Besides genes with a well-known role in DNA repair or replication, we also identified genes for which no function in the replication stress response has been described thus far (Fig. 2B/C). Interestingly, 30% of the top 30 hits were related to mitochondrial processes (Fig. 2C). This could indicate a relationship between mitochondrial functioning and the RS-response. Mitochondria are key regulators of cellular metabolism, their most prominent role being the production of ATP through oxidative phosphorylation (OXPHOS)²³⁰. Previously it has been proposed that energy adaptation through mitochondria is key under conditions of cellular stress^{231,232}. If cells that experience RS rely on mitochondrial genes, it suggests that the mitochondria normally create an environment that helps cells to deal with RS, or helps to reduce the overall level of RS. To first confirm the synthetic lethal interaction between mitochondrial genes and RS in our screens, we selected 2 of the mitochondrial-associated hits for knock-out generation. These 2 hits, *POLG2* and *MRPL23*, were selected because they carry out different functions within the mitochondrion and

were amongst the most prominent mitochondrial hits. We aimed to generate knock-outs by targeting CRISPR-Cas9 to the first exon of our gene of interest, followed by the insertion of a blasticidin resistance cassette at the broken DNA (Fig. 3A). Unfortunately, based on blasticidin resistance and PCR, successful knock-out generation could not be confirmed. Therefore, we turned to siRNA-mediated depletion of POLG2 and MRPL23 instead. Effective knock-down (~85%) of POLG2 and MRPL23 expression was confirmed by qRT-PCR (Fig. 3B). However, siMRPL23- and siPOLG2-treated cells did not show increased sensitivity to Aph or HU in growth assays, when compared to WT HAP1 cells (Fig. 3C/D), possibly due to residual POLG2 and MRPL23 expression.

Since knockouts of POLG2 and MRPL23 were difficult to obtain, we attempted to validate the mitochondrial hits in a different way. To this end, we set out to test functional mitochondrial dependency using oligomycin A, a drug that inhibits OXPHOS by blocking ATP synthase²³³. WT HAP1 cells were subjected to a growth assay in the presence of either Aph or HU alone, or in combination with oligomycin A. These results showed that oligomycin A treatment did not further sensitize cells to Aph or HU (Fig. 3E). This indicated that decreased OXPHOS was not the underlying cause of the observed enrichment of mitochondrial hits in our RS-screen. Thus, using growth assays we were not able to validate the mitochondrial dependency found in the RS-screens, not even when acutely inhibiting mitochondrial function.

Even though we were unable to validate the synthetic lethal interaction between loss of mitochondrial genes and RS observed in our screens, the prominent enrichment of mitochondrial hits prompted us to test other possibilities that could explain the observed interaction. An alternative explanation for the mitochondrial dependency in conditions of high RS could be that treatment with Aph or HU causes an increased energy demand in the cell^{231,232}. For example, the extra origin firing or the repair of lesions caused by RS could result in higher energy consumption rates. If so, losing mitochondrial genes could be detrimental as the energy demand caused by RS can no longer be met. To test this hypothesis, we set out to measure mitochondrial respiration using the mitochondrial stress test (Seahorse XFe analyzer²³⁴) (Fig. 3F). As a control for the sensitivity of this assay, siRNA-mediated depletion of succinate dehydrogenase complex, subunit A (SDHA) was used, since this is an essential component of complex II in the mitochondrial respiratory chain²³⁵. Using the Seahorse assay, we found that untreated (NT), Aph-treated, HU-treated or SDHA-depleted HAP1 cells displayed a similar oxygen consumption rate (OCR, a readout for glucose metabolism through OXPHOS) at baseline (Fig. 3F). The

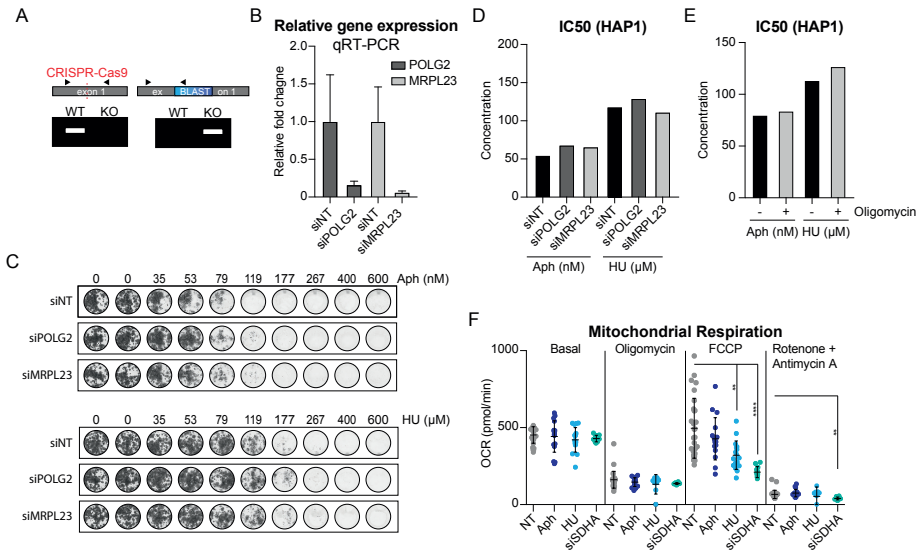


Figure 3: Mitochondrial reserve capacity might be important during replication stress.

(A) Schematic overview of the strategy to generate HAP1 knock-outs using CRISPR-Cas9 and blasticidin cassette integration (causing a frame shift). Knock-outs were first selected using blasticidin treatment, and confirmed by PCR. (B) Relative gene expression of *POLG2* and *MRPL23* in WT HAP1 cells, after siRNA mediated depletion (relative to non-targeting siRNA (siNT) control, normalized to GAPDH expression). Expression was measured by qRT-PCR, error bars represent standard deviation of three biological replicates from 1 experiment. (C) Growth assays of WT HAP1 and *POLG2* or *MRPL23* depleted cells, subjected to increasing doses of Aph or HU for 5 days. (D) IC50 of the growth assay displayed in (C), n=1. (E) Bar graph displaying the IC50 of a growth assay of HAP1 cells treated with Aph or HU, either alone or in combination with 2.5 μ M oligomycin A, n=1 (F) Oxygen consumption rate (OCR) of WT untreated, Aph (27.5 nM, 2 hours), HU (100 μ M, 2 hours) or siSDHA (3 days) treated HAP1 cells during different phases of the mitochondrial stress test. Dots represent individual wells, of multiple independent experiments (4 independent experiments for WT, 2 independent experiments for Aph and HU treated, and 1 independent experiment of siSDHA treated cells). Mean + SD, ** p<0.0025, **** p<0.0001 (unpaired students t-test).

only observed difference between the conditions was found after carbonyl cyanide 4-(trifluoromethoxy)-phenylhydrazone (FCCP) addition (Fig. 3F). FCCP causes a continuous electron flow through the respiratory chain, providing a read-out for the maximal OCR of cells²³⁶. The difference between the basal OCR and the maximum OCR observed after FCCP addition is the reserve respiratory capacity (RRC)²³⁶. In NT conditions, FCCP treatment resulted in a slightly positive RCC (Fig. 3F, compare NT basal OCR to NT FCCP OCR). This indicated that WT HAP1 cells have limited RRC. Previously, depletion of several SDH complex members has been shown to reduce the RRC of mitochondria^{232,235}. Indeed, depletion of SDHA, decreased the RRC dramatically (Fig. 3F) compared to NT conditions. Moreover, the OCR during FCCP addition was even lower than the basal OCR of siSDHA treated

cells, resulting in a negative RRC. Interestingly, HU treatment resulted in a decreased RRC compared to WT HAP1 cells. Like siSDHA treated cells, the RRC of HU-treated cells seemed negative, albeit this decrease was not as drastic as observed after SDHA depletion (Fig. 3F). These results suggest that RS can decrease the RRC of mitochondria. This decreased RRC could potentially be the explanation of the increased dependency on mitochondrial genes in our screens. For example, because cells under RS might need more energy to cope with RS.

Altogether, our screen data suggest that there is a possible role for mitochondrial genes in the coping with RS. However, validation of this interaction remained challenging. Thus, the exact contribution of mitochondria in the RS-response remains to be elucidated. Since knock-out generation of mitochondrial genes was unsuccessful, and there was no increased sensitivity of the oligomycin A-treated cells to RS, we decided to focus our attention on the hits with no apparent relation to mitochondrial function identified in the screen.

Loss of hnrnpa2b1 and gigyf2 show increased sensitivity to DNA-damage inducing agents

After excluding the mitochondria-related hits (depicted in Fig. 2C), we set out to validate the residual hits by generating knock-out cells as described in Fig. 3A. Some of the hits have already been implicated in the DNA damage repair (*RNASEH1*, *LIG3*, *UBR5*, *FANCL*, *BRIPI*, and *MDC1*). The RS-response makes use of DDR factors, like ATR and RPA²⁵. Additionally, during RS, the DDR is needed when DNA lesions occur²⁵. Interestingly, all our remaining hits were also found in a genetic screen of irradiated HAP1 cells (Feringa et al. unpublished). This suggested that our RS-screen led to the identification of common regulators of the DDR, and indicated that an impaired DDR is a common vulnerability for cells experiencing RS.

Successful knockout clones were confirmed by PCR for *RNASEH1*, *HNRNPA2B1*, *VEZT*, *GIGYF2*, *RANBP1*, *CDC42*, and *SEC63*. *RNASEH1* already has a proposed role in the RS-response, through the resolution of R-loops^{218,237,238}. These R-loops can be formed upon replication-transcription conflicts, and can cause DNA DSBs^{217,239}. Even though following up on *RNASEH1* might not yield novel insights in the RS-response, we took *RNASEH1* knock-outs along as a positive control. We subjected knock-outs to growth assays in the presence of Aph or HU, to determine their sensitivity to RS by calculating their IC50s (Fig. 4A). Indeed, the Δ *RNASEH1* cells were more sensitive to Aph and HU compared to WT HAP1 cells (Fig. 4A). Similarly, the *HNRNPA2B1*, *VEZT*, *GIGYF2*, *RANBP1*, *CDC42*, and *SEC63* knock-outs were also more sensitive to Aph and HU treatment, as evidenced by the decrease in IC50 compared to WT cells (Fig. 4A).

Prior work found heterogeneous nuclear ribonucleoproteins (hnRNPA/B family) to associate with nascent pre-mRNAs in order to control several RNA-related processes²⁴⁰. Moreover, hnRNPA2B1 was reported to play a role in RPA displacement at telomeres²⁴¹. Since our RS-screen probably yielded factors involved in DDR regulation, we were eager to test if loss of hnRNPA2B1 negatively affects the RS-response by changes in RPA displacement. We hypothesized that loss of hnRNPA2B1 could lead to an inability to release RPA, not only at telomeres but also in the context of RS. Changes in RPA dynamics could hamper the protection or further processing of ssDNA formed during RS, eventually leading to DSB formation. First, we further confirmed knock-out generation of hnRNPA2B1 by western blot (Fig. 4B). Subsequently, to test if Δ hnRNPA2B1 cells show hampered RPA dynamics, we measured phosphorylated serine 4/8 (ser4/8) RPA (pRPA) and γ H2AX levels by western-blot (Fig. 4C). The rationale being that if loss of hnRNPA2B1 influences RPA displacement, the RPA bound to ssDNA during replication should become hyperphosphorylated^{194,242}. This could lead to excessive activation of the downstream RS-response, through activation of ATR^{194,243}. Interestingly, Δ hnRNPA2B1 cells showed a baseline increase in phosphorylated RPA (pRPA) when compared to WT HAPI cells (Fig. 4C). However, although HU treatment did induce pRPA levels in WT HAPI cells, the pRPA levels were not exacerbated in Δ hnRNPA2B1 cells in response to RS. Importantly, we found an increase in γ H2AX (a marker for DSBs¹²⁶) after HU treatment, which was more prominent in Δ hnRNPA2B1 cells than WT HAPI cells. These findings indicate that Δ hnRNPA2B1 cells show signs of RS at baseline, which upon extra RS causes a further increase in DNA-damage. The finding that pRPA levels are not further increased in Δ hnRNPA2B1 cells upon HU treatment, while we did find increased levels of γ H2AX, could be explained by the fact that the nuclear pool of RPA is not infinite. Previously, it has been shown that in cells where nuclear RPA pools are exhausted, newly formed ssDNA is no longer coated by RPA²⁴⁴. Additionally, this increased the risk of fork collapse and breakage²⁴⁴. Therefore, we hypothesize that the compromised RPA turnover after loss of hnRNPA2B1 limits the availability of free RPA. During normal replication this is not problematic, and Δ hnRNPA2B1 cells progress through S-phase. However, upon RS, longer stretches of ssDNA or an increase in origin firing causes a higher demand for RPA, which in Δ hnRNPA2B1 cells cannot be met. Similar to what Toledo²⁴⁴ and colleagues showed, this RPA exhaustion can cause the observed increase in γ H2AX because replication forks can no longer be stabilized, thereby increasing the chance of fork collapse. We propose that the increased DSB in Δ hnRNPA2B1 cells enduring replication stress are the cause of the observed synthetic lethal interaction found in our RS-screen.

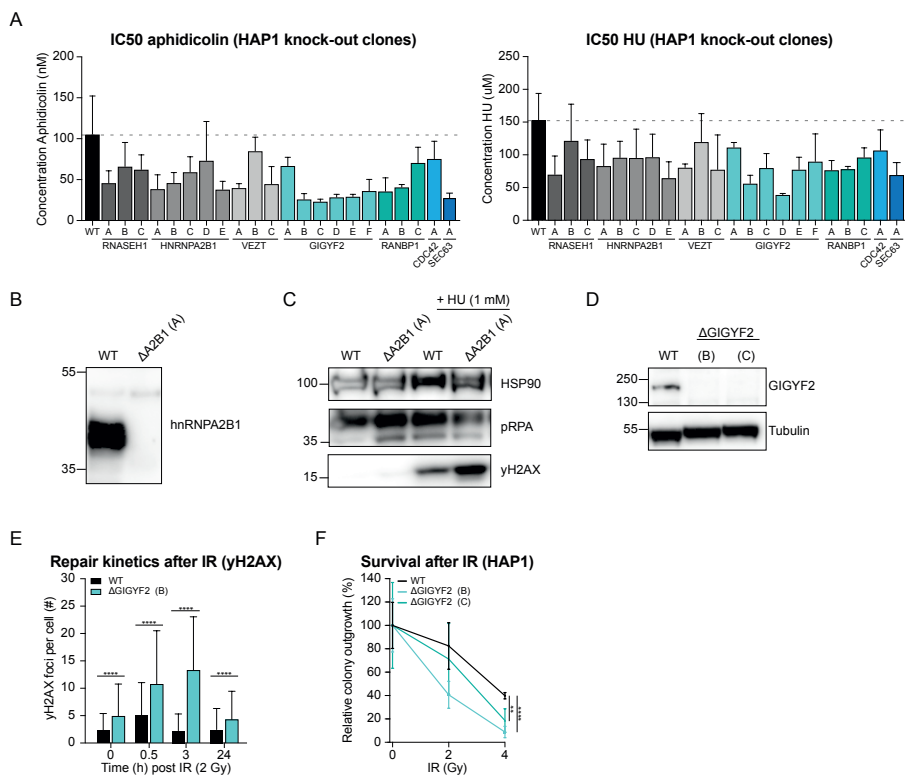


Figure 4: Loss of hnRNPA2B1 or GIGYF2 makes cells more vulnerable to replication stress.

(A) Average IC₅₀ of 2-8 independent growth assays for WT HAP cells and different knock-out clones. (B) Western blot confirming knock-out of hnRNPA2B1. (C) Western blot of pRPA (ser4/8) and yH2AX in WT and Δ hnRNPA2B1 HAP1 cells, with or without 3 hours of 1 mM HU treatment. HSP90 serves as a loading control. (D) Western blot confirming knock-out of GIGYF2 for two independent clones. (E) Number of yH2AX foci in asynchronous WT and Δ GIGYF2 HAP1 cells at indicated time points after IR, average of minimally 200 cells per condition, of 1 independent experiment. Mean + SD, **** $p < 0.0001$ (unpaired students t-test). (F) Relative outgrowth capacity of WT and Δ GIGYF2 HAP1 cells after increasing doses of IR, average of 4 independent experiments. Mean + SD, ** $p < 0.01$, **** $p < 0.0001$ (unpaired students t-test).

GIGYF2 knock-outs showed the highest sensitivity to Aph and HU. Therefore, we next aimed to understand the role of GIGYF2, a key component of the 4EHP-GYF2 multiprotein complex involved in repression of the initiation of translation²⁴⁵, in further detail. Knock-out generation of GIGYF2 was confirmed by western-blot (Fig. 4D). Unlike hnRNPA2B1, we had no clear hypothesis for the role of GIGYF2 in the RS-response. Because we found evidence our RS-screen yielded hits related to DDR function, we decided to test if Δ GIGYF2 cells show defects in DNA damage repair. First, we studied the repair kinetics of WT HAP1 and Δ GIGYF2 cells through measuring the amount of yH2AX foci at several time-points

after irradiation (IR) (Fig. 4E). Besides a baseline increase in the level of γ H2AX in Δ GIGYF2 cells compared to WT HAP1 cells (Fig. 4E, t=0), we also observed a repair delay (Fig. 4E, t=3), suggesting that GIGY2 might be a general repair factor. Moreover, we found that Δ GIGYF2 cells showed increased sensitivity to IR compared to WT HAP1 cells (Fig. 4F). These results indicate that GIGYF2 normally aids in reducing genomic instability, possibly through a yet to be defined role in DNA damage repair.

DISCUSSION

Replication stress is a severe threat to genomic stability, and highly evident in (pre-) cancerous lesions^{25,200}. Luckily, cells have evolved mechanisms to deal with RS, and use DNA repair pathways to resolve issues that originate from prolonged fork stalling^{25,26,194}. Since RS seems to be a cancer cell-specific feature, targeting the RS-response has been of therapeutic interest (reviewed by Ubhi et al.²⁰⁴ and Zhang et al.²⁰⁵). For example, it has been shown that therapies that induce DNA damage through radiation or chemotherapy^{205,246,247} enhance RS. This could push cancer cells over their tolerance limit for genomic instability (GIN), and could (partially) explain why such therapies work in the clinic. Using a different approach, recent studies have aimed to target the RS response itself, for example, by suppression of the ATR-induced checkpoint^{248,249}. Inhibition of ATR during RS will lead to cells entering mitosis with under-replicated DNA, eventually leading to cell death through mitotic catastrophe. While these efforts resulted in promising therapeutic approaches, their administration could create RS in normal tissue during treatment, which is a potential risk to form new pre-cancerous lesions. This highlights the need for additional targets, to effectively kill replication-stressed cancer cells. Moreover, conventional single therapy approaches have not eradicated cancer yet. Thus, additional (combination) targets are highly anticipated.

In this work, we set out to discover genes that are specifically essential for cells enduring RS, using a well-established haploid genetic screening approach¹⁶¹. We identified genes whose loss compromises proliferation of cells treated with RS-inducing drugs. While some of these genes have a well described role in the RS-response/DDR, we also discovered a set of mitochondrial genes, as well as a set of genes for which no function in replication/DDR had been described thus far. Of those genes, this work validated that *HNRNPA2B1* and *GIGYF2* are specifically required in cells suffering from RS.

The fact that we identify several genes with described roles in the RS-response/DDR indicates that these genes might be exploitable clinical targets. We showed that RNASEH1 knock-outs are more sensitive to RS-inducing drugs. RNASEH1 has a described role during RS, through the resolution of R-loops^{218,237,238}. Unresolved R-loops can create GIN by replication-transcription conflicts, leading to fork stalling and DSB formation^{217,239}. This might indicate that synthetic lethal interactions in cells enduring RS are the result of increased GIN. Moreover, we find that mutagenesis of Mdc1 and BRIP1 compromises cell viability in cells enduring RS. Besides a direct role in DNA damage repair²⁵⁰⁻²⁵², both Mdc1 and BRIP1 have been described to participate in the replication checkpoint^{229,253}, ultimately leading to ATR-Chk1 activation to enable DNA damage repair and replication restart^{27,229,253}. Interestingly, inhibition of the RS-response using ATR- or Chk1-inhibitors is currently being tested in clinical trials^{64,65}. The idea being that inhibiting ATR/Chk1 in cancer cells experiencing RS, will increase GIN to levels that induce cancer-specific cell killing. However, most pre-clinical studies have focused on combination, instead of mono-, therapies with ATR/Chk1 inhibition⁶⁴, indicating ATR/Chk1 inhibition alone might not be sufficient. We believe our set of DDR-related genes (*MDC1*, *BRIP1*, *FANCL*, *RNASEH1*, *LIG3*, and *UBR5*) yield potential druggable targets. Inhibiting (or depleting) these genes could specifically kill cancer cells enduring RS in a mechanism similar to ATR/Chk1 inhibition, namely by increasing the levels of GIN in cancer cells over the GIN-tolerance limit. It would be interesting to further validate these hits, and test if loss of these genes indeed elevates GIN levels during RS.

Mitochondria are mainly known as the energy factories of cells²³⁰, and the enrichment of mitochondrial genes in our RS-screen made us wonder if the energy state of a cell is important during RS. Unfortunately, knock-out generation of mitochondrial genes turned out to be challenging, thereby complicating validation of these hits. siRNA-mediated depletion of the mitochondrial hits *MRPL23* and *POLG2* showed no increased sensitivity to RS induced by Aph or HU. This was unexpected, because the screen predicted a high dependency on these mitochondrial genes during RS. We cannot exclude the possibility that our failure to validate these hits by siRNA-mediated depletion is a consequence of incomplete/too short knock-down. Although we could not confirm the mitochondrial gene dependency during RS, we did find that RS lowers the RRC of mitochondria. Previously, it has been shown that RS during mitochondrial DNA replication could lead to less total mitochondria²⁵⁴, which could of course lead to a decrease in RRC. Mitochondrial replication relies on import of dNTP's from the cytoplasm²⁵⁵, thus HU treatment could indeed result in RS in mitochondria. However, the mitochondrial polymerase γ is resistant

to Aph^{256,257}. Therefore, we do not believe that the reduction in RRC is a direct cause of RS in mitochondria. The RRC has been proposed to be critically important for cells to cope with stress, as it can help cells to adapt to an increased workload²³⁶. Because RS increases the demand of various cellular processes, cells under RS might already have a higher demand on the RRC. This could explain the decreased RRC that we observed during Aph or HU treatments. Possibly, this could explain the synthetic lethal interaction found in the screen; if RS causes a high energy consumption (and thereby a decrease in RRC), then loss of mitochondrial genes leaves no spare capacity to be called upon during RS. However, we did not find evidence for increased energy consumption in Aph/HU treatment, but did find a reduction in RRC. Moreover, the observed decrease below basal OCR after FCCP treatment is not well described, and therefore our results in this regard might reflect technical problems. Therefore, more precise measurements of mitochondrial respiration, for example by polarography²⁵⁸, should be executed. Nonetheless, even after acute siRNA depletion of mitochondrial genes, the synthetic lethal interaction observed in the screen was not recapitulated. Thus, although our screen results point towards a role for mitochondrial functioning in response to RS, further experiments are needed to truly validate this finding. For this, we propose to perform more experiments using acute depletion of the mitochondrial hits, for example by using an auxin-inducible degron or the CRISPRi system.

We next investigated the role of two genes that were previously not associated to RS, namely *HNRNPA2B1* and *GIGYF2*. We generated multiple knockout clones for both genes, which all displayed increased sensitivity to RS when compared to WT HAP1 cells. Therefore, we can conclude that *HNRNPA2B1* and *GIGYF2* are required for the cellular response to RS. We did not resolve the full mechanism by which these two proteins function in the RS-response, but did perform a few follow up experiments that allow us to speculate.

Besides the RNA-processing functions of hnRNPA2B1²⁴⁰, it has been proposed that hnRNPA2B1 promotes an RPA to POT1 switch at telomeres, thereby preventing DNA-damage checkpoint signaling through ATR²⁴¹. Loss of hnRNPA2B1 upon itself does not cause cells to arrest through RPA and ATR signaling, which is consistent with the fact that we were able to generate viable knock-outs. We found that untreated Δ hnRNPA2B1 cells show increased pRPA levels compared to WT HAP1 cells. We propose that loss of hnRNPA2B1 could limit RPA displacement, thereby leading to RPA retention, either at the telomere or at genomic regions experiencing RS. This persistent RPA retention could lead to ATR recruitment and the observed RPA hyperphosphorylation¹⁹⁴. Moreover, this limited RPA turn-over could

make Δ hnRNPA2B1 cells more prone to exhaust their nuclear RPA pool. Previously, it was shown that RPA exhaustion increases the amount of ssDNA devoid of RPA coating²⁴⁴. Subsequently, the unprotected ssDNA stretches have a high risk of causing replication fork collapse, resulting in DNA damage. Indeed, we found increased γ H2AX levels in Δ hnRNPA2B1 cells that experience RS. Therefore, we hypothesize that when Δ hnRNPA2B1 cells encounter RS, the increased demand of RPA binding to ssDNA structures cannot be met, resulting in increased DNA damage.

Nonetheless, a few observations warrant further investigation. First, ser4/8 hyperphosphorylation of RPA was previously shown to occur primarily in response to DSBs (caused by collapsed replication forks)²⁴². Therefore, it is somewhat surprising that we did not observe increased levels of γ H2AX at baseline in our Δ hnRNPA2B1 cells. This might be due to the detection limit on western-blot. Therefore, it would be interesting to measure γ H2AX levels in a different manner, for example using immunofluorescent analysis of γ H2AX foci. Second, we did not observe a further increase in pRPA levels during RS in Δ hnRNPA2B1 cells. Here, we propose RPA exhaustion could explain why we do not find a further increase in pRPA after HU treatment, as we might have reached maximum levels of RPA-ssDNA engagement in Δ hnRNPA2B1 cells already.

In order to test if limited RPA displacement/turn-over is the actual cause of the observed DNA-damage in Δ hnRNPA2B1 cells enduring RS, we propose to investigate the incidence of fork collapse in Δ hnRNPA2B1 cells treated with RS-inducing drugs using DNA-fiber assays. If our hypothesis is true, we would expect an increase in fork collapse in Δ hnRNPA2B1 cells. Additionally, it would be interesting to visualize if the ssDNA in Δ hnRNPA2B1 cells enduring RS indeed show lower RPA occupancy. Moreover, if expression of excess RPA protein²⁵⁹ complexes would reduce the observed DNA damage in Δ hnRNPA2B1 cells enduring RS, we would have strong evidence the observed defects are caused by defects in RPA turn-over. Alternatively, RS could induce an excessive DDR at telomeres in Δ hnRNPA2B1 cells, since hnRNPA2B1 was previously described to function at the telomere to limit DDR activity. In order to experimentally test if this is the underlying cause for synthetic lethality between hnRNPA2B1 loss and RS, one could look at DDR activity at telomeres by analysis of chromosome-end fusions in mitotic chromosome spreads^{260,261}.

The other hit we followed up, GIGYF2, is involved in repressing the initiation of translation²⁴⁵, but has no prior described role in replication or the DDR. We found that Δ GIGYF2 cells display an increase in DNA damage at baseline, and decreased repair kinetics compared

to WT HAP1 cells. This suggests that GIGYF2 aids in reducing genomic instability during the cell cycle, and probably plays a role in DNA damage repair. Since GIGYF2 has a role in translational repression²⁴⁵, it would be interesting to test if this causes specific protein imbalances that could explain the observed role in the DDR. Further work is needed to identify the exact role of GIGYF2 in preventing DSB formation upon the induction of RS.

Besides the mitochondrial hits, we experienced difficulties generating knock-outs of some of the remaining hits (namely; *EMC2*, *EEFSEC*, *BRIPI*, *DHX35*). This was somewhat unexpected, because the integration ratio of these genes in the WT screens ranges from 0.3 – 0.45. This suggests that deletion of these genes should not interfere much with cell viability in unchallenged conditions. Thus, it is unclear why the generation of knock-outs of these genes was problematic. It is possible that their role in DNA damage repair/tolerance challenges the generation of knock-out clones, that are generated via CRISPR-induced DNA breaks. Additionally, there is a remainder of hits that still await knock-out generation and validation (*SUMO2*, *PPP2R2A*, *ARPC2*, *ACTR3*, *CARS*, *NARS*; for which no roles have been defined in RS thus far).

Altogether, our RS-screens might be a valuable resource to identify RS-specific vulnerabilities. Even though we were not (yet) able to validate all hits, we provide strong evidence that cells under RS depend on a proper DDR. Our results compliment approaches taken in the clinic, which are also guided towards pushing replication-stressed cancer cells over the border of GIN-tolerance by interfering with the DDR through ATR inhibition^{65,248}. Besides known DDR factors, we validate two additional hits in this study, hnRNPA2B1 and GIGYF2, and identify that they have a potential role in the DDR. Future experiments are needed to specify their exact role in the DDR. Moreover, it would be interesting to test the sensitivity of the hnRNPA2B1 and GIGYF2 knock-outs to different DDR targeting drugs. For example, if these knock-outs are more sensitive to PARP inhibition than WT HAP1 cells, it could indicate that these genes play a role in homologous recombination repair (reflecting a similar sensitivity of HR-deficient BRCA mutant tumors to PARP inhibitors^{262–264}). This could aid in finding combination strategies for cancer therapy. Altogether, our data shows that our screen results might contain interesting therapeutic targets which await further validation.

METHODS

Cell culture

Human derived near-haploid HAP1 cells were cultured in IMDM (GIBCO) supplemented with 10% FCS, 1% GlutaMAX supplement (GIBCO), 100 U/ml penicillin, and 100 µg/ml streptomycin. siRNA transfections were performed using RNAiMax (Invitrogen) according to the manufacturer's guidelines. The following siRNAs were used in this study: siNon-Targetable (Dharmacon), siPOLG2 (Horizon, ON-TARGETplus, SMARTPool), siMRPL23 (Horizon, ON-TARGETplus, SMARTPool), siSDHA (Horizon, ON-TARGETplus, SMARTPool). All drugs (Aphidicolin, HU, Oligomycin, FCCP and Rotenone/Antimycin A) were dissolved in DMSO and used at indicated concentrations.

Growth assays

HAP1 cells were plated in 96-well plates, at a density of 1500 cells/well and treated as indicated for 5 days. After 5 days, cells were fixed using 100% methanol, and stained for 2h at room temperature using crystal violet. Subsequently, crystal violet was dissolved in 10% acetic acid, and intensity was measured using a BioTek Epoch Spectrophotometer at 595 nm. These measurements were used for IC50 calculations in PRISM, using nonlinear fit, sigmoidal, 4PL, X is log (concentration).

Immunofluorescence

Cells were grown on 9mm glass coverslips and fixed for 10 minutes at room temperature in 4% formaldehyde with 0.2% Triton X-100. The following antibodies were used: human anti-Crest (Cortex Biochem, cs1058), rabbit anti-pH3Ser10 (Campro, #07-081), mouse anti-ERCC6L (PICH) (Abnova, 000548421-b01p). All primary antibodies were incubated over night at 4°C. Secondary antibodies (Molecular probes, Invitrogen) and DAPI were incubated 2 hours at room temperature. Coverslips were mounted using ProLong Gold (Invitrogen). Images were acquired using a Deltavision deconvolution microscope (Applied Precision) with a 60x 1.40 NA oil objective. Softworx (Applied Precision), ImageJ, Adobe Photoshop and Illustrator CS6 were used to process acquired images.

Haploid insertional mutagenesis screens

Genes essential for survival of HAP1 cells treated with either Aph or HU were identified using a haploid insertional mutagenesis screen as described previously⁶¹. Mutagenized HAP1 cells were obtained from the Brummelkamp lab. In brief, mutagenesis of HAP1 cells was obtained as follows. Gene trap retrovirus was produced in HEK293T cells. Retrovirus

was harvested twice daily for a minimum of three days, and pelleted by centrifugation (2 hours, 21,000 rpm, 4°C using a SW28 rotor). Approximately 40 million HAPI cells were mutagenized by transduction of the concentrated gene trap virus in the presence of 8 µg/ml protamine sulfate in a T175 flask for at least two consecutive days. The mutagenized cells were frozen in IMDM medium containing 10% DMSO and 10% FCS. After thawing, mutagenized HAPI cells were passaged for 10 days in the presence of either 27.5 nM aphidicolin or 100 µM HU. After passaging, cells were collected by trypsin-EDTA followed by pelleting. Cells were fixed using fix buffer I (BD biosciences). To minimize confounding from diploid cells potentially harboring heterozygous mutations, fixed cells were stained with DAPI to allow sorting on G1 haploid DNA content using an Astrios Moflo. 30 million sorted cells were lysed overnight at 56°C to allow for de-crosslinking followed by genomic DNA isolation using a DNA mini kit (QIAGEN).

Insertion site mapping

The gene trap insertion sites were amplified by LAM-PCR, followed by capture, ssDNA linker ligation, and exponential amplification using primers containing illumina adapters prior to sequencing, as described previously¹⁶¹. Mapping and analysis of insertions sites is described previously¹⁶². Briefly, following sequencing on a HiSeq 2000 or HiSeq 2500 (Illumina), insertion sites were mapped to the human genome (h19) allowing one mismatch, and intersected with RefSeq coordinates to assign insertions sites to genes. Gene regions overlapping on opposite strands were not considered for analysis, while for genes overlapping on the same strand gene names were concatenated. For each replicate and for both drug treatments (Aph or HU) gene essentiality was determined by binomial test. Synthetic lethality was assessed by comparing the distribution of sense and antisense orientation integrations for each gene in the drug treated replicates with 4 wild-type control datasets previously published¹⁸⁸ (NCBI SRA accession number SRP058962) using Fisher's exact tests. A gene was considered a hit when it passed all Fisher's tests with a P value cutoff of 0.05 and an effect size of at least 15% (subtraction ratio > 0.15). By doing so, we selected RS-specific vulnerabilities when in the untreated setting the gene has a sense/total integration ratio around 0.5 (non-essential), but drops to a sense/total integration ratio of 0.35 or lower in all 3 screens performed in the presence of RS.

CRISPR-mediated generation of knockout cell-lines

Knockout cells were generated using CRISPR/Cas9 mediated genome editing. Guide sequences were designed using CRISPOR design. Guides to generate knockout cell lines were targeted against exon 1-3 of the gene of interest, and subsequently cloned into

the pX330 vector (Addgene plasmid #42230). pX330 and a donor vector containing a blasticidine resistance-cassette¹⁹⁰ were co-transfected in HAP1 cells and selected with 10 µg/ml blasticidin. Individual clones were selected and knockouts were confirmed using PCR to confirm integration of the blasticidin cassette at the correct locus, and by western blot analysis where indicated. The following guides were used:

Target gene	Forward	Reverse
RNASEH1	CACCGTCAGAAAGACCCCGGTCTTG	AAACCAAGACCGGGTCTTTCTGAC
HNRNPA2B1	CACCGAGGAAGACTACTACGAACAAT	AAACATTGTTCTAGTAGTTCCTC
VEZT	CACCGACACCGGAGTTTGACGAAG	AAACCTTCGTCAAACCTCCGGTGTG
GIGYF2	CACCGCTCCTCGTCTGTCAATCGC	AAACGCGATTGACAGGACGAGGAGC
RANBP1	CACCGATCGTTCTCAGAGGCAAAT	AAACATTTGCCTCTGAGAACGATC
CDC42	CACCGTTGTGGGCGATGGTGCTGT	AAACACAGCACCATCGCCACAAC
SEC63	CACCGTCCCGGCACATACTACCTC	AAACGAGGTAGTAGTCTGCGCCGGAC

RNA isolation and qRT-PCR

Cells were harvested by trypsinization 4 days post siRNA-transfection. RNA was isolated using the RNeasy kit (Qiagen) and quantified by NanoDrop (Thermo scientific). cDNA was synthesized using Bioscript Reverse Transcriptase (Bioline), random primers (Promega), dNTPs, and 800 ng of total RNA, according to manufacturer's protocol. Primers were designed with a Tm close to 60 °C to generate 90-120 bp amplicons, spanning introns. Subsequently, 10 ng of cDNA was amplified for 40 cycles on a Roche Lightcycler 480, using SYBR Green PCR Master Mix (applied Biosystems). Target cDNA levels were analyzed by comparative cycle (Ct) method and values were normalized to GAPDH expression levels. The following primers were used:

Target gene	Forward	Reverse
GAPDH	TGCACCACCAACTGCTTA	GGATGCAGGGATGATGTTT
POLG2	TGGGAAACTACGGGAGAACC	TCCAATCTGAGCAAGGCCAT
MRPL23	AGGATCAAGAAGCCGGACTA	TCAGGGCTCTCGTCTTTCTC

Mitochondrial stress assay

300,000 HAP1 cells were plated in each well of a XFe 24-well cell culture plate in 200 µL of IMDM. Four wells, A1, B4, C3 and D6 were left with medium only and used for background correction. For siRNA depletion of SDHA, cells were treated 3 days before plating the experiment. In the case of aphidicolin or HU treatments, cells were treated with 27.5 nM or 100 µM HU respectively for 2 hours before the analysis. The mito stress test cartridge was incubated overnight at 37°C without CO₂, in 1 mL of calibration buffer (Seahorse bioscience

100840-000). After overnight incubation at 37°C in 5% CO₂, cells were washed twice in PBS and IMDM was replaced with 700 µL base seahorse medium (Seahorse bioscience 102353-100) supplemented with 2 mM L-glutamine, 5.5 mM glucose, and sodium-pyruvate. Cells were then incubated at 37°C for 30 min without CO₂. Mitochondrial drugs were prepared at 10x concentrations, to be injected by the seahorse XFe24 extracellular flux analyzer; Oligomycin A (5 µg/mL), FCCP (10 µM), Rotenone (10 µM), Antimycin A (10 µM). Oxygen consumption rates (OCR) were measured using a XFe 24 extracellular flux analyzer (Agilent Technologies), at three different time-point during 4 different stages: basel/ no drugs, during oligomycin A, during FCCP and during rotenone + antimycin A. The XF mito stress test report automatically calculated the XF cell mito stress test parameters from Wave data. OCR is presented as the mean ± SD of 4 (WT), 2 (Aph, HU) or 1 (siSDHA) independent experiment(s), with 4 replicates and 3 time points per experiment.

Western-blot

Cells were lysed using Laemmli buffer (120 mM Tris pH 6.8, 4% SDS, 20% glycerol), and treated with drugs as indicated. Equal amounts of protein were separated on a polyacrylamide gel followed by transfer to a nitrocellulose membrane. Membranes were blocked in a 5% Milk/TBS solution. Antibodies were incubated in 2,5% milk in TBS containing 0,1% Tween. The following antibodies were used in this study: mouse anti- α -tubulin (Sigma, t5168), rabbit-anti-HSP90 (Santa Cruz, sc7947), mouse anti-yH2AX pSer139 (Upstate, #05-636), rabbit anti-RPA pSer4/pSer8 (Novus, NBPI-23017), mouse anti-hnRNPA2B1 (Santa Cruz, sc-374053), mouse anti-GIGYF2 (Santa Cruz, sc393918). HRP-coupled secondary antibodies (DAKO) were incubated for 2h at room temperature in a 1:2500 dilution. The immunopositive bands were visualized using Immobilon Western HRP Substrate (Millipore) and a ChemiDoc MP System (Biorad).

Quantification and Statistical Analysis

Significant differences between treatment conditions were calculated using a Student's t test. In all figures: *, p value < 0.05; **, p value < 0.01; ***, p value < 0.001; ****, p value < 0.0001.

Acknowledgments

We would like to thank the Medema, Brummelkamp, Rowland and Jacobs labs for helpful discussions, and J. Faria da Silva for advice on setting up the mitochondrial stress assay. This study was supported by funds from the Dutch Cancer Society (KWF- NKI-2015-7832), granted to R.H.M. and J.A.R.



SRBD1: A novel factor in sister chromatid decatenation?



Louise M.E. Janssen, Nuria Vaquero Siguero, Abdelghani Mazouzi, Leila Nahidiazar, Ahmed M.O. Elbatsh, Sarah C. Moser, Claire Hoencamp, Elmar Stickel, Kees Jalink, Jos Jonkers, Thijn R. Brummelkamp, Benjamin D. Rowland, René H. Medema, Jonne A. Raaijmakers

ABSTRACT

Proper chromosome segregation during mitosis is important to ensure chromosomal stability. Cancer cells show high levels of chromosomal instability (CIN), which creates a window of opportunity for targeted cancer therapy. One mechanism that ensures mitotic fidelity is chromosome compaction, which relies on condensin complexes, loss of which was shown to cause segregation errors. Here, we set out to identify factors that could either aggravate or rescue CIN (i.e. vulnerabilities or tolerance factors of CIN). To this end, we performed a genetic screen in condensin II-deficient cells. This screen identified SI RNA-binding domain-containing protein 1 (SRBD1) as a thus far undescribed essential factor for proper chromosome segregation. Loss of SRBD1 causes severe anaphase defects, closely resembling decatenation defects seen after catalytic inhibition of topoisomerase II (TOP2). The anaphase defects induced by SRBD1 loss, are not observed in condensin II-deficient cells, indicative of a genetic interaction between condensin II and SRBD1. Interestingly, we found that SRBD1 loss leads to enhanced levels of DNA-bound TOP2 complexes, indicating that SRBD1 either limits TOP2 activity directly, or prevents excessive binding of TOP2 to DNA. These altered TOP2 dynamics could be the cause of the severe anaphase defects. Together, we identified SRBD1 as a new player involved in preventing severe catenation defects, through a yet to be defined interplay with TOP2 and condensin II.

INTRODUCTION

Proper chromosome segregation during mitosis is important for maintaining genomic stability. Chromosome segregation errors can cause aneuploidy, chromosomal instability (CIN), and DNA damage, which can result in compromised cell viability^{36,92,118,121}. Interestingly, segregation errors are often found in cancer, where they contribute to tumor heterogeneity and are associated with poor prognostic outcome and therapy resistance⁹⁷⁻¹⁰⁰. In order to prevent segregation errors from occurring, cells deploy several pathways to ensure genomic stability.

One such pathway is chromosome condensation during mitosis. Instead of dividing long stretches of DNA, cells condense their chromosomes. This aids in sister chromatid resolution and generates compact, separable chromatids²⁶⁵. Condensation is established by highly conserved condensin complexes, which entrap and reel in the DNA (a process known as loop extrusion)²⁶⁶⁻²⁶⁸, thereby forming loops along the entire length of every chromosome. Metazoans possess two condensin complexes, I and II. These ring-shaped protein complexes contain the same structural maintenance of chromosomes (SMC) heterodimer (SMC2 & SMC4), but differ in their kleisin (CAPH/H2), and HEAT-repeat (CAPD2/D3 and CAPG/G2) subunits²⁶⁹⁻²⁷¹. While condensin II is present in the nucleus throughout the cell cycle, DNA only becomes accessible to condensin I upon nuclear envelope breakdown (NEB)²⁷². Therefore, it is thought that condensin I further condenses the chromosomes by forming nested loops within pre-established condensin II loops^{266,273}. Understandably, depletion of condensin causes segregation errors, such as lagging chromosomes and DNA bridges^{45,48,50,111-113,274}.

Besides chromosome shortening, condensation is also important to drive correct topoisomerase-mediated resolution DNA intertwines between sister chromatids (also known as DNA catenanes)^{45,48,50}. Topoisomerases are a family of protein complexes that resolve DNA topological problems such as DNA supercoils and catenanes⁴⁴. Topoisomerases act by generating transient DNA breaks and subsequent rejoining of the DNA. While most topoisomerase enzymes make single stranded breaks, type II topoisomerases (TOP2) enzymes generate double strand breaks (DSB) to perform their function⁴⁴. In vertebrates, two TOP2 enzymes exist: topoisomerase II α (TOP2A) and topoisomerase II β (TOP2B). TOP2A is essential for chromosome segregation^{47,50,275-279}, while TOP2B is more important during transcription⁴⁴. In interphase, both TOP2A and TOP2B are mobile²⁸⁰, and are localized in the nucleus (TOP2A is enriched in nucleoli)²⁸¹.

In mitosis, TOP2B is only present in the cytosol, while TOP2A remains chromatin bound, where it displays enrichment along the central axes of the chromatid arms and centromeres^{277,281,282}. The main role of TOP2A is to remove catenanes in mitosis⁴⁴. Catenane resolution is accomplished by generation of a double stranded break (DSB) in one of the intertwined strands. Thereafter, the other catenated strand is passed through the DSB, which is subsequently religated⁴⁴. The essential role TOP2A plays in mitosis, is reflected in the fact that TOP2A loss causes segregation errors^{50,276,278}, a function that cannot be taken over by TOP2B²⁷⁵. Thus, proper functioning of TOP2A is highly important to maintain genomic stability⁴⁴.

Condensin and TOP2 have been functionally linked in several studies^{45,46,48,50,51,276,283-285}. Condensins and TOP2 both localize to the axis of mitotic chromosomes^{282,283,286}. TOP2 has been implicated in condensation by aiding in the axial shortening of mitotic chromosomes and has also been shown to be important for the maintenance of the condensed state^{285,276,285,287}. Depletion of condensin was shown to delocalize TOP2 from the mitotic chromosome axis, and diminish decatenation activity^{50,286,288}. Moreover, it is thought that random TOP2 activity causes a high probability of creating DNA entanglements when DNA is in close proximity (reviewed in²⁸⁹). Condensin was shown to decrease this knotting probability by directing TOP2-activity towards decatenation⁴⁵. A proposed model for how condensin directs the decatenation activity of TOP2 has been put forward previously (reviewed in^{51,289}), where condensin either recruits TOP2 directly to a catenane, or the loop extrusion activity generates tension-mediated directionality to promote decatenation over catenation. Interestingly, it was shown that acute removal of condensin I in metaphase arrested drosophila embryos leads to TOP2-dependent *de novo* catenane formation⁴⁶, further indicating that TOP2's directionality and/or activity is restrained by condensin.

Here, we identified a prominent genetic interaction between condensin II and S1 RNA-binding domain-containing protein 1 (SRBD1). Loss of SRBD1 is detrimental to cell viability, but strikingly loss of SRBD1 in condensin II knock-outs is not lethal. We found that depletion of SRBD1 causes severe sister chromatid resolution defects that are rescued upon loss of condensin II. Here, we further untangle the function of SRBD1 and propose a role for SRBD1 in TOP2 biology.

RESULTS

Growth defect associated with loss of SRBD1 is rescued by loss of condensin II

In order to identify vulnerabilities and tolerance factors of chromosomal instability (CIN), a haploid genetic screen¹⁶¹ was performed in condensin II knock-out (Δ CAPH2) cells (Fig. S1A). Given that condensin II is involved in proper chromosome alignment^{50,111–113,273,274}, we hypothesized that synthetic lethal interactions with condensin II loss would involve spindle assembly checkpoint factors (SAC)¹⁶². Indeed, the strongest synthetic lethal interactors included SAC proteins MAD1L1 and MAD2L1 (Fig. S1B). Besides several additional synthetic lethal interactions (Fig. S1B), we also identified a small number of synthetic viable interactors (Fig. S1C). One of the most prominent synthetic viable hits was SI RNA-binding domain-containing protein 1 (SRBD1) (Fig. 1A, B, Fig. S1C). In wild type (WT) HAPI cells, disruption of SRBD1 was catastrophic for cell viability while, interestingly, its loss in Δ CAPH2 cells was far less detrimental (Fig. 1B/C, Fig. S2A/B). Thus far, little is described about the function of (SRBD1), but according to the Depmap portal¹²⁹⁰, SRBD1 is a common essential gene amongst many different cell lines.

In order to validate our screen results, we generated an auxin-inducible degron (AID)^{291,292} system for SRBD1 in HAPI tet-OstTIRI cells by integrating a mini-AID-HALO-3x-HA sequence at the C-terminus of the endogenous SRBD1 gene (Fig. 1D). We will further refer to this cell-line as SRBD1-AID. Upon doxycycline (DOX) addition, tet-OstTIRI HAPI cells express TIRI, which binds to several conserved endogenous proteins to form a SCF-ubiquitin ligase²⁹². This ligase rapidly degrades auxin (AUX)-bound mini-AID-fusion proteins²⁹² (Fig. 1D). SRBD1 degradation upon DOX/AUX addition was confirmed by western-blot (Fig. 1E). Colony outgrowth of the SRBD1-AID cells in the presence of DOX/AUX confirmed the lethality associated with SRBD1 loss (Fig. 1F). The additional knock-out of CAPH2 in the SRBD1-AID cell line rescued cell viability after SRBD1 depletion, thereby confirming our screen results (Fig. 1F, Fig. S1D).

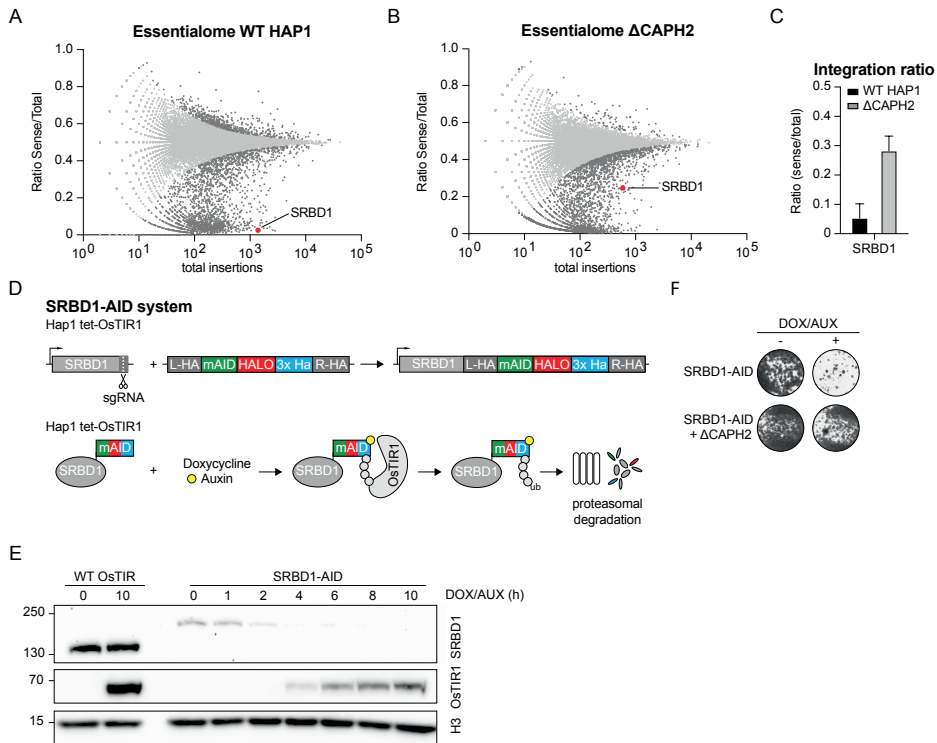


Figure 1: Growth defect associated with loss of SRBD1 is rescued by loss of condensin II

(A, B) Fishtail plots of gene-trap insertions in WT HAP1 and Δ CAPH2 cells. Each dot in the plot represents a single gene, and the number of integrations per gene is plotted on the x axis. On the y axis, the relative amount of sense integrations over the total amount of integrations (sense+antisense) is plotted. SRBD1 is highlighted in color. (C) Bar graph showing the average ratio of sense/total integrations in WT and Δ CAPH2 HAP1 cells. The data are extracted from 4 individual WT, and 2 Δ CAPH2 insertional mutagenesis screens. (D) Schematic representation of the generation of the mAID-HALO-3xHa tag on endogenous SRBD1. (TOP) The c-terminus of endogenous SRBD1 was targeted by CRISPR/Cas9 to induce a DSB. Repair of the break using a vector containing mini-AID (mAID), HALO-tag, 3xHa sequence, placed in between SRBD1 homologous sequences (homology arms) upstream (left, L-HA) and downstream (right, R-HA) of the DSB would lead to endogenously tagged SRBD1. (BOTTOM) Upon DOX addition, HAP1 OsTIR1 cells express a ubiquitin ligase that targets auxin tagged mAID-fusion proteins (in our case SRBD1) for proteasomal degradation. (E) Western blot of SRBD1, showing an increased protein size in SRBD1-AID cells due to the endogenous tag. Upon DOX addition, WT OsTIR1 and SRBD1-AID HAP1 cells express OsTIR1 after a few hours. Upon AUX addition, SRBD1 is specifically degraded in the SRBD1-AID cell line after 4 hours of DOX/AUX treatment. (F) Growth assay of SRBD1-AID and SRBD1-AID- Δ CAPH2 cells, either untreated or treated with DOX/AUX for 5 days.

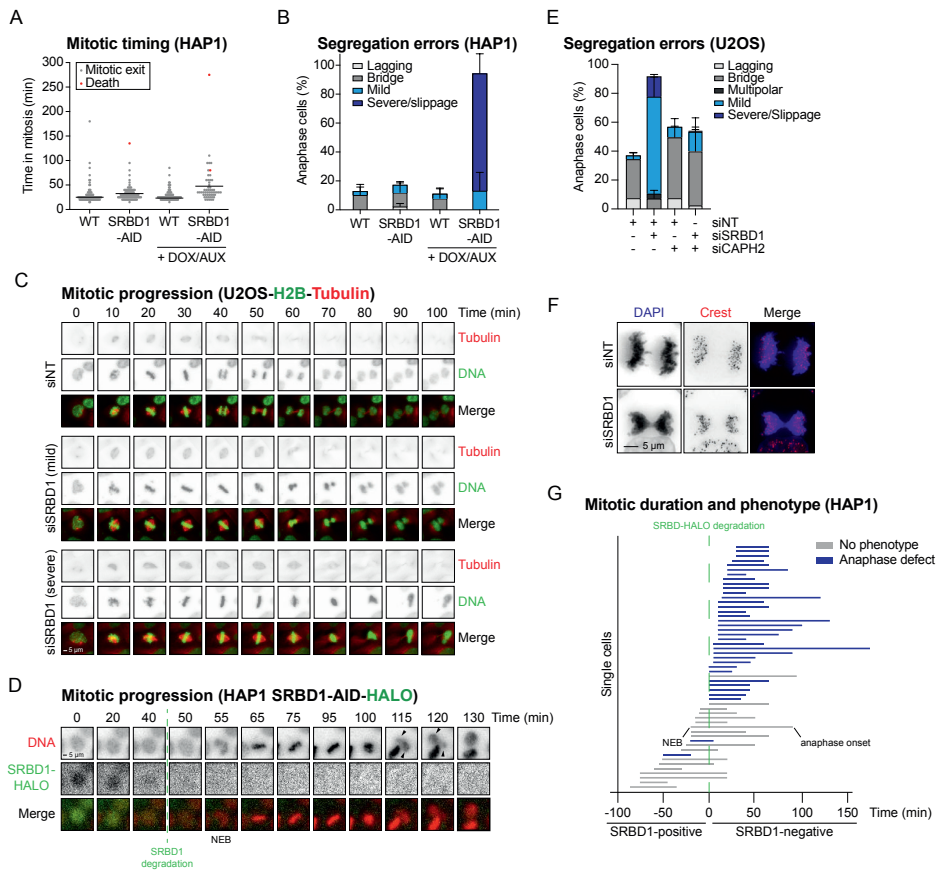


Figure 2: SRBD1-depletion causes severe anaphase defects

(A) Mitotic duration of WT Oostir1 and SRBD1-AID HAP1 cells, measured during live cell imaging. Drugs were added at start of movie. For the SRBD1-AID cells with DOX/AUX addition, all quantified cells were HALO positive. For the SRBD1-AID cells with DOX/AUX addition, only HALO negative cells were quantified. Pool of 3 independent experiments. (B) Segregation errors observed during anaphase of (A). Average of 3 independent experiments. (C) Representative images of the observed mitotic phenotypes in U2OS cells treated for 48 hours with a non-targeting siRNA (siNT) or siSRBD1. (D) Representative image of SRBD1-HALO degradation, and subsequent mitotic phenotype in SRBD1-AID HAP1 cells. Black arrows indicate two separate anaphase packs that cannot be equally divided. (E) Segregation errors during anaphase of U2OS cells depleted of SRBD1 and/or CAPH2 using siRNA's for 48 hours. Average of 2 independent experiments, minimally 100 cells per condition. (F) Representative immunofluorescence image of an anaphase U2OS cells treated for 48 hours with siNT or siSRBD1, stained for Dapi (DNA), and Crest (centromeres). (G) Graph displaying mitotic duration and the moment of SRBD1-HALO degradation in single cells. Every line represents a single cell, where the start represents NEB and the end of the line represents anaphase onset. Degradation of SRBD1 was determined by disappearance of the SRBD1-HALO signal. Blue lines indicate that that specific cell showed an anaphase defect. Pool of 3 independent experiments.

SRBD1 depletion causes severe anaphase defects

To understand the observed lethality of SRBD1-depletion, we set out to identify the cause of cell death using live-cell imaging. Mitotic timing was only slightly increased upon SRBD1-depletion (Fig. 2A), suggesting the early steps of mitosis are not severely affected. However, upon anaphase onset, SRBD1-depleted cells showed striking defects (Fig. 2B-E). Often, the DNA was not equally divided over two daughter cells, and seemed to be interconnected (Fig. 2C/D). This phenotype was often so severe, that the cells were unable to create two new daughter cells, resembling a slippage phenotype¹⁶⁷ (Fig. 2B-E). However, unlike previously described mitotic slippage, the DNA of SRBD1 depleted cells seemed to be subjected to pulling forces, reflected by the fact that the mitotic DNA appeared to be pulled away from the metaphase plate rather than decondense on the spot (Fig. 2D, indicated by arrows). Moreover, the tubulin signal showed clear indication of spindle midzone formation (Fig. 2C), and centromeres separated (Fig. 2F), suggestive of anaphase progression. Thus, SRBD1-depleted cells enter anaphase, but are unable to segregate their chromosomes properly, despite pulling forces being exerted. We could observe this anaphase phenotype in several different cell lines (HAPI, U2OS, RPE-1), using different approaches to deplete SRBD1: by auxin-induced degradation (HAPI) (Fig. 2B/D), by siRNA (Fig. 2C/E, Fig. S2B/C) and by CRISPRi (Fig. S2D/E). Moreover, overexpression of GFP-SRBD1 alleviated the anaphase defect upon CRISPRi-mediated depletion of endogenous SRBD1 (Fig. S2D/E). This further confirmed that the observed phenotypes can be attributed to SRBD1 loss. Importantly, the anaphase defects observed after SRBD1 depletion were rescued by additional CAPH2 depletion (Fig. 2E, Fig. S2C), which explains the rescue in cell viability upon co-depletion of SRBD1 and CAPH2 (Fig. 1F, Fig. S2A).

To pinpoint when SRBD1 acts, we utilized our SRBD1-AID cell-line. By visualizing SRBD1 using the introduced HALO-tag, we were able to determine the exact moment of SRBD1 degradation (Fig. 2D). When SRBD1 was depleted during mitosis (post nuclear envelope breakdown), we did not observe any anaphase phenotype (Fig. 2G, lower part of the graph), suggesting that SRBD1 is not important during the later stages of mitosis. In striking contrast, when SRBD1 was depleted prior to mitotic entry (just minutes before or at the exact moment of NEB), cells showed severe anaphase defects (Fig. 2G, upper part of the graph). Together, these data indicate that SRBD1 plays an essential role in prophase or early mitosis, to prevent severe anaphase defects.

SRBD1 localizes to the mitotic chromosome axis

To gain insight into SRBD1's function, we set out to understand its localization pattern. To this end, we generated a U2OS cell line stably expressing a GFP-fusion of WT SRBD1 (Fig. S2D/E). Using immunofluorescence, we found that GFP-SRBD1 localizes to the mitotic chromosome axis (Fig. 3A). Interestingly, several other proteins, including condensin I/II and TOP2A, were previously described to localize to the chromosome axis in mitosis^{282,283}, in a spiral-like organization^{286,293}. We found SRBD1 to localize in a similar higher-order structure by TIRF-STORM super resolution microscopy (Fig. 3B). Additionally, we confirmed the localization of HALO-CAPH2 and TOP2A to the mitotic chromosome axis in HAP1 cells by immunofluorescence (Fig. 3C), and found that SRBD1 localizes similarly to TOP2A to mitotic chromosomes (Fig. 3A). This chromosome axis, also referred to as the chromosome scaffold, contains non-histone proteins that play an important role in mitotic chromosome organization^{283,286}. Thus, the localization pattern of SRBD1 hinted toward a role in preserving mitotic chromosome architecture, possibly in collaboration with condensin II and TOP2A.

Functional dissection of SRBD1 domains

SRBD1 contains several structural domains: a N-terminal TEX-N domain, a central YqgF domain and a RuvA 2-like domain, and a C-terminal SI domain (Fig. 3D). TEX-N is a highly conserved protein domain, that can bind RNA and is involved in transcriptional processes²⁹⁴. YqgF-domains are RNase H-like structures that resemble RuvC holliday junction resolvases²⁹⁵. However, based on its sequence, this domain is predicted to be enzymatically inactive in SRBD1²⁹⁵. The RuvA-2-like domain has high similarity with domain 2 of RuvA, which has been implicated in holliday junction recognition²⁹⁶. Finally, the SI domain has been identified in *E. coli*, where it binds to RNA. Structurally, the SI domain closely resembles OB-folds, which are protein domains that frequently interact with DNA²⁹⁷. In order to identify which domains of SRBD1 are important for its functionality, we expressed several GFP-SRBD1-mutants in U2OS cells (Fig. 3D), and compared their localization to WT GFP-SRBD1 (Fig. 3E). WT GFP-SRBD1 localized to DNA, both in interphase and mitosis (Fig. 3E). All mutants showed nuclear localization in interphase (Fig. 3E). However, although WT SRBD1 enriched in nucleoli, this feature was disrupted in the Δ TEX-N and Δ RuvA 2-like mutants (Fig. 3E). Similarly, deletion of the TEX-N or RuvA-2-like domain disrupted chromatin localization of SRBD1 in mitosis, while the SI and YqgF domains seemed dispensable (Fig. 3E). Interestingly, only WT GFP-SRBD1 could rescue the observed anaphase defect after CRISPRi-mediated depletion of endogenous SRBD1 (Fig. 3F, Fig. S2D/E), indicating that all structural domains are required for proper SRBD1 function.

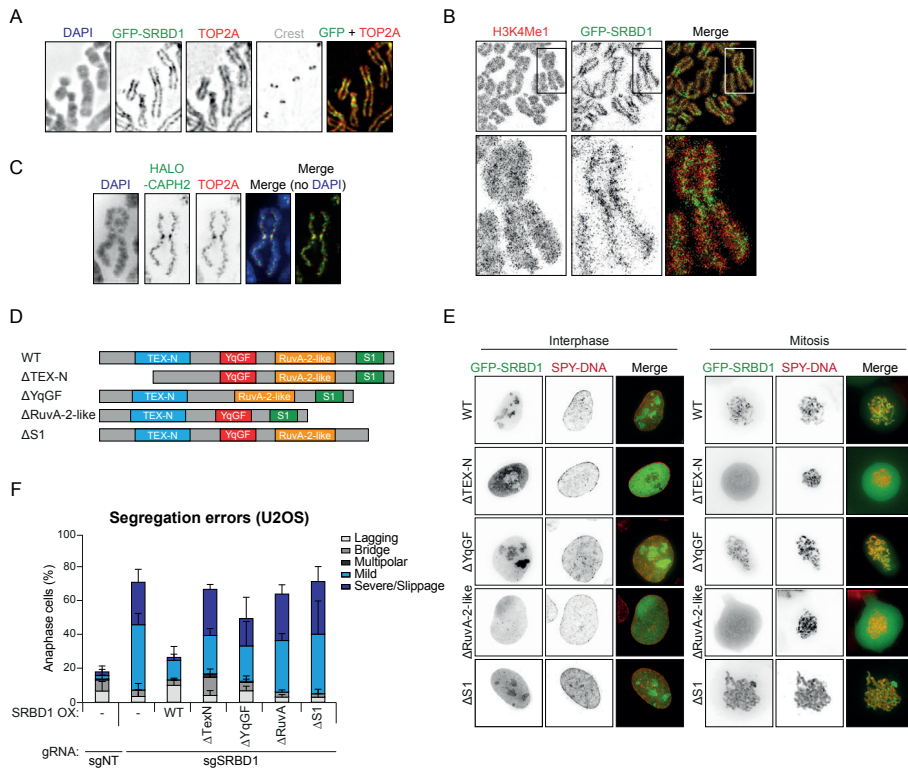


Figure 3: SRBD1 localizes to the mitotic chromosome axis

(A) Representative immunofluorescence image of a mitotic chromosome in U2OS cells, stained for Dapi (DNA), GFP (SRBD1), TOP2A and Crest (centromeres). (B) Representative image of GFP-SRBD1 localization on mitotic chromosomes in U2OS cells. Acquired by TIRF-STORM super-resolution. DNA is stained using H3K4me1. (C) Representative immunofluorescence image of a mitotic chromosome in HAPI cells, stained for Dapi (DNA), HALO (CAPH2), and TOP2A. (D) Schematic overview of several GFP-SRBD1 mutants. (E) Interphase and mitotic localization of WT GFP-SRBD1 and several GFP-SRBD1 mutants. DNA is visualized using Spy-DNA-555. (F) Segregation errors observed in anaphase of cells depleted of SRBD1 using a guide-RNA, and substituted with different GFP-SRBD1 (mutant) constructs. Average of minimally 2 independent experiments.

SRBD1 does not affect condensin II function nor dynamics

Our screen results implicate an interplay between condensin II and SRBD1. Therefore, we tested if loss of SRBD1 directly affects condensin II behavior. First, HALO-CAPH2 localization to the mitotic chromosome axis was not affected after siRNA-mediated SRBD1 depletion (Fig. 4A). Next, we studied if condensin II dynamics were perturbed after SRBD1 depletion. To this end, we performed a fluorescence recovery after photobleaching (FRAP) assay using an eGFP-CAPH2 plasmid¹³. As previously reported¹³, we found condensin II to be dynamic during interphase (Fig. 4B), and stable in metaphase (Fig. 4C). Depletion of SRBD1

did not affect these condensin II dynamics (Fig. 4B/C). To validate the condensation function of condensin after SRBD1-depletion, we measured the length of the longest three chromosomes²⁷³. As expected, Δ CAPH2 cells showed a significant increase in chromosome length compared to WT HAP1 cells (Fig. 4D). Depletion of SRBD1 in WT cells did not affect

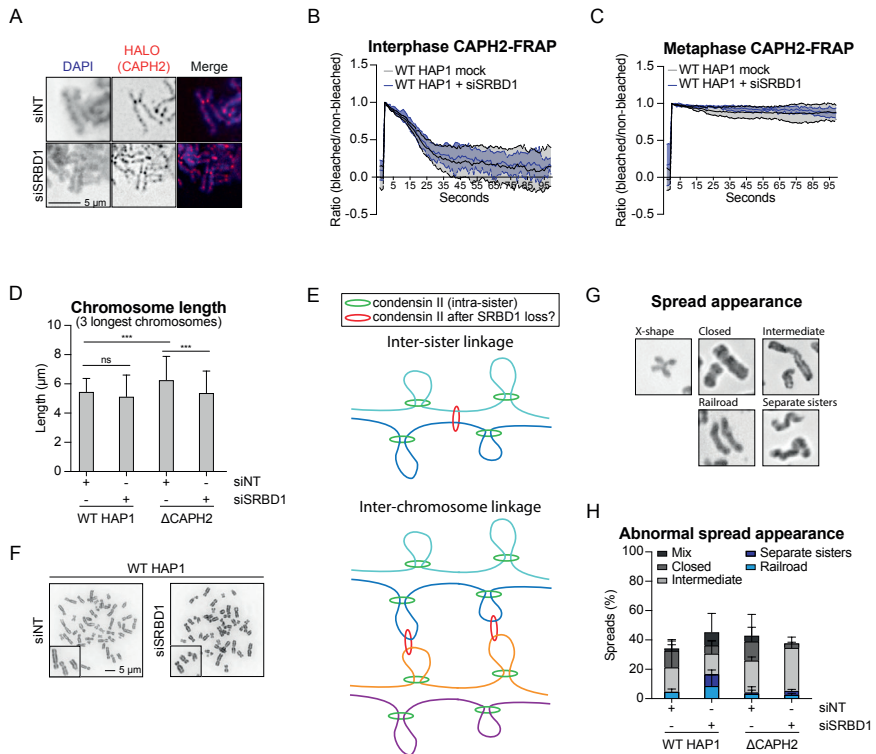


Figure 4: SRBD1 loss does not affect condensin II function nor dynamics

(A) Representative immunofluorescence image of a mitotic chromosome in HAP1 cells depleted for SRBD1. Stained for Dapi (DNA), and HALO (CAPH2). **(B)** FRAP of eGFP-CAPH2 in interphase HAP1 cells, treated for 96 hours with siNT or siSRBD1. Ratio of intensity in bleached/non-bleached area. Average of 1 experiment, with minimally 5 cells per condition. **(C)** FRAP of eGFP-CAPH2 in metaphase HAP1 cells, treated for 96 hours with siNT or siSRBD1. Ratio of intensity in bleached/non-bleached area. Average of 1 experiment, with minimally 2 cells per condition. **(D)** Average chromosome length of the 3 longest chromosomes in mitotic spreads of WT HAP1 and Δ CAPH2 cells treated with siNT or siSRBD1 for 96 hours. Average of 1 experiment, with minimally 80 chromosomes per condition. **(E)** Schematic of possible faulty condensin entrapments. Chromosomes could be either connected wrongly within two sister chromatids (inter-sister), or connections could be made between different chromosomes (inter-chromosome). **(F)** Representative images of chromosome spreads in WT HAP1 cells treated with 96 hours with siNT or siSRBD1, harvested after 5 hours of nocodazole treatment. **(G)** Example images of chromosome appearance in mitotic spreads. **(H)** Quantification of chromosome appearance in spreads of WT HAP1 and Δ CAPH2 cells treated for 96 hours with siNT or siSRBD1. Normal X-shape is not plotted, but accounts for the remaining percentage of spread appearance. Average of 2 independent experiments.

chromosome length, indicating that the condensation function of condensin I and II remains unaffected (Fig. 4C). Depleting SRBD1 in Δ CAPH2 cells showed a reduction in chromosome length as compared to deletion of CAPH2 by itself. This could indicate that SRBD1 antagonizes compaction, but only when condensin II is absent. Taken together, we did not find evidence that condensin II function was globally affected by loss of SRBD1.

Next, we hypothesized that the observed anaphase defect after SRBD1-depletion could be a consequence of faulty DNA-entrapment by condensin. For example, by entrapping the DNA of both sister chromatids (inter-sister linkage) or the DNA of two different chromosomes (inter-chromosome linkage) (Fig. 4E), condensin II-mediated DNA entrapment could lead to anaphase defects. Loss of condensin II would then rescue the SRBD1-depletion phenotype by preventing the generation of these faulty entrapments. To test the existence of such linkages, we generated chromosome spreads of cells arrested in prometaphase (Fig. 4F-H). We hypothesized that if condensin starts to generate inter-sister linkages (Fig. 4E), we would find an increase in closed chromosome arms (Fig. 4G). If condensin II would start to form inter-chromosome linkages (Fig. 4E), we expected to find severely distorted spreads, where chromosomes were fused to one another. However, we did not find clear evidence for such inter-chromosomal fusions (Fig. 4F). We next quantified the appearance of the chromosomes (Fig. 4G) as either X-shaped (normal chromosome appearance, not displayed in Fig. 4G but reflected by the remaining percentages), closed or intermediated closed (which can resemble cohesin retention²⁹⁸, incomplete sister chromatid resolution^{53,299}, or faulty entrapment of two sisters by condensin (Fig. 4E)), railroads or separate sisters (which reflect defects in sister chromatid cohesion^{300,301}). We found that depletion of SRBD1 did not increase the amount of (intermediate) closed chromosome arms compared to WT HAP1 cells (Fig. 4H). This suggests that there are no very prominent inter-chromosome or inter-sister chromatid connections present after loss of SRBD1, at least not along the entire length of the chromosomes. We observed a slight increase in railroad and separate sister chromatids, a phenotype that was not induced when depleting SRBD1 in Δ CAPH2 cells (Fig. 4H). However, this effect was mild and we did not observe any evidence for cohesin defects in our live cell imaging. Therefore, we did not follow-up on these results. Altogether, we conclude that SRBD1 does not (globally) affect condensin function.

SRBD1 depletion alters TOP2 behavior

The observed anaphase defect after SRBD1-depletion showed striking similarities to previously published phenotypes after ICRF-193 treatment (a catalytic inhibitor of

TOP2A/B)⁵³, and acute TOP2A depletion²⁷⁶. This could indicate that SRBD1 loss, like TOP2 inhibition, causes a defect in sister chromatid decatenation^{302,303}. Indeed, live cell imaging confirmed that treatment of U2OS cells with ICRF-193 resulted in a strikingly similar anaphase phenotype compared to SRBD1-depleted cells (Fig. 5A-C). Additionally, both SRBD1 (Fig. 2F) and TOP^{44,276} are specifically required in early mitosis. Moreover, TOP2A, unlike TOP2B, is active and chromatin bound during mitosis^{44,275,279}. Therefore, we hypothesized that the SRBD1-loss phenotype could potentially be attributed to dysfunction of TOP2A.

To test TOP2A function, we first quantified its localization to the mitotic chromosome axis. We did not observe apparent mislocalization of TOP2A after SRBD1-depletion (Fig. 5D/E). Next, we determined TOP2A function by visualizing decatenation defects by immunofluorescence imaging of the ultra-fine bridge (UFB) marker PICH^{37,52} (Fig. 5F). We found that depletion of SRBD1 increased the amount of PICH fibers in anaphase (anaphase was determined by the visual separation of 2 packs of centromeres, since we observed that centromere separation in anaphase was still occurring upon depletion of SRBD1, see Fig 2F) (Fig. 5F/G). Interestingly, most catenanes found after SRBD1-depletion originated from centromeres (Fig. S3), the location that generally harbors the majority of catenanes³⁷. Interestingly, CAPH2, TOP2A and GFP-SRBD1 were highly enriched at centromeres (Fig. 3A-C). Since we did not find indications of more intertwined sister chromatids along the length of the chromosomes (Fig. 4G), these data prompted us to test for decatenation defects specifically at centromeres. While removal of centromeric cohesin normally leads to premature sister chromatid separation, persistent DNA catenanes (induced by ICRF-193 treatment) were shown to keep sister chromatids together upon removal of centromeric cohesin⁵³. Therefore, we hypothesized that upon combined loss of SRBD1 and centromeric cohesin, chromosomes would remain connected if a large number of (centromeric) catenanes would indeed be present. To test this hypothesis, we depleted shugoshin 1 (Sgo1) by siRNA to induce premature loss of sister chromatid cohesion³⁰⁴⁻³⁰⁷ (Fig. 5H). Upon Sgo1 depletion, we indeed found a significant increase in railroad and separate sister chromatid structures (Fig 5H, siNT vs siSgo1), indicative for cohesin loss^{300,301}. As a positive control, we treated cells with ICRF-193 which significantly decreased the amount of separated sister chromatids (Fig. 5H, siSgo1 vs siSgo1 + ICRF), similar to previously published data⁵³. However, the combined depletion of SRBD1 and Sgo1 did not result in a rescue of separated sister chromatids (Fig. 5H, siSgo1 vs siSRBD1 + siSgo1). This either indicates that loss of SRBD1 does not lead to stable catenanes between sister chromatids, or that the decatenation defect upon SRBD1 loss is not sufficient to keep un-cohesed sister chromatids together.

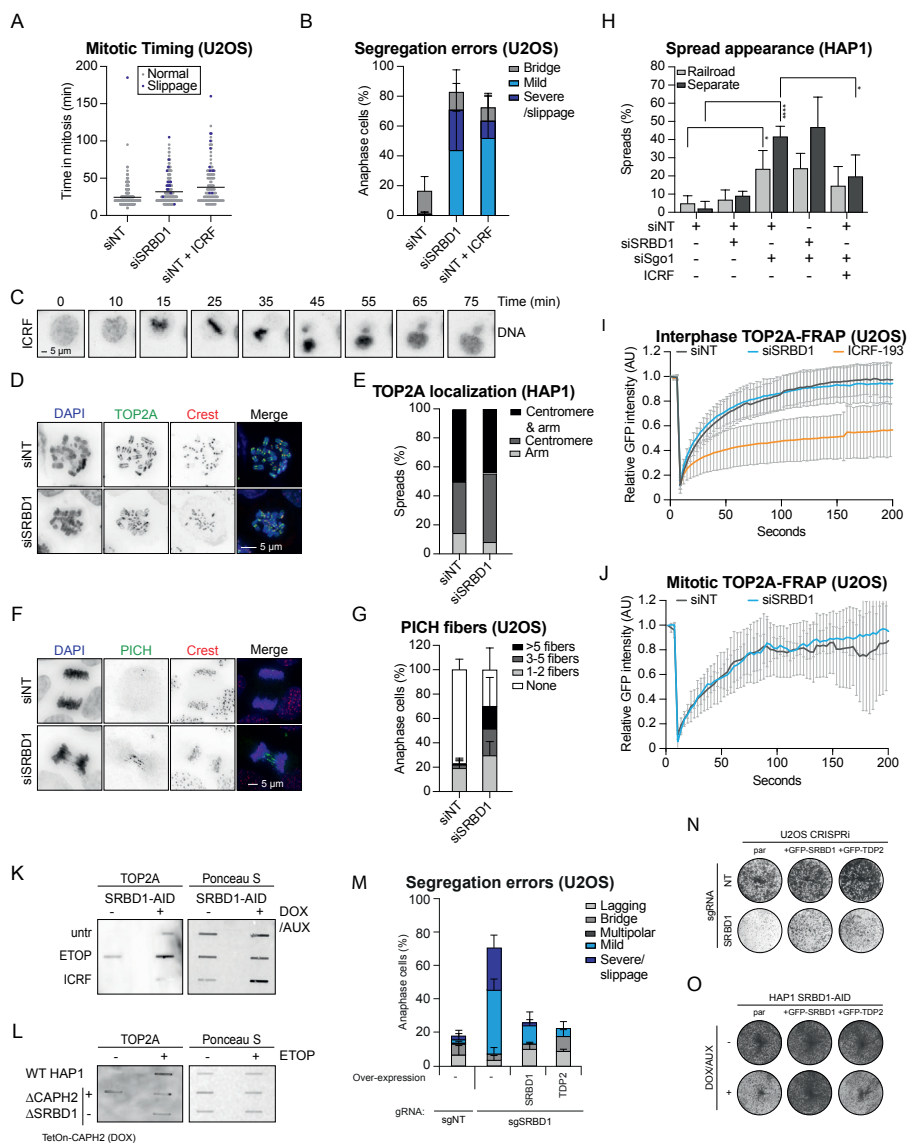


Figure 5: SRBD1 loss alters TOP2 behavior

(A) Mitotic duration measured during live cell imaging of U2OS cells treated with siNT or siSRBD1 for 48 hours, or 1.0 μ M of ICRF-193 2 hours before start of the movie. Pool of 5 independent experiments. (B) Segregation errors during anaphase of (A). Average of 5 independent experiments. (C) Representative images of the observed mitotic phenotypes in U2OS cells treated for with ICRF-193 in (A/B). (D) Representative immunofluorescence image of a mitotic chromosome spread in HAP1 cells depleted for SRBD1 using siRNA for 96 hours. Stained for Dapi (DNA), and TOP2A, and Crest (centromeres). (E) Quantification of TOP2 localization on mitotic chromosome arms as seen in (H). Percentages of one independent experiment, minimally 14 chromosome spreads per condition. (F) Representative immunofluorescence images of U2OS cells from (D), stained with Dapi (DNA), PICH (UFB), and Crest

(centromeres). **(G)** Quantification of PICH fibers in anaphase of U2OS cells treated with siNT or siSRBD1 for 48 hours. Mean of 5 independent experiments. Significant difference between samples having no PICH fibers (***). **(H)** Bar graph displaying the average spread appearance of cohesin depletion associated phenotypes (railroads and separate sisters) in WT HAP1 cells treated with a combination of siRNAs (siNT, siSRBD1 for 96 hours; siSgol for 24 hours) and/or ICRF-193 (24 hours). Average of four independent experiments. **(I)** FRAP of GFP-TOP2A in interphase U2OS cells, treated with siNT or siSRBD1 for 48 hours, or 1.0 μM of ICRF-193 for 30 min. Relative GFP intensity (A.U). Average of 1 experiment, with minimally 12 cells per condition. **(J)** FRAP of GFP-TOP2A in mitotic U2OS cells, treated with siNT or siSRBD1 for 48 hours. Relative GFP intensity (A.U). Average of 1 experiment, with minimally 4 cells per condition. **(K)** Western blot of the RADAR assay for TOP2A-DNA covalent complexes and Ponceau S. SRBD1-AID cells were either untreated and expressing GFP-SRBD1, or treated over-night with DOX/AUX (to deplete SRBD1). These samples were either untreated, or treated with etoposide (ETOP, 25 μM) or ICRF-193 (ICRF, 5 μM) for 30 minutes. **(L)** Western blot of the RADAR assay for TOP2A-DNA covalent complexes and Ponceau S. Double knock-out HAP1 cells ($\Delta\text{CAPH2}\Delta\text{SRBD1}$) expressing a DOX-inducible-CAPH2 were either untreated, or treated over-night with DOX (resembling a single ΔSRBD1). These samples were either untreated, or treated with etoposide (ETOP, 25 μM) for 30 minutes. **(M)** Segregation errors observed during anaphase in U2OS cells overexpressing GFP-SRBD1 or GFP-TDP2 after endogenous SRBD1 depletion. Average of 2 independent experiments. **(N)** Cell growth assay of U2OS cells with or without WT GFP-SRBD1 or TDP2-overexpression, depleted for SRBD1 using a guide-RNA. **(O)** Cell growth assay of SRBD1-AID HAP1 cells with or without WT GFP-SRBD1 or TDP2-overexpression, depleted for SRBD1 using DOX/AUX addition.

Next, we investigated the effect of SRBD1 depletion on TOP2 dynamics, using FRAP of GFP-TOP2A. ICRF-193 keeps TOP2 in a closed clamp state^{303,308}, which was shown to hamper TOP2A dynamics³⁰⁹. Indeed, we found that ICRF-193 treatment lowers TOP2A dynamics when compared to siNT treated cells (Fig. 5I). However, in contrast, depletion of SRBD1 did not affect GFP-TOP2A turn-over in interphase (Fig. 5I) nor mitosis (Fig. 5J), suggesting that TOP2 turnover is not globally affected.

We next performed a rapid approach to DNA-adduct recovery (RADAR) assay³¹⁰. This assay determines the amount of covalently bound TOP2 complexes to the DNA, for example TOP2 cleavage complexes (TOP2cc's). TOP2cc's are short-lived intermediates in the natural TOP2-DNA-cleavage-cycle³¹¹, where TOP2 is covalently bound to the DNA after it generated a DSB. Chemical inhibition of TOP2, for example by etoposide, locks TOP2 complexes in the cleavage stage, thereby strongly increasing the amount of (persistent) TOP2cc's^{303,312}. Indeed, we found that treatment with etoposide leads to an increase in the level of covalently-bound TOP2A (Fig. 5K/L) in WT cells. Interestingly, loss of SRBD1 resulted in increased covalently-bound TOP2A already in untreated conditions in two independent experiments, in two different HAP clones (Fig. 5K/L). The effect of etoposide addition on top of SRBD1 loss was not consistent in these 2 experiments, once showing no further increase, and once showing aggravation of covalent TOP2A binding (Fig 5K and L). Moreover, combined loss of SRBD1 and CAPH2 led to a reduction in the DNA-bound

TOP2A (Fig. 5L). This could indicate that the increased DNA-bound TOP2A is essential for the SRBD1 depletion phenotype observed in anaphase. Interesting to note is that ICRF-193 treatment did not result in increased covalently bound TOP2 complexes to the DNA (Fig. 5K), which might be explained by the fact that ICRF-193 does not lock TOP2 in a state covalently bound to the DNA^{303,308}. Altogether, our results thus far suggest that SRBD1 and ICRF can both affect TOP2 binding to DNA, but each has a completely different effect on the turnover of TOP2 complexes, despite their striking similar anaphase phenotype.

The obtained RADAR results could indicate that SRBD1 normally aids in the removal of TOP2 complexes that are covalently bound to the DNA. A similar function has been described for 5'-tyrosyl DNA phosphodiesterase 2 (TDP2), that aids in the removal of TOP2cc's³¹³⁻³¹⁵. Therefore, we reasoned that overexpression of TDP2 could potentially rescue the phenotype induced by loss of SRBD1. Indeed, overexpression of TDP2 rescued the anaphase defects in U2OS cells (Fig. 5M). Moreover, TDP2 overexpression increased cell outgrowth when SRBD1 was depleted in U2OS cells (Fig. 5N). However, TDP2 overexpression could not rescue cell viability in HAP1 SRBD1-AID cells (Fig. 5O). Possibly, the levels of TDP2 in HAP1 cells did not suffice to rescue the lethal SRBD1-depletion phenotype. Moreover, attempts to generate stable SRBD1 knockouts in TDP2 over-expressing HAP1 or U2OS cells were unsuccessful. Nevertheless, since TDP2 did rescue the phenotype in U2OS cells in a live setting, we tested if depletion of SRBD1 induced TOP2cc's by measuring DNA damage foci. However, we did not observe increased DNA damage upon SRBD1 depletion (Fig. S4A), something that is described for persistent TOP2cc's after etoposide treatment³¹⁶. Moreover, treatment with etoposide does not lead to anaphase defects as observed with ICRF-193 treatment or SRBD1 depletion (Fig. S4B). Altogether, we provide evidence that in the absence of SRBD1, there are more TOP2 complexes covalently bound to the DNA, however it is unlikely that these encompass persistent cleavage complexes.

Positive selection screen as an unbiased approach to unravel SRBD1 function

Our findings thus far indicated that loss of SRBD1 causes increased levels of covalently bound TOP2 to the DNA. However, if and how this can translate into the observed anaphase defect and the exact interplay between SRBD1, TOP2A and condensin II remained to be elucidated. To gain insight into the exact function of SRBD1, we setup an unbiased positive selection screen to search for factors that rescue the lethality of SRBD1 loss (Fig. 6A). First, we performed random mutagenesis by integrating a gene-trap virus (Fig. 6A). Five days post mutagenesis, we depleted SRBD1 using CRISPRi (sgSRBD1,

with a puromycin (PURO)-resistance cassette), which led to efficient cell killing (Fig. 6B). Mutants that rescue the lethality of SRBD1 loss are expected to enrich in the population after 10 days of growth (Fig. 6A, lower panel). We normalized the relative rescue to the enrichment observed in a population that was not treated with a guide RNA. Moreover, we performed parallel screens for a non-targeting guide (sgNT) that does not induce cell killing, and two unrelated essential genes, namely ATR and Aurora B (AurB) (Fig. 6A, B), as negative controls. This allowed us to filter out overlapping hits (most likely involving CRISPRi/ puromycin resistance regulators), and would thus allow for the identification of SRBD1-specific hits. Based on our initial observations, we expected gene-trap integrations in condensin II subunits to rescue the lethality of SRBD1-depletion (see Fig. 1), therefore serving as a positive control. Indeed, all 5 subunits of the condensin II complex (*SMC2*, *SMC4*, *NCAPH2*, *NCAPG2*, *NCAPD3*) were significantly enriched in the sgSRBD1 screen only (Fig. 6C/D, red dots), indicating our screen technically worked and further confirming our initial screen results. The remainder of SRBD1-specific rescue hits contained a variety of genes (Fig. 6E), involved in, but not limited to, RNA processing (*CELF1*, *TRIR*), histone acetylation (*KAT7*, *CREBBP*, *SMARCA4*), CENPA turnover (*KAT7*, *MIS18BP1*), and nuclear export (*RANBP3*, *XPO1*). As a first validation, we designed CRISPRi guides for a selection of the hitlist, containing a PURO-resistance cassette. On-target depletion of these genes, except *C16ORF72* and *TRIR*, using lentiviral infection was confirmed by qPCR (Fig 6F). After PURO selection, cells were infected with a second lentiviral CRISPRi guide, either sgNT or sgSRBD1, containing a zeocin (ZEO)-resistance cassette (Fig. 6G). We quantified the level of outgrowth by calculating the fold change of outgrowth in the sgSRBD1 (ZEO)-infected well over the sgNT (ZEO)-infected well (Fig. 6H). By doing so, a value of 1 would indicate that the SRBD1-depleted well was growing in a similar speed as the NT-depleted well, suggesting a complete rescue of the lethality of SRBD1-depletion. As expected, depletion of SRBD1 in the background of sgNT compromised cell viability (Fig. 6G, H). As expected, SRBD1-depletion in combination with *CAPH2*-depletion rescued cell viability (Fig. 6G/H), indicating that our approach worked. Using this system, we validated *KAT7*, *TRIR*, and *CELF1* (qPCR data of *TRIR* awaits further validation). Depletion of *XPO1* was lethal upon itself, which was expected based on the Depmap²⁹⁰ data. *RANBP3*, *C16ORF72* and *SMARCA4* did not validate, possibly due to incomplete knockdown or false positive hit selection, although this needs further validation. Additionally, *MIS18BP1*-depletion interfered dramatically with cell viability in control cells, hence its capability to rescue was difficult to interpret. Taken together, using a positive selection screen we identified gene candidates besides the entire condensin II complex, that are involved in the phenotype induced by SRBD1-loss. Further experiments are required to validate remaining hits and to determine the exact role of these rescue factors in relation to SRBD1.

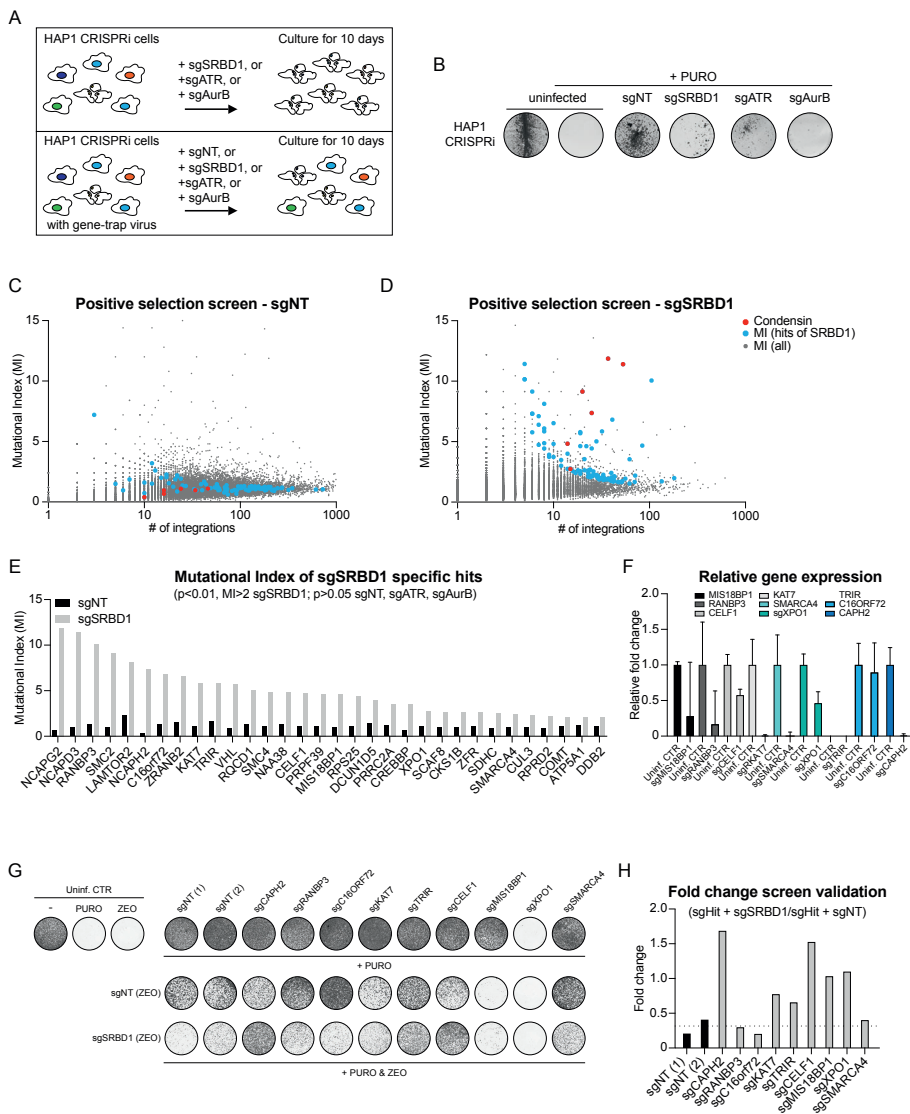


Figure 6: Positive selection screen as an unbiased approach to understand SRBD1 function

(A) Schematic representation of positive selection screen set-up. CRISPRi mediated depletion of essential genes (SRBD1, ATR, Aurora B (AurB)) will cause cell death. However, in the gene-trap background, synthetic viable interactions will grow out and this enrichment can be identified by sequencing. (B) Colony outgrowth of HAP1 CRISPRi cells, displaying uninfected control cells, and cells infected with guide RNAs targeting either NT, SRBD1, ATR or AurB and containing a puromycin resistance cassette. (C/D) Plots of the genes that were found back in the sgNT (C) and sgSRBD1 (D) screen. Each grey dot in the plot represents a single gene, and the number of integrations is plotted on the x axis. On the y axis, the mutational index (MI) is plotted, indicating how much this gene is enriched compared to WT essentialome screens. Blue and red dots represent specific hits of the sgSRBD1 screen, filtered by having $p < 0.05$, and $p > 0.05$ in the sgNT, sgATR and sgAurB screen. Red dots represent condensin II

related genes. **(E)** Bar graph displaying the MI of identified sgSRBD1 hits, in both the sgNT screen (black bars) and the sgSRBD1 screen (grey bars). Hitlist was generated by the following cutoffs: $p < 0.01$ and a MI > 2 in the sgSRBD1 screen, and $p > 0.05$ in the sgNT, sgATR and sgAurB screen. Indicating specific enrichment in the sgSRBD1 screen. **(F)** Relative gene expression of indicated genes after CRISPRi mediated depletion (relative to uninfected control, normalized to ribophorin expression). Expression was measured by qRT-PCR, error bars represent standard deviation of three biological replicates from 1 experiment. **(G)** Colony outgrowth of HAPI CRISPRi cells, displaying uninfected control cells, and cells infected with guide RNAs targeting the selected positive selection hits (puromycin resistant). Additionally, these cells were treated with CRISPRi guides for either sgNT or sgSRBD1, containing a zeocin resistance cassette. In this way, screen hits were validated when sgSRBD1 depletion did not compromise cell viability. **(H)** Bar graph showing the relative outgrowth using the fold change of sgSRBD1 over sgNT well intensity, after CRISPRi mediated depletion of positive selection screen hits. Dotted line represents average ratio of sgNT (1) and sgNT (2).

DISCUSSION

It has been shown that condensin and TOP2A act in concert to shorten chromosomes^{265,276,285,287} as well as to decatenate sister chromatids^{45,48,50,51,274,276,284}. It was proposed that condensin-mediated loop-extrusion guides catenanes to the basis of condensin loops^{45,51,289}. Here, TOP2's activity could be directed towards decatenation, because the loop-imposed tension could generate a bias towards correct re-ligation^{45,51,289}. Indeed, TOP2-mediated DNA intertwinings increase upon condensin depletion^{45,46}. However, how the interplay between condensin and TOP2 is regulated precisely remains uncertain^{51,289}.

Here, we identified a novel factor, SRBD1, that co-localizes with TOP2A and condensin to the chromatid axis. Upon loss of SRBD1, cells display severe segregation defects in anaphase, reflecting decatenation problems observed upon depletion of TOP2A or its chemical inhibition^{53,276}. Interestingly, loss of condensin II alleviates the anaphase defects observed after SRBD1 loss. In order to understand if and how SRBD1 loss causes these severe segregation defects, we first set out to test if condensin II and TOP2A still function properly. Our FRAP data indicate that loss of SRBD1 does not affect global condensin or TOP2A turnover. Remarkably, we did not observe severe defects in chromosome morphology and we found that sister chromatids still separated upon double depletion of centromeric cohesin and SRBD1. This could mean several things. First, the observed anaphase defect might be attributed to more subtle DNA-decatenation defects (either at the chromosome arm or centromere) and these catenanes might not be able to withstand forces generated during the mitotic spread procedure in the absence of cohesion. Secondly, loss of cohesin might generate tension on the catenanes, which in fact might aid to direct the decatenation activity of TOP2A, even in the absence of SRBD1. Finally, we cannot exclude that the phenotype is not caused by true DNA catenanes but by

inter-chromosomal connections generated by other factors (i.e. condensin for example, see Fig. 4D). Again, such a factor could be unable to withstand the forces generated during the spreading procedure, thereby explaining the successful separation of sister chromatids upon loss of centromeric cohesin.

Interestingly, even though loss of SRBD1 did not alter TOP2A dynamics, we did find an increase in TOP2A covalently bound to the DNA, which could be indicative for more TOP2cc's. Normally, TOP2cc's are transient in nature³¹¹, and persistent TOP2cc's are only found upon treatment with topoisomerase poisons like etoposide, that lock topoisomerase onto the broken DNA in a cleavage complex stage³⁰³. Thus, we explored the possibility that loss of SRBD1 affects the removal of TOP2cc's. Persistent TOP2cc's can be removed by nuclease dependent DSB-repair mechanisms, or by sumoylation and subsequent removal by TDP2^{314,315,317,318}. Interestingly, we have some evidence that overexpression of TDP2 can rescue the SRBD1 depletion phenotype. We therefore explored if SRBD1 is needed for TOP2cc removal. However, our experiments thus far hint that this is not the case. First, anaphase defects are not observed upon treatment with etoposide (Fig. S4B), while this treatment does result in enhanced levels of TOP2cc's on the DNA (Fig. 5K/L). Moreover, persistent TOP2cc's caused by etoposide treatment harbor broken DNA³¹⁶, and we do not observe increased DNA damage upon SRBD1-depletion (Fig. S4A). Thus, it is unlikely that persistent TOP2cc's are responsible for the anaphase defects upon loss of SRBD1. A more favorable explanation for the enhanced levels of covalently bound TOP2A in response to SRBD1 loss is that TOP2 DNA binding/activity is increased, which increases the amount of DNA-bound TOP2 at any given time (transient TOP2cc's). This could explain why loss of condensin II rescues the SRBD1 depletion phenotype, since loss of condensin has been shown to de-localize TOP2A^{50,266}, thereby limiting TOP2A engagement. Loss of SRBD1 could generate more substrates for TOP2, resulting in more covalently bound TOP2 molecules. Alternatively, SRBD1 could also directly compete with TOP2 for binding to the DNA under normal conditions (see Fig. 7), or act as a brake on TOP2 activity. Interestingly, undirected TOP2 activity has been shown to bias the knotting probability towards more entanglements⁴⁵. Thus, it is not unlikely that increased TOP2 activity in the absence of SRBD1 could actually create DNA catenations, and thereby contribute to the observed anaphase phenotype. In this regard, we can envision that TOP2 activity needs to be limited at specific topological abnormalities. Nonetheless, besides catenanes, different topological structures could underlie the observed anaphase defects after SRBD1 loss. In this regard, it is intriguing that the domains present in SRBD1 are related to holliday junction processing and RNA binding. Holliday junctions are homologous recombination

repair intermediates that result in hemicatenane formation, which can be resolved by endonucleases and topoisomerase III (TOP3)^{319,320}. It would be interesting to explore if SRBD1 could recognize holliday junction structures, hemicatenanes and/or structures involving RNA such as R-loops. Possibly, SRBD1 aids in the resolution or protection of such structures, in concert with other (topoisomerase) enzymes.

In order to test if undirected TOP2 activity or TOP2 hyperactivity are indeed the underlying cause of the observed anaphase defects after SRBD1 depletion, we aimed to co-deplete TOP2A. However, the essentiality of TOP2A²⁷⁶ made it technically challenging to find the right balance to establish a functional rescue. Additionally, TOP2A was also not identified as a rescue hit for SRBD1 depletion (Fig 6), which could again be attributed to its essentiality. Instead, we propose to either acutely deplete TOP2A in SRBD1-depleted cells using an AID-tagged TOP2A, or by preventing TOP2A binding to the DNA using aclarubicin, to test if reduced TOP2A activity can rescue the SRBD1-depletion phenotype. However, since acute loss of TOP2A was shown to also result in severe catenanes in anaphase²⁷⁶, this approach might still be unsuccessful. As an alternative, we suggest to perform kinetoplast decatenation assays³²¹ using extracts depleted of SRBD1. This could give indications of global TOP2 activity alterations. If TOP2 activity is not affected, the increase in DNA-bound TOP2A could underlie a more intricate defect, for example a location specific interplay between SRBD1 and TOP2A. To understand where SRBD1 binds in the genome and in proximity to which other factors, we plan to perform chromatin immunoprecipitation (ChIP) and rapid immunoprecipitation mass spectrometry of endogenous proteins (RIME) of SRBD1. Additionally, SRBD1 loss could create substrates for TOP2A binding or defects in direction of decatenation, for example due to changes in the chromatin environment. Therefore, it would be interesting to test condensin II and TOP2A binding to the genome using ChIP after SRBD1-depletion.

In order to gain further understanding into if and how SRBD1 prevents decatenation defects, we performed an unbiased positive selection screen. Besides all condensin II subunits, we identified other candidates that rescue cell viability after SRBD1-depletion. Interestingly, the hits comprised several RNA-processing factors (e.g. *CELF1*, *TRIR*, *ZRANB2*, *PRPF39*), histone acetylases (*KAT7*, *CREBBP*, *SMARCA4*), centromeric histone incorporation factors (*KAT7*, *MIS18BPI*), and nuclear export factors (*RANBP3*, *XPO1*). We were thus far able to validate that loss of *CELF1*, *KAT7* and *TRIR* indeed increases cell viability in combination with SRBD1-depletion. Although further experiments are required to validate the other hits and to understand these genetic interactions, we can speculate on these findings. *CELF1*

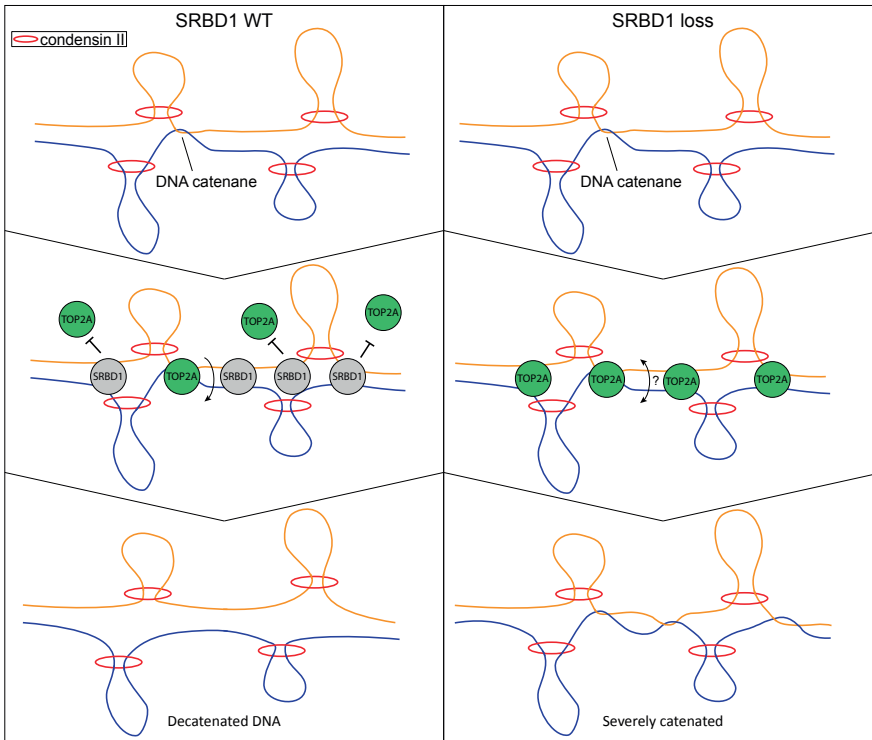


Figure 7: Speculative model of SRBD1's function

Schematic depiction of a speculative model on SRBD1's mode of action. When SRBD1 is present (left panel), decatenation activity of TOP2A is properly balanced by a yet to be defined mechanism of SRBD1. For example, SRBD1 could prevent TOP2A substrates from occurring, could directly compete with TOP2A for binding to the DNA, could change the (local) chromatin landscape to prevent TOP2A binding, or inhibit (local) TOP2A activity. Upon loss of SRBD1 (right panel), TOP2A binds excessively to the DNA, and catenation/decatenation activity occurs wrongly. This creates severely catenated DNA, which gives rise to the observed anaphase phenotype upon SRBD1 depletion.

depletion has been found to reduce TOP2A mRNA/protein levels³²². This would fit with the model postulated above for condensin, where loss of CELF1 would reduce TOP2A levels and thereby limit DNA-bound TOP2A. KAT7 was shown to aid in the deposition of CENPA at the centromere by promoting transcription^{323,324}. Transcription creates supercoils, and relaxation of these supercoils is shown to require TOP2 activity^{325,326}. Thus, loss of KAT7 could supposedly rescue the SRBD1 phenotype by reducing centromeric transcription and thereby reduce TOP2 engagement. Additionally, loss of KAT7 could change the histone landscape. This might underlie the phenotypic rescue, for example by reducing TOP2 engagement in general or by aiding in decatenation directionality in absence of SRBD1.

Further validation experiments are required to complete the list of rescue factors and to fully understand the molecular mechanisms underlying these interactions.

Altogether, even though some essential pieces of understanding the SRBD1 puzzle are missing, the indispensable role that SRBD1 plays in proper chromosome segregation and its interaction with condensin II are indisputable.

METHODS

Cell culture

Human derived near-haploid HAPI cells were cultured in IMDM (GIBCO) supplemented with 10% FCS, 1% GlutaMAX supplement (GIBCO), 100 U/ml penicillin, and 100 µg/ml streptomycin. U2OS cells were cultured in DMEM (Gibco) supplemented with 6% FCS, 1% GlutaMAX supplement (GIBCO), 100 U/ml penicillin, and 100 µg/ml streptomycin. siRNA transfections were performed using RNAiMax (Invitrogen) according to the manufacture's guidelines, and cells were incubated with the siRNA at the indicate times. The following siRNAs were used in this study: siNon-Targetable (Dharmacon), siCAPH2 (ON-TARGET plus NCAPH2 siRNA #9 Dharmacon), siSRBD1 (SMARTpool ON-TARGETplus Dharmacon), siSgo1 (ON-TARGETplus SMARTpool Dharmacon). All drugs were dissolved in DMSO, except for Auxin (dissolved in water) and used at indicated concentrations. For auxin every experiment uses 500 µM, for doxycycline every experiment uses 1 µg/ml.

Haploid insertional mutagenesis screens

Genes essential for survival of HAPI cells were identified as described previously¹⁶¹. In brief, mutagenesis of HAPI cells was obtained as follows. Gene trap retrovirus was produced in HEK293T cells. Retrovirus was harvested twice daily for a minimum of three days, and pelleted by centrifugation (2 hours, 21,000 rpm, 4°C using a SW28 rotor). Approximately 40 million HAPI cells were mutagenized by transduction of the concentrated gene trap virus in the presence of 8 µg/ml protamine sulfate in a T175 flask for at least two consecutive days. Mutagenized HAPI cells were passaged for 10 days. After passaging, cells were collected by trypsin-EDTA followed by pelleting. Cells were fixed using fix buffer I (BD biosciences). To minimize confounding from diploid cells potentially harboring heterozygous mutations, fixed cells were stained with DAPI to allow sorting on G1 haploid DNA content using an Astrios Moflo. 30 million sorted cells were lysed overnight at 56°C to allow for de-crosslinking followed by genomic DNA isolation using a DNA mini kit (QIAGEN).

For the positive selection screen, a similar protocol was followed for the mutagenesis of HAP1 CRISPRi cells. First, CRISPRi cells were obtained by lentiviral infection of a plasmid containing dCas9-KRAB-BFP-BLAST. CRISPRi expressing cells were obtained by BFP FACS sort. After mutagenesis, cells were infected with lentivirus containing pLV-mU6_Blp1_Ef1alpha_Puro-T2A-iRFP_sgRNA_CRISPRi with a non-targeting guide, or guides against SRBD1, ATR, or Aurora B. Cells were passaged for 10 days in the presence of puromycin, before fixing and following the steps mentioned above.

For validation experiments of the positive selection screen, CRISPRi guides were cloned into a pLV-mU6 with Blp1 and Ef1alpha Puro-T2A-sfGFP sgRNA_CRISPRi or into a pLV-mU6 with Blp1 and Ef1alpha Zeo-T2A-sfGFP sgRNA_. Subsequently, HAP1 CRISPRi cells were infected with lentivirus containing the sgRNA plasmid, and cells were selected with either puromycin (2 µg/ml) or zeocin (0.4 mg/ml). All guides were cloned using a DNA vector and the same reverse guide GTAATACGGTTATCCACGCGGCCCTAATGGATCCTAGTACTCGAGA (Rv). The following forward guides were used:

Target gene (CRISPRi)	Forward
NT	CCTTGGAGAACCACCTTGTGAACGACTAGTTAGGCGTGTAGTTAAGAGCTAAGCTGG
SRBD1	CCTTGGAGAACCACCTTGTGAACCCGCAAGACGACCGCCAGTTAAGAGCTAAGCTGG
Aurora B	CCTTGGAGAACCACCTTGTGGGCGCAAGGCCTGCGACAGGGTTAAGAGCTAAGCTGG
ATR	CCTTGGAGAACCACCTTGTGAGCCTCAGCATGGGGAAACAGTTAAGAGCTAAGCTGG
CAPH2	CCTTGGAGAACCACCTTGTGGGGCTGCCTTCCGAGGGGTAGTTAAGAGCTAAGCTGG
RANBP3	CCTTGGAGAACCACCTTGTGATGGCGGACCTGGCGAACGAGTTAAGAGCTAAGCTGG
CI6ORF72	CCTTGGAGAACCACCTTGTGGCGCAGCTCGGCCTGCACCGGTTAAGAGCTAAGCTGG
KAT7	CCTTGGAGAACCACCTTGTGCTGTATCAGTCCCAATCCTGGTTAAGAGCTAAGCTGG
CI9ORF43	CCTTGGAGAACCACCTTGTGGCGACAAAATGGCTGCCCGAGTTAAGAGCTAAGCTGG
CELF1	CCTTGGAGAACCACCTTGTGGGGATTTCGGCCTCAGCAGCGGTTAAGAGCTAAGCTGG
MISI8BP1	CCTTGGAGAACCACCTTGTGGGGCTCGCGCCTCAGGCCAGTTAAGAGCTAAGCTGG
XPO1	CCTTGGAGAACCACCTTGTGTGGAACAGGCACCGCCCGGTTAAGAGCTAAGCTGG
SMARCA4	CCTTGGAGAACCACCTTGTGGCCGCGCCGCCCAACGGTTAAGAGCTAAGCTGG

RNA isolation and qRT-PCR

Cells were harvested by trypsinization 4 days post siRNA-transfection. RNA was isolated using the RNeasy kit (Qiagen) and quantified by NanoDrop (Thermo scientific). cDNA was synthesized using Bioscript Reverse Transcriptase (Bioline), random primers (Promega), dNTPs, and 800 ng of total RNA, according to manufacturer's protocol. Primers were designed with a Tm close to 60 °C to generate 90-120 bp amplicons, spanning introns. Subsequently, 10 ng of cDNA was amplified for 40 cycles on a Roche Lightcycler 480,

using SYBR Green PCR Master Mix (applied Biosystems). Target cDNA levels were analyzed by comparative cycle (Ct) method and values were normalized to GAPDH or ribophorin expression levels. The following primers were used:

Target gene (qPCR)	Forward	Reverse
SRBD1	GTGTCAGCTTTGTGGAGTG	TCTCGTTGATAAAGGGTCCA
RANBP3	ATTGCTCCGCCCGTCTTT	AGGCTCCTCTCCCGAATCC
cl6orf72	TGGCACCTCTCCAGAACTC	CTGCGTTTGAAGGGGAC
KAT7	ACATCCCAGCATCTGCTC	AGTAAGCAGGCTCCTCAGTG
cl9orf43	GTCCGGGCTCCACACTTAG	TCTCCGCTTCTGCTTCTT
CELF1	GATAGGAGCCAAAACCCGC	TGGGAGGACTTTCATGTTGTG
MIS18BP1	AGCAGGAAAAGAAAGCACCA	ATGCTTTGTTTCGGGCTTCT
XPO1	TCGTCAGCTGCTTGATTTCAG	TGTGCAGTACTTCTTGAGCCA
SMARCA4	CTCAGGACAACATGCACCAG	CGCATCCCCATTCCTTTCAT
CAPH2	CTGGGCGAGTATCTGGAGG	GATCAACAACGCTGCCTCAA

Insertion site mapping

The gene trap insertion sites were amplified by LAM-PCR, followed by capture, ssDNA linker ligation, and an exponential amplification using primers containing illumina adapters prior to sequencing as described previously³³. Mapping and analysis of insertion sites is described previously¹⁹⁰. Briefly, following sequencing on a HiSeq 2000 or HiSeq 2500 (Illumina), insertion sites were mapped to the human genome (h19) allowing one mismatch, and intersected with RefSeq coordinates to assign insertion sites to genes. Gene regions overlapping on opposite strands were not considered for analysis, while for genes overlapping on the same strand gene names were concatenated. For each screen, gene essentiality or gene enrichment was determined by binomial test. Synthetic lethality was assessed by comparing the distribution of sense and antisense orientation integrations for each gene in the drug treated replicates with 4 wild-type control datasets previously published¹⁸⁸ (NCBI SRA accession number SRP058962) using Fisher's exact tests. A gene was considered a synthetic viable hit in the essentialome screens when it passed all Fisher's tests with a P value cut-off of 0.01, and a subtraction ratio of >0.075 (screen 1) or >0.05 (screen 2). Additionally, all genes on chromosome 8 were excluded of the analysis, as this chromosome is disomic in the Δ CAPH2 cells and could therefore not yield complete KO of a gene (as the gene-trap inserts randomly). A gene was considered a hit in the positive selection screen when it had an MI >2 and a p value of <0.05 in sgSRBD1, and a p>0.05 in sgNT, sgATR, and sgAurora B.

Plasmids

GFP-SRB1 constructs were generated in the lentiviral pTrip backbone. SRB1 was amplified from cDNA of HAP1 cells. Mutants were generated by digestions with flanking enzymes and Gibson cloning. GFP-TOP2A was also generated in the pTrip backbone by Gibson cloning two fragments of Top2A amplified from Hap1 cDNA. DOX-inducible CAPH2 expression was achieved by lentiviral infection of a pCW_pTight_CAPH2_PGK_PURO_T2A_BFP plasmid. CAPH2 was amplified from a pCI-eGFP-CAPH2 plasmid using Gibson cloning.

CRISPR-mediated generation of knockout cell-lines

Knockout cells were generated using CRISPR/Cas9 mediated genome editing (Zhang lab). Guide sequences were designed using CRISPOR design. Guides to generate knockout cell lines were targeted against exon 1-3 of the gene of interest, and subsequently cloned into the px330 vector (Addgene plasmid #42230). px330 and a donor vector containing a blasticidine resistance-cassette⁸⁵ were co-transfected in HAP1 cells and selected with 10 µg/ml blasticidin. Individual clones were selected and knockouts were confirmed using PCR to confirm integration of the blasticidin cassette at the correct locus, and by western blot analysis. The following guides were used:

Target gene (CRISPR)	Forward	Reverse
CAPH2	CACCGTTCTTGGTGAGGTCGCGGA	AAACTCCGCGACCTACCAAGAAC
SRB1	CACCGACCTGTACTTTCGCTCTTCT	AAACAGAAGAGCGAAAGTACAGGTC

AID cloning

The Hap1 tet-OsTIR1 cell line was generated and gifted by Sarah C. Moser. In short, the tet-OsTIR1-Puro cassette (pMK243, Addgene #72835) was integrated at the AAVS1 locus by targeting this locus with a CRISPR/Cas9 guide (px330). A Gblock (IDT) was designed containing c-terminal SRB1 homology arms (left and right, L-HA, R-HA, 250 bp each), with in between a linker (6 Gly), a mini-AID (mAID) sequence, a TEV site, a Halo-Tag sequence, and a 3x HA tag sequence. Insertion of the tag would lead to disruption of the sgRNA target sequence, thereby preventing re-cutting events. The Gblock was cloned into a Puc19 backbone (Gibson) using XbaI and KpnI restriction enzymes. In order to introduce this tag at the endogenous locus, HAP1 tet-OsTIR1 cells were transfected with the Puc19-SRB1-AID vector and a px459 vector containing a guide RNA targeting the c-terminus of SRB1 and Cas9. Transfections were performed according to manufacturer's protocol (FuGENE, Promega, 3:1). The vector containing CRISPR/Cas9 + a guide RNA targeting the last exon of SRB1 was used to generate a double-stranded break (DSB). By adding the Puc19-

SRBD1-AID donor vector that contained homology arms across the break site, a mini-AID, a HALO, and 3x a HA sequence, an endogenously-tagged SRBD1 would be obtained if this vector was used for homology-directed repair of the DSB. Cells were single cell plated, and clones were tested for AID integration by PCR. Subsequently, SRBD1-AID expressing clones were tested for functional SRBD1 degradation by western-blot and live cell imaging.

Target gene (CRISPR gRNA)	Forward	Reverse
SRBD1	CACCGTGTATGAGTATCCACGA	AAACTCGTGGGATACTCATAACAC

Target gene (PCR)	Forward	Reverse
SRBD1	TGTGTAGCATTGTAGAAGGAAGT	CAAGGCAGATGTTGGCAAGT
Mini-AID	AAGATCCAGCCAAACCTCCG	TTCCTCAAGTACGGTGCTCC
HALO	ATGGCAGAAATCGGTACTIONG	GCAGCGTACCCTCGATAAAA

Growth assays

HAP1 cells were plated in 96-well plates, at a density of 1500 cells/well and treated as indicated. Cells were fixed using 100% methanol, and stained for 2h at room temperature using crystal violet.

FRAP of eGFP-CAPH2 and GFP-TOP2A

Cells were plated at 70% confluency on 8-well glass-bottom dishes (LabTek) and imaged using a Deltavision deconvolution microscope (Applied Precision) equipped with a heat and CO₂ chamber. Cells were treated with siRNA's as indicated. For the eGFP-CAPH2 FRAP, HAP1 cells were transfected with an eGFP-CAPH2 containing plasmid (pCI-eGFP-CAPH2; gift from the Benjamin Rowland lab). For the GFP-TOP2A FRAP, U2OS cells expressing exogenous GFP-TOP2A were used. For DNA visualization, 250nM SiR-DNA (Spirochrome) was added 2 hours before imaging. Images were automatically acquired using a 100x (oil) objective, and a nuclear area was bleached using a 488 laser. Images were analyzed and processed using Softworx (Applied Precision) and ImageJ.

RADAR (rapid approach to DNA adduct recovery) assay

Cells were treated with etoposide (20 μ M) or ICRF-193 (10 μ M) for 30 min pre-lysis. After drug treatment, medium was removed by aspiration and cells were immediately lysed on the plate by addition of 1 ml of lysis reagent (MB buffer; 6 M GTC, 10 mM Tris-HCl (pH 6.5), 20 mM EDTA, 4% Triton X100, and 1% dithiothreitol). Thereafter, 800 μ l of the lysate was transferred to a 1.5 ml Eppendorf tube. 400 μ l (1/2 volume) of 100% ethanol was added

and briefly incubated low temperature (-20°C for 5 min). Samples were centrifuged for 15 min at maximum speed, at 4 degrees. The supernatant was aspirated, and the pellet was washed twice by vortexing in 1 ml of 75% ethanol, followed by 10 min centrifugation max speed cold in table top centrifuge. The nucleic acid pellet was promptly dissolved in 200µL of freshly made 8 mM NaOH after which samples were diluted 10x in TBS. 400µL of each sample was applied to a nitrocellulose membrane with a slot blotter (Schleicher & Scheull Minifold II) according to manufacturer's instructions. The membrane containing the samples was washed and stained with Ponceau S after which the membrane was blocked in 5% Milk in TBS. Primary antibodies (see western blot) were incubated overnight at 4 degrees Celsius in 2,5% milk/TBS solution. The next day, the membrane was washed twice with PBST and incubated for two hours with HRP-coupled secondary antibodies at RT. After 2 hours, the membrane was submerged in chemiluminiscent detection reagent and bands were visualized using a chemidoc (Biorad).

Western blot

Cells were lysed using Laemmli buffer (120 mM Tris pH 6.8, 4% SDS, 20% glycerol), and treated with drugs as indicated. Equal amounts of protein were separated on a polyacrylamide gel followed by transfer to a nitrocellulose membrane. Membranes were blocked in a 5% Milk/TBS solution. Antibodies were incubated in 2,5% milk in TBS containing 0,1% Tween. The following antibodies were used in this study: mouse anti-TOP2A (Topogen, Tg2010-1), mouse anti-TOP2B (Santa Cruz, sc-365071), rabbit anti-SRBD1 (Abcam, ab241572), rabbit anti-OstTIR1 (MBL, PD048), mouse anti-Histone H3 (Abcam, ab1791). HRP-coupled secondary antibodies (DAKO) were incubated for 2h at room temperature in a 1:2500 dilution. The immunopositive bands were visualized using Immobilon Western HRP Substrate (Millipore) and a ChemiDoc MP System (Biorad).

For immunoprecipitation, cells were cultured asynchronously or in the presence STLC for mitotic enrichment. In short, cells were harvested by trypsinization, and lysed using TNENI50-lysis buffer (50 mM Tris pH 7.5, 5 mM EDTA, 150 mM NaCl, 0.1% NP-40, protease inhibitor, phosphatase inhibitor). After 30 min incubation on ice, DNase was added for 1 hour at room-temperature. Supernatant was diluted 1:2 with TNENG (TNENI50 + 1% glycerol). Protein concentration of cell lysates was measured by Bradford assay. 1200 µg of protein was added to 30 µL anti-HA magnetic beads (Thermo Fisher), and rotated at 4 degrees Celsius over-night. Beads were washed 3 times on ice using TNENI25 (same base as TNENI50, with 125 mM NaCl, without protease/phosphatase inhibitors). For IP-MS, every condition consisted of three independent replicates.

Chromosome spreads & immunofluorescence staining

HAP1 cells were plated at 80% confluency in a 6-well plate. After cell adherence, nocodazole was added 1 hour before harvesting through mitotic shake-off. Cells were then incubated with 0.075M of KCl at 37°C for 10 minutes. Thereafter, a drop of fixative (methanol:acidic acid, in a 3:1 ratio made fresh) was added and the samples were centrifuged at 1500 rpm for 5 minutes. Supernatant was discarded and cells were fixed with 1 mL of fixative for 30 minutes. Fixative was then replaced by fixative + Dapi (1:1000). Subsequently, 15 μ L of the cell suspension was dropped from 5 cm distance onto an ethanol cleaned microscopic slide. Immunofluorescence staining was performed by incubating the cells fixed on the slide for 2 hours at room-temperature. Secondary antibodies (Molecular probes, Invitrogen) and DAPI were incubated 2 hours at room temperature. Coverslips were mounted using ProLong Gold (Invitrogen). Antibodies were incubated in PBS containing 0.1% Triton-X. The following antibodies were used in this study: human anti-Crest (Cortex Biochem, cs1058), mouse anti-ERCC6L (PICH) (Abnova, 000548421-b01p), mouse anti-TOP2A (Topogen, Tg2010-1), Janelia Fluor 549 HALO-Tag ligand (Promega), rabbit anti-TRF2 (Bethyl, A300-796A), rabbit anti-FANCD2 (Abcam, ab221932), mouse anti-yH2AX (Upstate, #05-636), rabbit anti-Geminin (Cell signaling, #52508). Edu was stained by incubating the cells fixed on the slide with Edu staining buffer (1 mM CuSO₄ in PBS), 100mM fresh ascorbic acid and Alexa Fluor-488 azide (Molecular Probes, 1:1000) for 30 minutes at room-temperature, and thereafter mounted using ProLong Gold. Images were acquired using a Deltavision deconvolution microscope (Applied Precision) with a 60x 1.40 NA oil objective. Softworx (Applied Precision), ImageJ, Adobe Photoshop and Illustrator CS6 were used to process acquired images.

For TIRF-STORM super resolution images, please refer to Leila Nahidiazar³²⁷ for a detailed protocol of buffers and settings. The following antibodies were used for super-resolution: rabbit anti-H3K4me1 (Abcam, ab8895), chicken anti-GFP (Abcam, ab13970).

Live cell imaging

Cells were plated at 70% confluency on 8-well glass-bottom dishes (LabTek) and imaged using a Deltavision deconvolution microscope (Applied Precision) equipped with a heat and CO₂ chamber. Cells were treated with drugs as indicated. For DNA visualization, 250nM SiR-DNA (Spirochrome) was added 2 hours before imaging. For SRBD1 visualization, 200 μ M Janelia Fluor 549 HALO-Tag (Promega) ligand was added together with spy505-DNA (Spirochrome) 2 hours before filming. Images were acquired every five minutes

using a 20x (0.25 NA) objective. Z stacks were acquired with 2 μm intervals. Images were analyzed and processed using Softworx (Applied Precision) and ImageJ.

Quantification and Statistical Analysis

Significant differences between treatment conditions were calculated using a Student's t test. In all figures: *, p value < 0.05; **, p value < 0.01; ***, p value < 0.001; ****, p value < 0.0001. Error bars represent standard deviation.

Acknowledgments

We would like to thank the Medema, Brummelkamp, Rowland and Jacobs labs for helpful discussions. This study was supported by funds from the Dutch Cancer Society (KWF- NKI-2015-7832), granted to R.H.M. and J.A.R.

SUPPLEMENTAL FIGURES

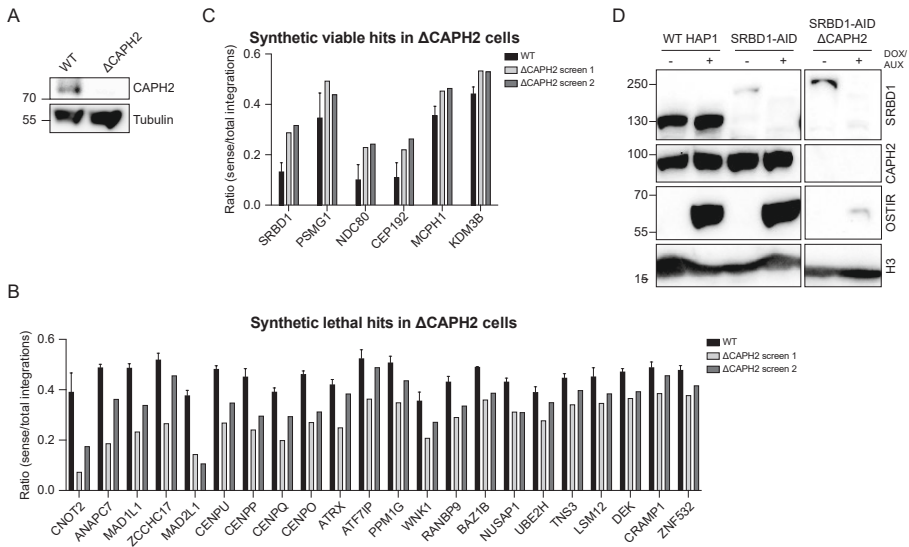


Figure S1: Haploid genetic screen in Δ CAPH2 cells.

(A) Western blot of CAPH2 and tubulin, confirming CAPH2 knock-out generation. **(B)** Bar graph showing the average ratio of sense/total integrations of synthetic lethal interactions picked up in the genetic insertional mutagenesis screen. Average ratio extracted from 4 individual screens. The ratio of the two Δ CAPH2 screens are plotted separately. The following criteria were used for hit selection: p-value < 0.01, absolute difference between WT and Δ CAPH2 ratio >0.09 (Δ CAPH2 screen 1) and >0.05 (Δ CAPH2 screen 2). **(C)** Bar graph showing the average ratio of sense/total integrations of synthetic viable interactions picked up in the genetic insertional mutagenesis screen. Average ratio extracted from 4 individual WT screens. The ratio of the two Δ CAPH2 screens are plotted separately. The following criteria were used for hit selection: p-value < 0.01, absolute difference between WT and Δ CAPH2 ratio >-0.075 (Δ CAPH2 screen 1) and >-0.05 (Δ CAPH2 screen 2). Genes on chromosome 8 were excluded, since this chromosome is disomic in Δ CAPH2 cells. **(D)** Western blot of SRBD1, CAPH2, OSTIR and histone 3 (H3), confirming CAPH2 knock-out generation in the SRBD1-AID cell line. Upon DOX/AUX addition (16h) cells express OSTIR, and SRBD1 is specifically degraded in the SRBD1-AID cell lines.

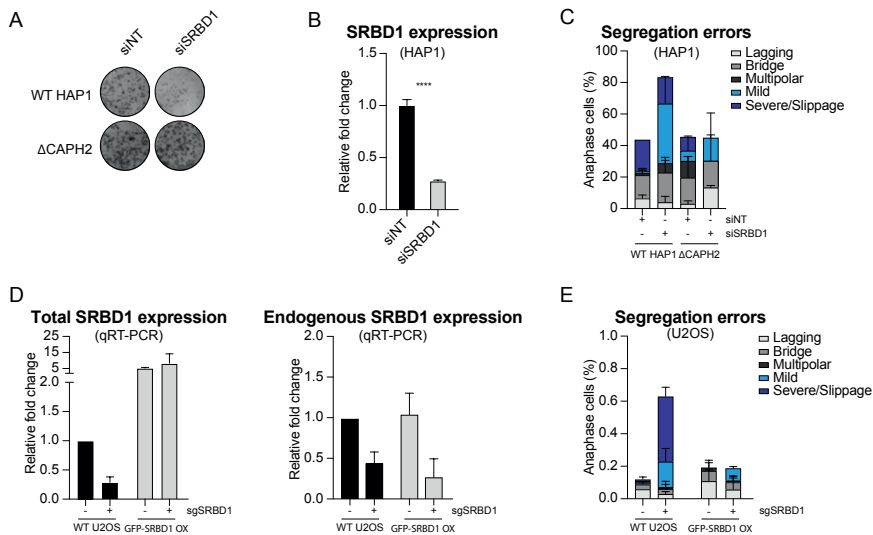


Figure S2: SRBD1 phenotype and phenotype-rescue in HAP1 and U2OS cells.

(A) Growth assay of WT HAP1 and Δ CAPH2 cells, treated with either siNT or siSRBD1 for 5 days. **(B)** Relative SRBD1 expression after siRNA mediated depletion (relative to siNT control, normalized to GAPDH expression) in HAP1 cells. Expression was measured by qRT-PCR, error bars represent standard deviation of three biological replicates from 1 experiment. **(C)** Segregation errors during anaphase of WT HAP1 and Δ CAPH2 cells, depleted of SRBD1 with siRNA. Error bars represent standard deviation of 2 independent experiments. **(D)** Relative endogenous or total SRBD1 expression after CRISPRi mediated depletion of SRBD1 (relative to uninfected control, normalized to GAPDH expression) in WT U2OS cells, or GFP-SRBD1 overexpressing U2OS cells. Expression was measured by qRT-PCR, error bars represent standard deviation of three biological replicates from 2 experiments. **(E)** Segregation errors observed during anaphase in WT U2OS cells, or U2OS cells overexpressing GFP-SRBD1, depleted of endogenous SRBD1 using CRISPRi. Error bars represent standard deviation of 2 independent experiments.

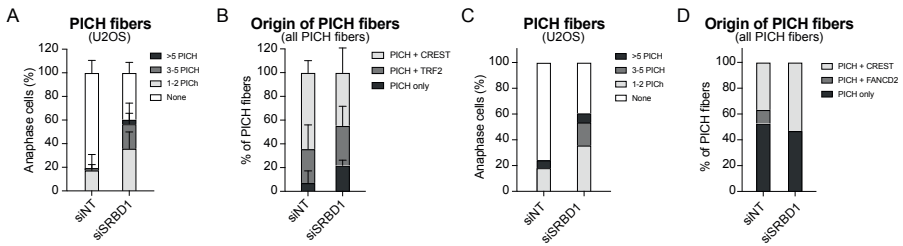


Figure S3: Origin of PICH fibers observed after SRBD1 loss

(A) Quantification of amount PICH fibers in anaphase of U2OS cells treated with siNT or siSRBD1 for 48 hours. Mean of 2 independent experiments. (B) Origin of all PICH fibers displayed in (A), determined by co-staining of PICH with centromeric marker CREST, or telomeric marker TRF2. (C) Quantification of amount PICH fibers in anaphase of U2OS cells treated with siNT or siSRBD1 for 48 hours. Data from 1 independent experiment. (D) Origin of all PICH fibers displayed in (C), determined by co-staining of PICH with centromeric marker CREST, or FANCD2 which marks UFBs originating from under-replicated regions⁵².

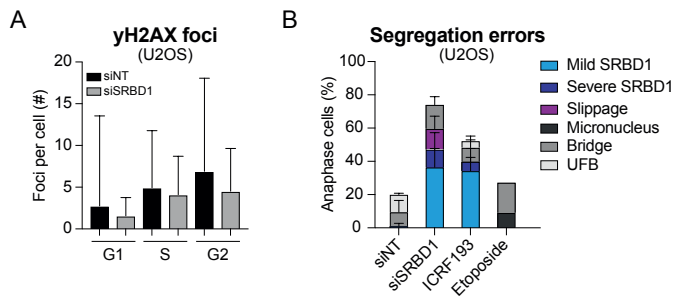


Figure S4: SRBD1 loss does not increase γ H2AX foci, and etoposide treatment does not resemble SRBD1 depletion in mitosis.

(A) DSB formation measured by immunofluorescent staining of γ H2AX in U2OS cells depleted of SRBD1 using siRNA (48h). Average and standard deviation of two independent experiments. Cell cycle was determined by co-staining of geminin (S/G2 marker) and Edu (S-phase marker). (B) Segregation errors observed during anaphase in WT U2OS cells depleted of SRBD1 using siRNA (48h), or WT U2OS cells treated with ICRF-193 (0.5 μ M added at start of live-cell imaging), or treated with etoposide (0.15 μ M added at start of live-cell imaging). Error bars represent standard deviation of 2 independent experiments. Etoposide was only taken along in one of those two experiments.



Identifying vulnerabilities of chromosomally unstable cells using haploid genetic approaches



Louise M.E. Janssen, Roy G.H.P. van Heesbeen, Ahmed M.O. Elbatsh, Abdelghani Mazouzi, Elmar Stickel, Thijn R. Brummelkamp, Benjamin D. Rowland, René H. Medema, Jonne A. Raaijmakers

ABSTRACT

To identify vulnerabilities associated with chromosomal instability (CIN), we performed several genetic screens in human haploid HAP1 cells (Chapters 2-4). In these screens, chromosomal instability (CIN) was induced using different methods; either by induction of spindle assembly checkpoint (SAC)-deficiency, induction of replication stress, or induction of chromosome condensation defects. By comparing all CIN screens, we identified 17 common genes that are essential for the survival of CIN cells, regardless of the method used to induce CIN. In addition, we found that multiple condensin II subunits become essential in both the SAC-deficient cells and the cells exposed to replication stress. We validated that loss of the condensin II subunit CAPH2, and loss of the common hit CENPO, a centromeric protein, increases sensitivity to chemical inhibition of the SAC and to replication stress-inducing drugs. Additionally, the common CIN hits were also identified in a genetic screen subjected to irradiation. This could indicate that we identified proteins involved in the DNA-damage response/repair. Alternatively, loss of any of the common hits could cause genomic instability, which then becomes synthetic lethal with CIN due to accumulative genomic instability. Taken together, we propose that increasing the level of genomic instability in CIN cells is a selective way of killing them.

INTRODUCTION

Maintaining genomic stability is important for cellular integrity, and is aided by e.g. cell cycle checkpoints and repair of DNA damage. Mutations in DNA repair genes or oncogene-induced replication stress (RS) can cause genomic instability (GIN). GIN refers to a cellular phenotype associated with the ongoing accumulation of genomic alterations, which can arise during all stages of the cell cycle. This GIN phenotype, also referred to as the “mutator phenotype³²⁸” is a specific characteristic of (pre-) cancerous cells⁵. Moreover, the ongoing accumulation of genetic alterations can promote cancer progression and therapy resistance^{25,205,329}. While GIN mostly causes mutations and small indels^{5,328}, most cancers also display larger genomic alterations involving whole or parts of chromosomes, referred to as aneuploidy (an aberrant karyotype). While aneuploidy can be stable, cancers often display unstable karyotypes. This specific form of GIN is called chromosomal instability (CIN), which is the ongoing process of segregation errors, leading to daughter cells with abnormal chromosome counts. While healthy cells rarely make mistakes during cell division⁹², a high percentage of cancer cells were shown to have high missegregation rates, but can continue to proliferate despite this CIN^{93,95}. However, when the CIN becomes too severe it can be disadvantageous, even for cancer cells¹⁴³, indicating there is a window of opportunity for cancer therapy.

Previously, we performed several screens to identify vulnerabilities of CIN cells (Chapters 2-4). We induced CIN through 3 different methods, each chosen to reflect a cancer-relevant mode of CIN. First, we deleted *Mad1* or *Mad2*^{102,162} to induce spindle assembly checkpoint (SAC)-deficiency. Although mutations in SAC genes are rare in cancer cells¹⁰⁶, SAC-deficiency clearly results in CIN¹⁰²⁻¹⁰⁴. Second, we interfered with chromosome condensation (by deletion of the condensin II subunit *CAPH2*¹¹²). Condensation defects have been found to induce segregation errors, comprising lagging chromosomes and anaphase bridges^{50,112,113,274}, and mutations in core condensin subunits are observed in cancer^{112,330}. Third, we induced CIN by treating cells with replication stress (RS)-inducing drugs, using a low dose of Aphidicolin (Aph)²⁰⁷ or Hydroxy Urea (HU)²⁰⁸. RS is frequently observed in a variety of cancers^{25,200}, and this was shown to lead to large chromosomal aberrations through induction of mitotic defects, like ultra-fine bridges (UFBs) and segregation errors^{32,38-40,52,203}. Altogether, this already illustrates that even though CIN is a cancer-specific trait^{93,95,97-100}, the causes of CIN will not be universal for all cancer cells. Since CIN is a cancer cell-specific trait, identifying common CIN vulnerabilities, that arise

independent of the mode in which CIN is induced, could yield interesting targets for (improved) anti-cancer therapies.

Therefore, we asked if we could identify common vulnerabilities of CIN, by comparing our screens that use different methods to render CIN. By comparing the data of our 4 CIN screens in human haploid HAP1 cells, we identified 17 genes that came up in all of our screens. These hits included several kinetochore proteins, ER proteins, ubiquitin ligases, a phosphatase and *RNASEH2A*. Besides these 17 genes, several subunits of the condensin II complex were identified as hits in the SAC-deficient and RS setting. In this chapter, we further validate *CAPH2* and *CENPO* as common CIN vulnerabilities. Additionally, we find hints that a common vulnerability of CIN cells is a further increase in the overall level of GIN.

RESULTS

Synthetic lethality screens identify common factors that are essential for cells that display various forms of chromosomal instability

To identify factors that are essential for the survival of CIN cells, we combined the hitlists of all previously described screens (Chapters 2-4). In every screen, CIN is induced in a different way; (1) spindle assembly checkpoint (SAC)-deficiency, (2) chromosome condensation defects or (3) enhanced RS (Fig. 1A). A gene was considered a common hit when its loss did not severely compromise cell viability in WT HAP1 cells, but did affect survival when lost in each of the CIN screens (determined by a reduced integration ratio of >0.075 compared to WT, in every CIN screen. See methods for details). Using this approach, we identified 17 genes (Fig. 1B), including several kinetochore components, endoplasmic reticulum components, ubiquitin ligases, a phosphatase and *RNASEH2A*.

Condensin II loss sensitizes cells to SAC-deficiency, RS, and IR

Besides using condensation defects as a means to induce CIN, we also found that loss of condensin II specific subunits (*NCAPH2*, *NCAPG2*, *NCAPD3*) is synthetic lethal with SAC-deficiency and enhanced RS (Fig. 1C). Condensin II is a ring-shaped protein complex involved in chromosome condensation, and has previously been implicated in chromosome alignment³³¹. This alignment function could explain why we found several condensin II subunits to be essential in SAC-deficient cells¹⁶². For our screen using condensation defects to induce CIN (Chapter 4), we had already generated *CAPH2* knockouts (Δ *CAPH2*) in HAP1 cells (Fig. 2F). Using live cell imaging, we quantified

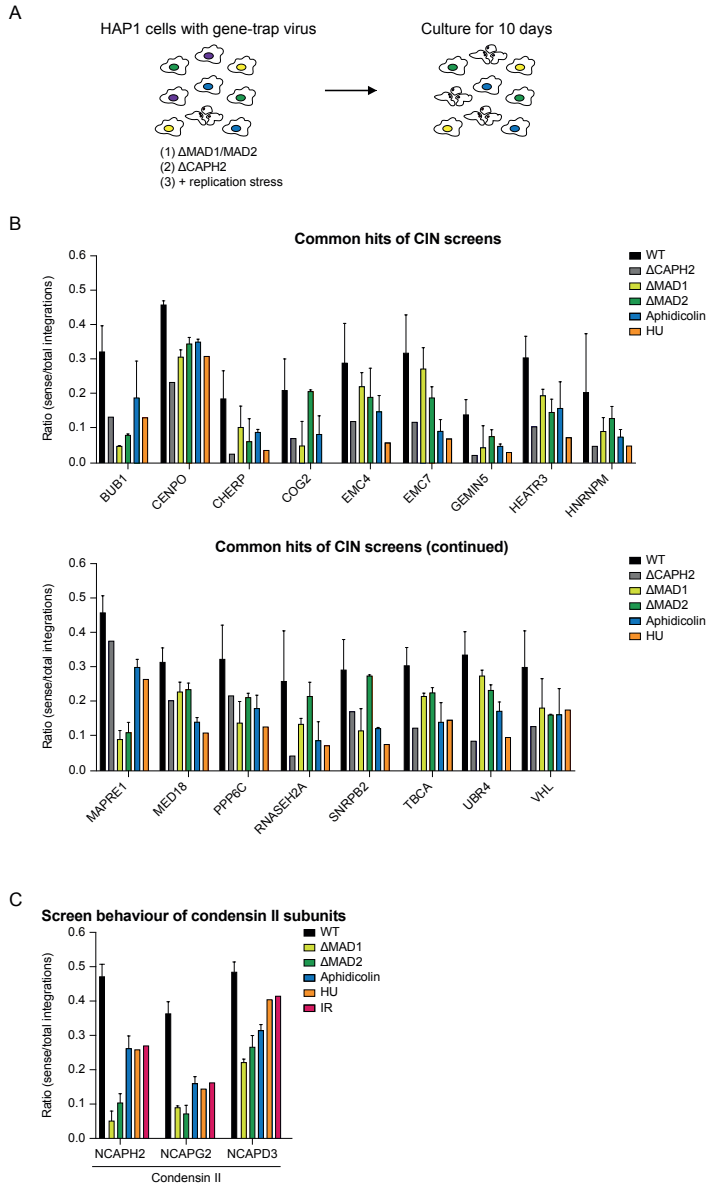


Figure 1: Synthetic lethality screens identify common factors that are essential for cells that display various forms of chromosomal instability

(A) Schematic representation of the multiple CIN screens. **(B)** Graph displaying the average ratio of sense/total integrations in WT, Δ CAPH2, Δ MAD1, Δ MAD2, or replication stressed HAP1 cells. The data are extracted from 4 individual WT screens, 1 individual Δ CAPH2 screen, 2 individual Δ MAD1 screens, 2 individual Δ MAD2 screens, 2 individual Aphidicolin screens, 1 individual HU screen and 1 individual IR screen. Graph contains 17 hits, that were selected based on a $p < 0.05$, and a subtraction ratio (ratio WT – ratio CIN-background) > 0.075 . Error bars represent SD of the individual screens. **(C)** Integration ratios of condensin II specific subunits in the CIN screens, and an irradiation screen. Error bars represent SD of the individual screens.

mitotic timing for WT HAP1 and Δ CAPH2 cells. We found that Δ CAPH2 cells spent more time in mitosis compared to WT HAP1 cells, with a delay in chromosome alignment and a delay in alignment to anaphase onset (Fig. 2A). This indicates that loss of condensin II causes chromosome congression defects in HAP1 cells. Indeed, when treated with an siRNA for Mad2 (to inactivate SAC-activity), the amount of segregation errors increased dramatically in Δ CAPH2 cells when compared to WT HAP1 cells (Fig. 2B). This could explain the observed synthetic lethality of CAPH2 loss and loss of the SAC proteins Mad1 or Mad2, since chromosome congression factors become essential upon induction of SAC-deficiency¹⁶².

Next, we aimed to explain the increased sensitivity of condensin II-deficient cells to RS. In line with previous work^{113,273,274,331,332}, Δ CAPH2 cells showed an increase in missegregations compared to WT HAP1 cells (Fig. 2B). These defects were shown to mainly involve DNA bridges, previously correlated to a function of condensin in decatenation^{45,48,273,274,332,333}. Defects in decatenation give rise to ultra-fine bridges (UFBs) in anaphase⁵². Similarly, RS is also known to induce UFBs⁵². Therefore, we hypothesized that the synthetic lethal interaction between CAPH2 loss and RS could be a consequence of an accumulation of segregation errors due to an increased number of UFBs. To test this, we measured the occurrence of UFBs in anaphase using immunofluorescent staining of PICH (a UFB marker^{40,52,215}). Untreated WT HAP1 cells showed about 8% of anaphases with at least one UFB, which increased to over 20% when treated with RS-inducing drugs (Aph or HU) for 48 hours (Fig. 2C). In untreated Δ CAPH2 cells, 25% of anaphases already harbored UFBs, which is comparable to WT HAP1 cells treated with RS-inducing drugs. This could indicate that decatenation defects in Δ CAPH2 cells and RS in WT HAP1 cells create similar levels of UFBs. Alternatively, it could suggest that loss of CAPH2 leads to RS. Interestingly, the level of UFBs was not exacerbated in Δ CAPH2 cells treated with Aph nor HU (Fig. 2C). This could be a consequence of cells not entering anaphase anymore due to too much decatenation/replication problems, which could explain the synthetic lethality. However, we were able to quantify similar numbers of anaphase cells in the UFB assay, indicating mitotic entry is not severely perturbed. Importantly, Δ CAPH2 cells were more sensitive to Aph and HU when compared to WT HAP1 cells in growth assays (Fig. 2D). This indicated that the Δ CAPH2 cells did not adapt to withstand continuous elevated levels of RS. Thus, the synthetic lethal interaction found between CAPH2 and RS might not be explained by a further increase of segregation errors. Alternatively, condensin II might have an additional function besides its well described role in mitotic chromosome condensation.

Higher organisms express two condensin complexes, condensin I and condensin II. While condensin I only gains access to the DNA after nuclear envelope breakdown (NEB), condensin II is located in the nucleus throughout the whole cell cycle³³¹. This could allow condensin II to perform additional roles, besides its function in mitotic chromosome condensation. All of the ring-shaped SMC complex protein family members, such as cohesin, SMC5/6 and condensin have previously been implicated in DNA damage repair³³⁴⁻³³⁶. A previous study hinted towards a role for condensin II in Homology Directed Repair³³⁷, known as homologous recombination (HR), but how condensin II mechanistically plays a role in HR has yet to be understood. Interestingly, our lab previously performed a screen that identified vulnerabilities of DNA lesions induced by ionizing irradiation (IR) (Feringa et al. unpublished), and the condensin II subunits were also identified as hits in this screen (Fig. 1C). This could indicate that condensin II indeed plays an important role in response to DNA damage. Indeed, Δ CAPH2 cells showed less outgrowth after 2 Gy of IR (Fig. 2E), confirming that Δ CAPH2 cells are more sensitive to IR than WT HAPI cells. Taken together, we next set out to explore a possible role for CAPH2/condensin II in the DNA damage response (DDR).

We showed that Δ CAPH2 cells are more sensitive than WT HAPI cells to RS (and IR), but do not show an increase in segregation errors when subjected to RS. Like IR, RS can inflict DNA damage^{25,32,201,214}. Therefore, we hypothesized that the increased sensitivity of Δ CAPH2 cells to RS and IR could be caused by persistent DNA-damage, for example due to a repair defect. To investigate this further, we measured phosphorylation of replication protein A (RPA) at ser4/8 (pRPA) (a readout for stalled replication forks that activate the DDR²⁴²) and γ H2AX (a DNA-damage marker¹²⁶) levels by western blot. Untreated WT HAPI and Δ CAPH2 cells did not show pRPA, and no difference was observed in γ H2AX on western blot (Fig. 2F). This indicates that Δ CAPH2 cells do not have a baseline increase in RS or DNA-damage. However, upon treatment with 1 mM of HU for 24 hours, pRPA levels increased more dramatically in Δ CAPH2 cells when compared to WT HAPI cells (Fig. 2F). In contrast, γ H2AX levels remained similar between WT HAPI and Δ CAPH2 cells after HU treatment (Fig. 2F).

The increase of pRPA could indicate persistent stretches of single stranded DNA, which could be a result of RS^{94,338}, or (defects in) resection-mediated repair^{94,338}, such as HR. Due to the previously described role for condensin II in HR³³⁷, we decided to investigate if HR-defects could explain the observed increase in pRPA. First, we tested repair-pathway dependencies in WT HAPI and Δ CAPH2 cells using growth assays in the presence of increasing doses of drugs that inhibit specific DNA-repair pathways. By inhibiting one repair pathway, cells will rely more on other pathways for double strand break (DSB) repair. For example, when

inhibiting non-homologous end joining (NHEJ), cells should rely more on HR to resolve a DSB³³⁹. We used DNA-PK inhibition (DNAPKi) to inhibit NHEJ²⁹, Rad51 inhibition (Rad51i) to inhibit HR³⁴⁰, or PARP inhibition (PARPi), which is toxic to HR-deficient cells²⁶²⁻²⁶⁴. DNA-PKi and Rad51i were combined with 2 Gy IR to activate the DDR. We did not combine IR with PARPi, since PARPi addition by itself can produce DNA lesions²⁶³. If Δ CAPH2 cells are more sensitive to DNAPKi and more sensitive to PARPi, this could hint towards a role for CAPH2 in HR. We found that Δ CAPH2 cells were not significantly more sensitive to DNA-PKi, even though a negative trend was observed (Fig. 2G). No difference in sensitivity to Rad51i was observed between WT HAPI and Δ CAPH2 cells (Fig. 2G). Similar to inhibition of DNA-Pk, Δ CAPH2 cells were not significantly more sensitive to PARPi, but a negative trend was observed (Fig. 2G/H). Given the known synthetic lethal interaction between PARPi and HR-deficiency^{262,264}, this result suggested that condensin II does not play a major role in HR. However, considering the earlier report on a possible role for condensin II in HR, combined with the small differences we observe in sensitivity to DNAPKi and PARPi, we decided to test the HR capacity of our Δ CAPH2 cells in a different manner. To this end, we made use of a well-established HR-reporter in U2OS cells³⁴¹. This DR-GFP reporter allowed us to directly measure HR-mediated repair of an I-SceI-induced DSB based on the occurrence of a GFP signal on FACS (Fig. 2I). We depleted CAPH2 with an siRNA and used non-targeting (NT), Rad51, and BRCA1 siRNAs as controls. After repair of the I-SceI-induced DSB, 34% of siNT-treated cells showed a GFP signal, generated through HR-directed repair (Fig. 2J). Upon depletion of Rad51 or BRCA1, both key players in HR^{35,38,340}, the percentage of GFP-positive cells dropped drastically (to 1% and 1.5%, respectively). Depletion of CAPH2 also reduced the percentage of GFP-positive cells when compared to siNT (a drop from 34% to 11% GFP-positive cells), but not as drastically as Rad51 or BRCA1 depletion (Fig. 2J). Importantly, loss of CAPH2 in U2OS cells affects cell viability. Therefore, after these promising preliminary results, we generated a DR-GFP reporter in the HAPI cell line, where loss of CAPH2 does not affect viability. We obtained two clones, A and B, that showed GFP-positive cells upon I-SceI-mediated DSB induction (Fig. 2K). Subsequently, we knocked out CAPH2. After allowing the repair of the I-SceI-induced DSB, we found no difference in GFP signal between WT HAPI and Δ CAPH2 DR-GFP cells (Fig. 2K). As a final approach to test HR-efficiency in Δ CAPH2 cells, we explored the occurrence of sister-chromatid exchanges (SCE) (Fig. 2L), a process that was previously reported to depend on HR factors³⁴². Our data (n=1) showed that about 50% of chromosomes in WT HAPI cells display one or more SCEs (Fig. 2M). By inhibiting HR with Rad51i, we observed a slight reduction in SCEs in WT HAPI cells (Fig. 2M). Our Δ CAPH2 cells showed reduced SCE levels compared to WT HAPI cells, and additional inhibition of HR through Rad51i did not change the SCE levels in Δ CAPH2 cells (Fig. 2M).

Altogether, our data indicate that loss of the condensin II subunit CAPH2 increases sensitivity to SAC-deficiency, RS, and IR. We propose that condensin II has dual roles; in chromosome congression and in the DDR or in replication. Our data show limited evidence to support the previously proposed role for condensin in HR. However, we did observe increased pRPA levels upon HU treatment in Δ CAPH2 cells. Instead of resected DNA, this could be indicative of stalled replication forks, eventually leading to fork collapse and DSB formation^{194,242,338}. Additional experiments are needed to determine a possible role for condensin II in the DDR and/or replication.

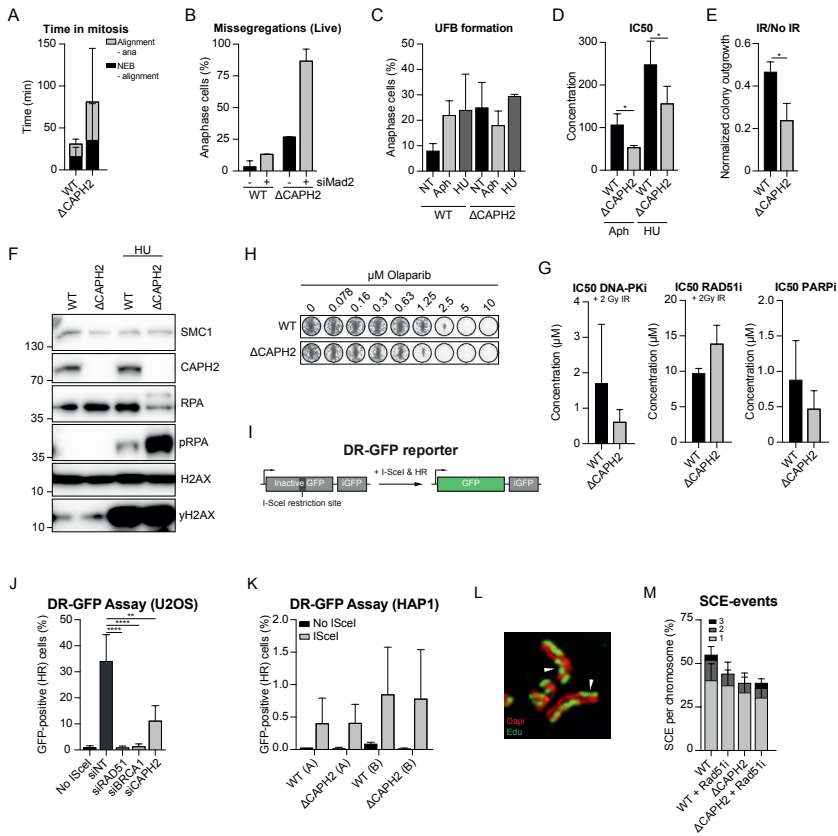


Figure 2: Condensin II loss sensitizes cells to SAC-deficiency, RS, and IR.

(A) Mitotic timing of WT HAP1 and Δ CAPH2 cells measured by live-cell imaging. (B) Segregation errors during anaphase visualized by live-cell imaging of WT HAP1 and Δ CAPH2 cells, treated with or without siRNA-mediated depletion of the SAC-component Mad2. (C) Quantification of PICH fibers in anaphase of WT HAP1 or Δ CAPH2 cells treated with 27.5 nM Aph (IC10) or 100 μ M HU (IC25) for 48 hours. Mean of 2 independent experiments, >50 cells per condition. (D) IC50 of HAP1 WT and CAPH2 knock-out cells showing increased sensitivity of CAPH2 knockouts to replication stress. Mean of 3 or 4 independent experiments of Aphidicolin (concentration in nM) or HU (concentration in μ M) respectively + SD, *

$p < 0.05$ (unpaired students t-test). **(E)** Colony outgrowth of WT HAP1 and Δ CAPH2 cells after 2 Gy of irradiation, normalized to colony outgrowth in unirradiated cells. Mean of 1 independent experiment, with 3 technical replicates, * $p < 0.05$. **(F)** Western blot of SMC1, CAPH2, RPA, ser4/8 pRPA, H2AX, and γ H2AX in WT and Δ CAPH2 HAP1 cells, with or without 24 hours of 1 mM HU treatment. **(G)** IC50 of WT HAP1 and Δ CAPH2 cells showing no significant difference in sensitivity of condensin II knockouts to PARP-inhibition (Olaparib), DNA-PK inhibition + 2 Gy IR or Rad51 inhibition + 2 Gy IR. Mean + SD of 4 independent experiments for Olaparib, and mean of 2 independent experiments for DNA-PK inhibitor and Rad51 inhibitor. All conditions ns (unpaired students t-test). **(H)** Representative colony formation assay of WT HAP1 and Δ CAPH2 cells subjected to increasing doses of Olaparib. **(I)** Schematic representation of DR-GFP assay. **(J)** DR-GFP assay performed in U2OS cells with siRNA-mediated depletion of a non-targeting (NT) control, Rad51, BRCA1 or CAPH2. Mean of 5 independent experiments + SD, ** $p < 0.01$, **** $p < 0.0001$ (unpaired students t-test). **(K)** DR-GFP assay performed in WT HAP1 and Δ CAPH2 cells. Mean of 2 independent experiments + SD. **(L)** Example of sister chromatid exchange events in mitotic spreads of HAP1 cells, stained with Dapi and Edu. **(M)** Quantification of sister chromatid exchange events, in untreated and 2 μ M Rad51 inhibitor treated, WT HAP1 and Δ CAPH2 cells. Preliminary data from 1 independent experiment, 20 mitotic spreads quantified per condition.

CENPO loss might be a common vulnerability of CIN cells

Next, we set out to validate some of the remaining common CIN hits (Fig. 1B). We selected CENPO, EMC7, and HEATR3 for further validation. First, because their integration ratio in WT HAP1 cells showed that loss of these genes was not affecting cell viability in unchallenged conditions (unlike *CHERP*, *COG2*, and *GEMIN5*). Second, they have not yet been implicated in chromosome congression or the DDR (unlike *BUB1*^{62,343-346}). In order to validate the synthetic lethal interaction found in our screens, knock-out cell lines were generated and subjected to growth assays in the presence of a monopolar spindle 1 (Mps1) inhibitor (mimicking SAC-deficiency)³⁴⁷ (Fig. 3A/B), or in the presence of Aphidicolin (Fig. 3C/D) or HU (Fig. 3E/F) to induce RS. Unfortunately, synthetic lethal interactions were not observed with EMC7 deletion, and the extent of sensitivity of Δ HEATR3 cells to the different drugs was mild. Only knock-out of CENPO showed consistent sensitivity to all three drugs. CENPO is a centromere component involved in chromosome congression³⁴⁸, which could explain why its loss sensitizes cells to Mps1 inhibition⁶². Future experiments could focus on understanding the synthetic lethal interaction between CENPO and RS. Additionally, experiments should aim to validate the synthetic lethal interaction between CENPO loss and condensation defects. Moreover, it would be important to identify which of the remainder of common hits validate, because these hits could entail additional targets for CIN+ cancer cell treatment. Interestingly, like the condensin II subunits, all the other common hits also became more essential in a genetic screen performed with IR (Fig. 3G) (Feringa et al. unpublished). This could indicate that the identified hits play a role in the DDR. Alternatively, these data could hint towards accumulative GIN being a common vulnerability of CIN cells, something that could possibly be exploited in (combination) therapies.

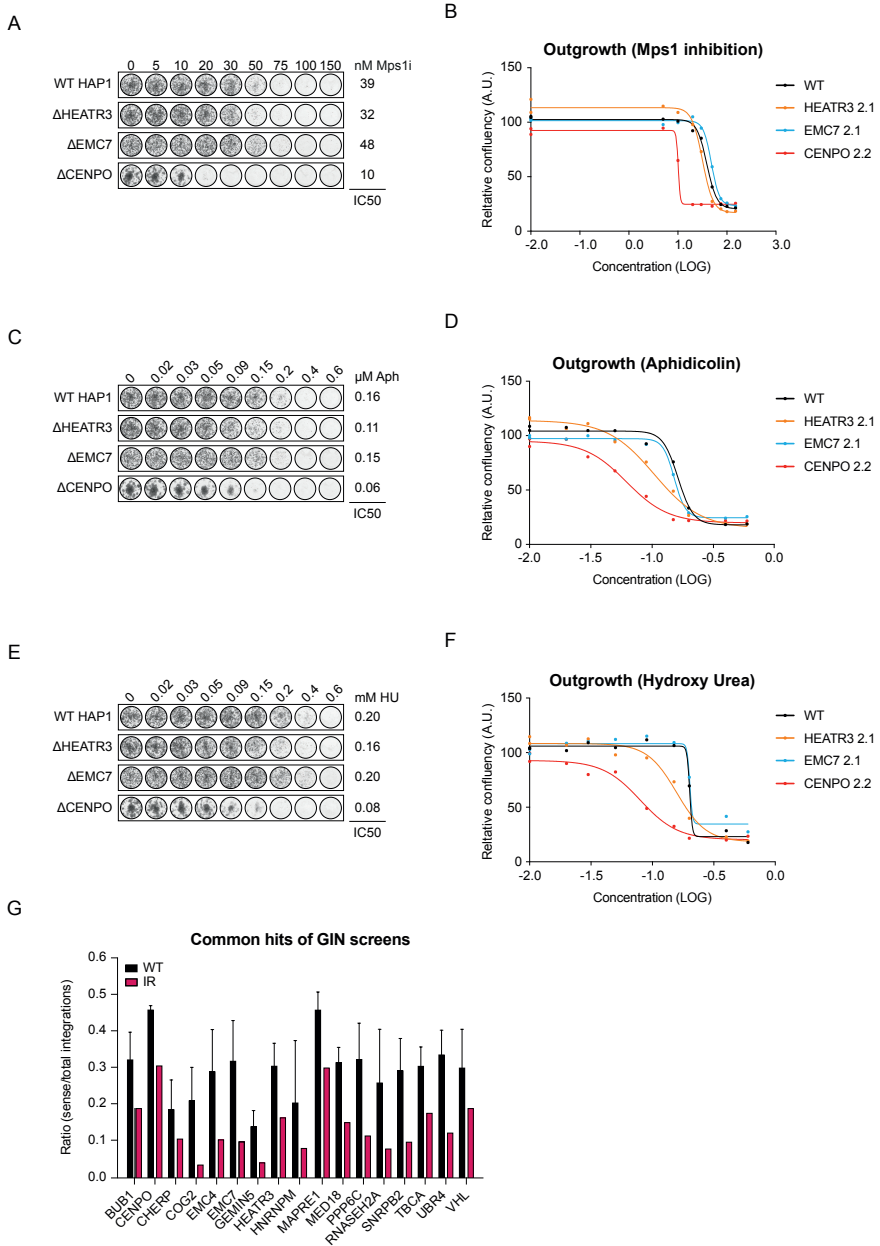


Figure 3: CENPO loss might be a common vulnerability of CIN cells.

(A, C, E) Growth assays of WT HAP1 cells, and CENPO, EMC7, and HEATR3 knock-out HAP1 cells treated with increasing doses of Mps1 inhibitor (NMS-P715), Aphidicolin or HU. IC50 concentration is annotated per cell-line, and calculated from the graphs displayed in (B, D, F). Preliminary data from 1 independent experiment. (G) Integration ratios of common hits in an irradiation screen. Error bars represent SD of the individual screens.

DISCUSSION

Genomic instability is a specific characteristic of cancer cells, which can promote tumor progression but also creates opportunities for cancer-specific vulnerabilities. One underlying cause of ongoing genomic instability is CIN^{39,95,97-100}. Here, we combined the data of multiple synthetic lethality screens to identify CIN-specific vulnerabilities. This led to a hitlist of 17 genes and to the notion that depletion of each of the individual condensin II subunits leads to sensitization to RS and SAC-deficiency.

By generating knock-outs of CAPH2, one of the accessory subunits of condensin II, we were able to confirm the synthetic lethal interaction between condensin II loss and SAC-deficiency, RS, and IR. We show that the Δ CAPH2 cells displayed increased alignment defects, leading to an increase in segregation errors during mitosis after Mad2 depletion. We showed previously that factors important for chromosome congression become essential upon SAC-deficiency¹⁶². Therefore, we believe that the increase in segregation errors explains the synthetic lethal interaction between condensin II loss, and Mad1 or Mad2 loss. Moreover, we show evidence that Δ CAPH2 cells are more sensitive to RS and IR, which could indicate a role for CAPH2 in DNA-damage repair. Due to the previously reported role of several SMC complex proteins in HR^{334-337,349}, we investigated if condensin II plays a role there. We found more ser4/8 pRPA after RS-inducing drug treatment in Δ CAPH2 cells than in WT HAP1 cells. One explanation for this data could be that loss of CAPH2 indeed causes a defect in resection-mediated repair (such as HR). The observed increase of pRPA could then reflect a failure to complete repair after initiation of DNA-end resection, causing pRPA to persist on ssDNA^{194,338}. However, our subsequent assays (chemical inhibition of different DSB repair pathways, DR-GFP and SCE) provided limited evidence that condensin II plays a role in HR. Therefore, we would like to speculate on the underlying cause of the observed synthetic lethality between condensin loss and RS.

Previously, condensin has been described to play a role in DNA decatenation^{48,50,273,274}, which could explain why we found an increase in UFBs upon CAPH2 loss. Interestingly, the level of UFBs in Δ CAPH2 cells remained stable after treatment with RS-inducing drugs. Possibly, the combination of Aph or HU treatment and defective decatenation caused by loss of condensin II is sufficient to prevent cell division, thus limiting the appearance of severe defects in anaphase. Moreover, this restrained cell division could explain the observed synthetic lethality. In order to test this hypothesis, we propose to compare the rate of mitotic entry in WT HAP1 and Δ CAPH2 cells treated with RS-inducing drugs. This

would indicate if Δ CAPH2 cells indeed stop proliferating in response to RS. To subsequently test if DNA decatenation defects could underly this synthetic lethality, we propose to test if a similar synthetic lethality can be observed between RS-inducing drugs and decatenation defects (for example by chemical inhibition of TOP2 using ICRF-193, a treatment that is known to cause decatenation problems^{53,302,308}).

Alternatively, the baseline increase in UFBs could also indicate that loss of CAPH2 causes RS^{40,52,215}. Again, limited mitotic entry might explain why we did not observe a further increase in UFBs after treatment with RS-inducing drugs. Additionally, accumulative RS in Δ CAPH2 cells after HU treatment could explain the observed increase in pRPA, and could indicate increased fork collapse^{194,338}. Our data might already be able to shed some light on this hypothesis. For example, besides the synthetic lethal interaction with HR-deficiency²⁶²⁻²⁶⁴, additional explanations for PARPi-mediated toxicity involve an interplay with replication^{263,350,351}. PARPi was shown to localize to stalled forks harboring ssDNA gaps, thereby promoting replication restart through resection³⁵⁰. Trapping of PARPi on the DNA by PARPi is shown to induce replication fork stalling and collapse^{263,350,351}. Thus, if CAPH2 loss induces RS and this is the explanation for the synthetic lethality with RS-inducing drugs, we would have expected to find a synthetic lethal interaction with the RS-inducing activities of PARPi treatment, similar to Aph or HU treatment. Moreover, it was recently shown that HR-independent SCE's can arise from under-replicated regions⁴². Following this data, we would expect SCE levels to increase if Δ CAPH2 cells would display levels of RS. Instead, we found that Δ CAPH2 cells show decreased SCE events compared to WT HAPI. This could indicate that loss of CAPH2 does not cause RS per se, or that not all Δ CAPH2 cells enter mitosis, thereby underestimating true SCE levels. If indeed not all Δ CAPH2 cells are able to enter mitosis, it would be interesting to test if SCE occurrence increases when forcing Δ CAPH2 cells into mitosis by inhibition of the RS-response kinase ATR^{64,212}. To more directly test if loss of CAPH2 causes RS, DNA fiber assays could be performed to look at replication fork progression and stability³⁵². If loss of CAPH2 indeed causes RS, it would be interesting to test CAPH2 localization to replication forks using isolation of proteins on nascent DNA (iPOND)³⁵³. If we find evidence for CAPH2 localization to replication forks, we could speculate on a role for condensin II in the RS-response.

Besides CAPH2, we followed up on three of the 17 common CIN-specific vulnerabilities; CENPO, EMC7 and HEATR3. Only the Δ CENPO cells showed increased sensitivity to both SAC-deficiency and RS. As CENPO already has proposed functions in the SAC and chromosome congression³⁵⁴, future experiments should focus on validating the synthetic lethal

interaction with RS and condensation defects. Once validated, it would be interesting to test if the segregation defects upon loss of CENPO³⁵⁴ are exacerbated upon addition of genotoxic stresses such as RS. If so, losing CENPO would create a state where segregation errors are already more prone to occur, and the further increase of these errors due to addition of genotoxic stresses could explain the synthetic lethal interaction in our screens. If no increase in missegregations is found upon RS, it could implicate that CENPO has dual roles: in alignment and for example in the RS-response, possibly similar to condensin II.

Interestingly, all the common hits were also identified as vulnerabilities in a previously performed irradiation screen that aimed to identify new regulators of the DDR (Feringa et al. unpublished). The fact that our common hits are also essential in this IR screen indicates that the DDR plays an important role during CIN. Surely, CIN can result in DNA-damage³⁶, which might explain the dependency of CIN+ cells on a well-functioning DDR. Interestingly, besides a role in chromosome congression, Bub1 has also been implicated in the DDR³⁴³⁻³⁴⁵. This could suggest that targeting genes with dual roles in the DDR and chromosome congression would be good treatment strategy to specifically kill CIN+ cells. Indeed, the combination of a Bub1 kinase inhibitor with paclitaxel, Olaparib or an ATR inhibitor has shown decreased tumor growth in a xenograft model³⁴⁴, implicating our hitlist entails potential targets for treatment combinations. Alternatively, our data could implicate that accumulative genotoxic stresses are killing CIN+ cells faster than non-CIN cells. For example, loss of CAPH2 or loss of Bub1 leads to genomic instability (condensation defects or congression defects respectively), and the addition of RS further increases that genomic instability independent of the function of CAPH2 or Bub1. This would indicate that the genes we identified will induce levels of CIN (or GIN) when lost, subsequently pushing cells over their CIN-tolerance when combined with SAC-deficiency, condensation defects, RS, or IR. This data fits with approaches currently taken in clinical trials, where combination therapies aim to overload cancer cells^{64,205}. For example, inhibition of the RS-response (ATR inhibition) combined with DNA-damage is currently of therapeutic interest^{64,65}. In this light, our hitlist might entail interesting targets that when lost, will lower the tolerance to additional CIN/GIN. Future research is needed to further validate the remaining common hitlist, and determine if the observed synthetic lethal interactions underly specific (dual) protein functions or are a consequence of genotoxic accumulation. Nonetheless, the biggest synthetic lethal interactions are found when looking at each CIN-screen separately. Therefore, cancer therapy might benefit more from identifying the underlying cause of the CIN in every cancer patient before choosing a treatment strategy, rather than relying on a common vulnerability to treat all cancer patients.

METHODS

Cell culture, siRNA transfections, and irradiation

Human derived near-haploid HAP1 cells were cultured in IMDM (GIBCO) supplemented with 10% FCS, 1% GlutaMAX supplement (GIBCO), 100 U/ml penicillin, and 100 µg/ml streptomycin. siRNA transfections were performed using RNAiMax (Invitrogen) according to the manufacture's guidelines. The following siRNAs were used in this study: siNon-Targetable (Dharmacon), siMad2 (SMARTpool ON-Targetplus Dharmacon), siCAPH2 (ON-TARGET plus NCAPH2 siRNA #9 Dharmacon), siRAD51 (SMARTpool ON-TARGETplus Dharmacon), siBRCA1 (SMARTpool ON-TARGETplus Dharmacon). All drugs (Aphidicolin, HU, PARPi (Olaparib), MPSi (NMS-P715), DNA-PKi (NU7441), Rad51i (B02) were dissolved in DMSO and used at indicated concentrations. Cells were γ -irradiated using a Gammacell Extractor (Best Theratronics) with a ¹³⁷Cs-source.

Combining haploid insertional mutagenesis screens

For details on gene-trap essentialome approaches, see Blomen et al.¹⁶¹ and Chapter 2-4 for screen details. The gene-trap randomly inserts into the genome, in either a sense (thereby inactivating the gene, equivalent to a knock-out of that gene due to the near haploid nature of this cell line) or antisense orientation (leaving gene expression intact). Therefore, cells with a sense integration in a gene that is essential for cell viability will drop out of the population. To identify the genes that are essential for cell viability upon CIN specifically, we compared the sense/total integration ratio for each gene in untreated WT HAP1 cells with the sense/total integration ratio in CIN HAP1 cells. Here, we used a subtraction ratio between WT HAP1 screens and CIN screens of >0.075 , p-value <0.05 in every screen to select CIN specific vulnerabilities. Average ratios were used from 4 WT HAP1, 2 Δ MAD1, 2 Δ MAD2, 2 aphidicolin treated, 1 HU treated, and 1 Δ CAPH2 screen.

CRISPR-mediated generation of knockout cell-lines

Knockout cells were generated using CRISPR/Cas9 mediated genome editing (Zhang lab). Guide sequences were designed using CRISPOR design. Guides to generate knockout cell lines were targeted against exon 1-3 of the gene of interest, and subsequently cloned into the pX330 vector (Addgene plasmid #42230). pX330 and a donor vector containing a blasticidine resistance-cassette¹⁹⁰ were co-transfected in HAP1 cells and selected with 10 µg/ml blasticidin. Individual clones were selected and knockouts were confirmed using PCR to confirm integration of the blasticidin cassette at the correct locus, and by western blot analysis where indicated. The following guides were used:

Target gene (CRISPR)	Forward	Reverse
CAPH2	CACCGTTCTTGGTGAGGTCGCGGA	AAACTCCGCGACCTCACCAAGAAC
CENPO	CACCGCTAGATGTGTTATCAGTCC	AAACGGACTGATAACACATCTAGC
EMC7	CACCGCAGATTTGATCCCGTTGAG	AAACCTCGAACGGGATCAAATCTGC
HEATR3	CACCGCAGGCGCACTCGCGGACCT	AAACAGGTCCGCGAGTGCGCCTGC

Growth assays

HAP1 cells were plated in 96-well plates, at a density of 1500 cells/well and treated as indicated for 5 days. After 5 days, cells were fixed using 100% methanol, and stained for 2h at room temperature using crystal violet. Subsequently, crystal violet was dissolved in 10% acetic acid, and intensity was measured using a BioTek Epoch Spectrophotometer at 595 nm. These measurements were used for IC50 calculations in PRISM, using nonlinear fit, sigmoidal, 4PL, X is log (concentration).

Colony outgrowth assay

250 HAP1 cells were plated in triplo in a 6-well plate. Plates were either left in culture, or irradiated with 2Gy. Colonies were left to grow out. Cells were fixed using 100% methanol, and stained for 2h at room temperature using crystal violet. Colonies were counted manually.

Live cell imaging

Cells were plated on 8-well glass-bottom dishes (LabTek) and imaged using a Deltavision deconvolution microscope (Applied Precision) equipped with a heat and CO2 chamber. For DNA visualization, 250nM SiR-DNA (Spirochrome) was added 2 hours before imaging. Images were acquired every five minutes using a 20x (0.25 NA) objective. Z stacks were acquired with 2 μ m intervals. Images were analyzed and processed using Softworx (Applied Precision) and ImageJ.

Immunofluorescence

Cells were grown on 9mm glass coverslips and fixed for 10 minutes at room temperature in 4% formaldehyde with 0.2% Triton X-100. The following antibodies were used: human anti-Crest (Cortex Biochem, cs1058), rabbit anti-pH3Ser10 (Campro, #07-081), mouse anti-ERCC6L (PICH) (Abnova, 000548421-b01p). All primary antibodies were incubated over night at 4°C. Secondary antibodies (Molecular probes, Invitrogen) and DAPI were incubated 2 hours at room temperature. Coverslips were mounted using ProLong Gold (Invitrogen). Images were acquired using a Deltavision deconvolution microscope (Applied Precision)

with a 60x 1.40 NA oil objective. Softworx (Applied Precision), ImageJ, Adobe Photoshop and Illustrator CS6 were used to process acquired images.

Western-blot

Cells were lysed using Laemmli buffer (120 mM Tris pH 6.8, 4% SDS, 20% glycerol), and treated with drugs as indicated. Equal amounts of protein were separated on a polyacrylamide gel followed by transfer to a nitrocellulose membrane. Membranes were blocked in a 5% Milk/TBS solution. Antibodies were incubated in 2,5% milk in TBS containing 0,1% Tween. The following antibodies were used in this study: mouse anti- γ H2AX pSer139 (Upstate, #05-636), rabbit anti-RPA pSer4/pSer8 (Novus, NBP1-23017), rabbit anti-CAPH2 (Abcam, A302-275a), rabbit anti-SMC1 (Abcam, A300-055a). HRP-coupled secondary antibodies (DAKO) were incubated for 2h at room temperature in a 1:2500 dilution. The immuno-positive bands were visualized using Immobilon Western HRP Substrate (Millipore) and a ChemiDoc MP System (Biorad).

DR-GFP assay

Details on the DR-GFP assay and protocol can be found in Gunn et al.³⁴¹. In short, DR-GFP U2OS cells were plated (with siRNA's) 3 days before I-SceI endonuclease transfection. Cells were placed in medium without antibiotics 2 hours prior to I-SceI transfection. Subsequently, I-SceI was transfected using Lipofectamine 2000 according to manufacturer's protocol. Cells were incubated for 3 hours, whereafter medium was replaced with medium containing 1:1000 triamcinolone acetone (TA), allowing the translocation of the I-SceI into the nucleus. Cells were then left to grow out for 3 additional days, before harvesting and fixation in 4% PFA + Dapi for FACS analysis of the GFP signal.

DR-GFP expressing HAP1 cells were obtained after transfection of a DR-GFP containing plasmid (Addgene #26475), using FuGENE (Promega, according to manufacturer's protocol). Single cell colonies were picked after puromycin selection. Clones were picked based on GFP-expression after following the DR-GFP assay described above.

Sister chromatid exchange

Hap1 cells were plated at 100% confluency in a 6-well plate. After cell adherence, 2 μ M Edu was added for 16 hours (all cells will go through S-phase at least once, both sister chromatids will have an Edu positive strand before going into mitosis). After 16 hours, Edu was washed away 3x using IMDM medium. Cells are then placed in Edu free medium, with or without 2 μ M Rad51i (B02) for 16 hours (second S-phase, where the new Edu

negative strand can exchange DNA with the Edu positive strand from the first S-phase). After 16 hours, nocodazole is added 1 hour before harvesting through shake-off. Cells were then incubated with 0.075M of KCl at 37°C for 10 minutes. Thereafter, a drop of fixative (methanol:acidic acid, in a 3:1 ratio made fresh) was added and the samples were centrifuged at 1500 rpm for 5 minutes. Supernatant was discarded and cells were fixed with 1 mL of fixative for 30 minutes. Fixative was then replaced by fixative + Dapi (1:1000). Subsequently, 15 μ L of the cell suspension was dropped from 5 cm distance onto an ethanol cleaned microscopic slide. Edu was stained by incubating the cells fixed on the slide with Edu staining buffer (1 mM CuSO₄ in PBS), 100mM fresh ascorbic acid and AF-488 azide (Invitrogen, 1:1000) for 30 minutes at room-temperature. After the cells were washed 2x in PBS-0.1% Tween and 1x in 100% ethanol, slides were dried and mounted with ProLong Gold (Invitrogen). Images were acquired using a Deltavision deconvolution microscope (Applied Precision) with a 100x 1.40 NA oil objective. Softworx (Applied Precision), ImageJ, Adobe Photoshop and Illustrator CS6 were used to process acquired images.

Quantification and Statistical Analysis

Significant differences between treatment conditions were calculated using a Student's t test. In all figures: *, p value < 0.05; **, p value < 0.01; ***, p value < 0.001; ****, p value < 0.0001.

Acknowledgments

We would like to thank the Medema, Brummelkamp, Rowland and Jacobs labs for helpful discussions. This study was supported by funds from the Dutch Cancer Society (KWF- NKI-2015-7832), granted to R.H.M. and J.A.R.



General discussion



Louise M.E. Janssen, René H. Medema, Jonne A. Raaijmakers

SUMMARY

During cell division, DNA needs to be duplicated and divided equally over two daughter cells. Cell division is highly controlled by cell cycle checkpoints in order to maintain tissue homeostasis. These checkpoints can be activated by DNA damage throughout the cell cycle, or faulty chromosome attachments in mitosis. Mutations or aberrant oncogenic signaling can perturb these control processes, causing carcinogenesis and contributing to tumor heterogeneity^{30,56,97-100,110-112}. Additionally, the perturbation of cell cycle checkpoints and DNA repair causes cancer cells to become genetically unstable, a state also referred to as genomic instability (GIN) and characterized by cumulative changes in the genome (e.g. mutations or aneuploidy). The fact that cancer cells thrive despite their genetic instability has been of longstanding interest, because it may yield cancer specific vulnerabilities.

In this thesis, we took multiple approaches to uncover the vulnerabilities of GIN+ cells. More precisely, we aimed to induce a specific form of GIN, chromosomal instability (CIN), in various ways. CIN, the ongoing missegregation of chromosomes, is a common cancer trait^{95,96} that causes genetic heterogeneity in a tumor^{36,93,97-100,203}. This can drive cancer evolution, leading to poor prognosis and increased therapy resistance in CIN+ tumors^{97,98,100}. By utilizing haploid genetic screens, we have mapped liabilities in several CIN-inducing backgrounds. The first pathway we hijacked to induce CIN, was the spindle-assembly checkpoint (SAC). By knock-out generation of essential components of the SAC (Mad1 and Mad2), we obtained SAC-deficient HAP1 cells, that display an elevated level of CIN. Using a haploid genetic screen approach, our lab demonstrated previously that SAC-deficiency becomes synthetic lethal with genes important for chromosome congression (not a part of this thesis). Additionally, this screen identified interesting synthetic viable interactions, addressed in this thesis. Specifically, we found that loss of Kif18A caused loss of kinetochore tension, which was associated with constitutive SAC-signaling while kinetochores were properly attached to the mitotic spindle (**chapter 2**). The persistent SAC-activation induced upon Kif18A loss, makes loss of Kif18A lethal in WT HAP1 cells, but Kif18A-depleted cells survive if the SAC is compromised. The second cancer-specific trait we exploited was replication stress, a common inducer of genomic instability in cancer^{30,56}. Moreover, replication stress has been linked to CIN^{38-40,355}. In this screen (**chapter 3**), we found hints that proper function of mitochondria might be required to cope with replication stress. Additionally, we identified several proteins with a thus far unidentified role in the replication-stress/DNA-damage response to become essential when cells endure replication stress. As a third inducer of CIN, we performed a screen in condensin II knock-

out cells. Although less common than replication stress, condensin defects are found in cancer¹¹². Moreover, condensin loss has been shown to induce chromosome bridges, thereby affecting genomic stability^{48,51,113,273,333}. Like the SAC-deficiency screen, we identified an interesting synthetic viable interaction; we found that loss of condensin II enables cells to survive upon loss of the essential protein SRBD1. We show that loss of SRBD1 causes severe anaphase defects in condensin II-proficient cells. We propose that the yet undefined role of SRBD1 lies in preventing DNA catenane formation, by limiting topoisomerase activity (**chapter 4**). As a final approach, we combined all screens in a search for common vulnerabilities of CIN+ conditions. By doing so, we identified the condensin subunit CAPH2 and the centromeric protein CENPO (**chapter 5**) as CIN-specific vulnerabilities.

Here, we will discuss our results from this thesis in relation to the current literature, and in relation to each other.

General discussion

1. Maintaining genomic stability: dividing it equally

As outlined in this thesis, genomic instability (GIN) and chromosomal instability (CIN) can have various causes. Both GIN and CIN can compromise cell viability and promote carcinogenesis^{5,356}. Thus, cells need to limit genotoxic events as much as possible. For this purpose, several checkpoints are in place. On the other hand, for an organism to survive, cells do need to duplicate even if conditions are not always optimal. Therefore, cells need to balance their decisions to either induce cell cycle arrest or tolerate low levels of GIN/CIN. In this thesis, we used haploid genetic screens to identify factors at the frontlines of this balance. By inducing CIN in several ways, we found genes that are important for survival under CIN-conditions. The uneven division of DNA due to mitotic errors (**chapter 2 and 4**), replication stress (**chapter 3**), or condensation defects (**chapter 4**), all leading to CIN, can create specific vulnerabilities. Thus, in a way, equal sharing is caring; the equal division of DNA over two daughter cells, takes care of forming healthy progeny.

2. Loss of the spindle assembly checkpoint sensitizes cells to loss of chromosome congression factors

Previously, we described the first human cell line that is viable without a functional SAC¹⁰⁵. We attribute the fact that HAPI cells can live without a functional SAC to their extremely efficient chromosome alignment^{105,357}. Using these cells, we identified Bub1 to become essential upon SAC-deficiency. We showed that loss of Bub1 does not severely affect SAC-activity, but loss of Bub1 does compromise SAC maintenance if the SAC is only partially

activated^{105,346,358}. More importantly, we found that loss of Bub1 causes chromosome congression defects, which lead to segregation errors when the SAC is lost¹⁶². Additionally, with this screen we identified similar trends in chromosome congression defects upon loss of Rod1 and several of the condensin II subunits^{162,359}. Thus, using this screen, we were able to reveal that chromosome congression factors become essential upon SAC-deficiency, indicating that CIN renders cells more sensitive to SAC-deficiency.

2.1 SAC-activity is not limited to kinetochore detachment: tension-less kinetochores can maintain/activate the SAC

Interestingly, we identified a synthetic viable interaction in the SAC-screens that we could not immediately comprehend (**chapter 2**). Loss of Kif18A, a protein with described roles in chromosome alignment^{163,165,166}, did not become more essential in SAC-deficient cells⁷⁸. The interaction we found turned out to be quite the opposite; loss of Kif18A was less detrimental in SAC-deficient cells. Given the fact that we previously showed that chromosome congression factors become essential in a SAC-deficient background, we decided to challenge the current understanding of Kif18A function. Based on our results, loss of Kif18A causes chromosome hyper-oscillations, in line with previous literature^{163,165,169,175}. However, in contrast, these hyper-oscillations did not lead to the previously described segregation errors^{163,165,166}. Additionally, we found that cell viability of Kif18A-deficient cells was rescued upon additional Mad1 or Mad2 loss, while the chromosome oscillations persisted. This further indicated that loss of Kif18A does not cause segregation defects. We found that loss of Kif18A leads to SAC activity at a subset of kinetochores (KTs). Interestingly, these SAC-signaling KT appeared to be fully attached, but showed a tension defect as measured by inter- and intra-kinetochore distance, and the absence of Astrin (normally recruited to KT-pairs once tension is established¹⁷¹). While the classic view is that the SAC is only activated at unattached KT, we observed that upon Kif18A-depletion, the majority of Mad1-positive kinetochores contained a prominent microtubule (MT) attachment. This finding disputes the model where SAC-activity is solely determined by KT-MT attachment status. It has been proposed that only lack of MT attachments allows SAC-activity, since Mps1 and microtubules (MTs) bind competitively to KT⁹⁴⁻⁸⁷¹⁷⁷. For example, it was shown that a non-phosphorylatable Hec1 mutant (HEC1-9A, which results in stable KT-MT attachment maintenance despite high Aurora B activity) could silence the SAC in conditions of low tension^{85,86}. These data fit with a model where MT detachment is needed for SAC activity, and indicate that a lack of tension is not directly sensed by the SAC. This also explains the need for the mitotic kinases Aurora B (and more recently Mps1³⁶⁰), which can revert erroneous, tensionless KT-MT attachments to unattached KT. As faulty attachments do

not create the same tension on KT-pairs as amphitelic attachments, Aurora B remains in proximity of KTs, and is able to phosphorylate KT components, making the attachment unstable. In turn, the unattached KT leads to SAC-activation and allows for proper re-attachment^{52,178}. However, the role of tension on SAC-activity in a setting where KTs are properly attached is still under debate.

Despite evidence in favor of unattached KTs as main SAC-activators, it needs to be noted that the role of tension is extremely difficult to study due to the tight interplay between tension and attachment. While it is possible to create a situation with low tension and stable MT attachments^{85,86}, creating a situation where there is tension without attachment is basically impossible. One moment where this situation occurs naturally, is when sister chromatids are split during anaphase. Here, KT-pairs are separated, and thus will lose tension while being properly connected to a MT. This setting has been used to study the effect of tension in SAC-activation⁷². By retaining the tension sensor Aurora B at centromeres throughout anaphase, this study showed that key SAC proteins (Mps1, BubR1, and Bub1) are recruited to the tensionless anaphase centromeres. Even though the recruitment of these SAC-components did not cause a substantial mitotic delay, MTs remained stably attached, indicating that tension-less kinetochore that are occupied with MTs are indeed capable of hosting SAC-proteins. Additionally, more recent evidence has shown that Mps1 is involved in error-correction in a similar manner as Aurora B³⁶⁰⁻³⁶³. This data shows that the main SAC-effector, Mps1, can sense tension-less KT-MT attachments. Moreover, this indicates that Mps1 does not always immediately compete with MTs to localize to the (unattached) KT to activate the SAC.

Resolving incorrect, tension-less, attachments ultimately requires MT-detachment to allow for proper re-attachment. Therefore, it remains difficult to pinpoint which step eventually causes SAC-activation. Our data provide strong indications that tension can also play a role in SAC-activity. By identifying a unique setting where there is a tension defect without chemically affecting MT dynamics, we were able to show that MT attached KTs under low tension display SAC-activity. We believe that KT-MT attachments in Kif8A-deficient cells are robust, since additional SAC-deficiency resulted in correct chromosome segregation. Moreover, additional SAC-deficiency rescued the cell death caused by prolonged mitotic (SAC-dependent) arrest. Together, our data dispute a model where the SAC is solely activated by unattached kinetochores.

2.2 Chromosome hyper-oscillations do not cause missegregations per se

An intriguing aspect of this data, is the fact that chromosomes hyper-oscillate upon Kif18A depletion, but do not cause missegregations. As we observe SAC-activity mainly at chromosomes outside of the metaphase plate (where tension is lowest/fluctuates most), how can it be that these chromosomes segregate normally upon SAC-deficiency? As we do not see karyotype changes, we believe the initial KT-MT attachments are made correctly (or are error-corrected). This idea is supported by the fact that Kif18A has been shown to move towards plus-ends from prometaphase to metaphase, and loss of Kif18A has been shown to affect movements of bioriented chromosomes^{163,175}. This makes it unlikely that Kif18A affects early KT-MT dynamics. The increased oscillatory movements seen upon Kif18A loss do make it more difficult to establish a steady metaphase plate, and most probably contribute to the observed tension defects. However, because the KT-MT attachments are correctly established beforehand, the pulling forces of the mitotic spindle will correctly separate the two sister chromatids over two daughter cells, albeit that the chromosomes are more spread out around the metaphase plate.

2.3 Kif18A and cancer therapy

Some recent studies have put Kif18A forward as a potential therapeutic target of CIN+ tumor cells^{6,364-366}. Taking a systematic approach with publicly available data, genetic dependencies were determined of CIN+ cancer cells (either aneuploid cancer cells or cancers cell lines displaying whole-genome doubling (WGD))^{364,365}. As could be expected from our SAC-deficiency screen, CIN+ tumor cells displayed increased sensitivity to loss of SAC-components, like *BUB1B* and *MAD2*. Additionally, both studies identified Kif18A as a common CIN-dependency^{364,365}. Moreover, in a smaller set-up, siRNA-mediated depletion was found to sensitize specifically CIN+ cell lines to Kif18A depletion³⁶⁶. These studies attribute this dependency to changes in spindle morphology or an increase in chromosomal burden in CIN+ cells. This in turn increases the chances of incorrect KT-MT attachments and chromosome missegregations upon Kif18A loss. Together, these data would support the idea that targeting Kif18A in CIN+ tumor cells could yield therapeutic benefit. However, as highlighted in this thesis (and by many others), CIN is not a homogenous phenotype^{36,93,97-100,203}. This is also reflected in the data of CIN+ dependency studies; the window of increased sensitivity is rather variable between the multiple cell lines used³⁶⁴⁻³⁶⁶. Our results indicate that complete loss of Kif18A is rather detrimental in low CIN, WT HAPI cells. Moreover, Kif18A loss is less detrimental in SAC-deficient HAPI cells that display high levels of CIN. This indicates that in certain conditions, CIN+ cells can tolerate loss of Kif18A rather well.

Altogether, our results in SAC-deficient cells and the results of the reports mentioned above do point towards one single direction: CIN+ cells are more dependent on proper SAC functioning than non-CIN cells. This is probably because SAC-deficiency increases the amount of missegregations to levels that CIN+ cells are no longer able to cope with. The difficulty for therapeutic intervention in this respect is that SAC-components are essential. Therefore, interfering with them could harbor severe side-effects (or even new cancer formation). To this end, pre-clinical studies in mice and early clinical trials have been performed using Mps1 inhibitors (as mono- or as combination therapy with microtubule interfering drugs) to inhibit SAC-activity. So far, results have included tumor regression, but also showed new aneuploidy induction, and toxicity^{367–371}. Thus, further studies are needed to understand how to play safely with fire: generating enough CIN to kill cancer cells, without severely affecting non-CIN cells.

3. Replication stress: a common cancer trait

GIN is a common cancer-specific trait. Therefore, targeting GIN has been of longstanding interest⁵. Most favorable would be to find common vulnerabilities that tackle the majority of cancer types. It is suggested that all cancer cells display some level of replication stress (RS)²⁰⁰. Moreover, it has been shown that normal cells, even highly proliferating ones, do not display high levels of RS²⁰⁵. Therefore, identifying vulnerabilities of RS could yield promising targets for cancer therapy. Efforts have already been made to specifically target RS therapeutically^{200,205,206}. To aid the identification of cancer-specific liabilities, we performed a haploid genetic screen in cells experiencing RS.

3.1 Identifying vulnerabilities of cells with replication stress

In order to identify additional RS-specific vulnerabilities, we performed a drop-out screen in cells treated with RS-inducing drugs (**chapter 3**). Using this approach, we have shown that loss of DNA-damage response (DDR) proteins compromises the survival of cells enduring RS. This data fits with approaches taken currently in pre-clinical settings, where targeting the DDR exacerbates GIN, and thereby is synthetic lethal with RS²⁰⁵. Additionally, we identified mitochondrial genes and genes with a yet undefined role in the DDR as RS-specific vulnerabilities. Determining the basis of the latter RS-specific vulnerabilities, might yield new therapeutic targets for combination strategies.

Our screen in cells experiencing RS identified several genes with described roles in the DDR (including *MDC1*, *BRIP1*, *FANCL*, *RNASEH1*, *LIG3*, and *UBR5*). This indicates that survival under RS requires a proper DDR, either for checkpoint activity and/or DNA damage repair. For example,

both Mdc1 and BRIP1 (also known as BACH1 or FANCI) have previously been implicated in the replication checkpoint^{229,253}. This checkpoint is initiated through an interaction of these proteins with the essential protein TopBP1, which has an important role in ATR-Chk1 activation²⁷. This indicates that interfering with the RS-response by limiting ATR-Chk1 activity is detrimental to cells experiencing RS, probably due to pushing these cells over their GIN-tolerance limit. In addition to replication checkpoint activation, Mdc1 and BRIP1 are also shown to play a direct role in DNA damage repair²⁵⁰⁻²⁵². This function could further compromise GIN-tolerance levels, by increasing the amount of DNA damage. In addition to the Fanconi Anemia (FA) complex member BRIP1, we also identified that loss of another FA member, FANCL, increased sensitivity to RS. While the FA members have been mainly implicated in interstrand crosslink (ICL) repair, where they work as a complex, more evidence is emerging of individual FA proteins having a role in protecting replication forks^{372,373}. This indicates once more that interfering with the RS response, in this case by losing fork protection, is specifically detrimental to cells enduring RS. Moreover, decreased fork protection could further increase GIN³⁷², and thus again push cells with RS over their tolerance limit. Taken these results together, it would be interesting to test if targeting these DDR genes leads to specific killing of cells experiencing RS. If so, targeting these proteins would be of therapeutic interest. We will come back to RS and cancer therapy in more detail in section 3.2.

It is important to note that all our RS-hits were also hits in a similar synthetic lethality screen performed in our lab, where cells were irradiated. This makes it likely that genes become essential during RS due to a role in DNA damage repair. The fact that we enrich for factors involved in the DDR complements the idea that prolonged RS causes GIN³²⁹. This is explained by the fact that prolonged RS leads to DNA damage^{25,374}, which if unrepaired forms a liability for cell survival. In the case of Mdc1, BRIP1, or FANCL loss, impaired replication checkpoint control or impaired DNA damage repair would make cells enduring RS more susceptible to DNA damage, which could explain their essential role during RS. Interestingly, other studies that aimed to identify vulnerabilities of RS also identified DNA repair proteins to be specifically essential in cells experiencing RS^{60,375,376}. For example, *CCNE1*-amplified tumors show increased sensitivity to *BRCA1* loss³⁷⁶. Another study, using an shRNA-based DDR library, *RECQL* was identified to be specifically essential during RS³⁷⁵. While our approach did not identify the same DDR factors as these studies, it strengthens our findings; cells experiencing RS are in higher need of a DDR than cells without RS. Interestingly, mapping the DNA damage response using a set of CRISPR screens in cells treated with multiple genotoxic agents, including HU, found no bias for a specific repair pathway being required during RS³⁷⁷. However, losing factors involved in ATR signaling or replication fork quality

control caused increased sensitivity to HU treatment. This implies that enhancing GIN is more important to tackle cells enduring RS than interfering with a specific DDR pathway.

Besides known DDR components, our screen also identified a large subset of mitochondrial genes to become essential during RS. Unfortunately, we were unable to indisputably confirm a synthetic lethal interaction between RS and our mitochondrial hits in follow-up experiments. First, we were unable to generate true knockouts for mitochondrial genes. Possibly due to stresses cells experience during the knockout generation, and a dependency on mitochondrial genes during these stresses. Second, experiments using acute siRNA-mediated inhibition of mitochondrial genes did not show increased sensitivity to RS inducing drugs. This could be a true effect, or due to insufficient knock-down. Third, blocking mitochondrial oxidative phosphorylation (OXPHOS) through oligomycin A treatment did not enhance sensitivity to RS-inducing drugs, indicating that OXPHOS is not critical during RS. Even though validation of mitochondrial gene dependency failed, we found evidence that RS can hamper mitochondrial metabolism. This might be part of a stress response, where RS is the stress inducer that increases the energy consumption of a cell²³⁶. Even if this is the underlying cause for the synthetic lethality found in the screen, we believe our follow up data show that mitochondrial genes might be tough to exploit therapeutically.

In addition to the mitochondrial genes, we followed up on some other hits of the RS screen. Thus far, we were able to validate that loss of *RNASEHI*, *HNRNPA2B1*, *VEZT*, *GIGYF2*, *RANBP1*, and *CDC42* increased sensitivity to RS. When following up on *HNRNPA2B1* and *GIGYF2*, we found that loss of these genes increased the baseline levels of pRPA or γ H2AX, respectively. Additionally, replication stress in both *HNRNPA2B1* and *GIGYF2* knock-out cells caused increased DNA damage compared to WT cells, which likely explains the synthetic lethal interaction found in the RS-screen. Additionally, this indicates that these genes play a role in the RS response, or in the downstream DNA repair pathway. As all our RS-hits were also identified in an irradiation screen, we propose it is most likely that *HNRNPA2B1* and *GIGYF2* play a role in DNA damage repair. It would be interesting to follow-up on where these proteins exert their function. Altogether, our data show that the biggest liability of RS is its demand for a proper DDR.

3.2 Replication stress as cancer treatment

Chemotherapeutic drugs like cisplatin (which cause ICLs), or radiotherapy (which causes DSBs), not only induce DNA damage but also increase RS²⁰⁵. While it is suggested

that exacerbating GIN in cancer cells experiencing RS would kill them, cisplatin and radiotherapy treatment have not eradicated all tumors with RS thus far. This highlights the importance of identifying additional factors in the RS/DDR response to achieve full synthetic lethality. The fact that >20% of the hits in our RS screen entailed proteins with already identified roles in the DDR, indicates that a major vulnerability of RS is the loss of DNA damage coping mechanisms. Our results indicate that exacerbating GIN in cells experiencing RS, through interfering with the RS-response or DNA damage repair, is detrimental to cells with RS. Therefore, inhibition of the RS-response by targeting ATR/Chk1, or increasing the persistence of DNA damage by interfering with DNA repair factors in cancer cells with RS could yield therapeutic benefit. Indeed, this idea has already been put forward previously^{205,329}, leading to the search for inhibitors that enhance RS/DNA-damage in cancer cells and thereby push them over the border of GIN-tolerance. For example, inhibition of the RS kinase ATR or its downstream target Chk1 will hamper the RS-response^{28,29,64,65}. This can lead to fork collapse, under-replicated DNA and DNA damage, which cause problems in subsequent mitosis²⁰⁵. Especially cancer cells with silencing mutations in other checkpoint proteins (such as p53 or ATM) are suspected to undergo mitotic catastrophe, since they will not be able to deal with the additional GIN⁶⁴. However, cancer cells might be able to utilize back-up repair mechanisms to cope with ATR/Chk1 inhibition. Therefore, pre-clinical studies have focused on combination, instead of mono-, therapies with ATR/Chk1 inhibition. For example, by combining ATR inhibitors with DNA-damaging agents, such as irradiation, PARP inhibition (Olaparib) or chemotherapy⁶⁴. In a similar fashion, inhibition of the G2/M checkpoint regulator WEE1 is also of therapeutic interest^{378,379}. By inhibiting WEE1, cells can enter mitosis with unrepaired DNA damage, for example caused by RS. WEE1 inhibition was also shown to cause cell death when combined with DNA-damaging agents, such as irradiation, cisplatin, Olaparib, but also when combined with ATR inhibition^{378,379}. While inhibiting ATR, Chk1 and WEE1 are more recent emerging approaches^{64,378,380}, these pre-clinical approaches implicate that mono-therapies are not sufficient to kill cancer cells. Therefore, our screen results might yield interesting targets to consider for combination therapy. For example, by increasing RS in cancer cells using ATR inhibition, in combination with targeting one of our screen hits. However, the response in healthy cells to such combination therapies should be tightly monitored, as RS and its associated GIN lie at the basis of *de novo* tumor formation.

4. Decatenation defects in time and space

DNA intertwines, also known as DNA catenanes, can arise during replication^{43,381,382}. Due to the action of topoisomerase II (TOP2), DNA catenanes are mostly removed during

S-phase³⁸³. Nonetheless, TOP2 is still needed in mitosis to resolve remaining DNA catenanes^{48,276}, a function that is suggested to depend on condensin function^{45,48}. While persistent DNA catenanes are a threat to genome stability³⁷, they are also used as an extra layer of sister chromatid cohesion^{24,384}. This intricate balance is important for the correct segregation of sister chromatids in mitosis^{47,48,53,274,385}. Additionally, correct DNA decatenation in mitosis prevents breakage of the DNA catenane in anaphase³⁸⁶, when sister chromatids are pulled apart. Since loss of condensin II was found to induce segregation errors, probably reflecting defects in decatenation^{45,48,50,51,113,331,333}, we used condensin II knock-out cells as a third means to induce CIN. By performing a haploid genetic screen in these condensin II knock-out cells (**chapter 4**), we identified SRBD1 as a suppressor of DNA catenanes. We find that SRBD1's actions in prophase either stimulate the resolution of catenanes, or actively prevent their formation. When SRBD1 was lost, we observed severe anaphase defects as a consequence of high levels of sister chromatid catenanes. Interestingly, this anaphase defect was rescued after additional loss of condensin II. Because we used loss of condensin II initially to mimic decatenation defects, we set out to understand this intriguing genetic interaction.

4.1 The interplay between condensin and topoisomerase II

First, we will summarize the current understanding of both condensin and TOP2, and their role in sister chromatid resolution. Condensins are ring shaped multi-protein molecules that can entrap and condense DNA through loop extrusion^{266–268,273}. Depletion of condensin has been shown to increase segregation errors and DNA bridges as a consequence of impaired sister chromatid resolution^{113,273,274}. This decatenation defect has been linked to malfunctioning of TOP2^{45,48,50,289}. Topoisomerases are a group of enzymes that can act to resolve topological problems⁴⁴. For example, human TOP2 enzymes (topoisomerase II α (TOP2A) and topoisomerase II β) can relax supercoiled DNA and decatenate DNA intertwinings. With respect to decatenation, human TOP2A (and TOP2 in yeast) has been shown to be essential for chromosome segregation due to its decatenation activity^{44,276,387,388}. The decatenation defects observed after depletion of condensin have been linked to the delocalization of TOP2^{50,286} (more specifically TOP2A in vertebrate cells, and TOP2 in yeast). Therefore, it is easy to assume that the main role of condensin in the decatenation process is to guide TOP2 to the right spot. However, condensin has also been shown to directly stimulate topoisomerase activity in *E.Coli*^{389,390}, although in eukaryotes this link seems to be less direct⁵¹. Interestingly, it has been shown that TOP2 activity increases, instead of decreases, the knotting probability of DNA^{45,289,391}. This implicates that TOP2 needs to be directed towards decatenation by external factors.

Recently, it was shown that condensin minimizes TOP2-mediated entanglements⁴⁵. Why would specifically condensin be needed for this? It is thought that by the loop-extrusion activities of condensin, DNA catenanes are tightened^{45,51,289,392,393}. The tension exerted by the loop extrusion directs the TOP2 activity towards decatenation, and not towards further entanglement. Experimental data also supports the fact that condensin activity promotes decatenation; it was shown that depletion of metaphase condensin caused newly formed DNA catenanes^{46,289}. Whether the loop-extrusion activities of condensin really direct TOP2-mediated decatenation still needs to be experimentally validated. Nevertheless, we could observe a (mild) increase in the number of ultrafine bridges in the absence of condensin II, therefore indeed suggesting that condensin II also aids in the decatenation process in HAPI cells. Identifying other factors that influence the DNA knotting balance might aid in understanding TOP2-mediated DNA (de)knotting.

4.2 SRBD1: a novel guardian of chromosomal stability

By performing a screen in condensin II (CAPH2) knock-out cells, we set out to identify players involved in proper chromosome segregation (**chapter 4**). We found that loss of the SI RNA-binding domain-containing protein 1 (SRBD1) was lethal in WT HAPI cells, but not in Δ CAPH2 cells. We observed that loss of SRBD1 caused severe anaphase defects in WT cells, resembling excessive decatenation defects. Indeed, additional loss of condensin II abolished this phenotype. This finding was unexpected, due to the described role for condensin II in sister chromatid resolution^{50,113,273,274}. Therefore, we set out to understand this unexpected interplay. We found that depletion of SRBD1 just before nuclear envelope breakdown (NEB) is sufficient to generate the anaphase defects, while depletion of SRBD1 after NEB did not create this phenotype. Interestingly, it has been shown previously that sister chromatid decatenation is largely completed by the end of prophase, and depends on both TOP2A and condensin activity³³². Where condensin is thought to aid in sister chromatid decatenation by localizing TOP2 and/or creating a decatenation-directed environment^{48,50,284,289}, our data suggests that SRBD1 also plays an important role in this pathway. While loss of SRBD1 did not seem to affect condensin function, we showed that loss of SRBD1 increased the levels of covalently bound TOP2 complexes to the DNA. This could indicate that the release function of TOP2 is affected by SRBD1 depletion, however global TOP2 dynamics did not seem to be affected based on FRAP assays. Higher levels of covalently bound TOP2 to the DNA could also be an indication of increased TOP2 enzymatic function⁴⁴, leading to an overall increase of DNA-engaged TOP2 at any given time. This increase in TOP2 activity/DNA-engagement could be a direct consequence of SRBD1 depletion, for example if TOP2 and SRBD1 bind to the DNA in a competitive manner.

Alternatively, the increase in covalently bound TOP2 complexes to the DNA could reflect a higher demand for TOP2 processing⁴⁴, for example if loss of SRBD1 increases the amount of DNA catenanes, changes the chromatin environment, or changes transcriptional activity.

In order to gain further insight in the exact function of SRBD1, we performed a positive selection screen to find factors that rescue the lethality of SRBD1 loss. Besides all the condensin II complex members, we also identified other SRBD1-specific rescue hits, involved in, but not limited to, RNA processing (*CELF1*, *TRIR*), histone acetylation (*KAT7*, *CREBBP*, *SMARCA4*), CENPA turnover (*KAT7*, *MIS18BP1*), and nuclear export (*RANBP3*, *XPO1*). Thus far, we were able to validate that loss of *CELF1*, *KAT7* and *TRIR* indeed increases cell viability in combination with SRBD1-depletion. Interestingly, *CELF1* depletion has been found previously to reduce TOP2A mRNA/protein levels³²². This indicates that reducing TOP2A levels might limit the toxic effects of DNA-bound TOP2A after SRBD1 depletion. However, we did not pick up TOP2A in the positive selection screen. This could be because TOP2A is essential for cell survival^{276,290}. Nonetheless, these results underline the importance of understanding if the increased TOP2-DNA-engagement is the underlying cause of the SRBD1-depletion phenotype. One way to experimentally test this would be to prevent TOP2A association with the DNA by for example aclarubicin treatment, and see if this would rescue the anaphase defect upon SRBD1 depletion. The observed interplay between SRBD1 and *KAT7* or *C19ORF43* might be more indirect. For example, *KAT7* was shown to deposit CENPA at the centromere by activating transcription, allowing for histone turnover³²³. While transcription requires TOP2 activity^{44,325,326}, more direct changes caused to the histone landscape upon *KAT7* loss could also underly the phenotypic rescue, for example by aiding in decatenation directionality. Further hit validation awaits, and will hopefully help us understand how loss of SRBD1 causes the observed anaphase defect.

4.3 Untangling the function of SRBD1

Altogether, our results indicate that we found a novel factor in DNA catenane biology. How exactly SRBD1 acts to prevent catenane formation, or resolve them, still needs to be elucidated. We hypothesize that the anaphase defects observed are caused by a high number of catenanes as a result of malfunctioning TOP2. First, because enzymatic inhibition of TOP2 phenocopies the loss of SRBD1. Second, because we see an increase in DNA bound TOP2 upon SRBD1 depletion. We postulate two ways in which SRBD1 loss could cause this increase: (1) by interfering with TOP2 release from the DNA, or (2) by hyper-activity of TOP2. Our data thus far do not completely support the first hypothesis. As we did not identify a direct interaction between TOP2 and SRBD1 (based on mass-

spectrometry) nor changes in TOP2 dynamics (based on FRAP), we believe SRBD1 does not play a direct role in removing TOP2 from the DNA, or at least not globally. We cannot exclude that SRBD1 fulfills such a function more locally, for example at centromeres. We propose that the observed increase in DNA-bound TOP2 reflects increased TOP2 activity or DNA-engagement upon SRBD1 loss. Keeping in mind that unlimited TOP2 activity has been shown to create massive DNA entanglements^{45,289}, cells need to have mechanisms in place to limit and direct TOP2 activity. Taken together, we hypothesize that SRBD1 normally acts to suppress TOP2 activity/DNA binding, thereby preventing erroneous (de)catenation by directing TOP2 towards decatenation. SRBD1 could do so by direct competition with TOP2 for binding to the DNA, or more indirect, for example by changing the epigenetic landscape. As a result, SRBD1's actions would limit the toxic effect that TOP2 activity can have. We propose that loss of SRBD1 and the subsequent change in TOP2 biology causes massive DNA entanglements, either due to the high TOP2 activity itself or due to a lack of directionality, leading to the severe anaphase defects observed. Loss of factors that influence TOP2 activity in turn rescue the SRBD1 phenotype. For example, loss of condensin II has been shown to cause de-localization of TOP2, and could thereby limit TOP2 engagement with the DNA and rescue the SRBD1 depletion phenotype.

In order to test if SRBD1 loss causes the anaphase phenotype due to increased TOP2 activity, we would like to test TOP2 activity of SRBD1-depleted cell lysates in kinetoplast decatenation assays. To further understand why SRBD1 loss causes increased TOP2 activity/engagement with the DNA, we would like to explore several things. If TOP2 activity is not affected, the increase in DNA-bound TOP2A could underly a more intricate defect, for example defects in direction of decatenation due to changes in the chromatin environment upon SRBD1 loss. Next, it would be important to test if the observed increase in DNA-bound TOP2 is indeed the cause of the SRBD1-depletion phenotype. For this, we would like to (chemically) interfere with TOP2 binding to the DNA to test if this rescues the observed anaphase defects after SRBD1 depletion. However, loss of TOP2A was shown to create similar anaphase defects²⁷⁸, making interpretation of these results difficult. Therefore, it might help to understand why SRBD1 loss causes increased TOP2A engagement/activity on the DNA. This could be by a direct role in topoisomerase biology, or more indirect by affecting specific genomic regions. In order to elucidate this, we aim to further study the localization pattern of SRBD1 and correlate this to genomic regions, histone marks, and topoisomerase proteins. For this, we plan to perform chromatin immunoprecipitation (ChIP) and rapid immunoprecipitation mass spectrometry of endogenous proteins (RIME) on SRBD1. This could give us more insights where SRBD1 acts, and in concert with (or exclusion of) what

proteins/chromatin environments. Moreover, we would like to further validate why our hits of the positive selection screen rescue lethality of SRBD1 depletion. Altogether, the essential role that SRBD1 plays in proper chromosome segregation is undeniable, and puts another view on how condensin and topoisomerases act during the decatenation process.

5. Combining it all: common vulnerabilities of CIN+ cells

As highlighted in this thesis, CIN is a common cancer trait and can be induced in a variety of ways. To tackle cancer cells specifically, targeting their unique vulnerabilities has been of longstanding interest. By combining our CIN screens (utilizing SAC-deficiency, RS, and condensation defects) (**chapter 5**), we aimed to find common vulnerabilities of CIN+ cells. We identified several kinetochore proteins, ER proteins, ubiquitin ligases, a phosphatase and RNASEH2A. Besides these 17 genes, subunits of the condensin II complex were hits in the SAC-deficient and RS screens. Interestingly, all the common hits were also identified as vulnerability in a previously performed irradiation screen (Feringa et al. unpublished). This indicates that the DDR is an important process in the protection of/tolerance towards CIN, regardless of the underlying CIN-mechanism. Alternatively, using this approach we might have identified genes that when lost, cause CIN/GIN. In that case, the accumulation of CIN exerted by our CIN screen-background is toxic. This would indicate that the accumulation of genotoxic stresses is a specific way to specifically kill CIN+ cancer cells.

5.1 Loss of CAPH2, CENPO or BUB1 is toxic to CIN+ cells

Even though we utilized loss of condensin II as a way to induce CIN, subunits of the condensin II complex were also identified in our SAC-deficient and RS screens. While the synthetic lethality between SAC-deficiency and condensin II loss might be attributed to the role of condensin II in chromosome congression, the interplay between condensin II and replication or DNA-damage was less clear. Since we found condensin II subunits in the RS and irradiation screen, we investigated the role of condensin II in the DDR. In yeast, condensin has previously been proposed to play a role in DNA-damage repair^{336,394}. Additionally, a previous study reported a decreased HR-efficiency upon condensin II depletion³³⁷. However, our data provided limited evidence that condensin II plays a role in HR.

How loss of condensin II sensitizes cells to RS remains to be elucidated. Condensin II depleted cells showed a base-line increase in ultra-fine bridges (UFBs), which could be the result of decatenation defects^{48,50,274} or RS^{40,52,215}. Interestingly, the amount of UFBs did not increase when condensin II depleted cells experienced RS. This could be a consequence

of cells failing to enter mitosis due to increased decatenation defects/RS, or it could indicate that there is a different cause to the synthetic lethal interaction. Therefore, it would be interesting to test if mitotic entry is affected in condensin II depleted cells enduring RS. Next, we could push cells into mitosis (for example using ATR or WEE1 inhibitors, mentioned in section 3.2), and test if this causes condensin II depleted cells to increase their UFB levels in response to RS. Interestingly, we did observe an increase in phosphorylated RPA (ser4/8) in condensin II depleted cells treated with the RS-inducing drug HU, indicative of collapsed replication forks^{194,338}. This might indicate that condensin II can prevent fork collapse, which could be the underlying cause of the synthetic lethal interaction observed. Alternatively, condensin II could aid in stabilizing broken forks/DSB, which could explain the synthetic lethal interaction observed in the RS and irradiation screen. Interestingly, previous studies have implicated functions for related SMC complexes in DNA-damage repair³³⁵. This might hint towards a similar role for condensin II. For example, the SMC1/3 containing protein complex, cohesin, is thought to aid in HR-repair by keeping the sister chromatids in close proximity of each other³³⁵, and plays a role in checkpoint activation^{335,395}. We speculate that condensin II could aid in stalled replication fork/DSB stability, for example by entrapping these structures. However, further experiments are needed to determine the cause of the synthetic lethality first.

Besides condensin II, we also identified the kinetochore protein Bub1 as a common CIN vulnerability. Interestingly, Bub1 has a proposed role in DSB-repair^{343,345}. Loss of Bub1 was found to delay DSB repair, and increase sensitivity to irradiation³⁴³. It was shown that Bub1 localizes to a DSB and promotes NHEJ³⁴⁵. Additionally, depletion of Bub1 was shown to sensitize breast cancer cells to irradiation³⁹⁶. The link between the SAC and DDR is rather complex: DNA damage is shown to activate the SAC³⁹⁷⁻⁴⁰⁰, but this could be a consequence of disrupted KT-MT attachments^{398,400,401}. As repair in mitosis is limited⁴⁰², disrupted KT-MTs could persist and increase the chance of missegregations. It could be that Bub1 plays a role in reacting to DSBs in mitosis in order to prevent CIN. However, it was also shown that Bub1 plays a role in the DDR outside of mitosis^{343,345,396}. In addition to Bub1, we also identified another kinetochore component (CENPO) as a common CIN vulnerability. We validated that CENPO knock-outs were more sensitive to SAC-deficiency (Mps1 inhibition) and RS (Aphidicolin and HU). Its enhanced sensitivity to SAC-deficiency could be explained by its established role in chromosome alignment⁴⁰³. Based on the fact that our combined hitlist seems to enrich for DDR-factors, we propose that future experiments should focus on characterizing the potential role of CENPO in the DDR.

As our SAC-deficiency screen identified players in chromosome congression and not many DDR factors, it is most likely that genes that are identified by combining all CIN screens have dual roles in CIN tolerance. For example, like Bub1, a role in chromosome congression and a different role in the DDR, thereby explaining their general requirement under many conditions. Alternatively, our common hitlist might entail factors that when lost, induce CIN. This would fit with approaches tested in pre-clinical settings^{6,63,64,205,339}, where accumulative genotoxic stresses kill (chromosomal unstable) cancer cells faster than non-CIN cells.

5.2 Targeting the DNA-damage response in cancer

As CIN is a cancer-specific characteristic⁵, and our combined CIN screens hint towards the DDR as a common vulnerability, it seems that we should target the DDR to specifically kill cancer cells⁴⁰⁴. Indeed, CIN can result in DNA damage³⁶, which might explain the dependency on DDR factors. Loss of specific DDR pathways have already proven to be clinically exploitable. A well-known example is the synthetic lethal interaction found between BRCA1/2-mutated tumors and PARP inhibitors^{262,264}. Additionally, as mentioned before, therapeutic approaches targeting the replication stress/DDR kinase ATR and its downstream target Chk1 are emerging^{64,65,404}. Interestingly, the combination of a Bub1 kinase inhibitor with paclitaxel, PARP inhibitor (Olaparib) or ATR inhibitor showed increased mitotic defects and decreased tumor growth in a xenograft model³⁴⁴. This indicates that our screens might yield therapeutic targets that could be exploited in cancer (combination) therapies. While CIN is a cancer-specific trait, the DDR is needed in all cells of our body. Therefore, targeting the DDR comes with the potential risk of severe side effects. Additionally, as PARP inhibitors are shown to work in specific tumor backgrounds, targeting the DDR as a common cancer therapy will probably not be trivial. As a way to still use the DDR as a therapeutic target, combination therapy with (local) irradiation could enhance tumor cell killing⁴⁰⁴.

Even though the tumor-specific background might influence the sensitivity to loss of DDR components, our screen results suggests that the DDR is a common Achilles' heel of CIN cells. Alternatively, the accumulation of genotoxic stresses might kill CIN+ cells faster than non-CIN cells. Besides further validating the common hitlist, it will be important to determine if the observed synthetic lethal interactions underly specific (dual) protein functions, or if they are a consequence of genotoxic accumulation. Nevertheless, the biggest synthetic lethal interactions were found when looking at each screen separately (**chapter 2-4**). Therefore, it is better to pick the optimal treatment strategy based on the underlying cause of CIN in each cancer patient, instead of relying on a common vulnerability to treat all cancer patients.



Addendum

References

Nederlandse samenvatting

Curriculum Vitae

Publication list

Acknowledgments

REFERENCES

1. Massagué, J. G1 cell-cycle control and cancer. *Nature* 2004 432:7015 **432**, 298–306 (2004).
2. Blagosklonny, M. v. & Pardee, A. B. The Restriction Point of the Cell Cycle. (2013).
3. Fragkos, M., Ganier, O., Coulombe, P. & Méchali, M. DNA replication origin activation in space and time. *Nature Reviews Molecular Cell Biology* 2015 16:6 **16**, 360–374 (2015).
4. Shaltiel, I. A., Krenning, L., Bruinsma, W. & Medema, R. H. The same, only different – DNA damage checkpoints and their reversal throughout the cell cycle. *Journal of Cell Science* **128**, 607–620 (2015).
5. Negrini, S., Gorgoulis, V. G. & Halazonetis, T. D. Genomic instability – an evolving hallmark of cancer. *Nature Reviews Molecular Cell Biology* 2010 11:3 **11**, 220–228 (2010).
6. Bielski, C. M. & Taylor, B. S. Homing in on genomic instability as a therapeutic target in cancer. *Nature Communications* **12**, (2021).
7. Blow, J. J. & Gillespie, P. J. Replication licensing and cancer--a fatal entanglement? *Nat Rev Cancer* **8**, 799–806 (2008).
8. Jackson, S. P. & Bartek, J. The DNA-damage response in human biology and disease. *Nature* **461**, 1071 (2009).
9. Chapman, J. R., Taylor, M. R. G. & Boulton, S. J. Playing the End Game: DNA Double-Strand Break Repair Pathway Choice. *Molecular Cell* **47**, 497–510 (2012).
10. Chehab, N. H., Malikzay, A., Appel, M. & Halazonetis, T. D. Chk2/hCds1 functions as a DNA damage checkpoint in G1 by stabilizing p53. *Genes & Development* **14**, 278 (2000).
11. Maréchal, A. & Zou, L. DNA Damage Sensing by the ATM and ATR Kinases. *Cold Spring Harbor Perspectives in Biology* **5**, (2013).
12. Levine, A. J. p53, the Cellular Gatekeeper for Growth and Division. *Cell* **88**, 323–331 (1997).
13. Shaltiel, I. A. *et al.* Distinct phosphatases antagonize the p53 response in different phases of the cell cycle. *Proc Natl Acad Sci U S A* **111**, 7313–7318 (2014).
14. García-Gutiérrez, L., Delgado, M. D. & León, J. MYC Oncogene Contributions to Release of Cell Cycle Brakes. *Genes (Basel)* **10**, (2019).
15. Loeb, K. R. *et al.* A mouse model for cyclin E-dependent genetic instability and tumorigenesis. *Cancer Cell* **8**, 35–47 (2005).
16. Schraml, P. *et al.* Cyclin E overexpression and amplification in human tumours. *J Pathol* **200**, 375–382 (2003).
17. Meyer, N. & Penn, L. Z. Reflecting on 25 years with MYC. *Nature Reviews Cancer* 2008 8:12 **8**, 976–990 (2008).
18. Hwang, H. C. & Clurman, B. E. Cyclin E in normal and neoplastic cell cycles. *Oncogene* 2005 24:17 **24**, 2776–2786 (2005).
19. Bochman, M. L. & Schwacha, A. The Mcm2-7 Complex Has In Vitro Helicase Activity. *Molecular Cell* **31**, 287–293 (2008).
20. Langston, L. D. & O'donnell, M. Short Review DNA Replication: Keep Moving and Don't Mind the Gap. *Molecular Cell* **23**, 155–160 (2006).
21. Burgers, P. M. J. Polymerase dynamics at the eukaryotic DNA replication fork. *J Biol Chem* **284**, 4041–4045 (2009).
22. Heller, R. C. *et al.* Eukaryotic origin-dependent DNA replication in vitro reveals sequential action of DDK and S-CDK kinases. *Cell* **146**, 80–91 (2011).
23. Haarhuis, J. H. I., Elbatsh, A. M. O. & Rowland, B. D. Cohesin and its regulation: on the logic of X-shaped chromosomes. *Dev Cell* **31**, 7–18 (2014).
24. Farcas, A. M., Uluocak, P., Helmhart, W. & Nasmyth, K. Cohesin's concatenation of sister DNAs maintains their intertwining. *Mol Cell* **44**, 97–107 (2011).
25. Zeman, M. K. & Cimprich, K. A. Causes and consequences of replication stress. *Nature Cell Biology* **16**, 2–9 (2014).
26. Zou, L. & Elledge, S. J. Sensing DNA damage through ATRIP recognition of RPA-ssDNA complexes. *Science* **300**, 1542–1548 (2003).
27. Burrows, A. E. & Elledge, S. J. How ATR turns on: TopBP1 goes on ATRIP with ATR. *Genes & Development* **22**, 1416 (2008).
28. Saldivar, J. C., Cortez, D. & Cimprich, K. A. The essential kinase ATR: ensuring faithful duplication of a challenging genome. *Nat Rev Mol Cell Biol* **18**, 622 (2017).
29. Cimprich, K. A. & Cortez, D. ATR: An essential regulator of genome integrity. *Nature Reviews Molecular Cell Biology* **9**, 616–627 (2008).
30. Zeman, M. K. & Cimprich, K. A. Causes and consequences of replication stress. *Nat Cell Biol* **16**, 2–9 (2014).
31. Neelsen, K. J. & Lopes, M. Replication fork reversal in eukaryotes: From dead end to dynamic response. *Nature Reviews Molecular Cell Biology* **16**, 207–220 (2015).
32. Petermann, E., Orta, M. L., Issaeva, N., Schultz, N. & Helleday, T. Hydroxyurea-stalled replication forks become progressively inactivated and require two different RAD51-mediated pathways for restart and repair. *Mol Cell* **37**, 492–502 (2010).
33. Kawabata, T. *et al.* Stalled Fork Rescue via Dormant Replication Origins in Unchallenged S Phase Promotes Proper Chromosome Segregation and Tumor Suppression. *Molecular Cell* **41**, 543–553 (2011).
34. Hashimoto, Y., Puddu, F. & Costanzo, V. RAD51- and MRE11-dependent reassembly of uncoupled CMG helicase complex at collapsed replication forks. *Nature Structural and Molecular Biology* **19**, 17–25 (2012).
35. Lopes, M. *et al.* The DNA replication checkpoint response stabilizes stalled replication forks. *Nature* **412**, 557–561 (2001).
36. Soto, M., Raaijmakers, J. A. & Medema, R. H. Consequences of Genomic Diversification Induced by Segregation Errors. *Trends Genet* **35**, 279–291 (2019).
37. Fernández-Casañas, M. & Chan, K.-L. The Unresolved Problem of DNA Bridging. doi:10.3390/genes9120623.

38. Wilhelm, T. *et al.* Mild replication stress causes chromosome mis-segregation via premature centriole disengagement. *Nature Communications* 2019 10:1 **10**, 1–14 (2019).
39. Burrell, R. A. *et al.* Replication stress links structural and numerical cancer chromosomal instability. *Nature* **494**, 492–496 (2013).
40. Chan, K. L., Palmai-Pallag, T., Ying, S. & Hickson, I. D. Replication stress induces sister-chromatid bridging at fragile site loci in mitosis. *Nature Cell Biology* **11**, 753–760 (2009).
41. Wang, L. *et al.* Aphidicolin-Induced FRA3B Breakpoints Cluster in Two Distinct Regions. *Genomics* **41**, 485–488 (1997).
42. Heijink, A. M. *et al.* Sister chromatid exchanges induced by perturbed replication are formed independently of homologous recombination factors. *bioRxiv* 2021.09.17.460736 (2021) doi:10.1101/2021.09.17.460736.
43. Heintzman, D. R., Campos, L. v., Byl, J. A. W., Osheroﬀ, N. & Dewar, J. M. Topoisomerase II Is Crucial for Fork Convergence during Vertebrate Replication Termination. *Cell Reports* **29**, 422–436.e5 (2019).
44. Pommier, Y., Sun, Y., Huang, S. Y. N. & Nitiss, J. L. Roles of eukaryotic topoisomerases in transcription, replication and genomic stability. *Nature Reviews Molecular Cell Biology* (2016) doi:10.1038/nrm.2016.111.
45. Dyson, S., Segura, J., Martínez-García, B., Valdés, A. & Roca, J. Condensin minimizes topoisomerase II-mediated entanglements of DNA in vivo. *The EMBO Journal* **40**, e105393 (2021).
46. Piskadlo, E., Tavares, A. & Oliveira, R. A. Metaphase chromosome structure is dynamically maintained by condensin I-directed DNA (de)catenation. *Elife* **6**, (2017).
47. Luo, K., Yuan, J., Chen, J. & Lou, Z. Topoisomerase II α controls the decatenation checkpoint. *Nature Cell Biology* **11**, 204–210 (2009).
48. Charbin, A., Bouchoux, C. & Uhlmann, F. Condensin aids sister chromatid decatenation by topoisomerase II. *Nucleic Acids Research* **42**, 340 (2014).
49. D'Ambrosio, C., Kelly, G., Shirahige, K. & Uhlmann, F. Condensin-Dependent rDNA Decatenation Introduces a Temporal Pattern to Chromosome Segregation. *Current Biology* **18**, 1084–1089 (2008).
50. Coelho, P. A., Queiroz-Machado, J. & Sunkel, C. E. Condensin-dependent localisation of topoisomerase II to an axial chromosomal structure is required for sister chromatid resolution during mitosis. *Journal of Cell Science* (2003) doi:10.1242/jcs.00799.
51. Cuylen, S. & Haering, C. H. Deciphering condensin action during chromosome segregation. *Trends in Cell Biology* **21**, 552–559 (2011).
52. Chan, K. L. & Hickson, I. D. On the origins of ultra-fine anaphase bridges. *Cell Cycle* **8**, 3065–3066 (2009).
53. Wang, L. H. C., Mayer, B., Stemmann, O. & Nigg, E. A. Centromere DNA decatenation depends on cohesin removal and is required for mammalian cell division. *J Cell Sci* **123**, 806–813 (2010).
54. Rouzeau, S. *et al.* Bloom's Syndrome and PICH Helicases Cooperate with Topoisomerase II α in Centromere Disjunction before Anaphase. *PLOS ONE* **7**, e33905 (2012).
55. Chan, Y. W., Fugger, K. & West, S. C. Unresolved recombination intermediates lead to ultra-fine anaphase bridges, chromosome breaks and aberrations. *Nat Cell Biol* **20**, 92 (2018).
56. Bester, A. C. *et al.* Nucleotide deficiency promotes genomic instability in early stages of cancer development. *Cell* **145**, 435–446 (2011).
57. Jansen-Durr, P. *et al.* Differential modulation of cyclin gene expression by MYC. *Proceedings of the National Academy of Sciences* **90**, 3685–3689 (1993).
58. Steiner, P. *et al.* Identification of a Myc-dependent step during the formation of active G1 cyclin-cdk complexes. *The EMBO Journal* **14**, 4814 (1995).
59. Jones, R. M. *et al.* Increased replication initiation and conflicts with transcription underlie Cyclin E-induced replication stress. *Oncogene* **32**, 3744–3753 (2013).
60. Benedict, B. *et al.* Loss of p53 suppresses replication-stress-induced DNA breakage in G1/S checkpoint deficient cells. *Elife* **7**, (2018).
61. Kok, Y. P. *et al.* Overexpression of Cyclin E1 or Cdc25A leads to replication stress, mitotic aberrancies, and increased sensitivity to replication checkpoint inhibitors. *Oncogenesis* 2020 9:10 **9**, 1–15 (2020).
62. Ghelli Luserna Di Rorà, A., Cerchione, C., Martinelli, G. & Simonetti, G. A WEE1 family business: regulation of mitosis, cancer progression, and therapeutic target. *Journal of Hematology & Oncology* 2020 13:1 **13**, 1–17 (2020).
63. de Witt Hamer, P. C., Mir, S. E., Noske, D., van Noorden, C. J. F. & Würdinger, T. WEE1 kinase targeting combined with DNA-damaging cancer therapy catalyzes mitotic catastrophe. *Clin Cancer Res* **17**, 4200–4207 (2011).
64. Bradbury, A., Hall, S., Curtin, N. & Drew, Y. Targeting ATR as Cancer Therapy: A new era for synthetic lethality and synergistic combinations? *Pharmacology & Therapeutics* **207**, 107450 (2020).
65. Fokas, E. *et al.* Targeting ATR in DNA damage response and cancer therapeutics. *Cancer Treat Rev* **40**, 109–117 (2014).
66. Brown, E. J. & Baltimore, D. ATR disruption leads to chromosomal fragmentation and early embryonic lethality. *Genes & Development* **14**, 397 (2000).
67. Lam, M. H., Liu, Q., Elledge, S. J. & Rosen, J. M. Chk1 is haploinsufficient for multiple functions critical to tumor suppression. *Cancer Cell* **6**, 45–59 (2004).
68. Stark, G. R. & Taylor, W. R. Analyzing the G2/M checkpoint. *Methods Mol Biol* **280**, 51–82 (2004).
69. Gibcus, J. H. *et al.* A pathway for mitotic chromosome formation. *Science* **359**, (2018).
70. Tanenbaum, M. E. & Medema, R. H. Mechanisms of Centrosome Separation and Bipolar Spindle Assembly. *Developmental Cell* **19**, 797–806 (2010).
71. Cheeseman, I. M. The Kinetochore. *Cold Spring Harbor Perspectives in Biology* **6**, (2014).
72. Musacchio, A. The Molecular Biology of Spindle Assembly Checkpoint Signaling Dynamics. *Current Biology* **25**, R1002–R1018 (2015).
73. Sacristan, C. & Kops, G. J. P. L. Joined at the hip: Kinetochores, microtubules, and spindle assembly checkpoint signaling. *Trends in Cell Biology* **25**, 21–28 (2015).



74. Cimini, D. Merotelic kinetochore orientation, aneuploidy, and cancer. *Biochimica et Biophysica Acta (BBA) – Reviews on Cancer* **1786**, 32–40 (2008).
75. Foley, E. A. & Kapoor, T. M. Microtubule attachment and spindle assembly checkpoint signalling at the kinetochore. *Nature Reviews Molecular Cell Biology* **14**, 25–37 (2013).
76. Bakhoun, S. F., Genovese, G. & Compton, D. A. Deviant kinetochore microtubule dynamics underlie chromosomal instability. *Curr Biol* **19**, 1937–1942 (2009).
77. Ertych, N. *et al.* Increased microtubule assembly rates influence chromosomal instability in colorectal cancer cells. *Nat Cell Biol* **16**, 779–791 (2014).
78. Janssen, L. M. E., Averink, T. v., Blomen, V. A. & Brummelkamp, T. R. Loss of Kif18A Results in Spindle Assembly Checkpoint Activation at Microtubule-Attached Kinetochores. *Current Biology* **28**, 2685–2696.e4 (2018).
79. Foley, E. A. & Kapoor, T. M. Microtubule attachment and spindle assembly checkpoint signalling at the kinetochore. *Nat Rev Mol Cell Biol* **14**, 25–37 (2013).
80. Yamagishi, Y., Yang, C. H., Tanno, Y. & Watanabe, Y. MPS1/Mph phosphorylates the kinetochore protein KNL1/Spc7 to recruit SAC components. *Nature Cell Biology* **2012 14:7** **14**, 746–752 (2012).
81. Musacchio, A. The Molecular Biology of Spindle Assembly Checkpoint Signaling Dynamics. *Curr Biol* **25**, R1002–R1018 (2015).
82. Sudakin, V., Chan, G. K. T. & Yen, T. J. Checkpoint inhibition of the APC/C in HeLa cells is mediated by a complex of BUBR1, BUB3, CDC20, and MAD2. *Journal of Cell Biology* **154**, 925–936 (2001).
83. Hwang, L. H. *et al.* Budding yeast Cdc20: a target of the spindle checkpoint. *Science* **279**, 1041–1044 (1998).
84. Joglekar, A. P., Bouck, D. C., Molk, J. N., Bloom, K. S. & Salmon, E. D. Molecular architecture of a kinetochore-microtubule attachment site. *Nature Cell Biology* **8**, 581–585 (2006).
85. Etemad, B., Kuijt, T. E. F. & Kops, G. J. P. L. Kinetochore-microtubule attachment is sufficient to satisfy the human spindle assembly checkpoint. *Nature Communications* **6**, 1–8 (2015).
86. Tauchman, E. C., Boehm, F. J. & DeLuca, J. G. Stable kinetochore-microtubule attachment is sufficient to silence the spindle assembly checkpoint in human cells. *Nature Communications* **6**, 1–9 (2015).
87. Ji, Z., Gao, H. & Yu, H. Kinetochore attachment sensed by competitive Mps1 and microtubule binding to Ndc80C. *Science (1979)* **348**, 1260–1264 (2015).
88. Peters, J. M. The anaphase promoting complex/cyclosome: a machine designed to destroy. *Nat Rev Mol Cell Biol* **7**, 644–656 (2006).
89. Sacristan, C. & Kops, G. J. P. L. Joined at the hip: kinetochores, microtubules, and spindle assembly checkpoint signaling. *Trends in Cell Biology* **25**, 21–28 (2015).
90. Gregan, J., Polakova, S., Zhang, L., Tolić-Nørrelykke, I. M. & Cimini, D. Merotelic kinetochore attachment: causes and effects. *Trends Cell Biol* **21**, 374–381 (2011).
91. Lampson, M. A. & Cheeseman, I. M. Sensing centromere tension: Aurora B and the regulation of kinetochore function. *Trends Cell Biol* **21**, 133–140 (2011).
92. Knouse, K. A., Wu, J., Whittaker, C. A. & Amon, A. Single cell sequencing reveals low levels of aneuploidy across mammalian tissues. *Proc Natl Acad Sci U S A* **111**, 13409–13414 (2014).
93. Naylor, R. M. & van Deursen, J. M. Aneuploidy in Cancer and Aging. *Annu Rev Genet* **50**, 45 (2016).
94. T. H. & P. H. To err (meiotically) is human: the genesis of human aneuploidy. *Nat Rev Genet* **2**, (2001).
95. Sansregret, L., Vanhaesebroeck, B. & Swanton, C. Determinants and clinical implications of chromosomal instability in cancer. *Nature Reviews Clinical Oncology* **2018 15:3** **15**, 139–150 (2018).
96. BOVERI & T. Uber mehrpolige Mitosen als Mittel zur Analyse des Zellkerns. *Verhandl Phys-med Ges (Wulzburg)* **NF 35**, 67–90 (1902).
97. Carter, S. L., Eklund, A. C., Kohane, I. S., Harris, L. N. & Szallasi, Z. A signature of chromosomal instability inferred from gene expression profiles predicts clinical outcome in multiple human cancers. *Nat Genet* **38**, 1043–1048 (2006).
98. Vargas-Rondón, N., Villegas, V. E. & Rondón-Lagos, M. The Role of Chromosomal Instability in Cancer and Therapeutic Responses. *Cancers (Basel)* **10**, (2017).
99. McClelland, S. E. & McClelland, S. E. Role of chromosomal instability in cancer progression. *Endocrine-Related Cancer* **24**, T23–T31 (2017).
100. McGranahan, N., Burrell, R. A., Endesfelder, D., Novelli, M. R. & Swanton, C. Cancer chromosomal instability: therapeutic and diagnostic challenges. *EMBO Rep* **13**, 528–538 (2012).
101. Janssen, A., Kops, G. J. P. L. & Medema, R. H. Elevating the frequency of chromosome mis-segregation as a strategy to kill tumor cells. *Proceedings of the National Academy of Sciences* **106**, 19108–19113 (2009).
102. Dobles, M., Liberal, V., Scott, M. L., Benezra, R. & Sorger, P. K. Chromosome Missegregation and Apoptosis in Mice Lacking the Mitotic Checkpoint Protein Mad2. *Cell* **101**, 635–645 (2000).
103. Folger, F. *et al.* Chromosome instability induced by Mps1 and p53 mutation generates aggressive lymphomas exhibiting aneuploidy-induced stress. *Proc Natl Acad Sci U S A* **111**, 13427–13432 (2014).
104. Kops, G. J. P. L., Foltz, D. R. & Cleveland, D. W. Lethality to human cancer cells through massive chromosome loss by inhibition of the mitotic checkpoint. *Proceedings of the National Academy of Sciences* **101**, 8699–8704 (2004).
105. Raaijmakers, J. A. *et al.* BUB1 Is Essential for the Viability of Human Cells in which the Spindle Assembly Checkpoint Is Compromised. *Cell Reports* **22**, 1424–1438 (2018).
106. Schwartzman, J. M., Sotillo, R. & Benezra, R. Mitotic chromosomal instability and cancer: mouse modelling of the human disease. *Nature Reviews Cancer* **2010 10:2** **10**, 102–115 (2010).
107. Baker, D. J. *et al.* Increased expression of BubR1 protects against aneuploidy and cancer and extends healthy lifespan. *Nat Cell Biol* **15**, 96–102 (2013).
108. Sotillo, R. *et al.* Mad2 overexpression promotes aneuploidy and tumorigenesis in mice. *Cancer Cell* **11**, 9–23 (2007).
109. Thiru, P. *et al.* Kinetochore genes are coordinately up-regulated in human tumors as part of a FoxM1-related cell division program. *Molecular Biology of the Cell* **25**, 1983 (2014).

110. Barber, T. D. *et al.* Chromatid cohesion defects may underlie chromosome instability in human colorectal cancers. *Proceedings of the National Academy of Sciences* **105**, 3443–3448 (2008).
111. Solomon, D. A. *et al.* Mutational inactivation of STAG2 causes aneuploidy in human cancer. *Science* **333**, 1039–1043 (2011).
112. Weyburne, E. & Bosco, G. Cancer-associated mutations in the condensin II subunit CAPH2 cause genomic instability through telomere dysfunction and anaphase chromosome bridges. *Journal of Cellular Physiology* **236**, 3579–3598 (2021).
113. Gerlich, D., Hirota, T., Koch, B., Peters, J. M. & Ellenberg, J. Condensin I stabilizes chromosomes mechanically through a dynamic interaction in live cells. *Curr Biol* **16**, 333–344 (2006).
114. Ganem, N. J., Godinho, S. A. & Pellman, D. A mechanism linking extra centrosomes to chromosomal instability. *Nature* 2009 460:7252 **460**, 278–282 (2009).
115. Cornforth, M. N. & Goodwin, E. H. Transmission of radiation-induced acentric chromosomal fragments to micronuclei in normal human fibroblasts. *Radiation Research* **126**, 210–217 (1991).
116. Kaye, J. A. *et al.* DNA breaks promote genomic instability by impeding proper chromosome segregation. *Current Biology* **14**, 2096–2106 (2004).
117. Bakhoum, S. F., Kabeche, L., Murnane, J. P., Zaki, B. I. & Compton, D. A. DNA-damage response during mitosis induces whole-chromosome missegregation. *Cancer Discov* **4**, 1281–1289 (2014).
118. Sheltzer, J. M. *et al.* Aneuploidy drives genomic instability in yeast. *Science* **333**, 1026–1030 (2011).
119. Passerini, V. *et al.* The presence of extra chromosomes leads to genomic instability. *Nature Communications* 2016 7:1 **7**, 1–12 (2016).
120. Chunduri, N. K. *et al.* Systems approaches identify the consequences of monosomy in somatic human cells. *Nature Communications* 2021 12:1 **12**, 1–17 (2021).
121. Hintzen, D. C. *et al.* Monosomies, trisomies and segmental aneuploidies differentially affect chromosomal stability. *bioRxiv* 2021.08.31.458318 (2021) doi:10.1101/2021.08.31.458318.
122. Nicholson, J. M. *et al.* Chromosome mis-segregation and cytokinesis failure in trisomic human cells. *Elife* **4**, (2015).
123. Oromedia, A. B., Dodgson, S. E. & Amon, A. Aneuploidy causes proteotoxic stress in yeast. *Genes Dev* **26**, 2696–2708 (2012).
124. Larrimore, K. E., Barattin-Voynova, N. S., Reid, D. W. & Ng, D. T. W. Aneuploidy-induced proteotoxic stress can be effectively tolerated without dosage compensation, genetic mutations, or stress responses. *BMC Biology* **18**, 1–19 (2020).
125. Panier, S. & Durocher, D. Push back to respond better: regulatory inhibition of the DNA double-strand break response. *Nature Reviews Molecular Cell Biology* 2013 14:10 **14**, 661–672 (2013).
126. Mah, L. J., El-Osta, A. & Karagiannis, T. C. γH2AX: a sensitive molecular marker of DNA damage and repair. *Leukemia* 2010 24:4 **24**, 679–686 (2010).
127. Tang, J. *et al.* Acetylation limits 53BP1 association with damaged chromatin to promote homologous recombination. *Nature Structural & Molecular Biology* 2013 20:3 **20**, 317–325 (2013).
128. Lieber, M. R. The mechanism of double-strand DNA break repair by the nonhomologous DNA end-joining pathway. *Annu Rev Biochem* **79**, 181–211 (2010).
129. Burma, S., Chen, B. P. C. & Chen, D. J. Role of non-homologous end joining (NHEJ) in maintaining genomic integrity. *DNA Repair (Amst)* **5**, 1042–1048 (2006).
130. Krenning, L., van den Berg, J. & Medema, R. H. Life or Death after a Break: What Determines the Choice? *Mol Cell* **76**, 346–358 (2019).
131. Sishc, B. J. & Davis, A. J. The Role of the Core Non-Homologous End Joining Factors in Carcinogenesis and Cancer. *Cancers (Basel)* **9**, (2017).
132. Symington, L. S. & Gautier, J. Double-strand break end resection and repair pathway choice. *Annu Rev Genet* **45**, 247–271 (2011).
133. van Sluis, M. & McStay, B. A localized nucleolar DNA damage response facilitates recruitment of the homology-directed repair machinery independent of cell cycle stage. *Genes Dev* **29**, 1151–1163 (2015).
134. Uziel, T. *et al.* Requirement of the MRN complex for ATM activation by DNA damage. *EMBO J* **22**, 5612–5621 (2003).
135. Davies, A. A. *et al.* Role of BRCA2 in control of the RAD51 recombination and DNA repair protein. *Mol Cell* **7**, 273–282 (2001).
136. Heyer, W. D. Recombination: Holliday Junction Resolution and Crossover Formation. *Current Biology* **14**, R56–R58 (2004).
137. Wechsler, T., Newman, S. & West, S. C. Aberrant chromosome morphology in human cells defective for Holliday junction resolution. *Nature* **471**, 642–646 (2011).
138. Prakash, R., Zhang, Y., Feng, W. & Jasin, M. Homologous Recombination and Human Health: The Roles of BRCA1, BRCA2, and Associated Proteins. *Cold Spring Harbor Perspectives in Biology* **7**, (2015).
139. Miki, Y. *et al.* A strong candidate for the breast and ovarian cancer susceptibility gene BRCA1. *Science* **266**, 66–71 (1994).
140. Wooster, R. *et al.* Identification of the breast cancer susceptibility gene BRCA2. *Nature* 1995 378:6559 **378**, 789–792 (1995).
141. Helleday, T. Homologous recombination in cancer development, treatment and development of drug resistance. *Carcinogenesis* **31**, 955–960 (2010).
142. Raaijmakers, J. A. *Mitotic spindle organization: by dynein & kinetochores.* (2014).
143. Gordon, D. J., Resio, B. & Pellman, D. Causes and consequences of aneuploidy in cancer. *Nature Reviews Genetics* **13**, 189–203 (2012).
144. Lara-Gonzalez, P., Westhorpe, F. G. & Taylor, S. S. The spindle assembly checkpoint. *Curr Biol* **22**, (2012).
145. Yamagishi, Y., Yang, C. H., Tanno, Y. & Watanabe, Y. MPS1/Mph1 phosphorylates the kinetochore protein KNL1/Spc7 to recruit SAC components. *Nature Cell Biology* **14**, 746–752 (2012).

146. Kulukian, A., Han, J. S. & Cleveland, D. W. Unattached Kinetochores Catalyze Production of an Anaphase Inhibitor that Requires a Mad2 Template to Prime Cdc20 for BubR1 Binding. *Developmental Cell* **16**, 105–117 (2009).
147. Han, J. S. *et al.* Catalytic assembly of the mitotic checkpoint inhibitor BubR1–Cdc20 by a Mad2-induced functional switch in Cdc20. *Mol Cell* **51**, 92–104 (2013).
148. Alfieri, C. *et al.* Molecular basis of APC/C regulation by the spindle assembly checkpoint. *Nature* **536**, 431–436 (2016).
149. Acquaviva, C. & Pines, J. The anaphase-promoting complex/cyclosome: APC/C. *Journal of Cell Science* **119**, 2401–2404 (2006).
150. Akeru, T. & Watanabe, Y. The spindle assembly checkpoint promotes chromosome bi-orientation: A novel Mad1 role in chromosome alignment. *Cell Cycle* **15**, 493–497 (2016).
151. Knowlton, A. L., Lan, W. & Stukenberg, P. T. Aurora B is enriched at merotelic attachment sites, where it regulates MCAK. *Curr Biol* **16**, 1705–1710 (2006).
152. Cimini, D. Detection and correction of merotelic kinetochore orientation by Aurora B and its partners. *Cell Cycle* **6**, 1558–1564 (2007).
153. Biggins, S. & Murray, A. W. The budding yeast protein kinase Ipl1/Aurora allows the absence of tension to activate the spindle checkpoint. *Genes & Development* **15**, 3118 (2001).
154. Rieder, C. L., Cole, R. W., Khodjakov, A. & Sluder, G. The checkpoint delaying anaphase in response to chromosome monoorientation is mediated by an inhibitory signal produced by unattached kinetochores. *J Cell Biol* **130**, 941–948 (1995).
155. Waters, J. C., Chen, R. H., Murray, A. W. & Salmon, E. D. Localization of Mad2 to kinetochores depends on microtubule attachment, not tension. *J Cell Biol* **141**, 1181–1191 (1998).
156. Mansfeld, J., Collin, P., Collins, M. O., Choudhary, J. S. & Pines, J. APC15 drives the turnover of MCC-CDC20 to make the spindle assembly checkpoint responsive to kinetochore attachment. *Nature Cell Biology* **13**, 1234–1243 (2011).
157. Jin, F. & Wang, Y. The signaling network that silences the spindle assembly checkpoint upon the establishment of chromosome bipolar attachment. *Proc Natl Acad Sci U S A* **110**, 21036–21041 (2013).
158. Zhou, J., Yao, J. & Joshi, H. C. Attachment and tension in the spindle assembly checkpoint. *J Cell Sci* **115**, 3547–3555 (2002).
159. Nicklas, R. B., Waters, J. C., Salmon, E. D. & Ward, S. C. Checkpoint signals in grasshopper meiosis are sensitive to microtubule attachment, but tension is still essential. *J Cell Sci* **114**, 4173–4183 (2001).
160. Shannon, K. B., Canman, J. C. & Salmon, E. D. Mad2 and BubR1 function in a single checkpoint pathway that responds to a loss of tension. *Mol Biol Cell* **13**, 3706–3719 (2002).
161. Blomen, V. A. *et al.* Gene essentiality and synthetic lethality in haploid human cells. *Science* (1979) **350**, 1092–1096 (2015).
162. Raaijmakers, J. A. *et al.* BUB1 Is Essential for the Viability of Human Cells in which the Spindle Assembly Checkpoint Is Compromised. *Cell Rep* **22**, 1424–1438 (2018).
163. Mayr, M. I. *et al.* The Human Kinesin Kif18A Is a Motile Microtubule Depolymerase Essential for Chromosome Congression. *Current Biology* **17**, 488–498 (2007).
164. Du, Y., English, C. A. & Ohi, R. The Kinesin-8 Kif18A Dampens Microtubule Plus-End Dynamics. *Current Biology* **20**, 374–380 (2010).
165. Höfner, J., Mayr, M. I., Möckel, M. M. & Mayer, T. U. Pre-anaphase chromosome oscillations are regulated by the antagonistic activities of Cdk1 and PPI on Kif18A. *Nature Communications* **5**, 1–14 (2014).
166. Manning, A. L. *et al.* CLASPI, astrin and Kif2b form a molecular switch that regulates kinetochore-microtubule dynamics to promote mitotic progression and fidelity. *EMBO Journal* **29**, 3531–3543 (2010).
167. Brito, D. A. & Rieder, C. L. Mitotic Checkpoint Slippage in Humans Occurs via Cyclin B Destruction in the Presence of an Active Checkpoint. *Current Biology* **16**, 1194–1200 (2006).
168. Czechanski, A. *et al.* Kif18a is specifically required for mitotic progression during germ line development. *Developmental Biology* **402**, 253–262 (2015).
169. Stumpff, J., Wagenbach, M., Franck, A., Asbury, C. L. & Wordeman, L. Kif18A and Chromokinesins Confine Centromere Movements via Microtubule Growth Suppression and Spatial Control of Kinetochore Tension. *Developmental Cell* **22**, 1017–1029 (2012).
170. Maresca, T. J. & Salmon, E. D. Intrakinetochores stretch is associated with changes in kinetochore phosphorylation and spindle assembly checkpoint activity. *Journal of Cell Biology* **184**, 373–381 (2009).
171. Schmidt, J. C. *et al.* Aurora B kinase controls the targeting of the Astrin–SKAP complex to bi-oriented kinetochores. *Journal of Cell Biology* **191**, 269–280 (2010).
172. Vázquez-Novelle, M. D. & Petronczki, M. Relocation of the Chromosomal Passenger Complex Prevents Mitotic Checkpoint Engagement at Anaphase. *Current Biology* **20**, 1402–1407 (2010).
173. Kajtez, J. *et al.* Overlap microtubules link sister k-fibres and balance the forces on bi-oriented kinetochores. *Nature Communications* **7**, (2016).
174. Stumpff, J. *et al.* A Tethering Mechanism Controls the Processivity and Kinetochore–Microtubule Plus-End Enrichment of the Kinesin-8 Kif18A. *Molecular Cell* **43**, 764–775 (2011).
175. Stumpff, J., von Dassow, G., Wagenbach, M., Asbury, C. & Wordeman, L. The Kinesin-8 Motor Kif18A Suppresses Kinetochore Movements to Control Mitotic Chromosome Alignment. *Developmental Cell* **14**, 252–262 (2008).
176. Ji, Z., Gao, H. & Yu, H. CELL DIVISION CYCLE. Kinetochore attachment sensed by competitive Mps1 and microtubule binding to Ndc80C. *Science* **348**, 1260–1264 (2015).
177. Hiruma, Y. *et al.* Competition between MPS1 and microtubules at kinetochores regulates spindle checkpoint signaling. *Science* (1979) **348**, 1264–1267 (2015).
178. Krenn, V. & Musacchio, A. The Aurora B kinase in chromosome bi-orientation and spindle checkpoint signaling. *Frontiers in Oncology* **5**, (2015).

179. Logarinho, E. *et al.* Different spindle checkpoint proteins monitor microtubule attachment and tension at kinetochores in *Drosophila* cells. *J Cell Sci* **117**, 1757–1771 (2004).
180. Musacchio, A. & Salmon, E. D. The spindle-assembly checkpoint in space and time. *Nature Reviews Molecular Cell Biology* **8**, 379–393 (2007).
181. King, J. M. & Nicklas, R. B. Tension on chromosomes increases the number of kinetochore microtubules but only within limits. *Journal of Cell Science* **113**, 3815–3823 (2000).
182. Shonn, M. A., McCarroll, R. & Murray, A. W. Requirement of the spindle checkpoint for proper chromosome segregation in budding yeast meiosis. *Science* **289**, 300–303 (2000).
183. Stern, B. M. & Murray, A. W. Lack of tension at kinetochores activates the spindle checkpoint in budding yeast. *Current Biology* **11**, 1462–1467 (2001).
184. Kuhn, J. & Dumont, S. Spindle assembly checkpoint satisfaction occurs via end-on but not lateral attachments under tension. *Journal of Cell Biology* **216**, 1533–1542 (2017).
185. Kim, H. & Stumpff, J. Kif18A promotes Hec1 dephosphorylation to coordinate chromosome alignment with kinetochore microtubule attachment. *bioRxiv* 304147 (2018) doi:10.1101/304147.
186. Jae, L. T. *et al.* Deciphering the glycosylome of dystroglycanopathies using haploid screens for lassa virus entry. *Science* **340**, 479–483 (2013).
187. Langmead, B., Trapnell, C., Pop, M. & Salzberg, S. L. Ultrafast and memory-efficient alignment of short DNA sequences to the human genome. *Genome Biology* **10**, (2009).
188. Quinlan, A. R. & Hall, I. M. BEDTools: a flexible suite of utilities for comparing genomic features. *Bioinformatics* **26**, 841 (2010).
189. Cong, L. *et al.* Multiplex genome engineering using CRISPR/Cas systems. *Science* **339**, 819–823 (2013).
190. Lockner, D. H. *et al.* A generic strategy for CRISPR-Cas9-mediated gene tagging. *Nature Communications* **6**, 4–10 (2015).
191. Koch, A., Maia, A., Janssen, A. & Medema, R. H. Molecular basis underlying resistance to Mps1/TTK inhibitors. *Oncogene* **35**, 2518–2528 (2016).
192. Burgers, P. M. J. Polymerase dynamics at the eukaryotic DNA replication fork. *J Biol Chem* **284**, 4041–4045 (2009).
193. Byun, T. S., Pacek, M., Yee, M. C., Walter, J. C. & Cimprich, K. A. Functional uncoupling of MCM helicase and DNA polymerase activities activates the ATR-dependent checkpoint. *Genes Dev* **19**, 1040–1052 (2005).
194. Maréchal, A. & Zou, L. RPA-coated single-stranded DNA as a platform for post-translational modifications in the DNA damage response. *Nature Publishing Group* **25**, 9–23 (2015).
195. Woodward, A. M. *et al.* Excess Mcm2–7 license dormant origins of replication that can be used under conditions of replicative stress. *Journal of Cell Biology* **173**, 673–683 (2006).
196. Ge, X. Q., Jackson, D. A. & Blow, J. J. Dormant origins licensed by excess Mcm2–7 are required for human cells to survive replicative stress. *Genes & Development* **21**, 3331–3341 (2007).
197. Naim, V. & Rosselli, F. The FANCD1 pathway and BLM collaborate during mitosis to prevent micro-nucleation and chromosome abnormalities. *Nature Cell Biology* **2009** *11*:6 **11**, 761–768 (2009).
198. Bi, X. Mechanism of DNA damage tolerance. *World Journal of Biological Chemistry* **6**, 48 (2015).
199. Liu, Y., Nielsen, C. F., Yao, Q. & Hickson, I. D. The origins and processing of ultra fine anaphase DNA bridges. *Curr Opin Genet Dev* **26**, 1–5 (2014).
200. Macheret, M. & Halazonetis, T. D. DNA replication stress as a hallmark of cancer. *Annu Rev Pathol* **10**, 425–448 (2015).
201. Gorgoulis, V. G. *et al.* Activation of the DNA damage checkpoint and genomic instability in human precancerous lesions. *Nature* **2005** *434*:7035 **434**, 907–913 (2005).
202. Dereli-Öz, A., Versini, G. & Halazonetis, T. D. Studies of genomic copy number changes in human cancers reveal signatures of DNA replication stress. *Mol Oncol* **5**, 308–314 (2011).
203. Burrell, R. A., McGranahan, N., Bartek, J. & Swanton, C. The causes and consequences of genetic heterogeneity in cancer evolution. *Nature* **2013** *501*:7467 **501**, 338–345 (2013).
204. Ubhi, T. & Brown, G. W. Exploiting DNA Replication Stress for Cancer Treatment. *Cancer Research* **79**, 1730–1739 (2019).
205. Zhang, J., Dai, Q., Park, D. & Deng, X. Targeting DNA Replication Stress for Cancer Therapy. *Genes (Basel)* **7**, (2016).
206. Ngoi, N. Y. L., Pham, M. M., Tan, D. S. P. & Yap, T. A. Targeting the replication stress response through synthetic lethal strategies in cancer medicine. *Trends Cancer* **7**, (2021).
207. Ikegami, S. *et al.* Aphidicolin prevents mitotic cell division by interfering with the activity of DNA polymerase- α . *Nature* **1978** *275*:5679 **275**, 458–460 (1978).
208. Rosenkranz, H. S. & Levy, J. A. HYDROXYUREA: A SPECIFIC INHIBITOR OF DEOXYRIBONUCLEIC ACID SYNTHESIS. *Biochim Biophys Acta* **95**, 181–183 (1965).
209. Branzel, D. & Foiani, M. The checkpoint response to replication stress. *DNA Repair* **8**, 1038–1046 (2009).
210. Magiera, M. M., Gueydon, E. & Schwob, E. DNA replication and spindle checkpoints cooperate during S phase to delay mitosis and preserve genome integrity. *Journal of Cell Biology* **204**, 165–175 (2014).
211. Willis, N. & Rhind, N. Regulation of DNA replication by the S-phase DNA damage checkpoint. *Cell Division* **4**, 1–10 (2009).
212. Saldivar, J. C. *et al.* An intrinsic S/G2 checkpoint enforced by ATR. *Science* **361**, 806 (2018).
213. Haahr, P. *et al.* Activation of the ATR kinase by the RPA-binding protein ETAA1. *Nat Cell Biol* **18**, 1196–1207 (2016).
214. Harrigan, J. A. *et al.* Replication stress induces 53BP1-containing OPT domains in G1 cells. *J Cell Biol* **193**, 97–108 (2011).
215. Chan, K. L., North, P. S. & Hickson, I. D. BLM is required for faithful chromosome segregation and its localization defines a class of ultrafine anaphase bridges. *EMBO J* **26**, 3397–3409 (2007).
216. Carette, J. E. *et al.* Ebola virus entry requires the cholesterol transporter Niemann-Pick C1. *Nature* **477**, 340–343 (2011).

217. Gan, W. *et al.* R-loop-mediated genomic instability is caused by impairment of replication fork progression. *Genes Dev* **25**, 2041–2056 (2011).
218. Nguyen, H. D. *et al.* Functions of Replication Protein A as a Sensor of R Loops and a Regulator of RNaseH1. *Mol Cell* **65**, 832–847.e4 (2017).
219. Abdou, I., Poirier, G. G., Hendzel, M. J. & Weinfeld, M. DNA ligase III acts as a DNA strand break sensor in the cellular orchestration of DNA strand break repair. *Nucleic Acids Res* **43**, 875–892 (2015).
220. Lu, G. *et al.* Ligase I and ligase III mediate the DNA double-strand break ligation in alternative end-joining. *Proc Natl Acad Sci U S A* **113**, 1256–1260 (2016).
221. Paes Dias, M. *et al.* Loss of nuclear DNA ligase III reverts PARP inhibitor resistance in BRCA1/53BP1 double-deficient cells by exposing ssDNA gaps. *Mol Cell* **81**, 4692–4708.e9 (2021).
222. Cipolla, L. *et al.* UBR5 interacts with the replication fork and protects DNA replication from DNA polymerase η toxicity. *Nucleic Acids Res* **47**, 11268–11283 (2019).
223. Li, C. G. *et al.* PPAR γ and Interaction with UBR5/ATMIN Promotes DNA Repair to Maintain Endothelial Homeostasis. *Cell Reports* **26**, 1333–1343 (2019).
224. Zhang, T., Cronshaw, J., Kanu, N., Snijders, A. P. & Behrens, A. UBR5-mediated ubiquitination of ATMIN is required for ionizing radiation-induced ATM signaling and function. *Proc Natl Acad Sci U S A* **111**, 12091–12096 (2014).
225. Xu, X. *et al.* Fanconi anemia proteins participate in a break-induced-replication-like pathway to counter replication stress. *Nat Struct Mol Biol* **28**, 487–500 (2021).
226. Howlett, N. G., Taniguchi, T., Durkin, S. G., D'Andrea, A. D. & Glover, T. W. The Fanconi anemia pathway is required for the DNA replication stress response and for the regulation of common fragile site stability. *Hum Mol Genet* **14**, 693–701 (2005).
227. Datta, A. & Brosh, R. M. Holding All the Cards—How Fanconi Anemia Proteins Deal with Replication Stress and Preserve Genomic Stability. *Genes (Basel)* **10**, (2019).
228. Zhang, F., Fan, Q., Ren, K., Auerbach, A. D. & Andreassen, P. R. FANCD2/BRIPI recruitment and regulation of FANCD2 in DNA damage responses. *Chromosoma* **119**, 637 (2010).
229. Wang, J., Gong, Z. & Chen, J. MDC1 collaborates with TopBP1 in DNA replication checkpoint control. *The Journal of Cell Biology* **193**, 267 (2011).
230. Formosa, L. E., Dibley, M. G., Stroud, D. A. & Ryan, M. T. Building a complex complex: Assembly of mitochondrial respiratory chain complex I. *Seminars in Cell & Developmental Biology* **76**, 154–162 (2018).
231. Picard, M., McEwen, B. S., Epel, E. S. & Sandi, C. An energetic view of stress: Focus on mitochondria. *Front Neuroendocrinol* **49**, 72–85 (2018).
232. Pflieger, J., He, M. & Abdellatif, M. Mitochondrial complex II is a source of the reserve respiratory capacity that is regulated by metabolic sensors and promotes cell survival. *Cell Death & Disease* **6**, e1835 (2015).
233. Lardy, H. A., Johnson, D. & McMurray, W. C. Antibiotics as tools for metabolic studies. I. A survey of toxic antibiotics in respiratory, phosphorylative and glycolytic systems. *Archives of Biochemistry and Biophysics* **78**, 587–597 (1958).
234. Divakaruni, A. S., Paradyse, A., Ferrick, D. A., Murphy, A. N. & Jastroch, M. Analysis and interpretation of microplate-based oxygen consumption and pH data. *Methods Enzymol* **547**, 309–354 (2014).
235. Aspuria, P.-J. P. *et al.* Succinate dehydrogenase inhibition leads to epithelial-mesenchymal transition and reprogrammed carbon metabolism. *Cancer & Metabolism* **2014** *2:1*, 1–15 (2014).
236. Marchetti, P., Fovez, Q., Germain, N., Khamari, R. & Kluz, J. Mitochondrial spare respiratory capacity: Mechanisms, regulation, and significance in non-transformed and cancer cells. *The FASEB Journal* **34**, 13106–13124 (2020).
237. Garcia-Muse, T. & Aguilera, A. Transcription–replication conflicts: how they occur and how they are resolved. *Nature Reviews Molecular Cell Biology* **2016** *17:9* **17**, 553–563 (2016).
238. Zhao, H., Zhu, M., Limbo, O. & Russell, P. RNase H eliminates R-loops that disrupt DNA replication but is nonessential for efficient DSB repair. *EMBO Rep* **19**, e45335 (2018).
239. Tuduri, S. *et al.* Topoisomerase I suppresses genomic instability by preventing interference between replication and transcription. *Nat Cell Biol* **11**, 1315–1324 (2009).
240. He, Y. & Smith, R. Nuclear functions of heterogeneous nuclear ribonucleoproteins A/B. *Cell Mol Life Sci* **66**, 1239–1256 (2009).
241. Flynn, R. L. *et al.* TERRA and hnRNP1 orchestrate an RPA-to-POT1 switch on telomeric single-stranded DNA. *Nature* **471**, 532–538 (2011).
242. Liaw, H., Lee, D. & Myung, K. DNA-PK-Dependent RPA2 Hyperphosphorylation Facilitates DNA Repair and Suppresses Sister Chromatid Exchange. *PLOS ONE* **6**, e21424 (2011).
243. Sugiyama, T. & Kowalczykowski, S. C. Rad52 protein associates with replication protein A (RPA)-single-stranded DNA to accelerate Rad51-mediated displacement of RPA and presynaptic complex formation. *J Biol Chem* **277**, 31663–31672 (2002).
244. Toledo, L. I. *et al.* ATR Prohibits Replication Catastrophe by Preventing Global Exhaustion of RPA. *Cell* **155**, 1088–1103 (2013).
245. Morita, M. *et al.* A Novel 4EHP-GIGYF2 Translational Repressor Complex Is Essential for Mammalian Development. *Molecular and Cellular Biology* **32**, 3585 (2012).
246. Deans, A. J. & West, S. C. DNA interstrand crosslink repair and cancer. *Nat Rev Cancer* **11**, 467 (2011).
247. Lomax, M. E., Folkes, L. K. & O'Neill, P. Biological consequences of radiation-induced DNA damage: relevance to radiotherapy. *Clin Oncol (R Coll Radiol)* **25**, 578–585 (2013).
248. Bradbury, A., Hall, S., Curtin, N. & Drew, Y. Targeting ATR as Cancer Therapy: A new era for synthetic lethality and synergistic combinations? *Pharmacol Ther* **207**, (2020).
249. Konstantinopoulos, P. A. *et al.* A Replication stress biomarker is associated with response to gemcitabine versus combined gemcitabine and ATR inhibitor therapy in ovarian cancer. *Nature Communications* **2021** *12:1* **12**, 1–8 (2021).

250. Litman, R. *et al.* BACH1 is critical for homologous recombination and appears to be the Fanconi anemia gene product FANCF. *Cancer Cell* **8**, 255–265 (2005).
251. Cantor, S. B. *et al.* BACH1, a novel helicase-like protein, interacts directly with BRCA1 and contributes to its DNA repair function. *Cell* **105**, 149–160 (2001).
252. Coster, G. & Goldberg, M. The cellular response to DNA damage: A focus on MDC1 and its interacting proteins. *Nucleus* **1**, 166 (2010).
253. Gong, Z., Kim, J. E., Leung, C. C. Y., Glover, J. N. M. & Chen, J. BACH1/FANCF Acts with TopBP1 and Participates Early in DNA Replication Checkpoint Control. *Molecular Cell* **37**, 438–446 (2010).
254. Ricchetti, M. Replication stress in mitochondria. *Mutation Research/Fundamental and Molecular Mechanisms of Mutagenesis* **808**, 93–102 (2018).
255. Gandhi, V. v. & Samuels, D. C. A review comparing deoxyribonucleoside triphosphate (dNTP) concentrations in the mitochondrial and cytoplasmic compartments of normal and transformed cells. *Nucleosides, Nucleotides and Nucleic Acids* (2011) doi:10.1080/15257770.2011.586955.
256. Geuskens, M., Hardt, N., Pedrali-Noy3, G. & Spadari3, S. Nucleic Acids Research An autoradiographic demonstration of nuclear DNA replication by DNA polymerase α and of mitochondrial DNA synthesis by DNA polymerase γ . 1981.
257. Zimmermann, W., Chen, S. M., Bolden, A. & Weissbach, A. Mitochondrial DNA replication does not involve DNA polymerase α . *Journal of Biological Chemistry* **255**, 11847–11852 (1980).
258. Barrientos, A., Fontanesi, F. & Díaz, F. Evaluation of the Mitochondrial Respiratory Chain and Oxidative Phosphorylation System using Polarography and Spectrophotometric Enzyme Assays. *Current protocols in human genetics / editorial board, Jonathan L. Haines ... [et al.]* CHAPTER, Unit19.3 (2009).
259. Henriksens, L. A., Umbricht, C. B. & Woldsi, M. S. THE JOURNAL OF BIOUXICAL CHEMISTRY Recombinant Replication Protein A Expression, Complex Formation, and Functional Characterization*. **269**, 11121–11132 (1994).
260. Arnoult, N. & Karlseder, J. Complex interactions between the DNA-damage response and mammalian telomeres. *Nat Struct Mol Biol* **22**, 859 (2015).
261. Lazzerini-Denchi, E. & Sfeir, A. Stop pulling my strings – what telomeres taught us about the DNA damage response. *Nature Reviews Molecular Cell Biology* 2016 17:6 **17**, 364–378 (2016).
262. Bryant, H. E. *et al.* Specific killing of BRCA2-deficient tumours with inhibitors of poly(ADP-ribose) polymerase. *Nature* 2005 434:7035 **434**, 913–917 (2005).
263. Helleday, T. The underlying mechanism for the PARP and BRCA synthetic lethality: clearing up the misunderstandings. *Mol Oncol* **5**, 387–393 (2011).
264. Farmer, H. *et al.* Targeting the DNA repair defect in BRCA mutant cells as a therapeutic strategy. *Nature* 2005 434:7035 **434**, 917–921 (2005).
265. Piskadlo, E. & Oliveira, R. A. Novel insights into mitotic chromosome condensation [version 1; referees: 2 approved]. *F1000Res* **5**, (2016).
266. Gibcus, J. H. *et al.* A pathway for mitotic chromosome formation. *Science* **359**, (2018).
267. Ganji, M. *et al.* Real-time imaging of DNA loop extrusion by condensin. *Science* (1979) **360**, 102–105 (2018).
268. Kim, E., Kerssemakers, J., Shaltiel, I. A., Haering, C. H. & Dekker, C. DNA-loop extruding condensin complexes can traverse one another. *Nature* 2020 579:7799 **579**, 438–442 (2020).
269. Hirano, T. & Mitchison, T. J. A heterodimeric coiled-coil protein required for mitotic chromosome condensation in vitro. *Cell* **79**, 449–458 (1994).
270. Ono, T. *et al.* Differential contributions of condensin I and condensin II to mitotic chromosome architecture in vertebrate cells. *Cell* (2003) doi:10.1016/S0092-8674(03)00724-4.
271. Hirota, T., Gerlich, D., Koch, B., Ellenberg, J. & Peters, J. M. Distinct functions of condensin I and II in mitotic chromosome assembly. *Journal of Cell Science* **117**, 6435–6445 (2004).
272. Hirano, T. Condensins: universal organizers of chromosomes with diverse functions. *Genes & Development* **26**, 1659 (2012).
273. Elbatsh, A. M. O. *et al.* Distinct Roles for Condensin's Two ATPase Sites in Chromosome Condensation. *Mol Cell* **76**, 724–737.e5 (2019).
274. Martin, C. A. *et al.* Mutations in genes encoding condensin complex proteins cause microcephaly through decatenation failure at mitosis. *Genes and Development* **30**, 2158–2172 (2016).
275. Grue, P. *et al.* Essential Mitotic Functions of DNA Topoisomerase II α Are Not Adopted by Topoisomerase II β in Human H69 Cells *. *Journal of Biological Chemistry* **273**, 33660–33666 (1998).
276. Nielsen, C. F., Zhang, T., Barisic, M., Kalitsis, P. & Hudson, D. F. Topoisomerase II α is essential for maintenance of mitotic chromosome structure. *Proc Natl Acad Sci U S A* (2020) doi:10.1073/pnas.2001760117.
277. Warburton, P. E. & Earnshaw, W. C. Untangling the role of DNA topoisomerase II in mitotic chromosome structure and function. *BioEssays* **19**, 97–99 (1997).
278. Spence, J. M. *et al.* Depletion of topoisomerase II α leads to shortening of the metaphase interkinetochore distance and abnormal persistence of PICH-coated anaphase threads. *J Cell Sci* **120**, 3952–3964 (2007).
279. Gonzalez, R. E. *et al.* Effects of conditional depletion of topoisomerase II on cell cycle progression in mammalian cells. *Cell Cycle* **10**, 3505–3514 (2011).
280. Christensen, M. O. *et al.* Dynamics of human DNA topoisomerases II α and II β in living cells. *J Cell Biol* **157**, 31–44 (2002).
281. Meyer, K. N. *et al.* Cell Cycle-coupled Relocation of Types I and II Topoisomerases and Modulation of Catalytic Enzyme Activities. *Journal of Cell Biology* **136**, 775–788 (1997).
282. Maeshima, K. & Laemmli, U. K. A Two-step scaffolding model for mitotic chromosome assembly. *Developmental Cell* (2003) doi:10.1016/S1534-5807(03)00092-3.
283. Green, L. C. *et al.* Contrasting roles of condensin I and condensin II in mitotic chromosome formation. *Journal of Cell Science* (2012) doi:10.1242/jcs.097790.

284. Baxter, J. *et al.* Positive supercoiling of mitotic DNA drives decatenation by topoisomerase II in eukaryotes. *Science* **331**, 1328–1332 (2011).
285. Farr, C. J., Antoniou-Kourouniotti, M., Mimmack, M. L., Volkov, A. & Porter, A. C. G. The α isoform of topoisomerase II is required for hypercompaction of mitotic chromosomes in human cells. *Nucleic Acids Research* **42**, 4414–4426 (2014).
286. Poonperm, R. *et al.* Chromosome Scaffold is a Double-Stranded Assembly of Scaffold Proteins. *Scientific Reports* (2015) doi:10.1038/srep11916.
287. Adachi, Y., Luke, M. & Laemmli, U. K. Chromosome assembly in vitro: Topoisomerase II is required for condensation. *Cell* **64**, 137–148 (1991).
288. Hudson, D. F., Vagnarelli, P., Gassmann, R. & Earnshaw, W. C. Condensin Is Required for Nonhistone Protein Assembly and Structural Integrity of Vertebrate Mitotic Chromosomes. *Developmental Cell* **5**, 323–336 (2003).
289. Roca, J., Dyson, S., Segura, J., Valdés, A. & Martínez-García, B. Keeping intracellular DNA untangled: A new role for condensin? *Bioessays* (2021) doi:10.1002/BIES.202100187.
290. Tsherniak, A. *et al.* Defining a Cancer Dependency Map. *Cell* **170**, 564–576.e16 (2017).
291. Holland, A. J., Fachinetti, D., Han, J. S. & Cleveland, D. W. Inducible, reversible system for the rapid and complete degradation of proteins in mammalian cells. *Proc Natl Acad Sci U S A* **109**, E3350–E3357 (2012).
292. Natsume, T., Kiyomitsu, T., Saga, Y. & Kanemaki, M. T. Rapid Protein Depletion in Human Cells by Auxin-Inducible Degron Tagging with Short Homology Donors. *Cell Reports* **15**, 210–218 (2016).
293. Chu, L. *et al.* The 3D Topography of Mitotic Chromosomes. *Molecular Cell* (2020) doi:10.1016/j.molcel.2020.07.002.
294. Johnson, S. J. *et al.* Crystal Structure and RNA binding of the Tex protein from *Pseudomonas aeruginosa*. *J Mol Biol* **377**, 1460 (2008).
295. Aravind, L., Makarova, K. S. & Koonin, E. v. SURVEY AND SUMMARY Holliday junction resolvases and related nucleases: identification of new families, phyletic distribution and evolutionary trajectories. *Nucleic Acids Research* **28**, 3417–3432 (2000).
296. West, S. C. & Connolly, B. Biological roles of the *Escherichia coli* RuvA, RuvB and RuvC proteins revealed. *Mol Microbiol* **6**, 2755–2759 (1992).
297. Bycroft, M., Hubbard, T. J. P., Proctor, M., Freund, S. M. V. & Murzin, A. G. The Solution Structure of the SI RNA Binding Domain: A Member of an Ancient Nucleic Acid-Binding Fold. *Cell* **88**, 235–242 (1997).
298. Haarhuis, J. H. I. *et al.* WAPL-mediated removal of cohesin protects against segregation errors and aneuploidy. *Current Biology* **23**, 2071–2077 (2013).
299. Nielsen, C. F. *et al.* PICH promotes sister chromatid disjunction and co-operates with topoisomerase II in mitosis. *Nature Communications* **2015** 6:1 6, 1–15 (2015).
300. van der Lelij, P. *et al.* Warsaw Breakage Syndrome, a Cohesinopathy Associated with Mutations in the XPD Helicase Family Member DDX11/ChIR1. *American Journal of Human Genetics* **86**, 262–266 (2010).
301. Whelan, G. *et al.* Cohesin acetyltransferase Esco2 is a cell viability factor and is required for cohesion in pericentric heterochromatin. *The EMBO Journal* **31**, 71–82 (2012).
302. Morris, S. K., Baird, C. L. & Lindsley, J. E. Steady-state and Rapid Kinetic Analysis of Topoisomerase II Trapped as the Closed-clamp Intermediate by ICRF-193*. *Journal of Biological Chemistry* **275**, 2613–2618 (2000).
303. Nitiss, J. L. Targeting DNA topoisomerase II in cancer chemotherapy. *Nature Reviews Cancer* **2009** 9:5 9, 338–350 (2009).
304. Watanabe, Y., Kitajima, T. S., Hyman, T., Yanagida, M. & Hirano, T. Shugoshin protects cohesin complexes at centromeres. *Philosophical Transactions of the Royal Society B: Biological Sciences* **360**, 515–521 (2005).
305. Kitajima, T. S. *et al.* Shugoshin collaborates with protein phosphatase 2A to protect cohesin. *Nature* **441**, 46–52 (2006).
306. McGuinness, B. E., Hirota, T., Kudo, N. R., Peters, J. M. & Nasmyth, K. Shugoshin Prevents Dissociation of Cohesin from Centromeres During Mitosis in Vertebrate Cells. *PLOS Biology* **3**, e86 (2005).
307. Watanabe, Y. Shugoshin: guardian spirit at the centromere. *Curr Opin Cell Biol* **17**, 590–595 (2005).
308. Roca, J., Ishida, R., Berger, J. M., Andoh, T. & Wang, J. C. Antitumor bisdioxopiperazines inhibit yeast DNA topoisomerase II by trapping the enzyme in the form of a closed protein clamp. *Proc Natl Acad Sci U S A* **91**, 1781 (1994).
309. Carpenter, A. J. & Porter, A. C. G. Construction, characterization, and complementation of a conditional-lethal DNA topoisomerase II α mutant human cell line. *Molecular Biology of the Cell* **15**, 5700–5711 (2004).
310. Kiianitsa, K. & Maizels, N. A rapid and sensitive assay for DNA–protein covalent complexes in living cells. *Nucleic Acids Research* **41**, e104 (2013).
311. McClendon, A. K. & Osheroff, N. DNA Topoisomerase II, Genotoxicity, and Cancer. *Mutat Res* **623**, 83 (2007).
312. Sun, Y. *et al.* A conserved SUMO pathway repairs topoisomerase DNA–protein cross-links by engaging ubiquitin-mediated proteasomal degradation. *Science Advances* **6**, (2020).
313. Ledesma, F. C., el Khamisy, S. F., Zuma, M. C., Osborn, K. & Caldecott, K. W. A human 5'-tyrosyl DNA phosphodiesterase that repairs topoisomerase-mediated DNA damage. *Nature* **461**, 674–678 (2009).
314. Schellenberg, M. J. *et al.* Mechanism of repair of 5'-topoisomerase II-DNA adducts by mammalian tyrosyl-DNA phosphodiesterase 2. *Nat Struct Mol Biol* **19**, 1363–1371 (2012).
315. Schellenberg, M. J. *et al.* Reversal of DNA damage induced Topoisomerase 2 DNA–protein crosslinks by Tdp2. *Nucleic Acids Research* **44**, 3829 (2016).
316. Fan, J. R. *et al.* Cellular processing pathways contribute to the activation of etoposide-induced DNA damage responses. *DNA Repair* **7**, 452–463 (2008).
317. Zagnoli-Vieira, G. & Caldecott, K. W. TDP2, TOP2, and SUMO: what is ZATT about? *Cell Research* **2017** 27:12 27, 1405–1406 (2017).
318. Sun, Y. *et al.* A conserved SUMO pathway repairs topoisomerase DNA–protein cross-links by engaging ubiquitin-mediated proteasomal degradation. *Sci Adv* **6**, (2020).

319. Wyatt, H. D. M. & West, S. C. Holliday junction resolvases. *Cold Spring Harbor Perspectives in Biology* (2014) doi:10.1101/cshperspect.a023192.
320. Cejka, P., Plank, J. L., Bachrati, C. Z., Hickson, I. D. & Kowalczykowski, S. C. Rmi1 stimulates decatenation of double Holliday junctions during dissolution by Sgs1-Top3. *Nature Structural and Molecular Biology* (2010) doi:10.1038/nsmb.1919.
321. Nitiss, J. L., Soans, E., Rogojina, A., Seth, A. & Mishina, M. Topoisomerase Assays. *Current Protocols in Pharmacology* **CHAPTER**, Unit3.3 (2012).
322. Cifdaloz, M. *et al.* Systems analysis identifies melanoma-enriched pro-oncogenic networks controlled by the RNA binding protein CELF1. doi:10.1038/s41467-017-02353-y.
323. Palladino, J. & Mellone, B. G. The KAT's Out of the Bag: Histone Acetylation Promotes Centromere Assembly. *Developmental Cell* **37**, 389–390 (2016).
324. Bobkov, G. O. M., Gilbert, N. & Heun, P. Centromere transcription allows CENP-A to transit from chromatin association to stable incorporation. *Journal of Cell Biology* **217**, 1957–1972 (2018).
325. Canela, A. *et al.* Topoisomerase II-Induced Chromosome Breakage and Translocation Is Determined by Chromosome Architecture and Transcriptional Activity. *Molecular Cell* **75**, 252–266.e8 (2019).
326. Valdés, A. *et al.* Transcriptional supercoiling boosts topoisomerase II-mediated knotting of intracellular DNA. *Nucleic Acids Research* **47**, 6946–6955 (2019).
327. Nahidiazar, L., Agronskaia, A. v., Broertjes, J., van Broek, B. den & Jalink, K. Optimizing Imaging Conditions for Demanding Multi-Color Super Resolution Localization Microscopy. *PLoS ONE* **11**, e0158884 (2016).
328. Loeb, L. A. Human cancers express mutator phenotypes: origin, consequences and targeting. *Nature Reviews Cancer* **2011**, 450–457 (2011).
329. Gaillard, H., García-Muse, T. & Aguilera, A. Replication stress and cancer. *Nature Reviews Cancer* **15**, 276–280 (2015).
330. Leiserson, M. D. M. *et al.* Pan-cancer network analysis identifies combinations of rare somatic mutations across pathways and protein complexes. *Nat Genet* **47**, 106–114 (2015).
331. Ono, T., Fang, Y., Spector, D. L. & Hirano, T. Spatial and temporal regulation of condensins I and II in mitotic chromosome assembly in human cells. *Molecular Biology of the Cell* **15**, 3296–3308 (2004).
332. Nagasaka, K., Hossain, M. J., Roberti, M. J., Ellenberg, J. & Hirota, T. Sister chromatid resolution is an intrinsic part of chromosome organization in prophase. *Nature Cell Biology* **2016**, 18:6, 692–699 (2016).
333. Ono, T., Yamashita, D. & Hirano, T. Condensin II initiates sister chromatid resolution during S phase. *Journal of Cell Biology* **200**, 429–441 (2013).
334. Potts, P. R., Porteus, M. H. & Yu, H. Human SMC5/6 complex promotes sister chromatid homologous recombination by recruiting the SMC1/3 cohesin complex to double-strand breaks. *EMBO J* **25**, 3377–3388 (2006).
335. Wu, N. & Yu, H. The Smc complexes in DNA damage response. *Cell and Bioscience* **2**, 1–11 (2012).
336. Aono, N., Sutani, T., Tomonaga, T., Mochida, S. & Yanagida, M. Cnd2 has dual roles in mitotic condensation and interphase. *Nature* **417**, 197–202 (2002).
337. Wood, J. L., Liang, Y., Li, K. & Chen, J. Microcephalin/MCPH1 associates with the Condensin II complex to function in homologous recombination repair. *J Biol Chem* **283**, 29586–29592 (2008).
338. Ashley, A. K. *et al.* DNA-PK phosphorylation of RPA32 Ser4/Ser8 regulates replication stress checkpoint activation, fork restart, homologous recombination and mitotic catastrophe. *DNA Repair (Amst)* **21**, 131–139 (2014).
339. Albarakati, N. *et al.* Targeting BRCA1-BER deficient breast cancer by ATM or DNA-PKcs blockade either alone or in combination with cisplatin for personalized therapy. *Molecular Oncology* **9**, 204 (2015).
340. Alagupulinsa, D. A., Ayyadevara, S. & Shmookler Reis, R. J. A small molecule inhibitor of RAD51 reduces homologous recombination and sensitizes multiple myeloma cells to doxorubicin. *Frontiers in Oncology* **4**, 289 (2014).
341. Gunn, A. & Stark, J. M. I-SceI-based assays to examine distinct repair outcomes of mammalian chromosomal double strand breaks. *Methods Mol Biol* **920**, 379–391 (2012).
342. Sonoda, E. *et al.* Sister chromatid exchanges are mediated by homologous recombination in vertebrate cells. *Mol Cell Biol* **19**, 5166–5169 (1999).
343. Yang, C. *et al.* The kinetochore protein Bubl1 participates in the DNA damage response. *DNA Repair (Amst)* **11**, 185 (2012).
344. Siemeister, G. *et al.* Inhibition of BUB1 Kinase by BAY 1816032 Sensitizes Tumor Cells toward Taxanes, ATR, and PARP Inhibitors In Vitro and In Vivo. *Clinical Cancer Research* **25**, 1404–1414 (2019).
345. Jessulat, M. *et al.* Spindle Checkpoint Factors Bub1 and Bub2 Promote DNA Double-Strand Break Repair by Nonhomologous End Joining. *Molecular and Cellular Biology* **35**, 2448–2463 (2015).
346. Raaijmakers, J. A. & Medema, R. H. Killing a zombie: a full deletion of the BUB1 gene in HAP1 cells. *The EMBO Journal* **38**, e102423 (2019).
347. Colombo, R. *et al.* Targeting the mitotic checkpoint for cancer therapy with NMS-P715, an inhibitor of MPS1 kinase. *Cancer Res* **70**, 10255–10264 (2010).
348. Nguyen, A. L., Fadel, M. D. & Cheeseman, I. M. Differential requirements for the CENP-O complex reveal parallel PLK1 kinetochore recruitment pathways. *Molecular Biology of the Cell* **32**, 712–721 (2021).
349. Cui, Y., Petrushenko, Z. M. & Rybenkov, V. v. MukB acts as a macromolecular clamp in DNA condensation. *Nat Struct Mol Biol* **15**, 411–418 (2008).
350. Bryant, H. E. *et al.* PARP is activated at stalled forks to mediate Mre11-dependent replication restart and recombination. *The EMBO Journal* **28**, 2601–2615 (2009).
351. Maya-Mendoza, A. *et al.* High speed of fork progression induces DNA replication stress and genomic instability. *Nature* **559**, 279–284 (2018).
352. Nieminszczy, J., Schwab, R. A. & Niedzwiedz, W. The DNA fibre technique – tracking helicases at work. *Methods* **108**, 92–98 (2016).
353. Sirbu, B. M. *et al.* Analysis of protein dynamics at active, stalled, and collapsed replication forks. *Genes & Development* **25**, 1320–1327 (2011).



354. McAinsh, A. D., Meraldi, P., Draviam, V. M., Toso, A. & Sorger, P. K. The human kinetochore proteins Nnf1R and Mcm21R are required for accurate chromosome segregation. *The EMBO Journal* **25**, 4033 (2006).
355. Replication, D. N. A., Drives, S. & Instability, C. DNA replication stress drives chromosomal instability. *Cancer Discovery* **3**, 372 (2013).
356. Cahill, D. P., Kinzler, K. W., Vogelstein, B. & Lengauer, C. Genetic instability and darwinian selection in tumours. *Trends in Cell Biology* **9**, M57–M60 (1999).
357. Buffin, E., Emre, D. & Karesse, R. E. Flies without a spindle checkpoint. *Nat Cell Biol* **9**, 565–572 (2007).
358. Zhang, G. *et al.* Efficient mitotic checkpoint signaling depends on integrated activities of Bub1 and the RZZ complex. *EMBO J* **38**, (2019).
359. van Heesbeen, R. G. *Mitotic Spindle Assembly: may the force be with you.* (2015).
360. Sarangapani, K. K., Koch, L. B., Nelson, C. R., Asbury, C. L. & Biggins, S. Kinetochore-bound Mps1 regulates kinetochore–microtubule attachments via Ndc80 phosphorylation. *Journal of Cell Biology* **220**, (2021).
361. Benzi, G. *et al.* A common molecular mechanism underlies the role of Mps1 in chromosome biorientation and the spindle assembly checkpoint. *EMBO Rep* **21**, e50257 (2020).
362. Maure, J. F., Kitamura, E. & Tanaka, T. U. Mps1 Kinase Promotes Sister-Kinetochore Bi-orientation by a Tension-Dependent Mechanism. *Current Biology* **17**, 2175–2182 (2007).
363. Meyer, R. E. *et al.* Mps1 and Ip11/Aurora B act sequentially to correctly orient chromosomes on the meiotic spindle of budding yeast. *Science (1979)* **339**, 1071–1074 (2013).
364. Cohen-Sharir, Y. *et al.* Aneuploidy renders cancer cells vulnerable to mitotic checkpoint inhibition. *Nature* **2021** 590:7846 **590**, 486–491 (2021).
365. Quinton, R. J. *et al.* Whole-genome doubling confers unique genetic vulnerabilities on tumour cells. *Nature* **590**, 492–497 (2021).
366. Marquis, C. *et al.* Chromosomally unstable tumor cells specifically require KIF18A for proliferation. *Nature Communications* **12**, (2021).
367. Maia, A. R. R. *et al.* Mps1 inhibitors synergise with low doses of taxanes in promoting tumour cell death by enhancement of errors in cell division. *British Journal of Cancer* **2018** 118:12 **118**, 1586–1595 (2018).
368. Mason, J. M. *et al.* Functional characterization of CFI-402257, a potent and selective Mps1/TTK kinase inhibitor, for the treatment of cancer. *Proc Natl Acad Sci U S A* **114**, 3127–3132 (2017).
369. Pauer, L. R. *et al.* Phase I study of oral CI-994 in combination with carboplatin and paclitaxel in the treatment of patients with advanced solid tumors. *Cancer Invest* **22**, 886–896 (2004).
370. Lorusso, P. *et al.* First-in-human study of the monopolar spindle 1 (Mps1) kinase inhibitor BAY 1161909 in combination with paclitaxel in subjects with advanced malignancies. *Annals of Oncology* **29**, viii138 (2018).
371. Atrafi, F. *et al.* A Phase I Study of an MPS1 Inhibitor (BAY 1217389) in Combination with Paclitaxel Using a Novel Randomized Continual Reassessment Method for Dose Escalation. *Clinical Cancer Research* **27**, 6366–6375 (2021).
372. Kolinjivadi, A. M., Crismani, W. & Ngeow, J. Emerging functions of Fanconi anemia genes in replication fork protection pathways. *Hum Mol Genet* **29**, RI58–RI64 (2020).
373. Räschle, M. *et al.* Mechanism of replication-coupled DNA interstrand cross-link repair. *Cell* **134**, 969 (2008).
374. Mazouzi, A., Velimezi, G. & Loizou, J. I. DNA replication stress: Causes, resolution and disease. *Experimental Cell Research* **329**, 85–93 (2014).
375. Benedict, B. *et al.* The RECQL helicase prevents replication fork collapse during replication stress. *Life Science Alliance* **3**, (2020).
376. Etemadmoghadam, D. *et al.* Synthetic lethality between CCNE1 amplification and loss of BRCA1. *Proc Natl Acad Sci U S A* **110**, 19489–19494 (2013).
377. Olivieri, M. *et al.* A Genetic Map of the Response to DNA Damage in Human Cells. *Cell* **182**, 481–496.e21 (2020).
378. Ha, D. H. *et al.* Antitumor effect of a WEE1 inhibitor and potentiation of olaparib sensitivity by DNA damage response modulation in triple-negative breast cancer. *Scientific Reports* **2020** 10:1 **10**, 1–13 (2020).
379. PosthumaDeBoer, J. *et al.* WEE1 inhibition sensitizes osteosarcoma to radiotherapy. *BMC Cancer* **11**, (2011).
380. Baillie, K. E. & Stirling, P. C. Beyond Kinases: Targeting Replication Stress Proteins in Cancer Therapy. *Trends in Cancer* **7**, 430–446 (2021).
381. Dewar, J. M. & Walter, J. C. Mechanisms of DNA replication termination. *Nat Rev Mol Cell Biol* **18**, 507 (2017).
382. Postow, L., Crisona, N. J., Peter, B. J., Hardy, C. D. & Cozzarelli, N. R. Topological challenges to DNA replication: Conformations at the fork. *PNAS* **98**, 2021 (2001).
383. Baxter, J. & Diffley, J. F. X. Topoisomerase II Inactivation Prevents the Completion of DNA Replication in Budding Yeast. *Molecular Cell* **30**, 790–802 (2008).
384. Minchell, N. E., Keszthelyi, A. & Baxter, J. Cohesin Causes Replicative DNA Damage by Trapping DNA Topological Stress. *Molecular Cell* **78**, 739–751.e8 (2020).
385. Skoufias, D. A., Lacroix, F. B., Andreassen, P. R., Wilson, L. & Margolis, R. L. Inhibition of DNA Decatenation, but Not DNA Damage, Arrests Cells at Metaphase. *Molecular Cell* **15**, 977–990 (2004).
386. Darmlin, M. & Bestor, T. H. The decatenation checkpoint. *British Journal of Cancer* **96**, 201 (2007).
387. Earnshaw, W. C., Holligan, B., Cooke, C. A., Heck, M. M. S. & Liu, L. F. Topoisomerase II is a structural component of mitotic chromosome scaffolds. *Journal of Cell Biology* (1985) doi:10.1083/jcb.100.5.1706.
388. Lee, J. H. & Berger, J. M. Cell cycle-dependent control and roles of DNA topoisomerase II. *Genes* (2019) doi:10.3390/genes10110859.
389. Li, Y. *et al.* Escherichia coli condensin MukB stimulates topoisomerase IV activity by a direct physical interaction. *Proc Natl Acad Sci U S A* **107**, 18832–18837 (2010).
390. Hayama, R. & Mariani, K. J. Physical and functional interaction between the condensin MukB and the decatenase topoisomerase IV in Escherichia coli. *Proceedings of the National Academy of Sciences* **107**, 18826–18831 (2010).
391. Rybenkov, V. v., Ullsperger, C., Vologodskii, A. v. & Cozzarelli, N. R. Simplification of DNA Topology Below Equilibrium Values by Type II Topoisomerases. *Science (1979)* **277**, 690–693 (1997).

392. Orlandini, E., Marenduzzo, D. & Michieletto, D. Synergy of topoisomerase and structural-maintenance-of-chromosomes proteins creates a universal pathway to simplify genome topology. *Proc Natl Acad Sci U S A* **116**, 8149–8154 (2019).
393. Racko, D., Benedetti, F., Goundaroulis, D. & Stasiak, A. Chromatin Loop Extrusion and Chromatin Unknotting. *Polymers* **2018**, Vol. 10, Page 1126 **10**, 1126 (2018).
394. Chen, E. S., Sutani, T. & Yanagida, M. Ctl1/CID interacts with condensin SMC hinge and supports the DNA repair function of condensin. *Proc Natl Acad Sci U S A* **101**, 8078–8083 (2004).
395. Litwin, I., Pilarczyk, E. & Wysocki, R. The Emerging Role of Cohesin in the DNA Damage Response. *Genes (Basel)* **9**, (2018).
396. Han, J. Y. *et al.* Bubl is required for maintaining cancer stem cells in breast cancer cell lines. *Scientific Reports* **5**, (2015).
397. Eun, M. K. & Burke, D. J. DNA damage activates the SAC in an ATM/ATR-dependent manner, independently of the kinetochore. *PLoS Genet* **4**, (2008).
398. Nitta, M. *et al.* Spindle checkpoint function is required for mitotic catastrophe induced by DNA-damaging agents. *Oncogene* **2004** 23:39 **23**, 6548–6558 (2004).
399. Searle, J. S., Schollaert, K. L., Wilkins, B. J. & Sanchez, Y. The DNA damage checkpoint and PKA pathways converge on APC substrates and Cdc20 to regulate mitotic progression. *Nature Cell Biology* **2004** 6:2 **6**, 138–145 (2004).
400. Mikhailov, A., Cole, R. W. & Rieder, C. L. DNA Damage during Mitosis in Human Cells Delays the Metaphase/Anaphase Transition via the Spindle-Assembly Checkpoint. *Current Biology* **12**, 1797–1806 (2002).
401. Dotiwala, F., Harrison, J. C., Jain, S., Sugawara, N. & Haber, J. E. Mad2 prolongs DNA damage checkpoint arrest caused by a double-strand break via a centromere-dependent mechanism. *Curr Biol* **20**, 328–332 (2010).
402. Heijink, A. M., Krajewska, M. & van Vugt, M. A. T. M. The DNA damage response during mitosis. *Mutation Research/Fundamental and Molecular Mechanisms of Mutagenesis* **750**, 45–55 (2013).
403. Hori, T., Okada, M., Maenaka, K. & Fukagawa, T. CENP-O Class Proteins Form a Stable Complex and Are Required for Proper Kinetochore Function. *Molecular Biology of the Cell* **19**, 843 (2008).
404. O'Connor, M. J. Targeting the DNA Damage Response in Cancer. *Molecular Cell* **60**, 547–560 (2015).

NEDERLANDSE SAMENVATTING

Elk mens bestaat uit biljoenen cellen. Deze hoeveelheid cellen wordt bereikt door meerdere rondes van celdeling. Celdeling is niet alleen belangrijk voor de ontwikkeling van een organisme, maar ook gedurende hun leven om weefsels te kunnen onderhouden. Tijdens celdeling, wordt er een exacte kopie gemaakt van de genetische informatie (ook wel DNA genoemd) die is opgeslagen in elke cel. Tijdens dit proces van replicatie, wordt het DNA van alle 46 chromosomen gedupliceerd. Vervolgens wordt het gedupliceerde DNA eerlijk verdeeld over twee dochtercellen, in een proces dat mitose heet. Het is belangrijk dat deze processen foutloos verlopen, aangezien genetische instabiliteit een gevaar is voor de levensvatbaarheid van cellen. Om het genoom stabiel te houden, maken cellen gebruik van verschillende controlepunten (checkpoints). Deze checkpoints kunnen bijvoorbeeld DNA-schade of fouten in de verdeling van chromosomen in mitose opsporen. Door het activeren van deze checkpoints wordt de celdeling gepauzeerd zodat de problemen opgelost kunnen worden. Als de problemen te groot zijn, kan een cel ook geprogrammeerde celdood (apoptose) ondergaan. Samen zorgen deze processen ervoor dat er twee gezonde, genetisch stabiele, dochtercellen ontstaan na elke celdeling.

Wanneer er mutaties ontstaan in deze controlesystemen, kunnen cellen sneller gaan delen en/of minder goed reageren op DNA-defecten. Dit kan leiden tot de formatie van kanker: ongecontroleerde celdeling, die over tijd agressiever van aard wordt. Kanker is een van de dodelijkste ziekten op aarde, en is gekarakteriseerd door genetische instabiliteit. Daarom is het belangrijk om te begrijpen waarom kankercellen, in tegenstelling tot normale cellen, kunnen overleven terwijl zij genetisch zo instabiel zijn. Als we dit begrijpen, kunnen we deze specifieke kanker-eigenschap misschien uitbuiten als kanker-specifieke kwetsbaarheid in (nieuwe) kankertherapieën.

In dit proefschrift hebben we getracht om de specifieke kwetsbaarheden van genetische instabiliteit bloot te leggen. Om meer precies te zijn, hebben we een specifieke vorm van genetische instabiliteit bestudeerd, namelijk chromosomale instabiliteit. Bij chromosomale instabiliteit worden chromosomen tijdens mitose meermaals oneerlijk verdeeld over twee dochtercellen. Hierdoor varieert de genetische informatie van de dochtercellen, iets wat kan bijdragen aan resistentie tegen kankermedicijnen. Kankercellen hebben vaker chromosomale instabiliteit dan normale cellen, en daarom kan chromosomale instabiliteit een kanker-specifieke kwetsbaarheid zijn. Om deze kwetsbaarheden bloot

te leggen, hebben wij verschillende genetische screens uitgevoerd in cellen met chromosomale instabiliteit.

In **hoofdstuk 2** hebben wij chromosomale instabiliteit geïnduceerd door essentiële componenten van het mitotische checkpoint te verwijderen. Hierdoor kan een cel geen halt oproepen wanneer er chromosomen ongelijk verdeeld dreigen te worden over de twee dochtercellen. Wij ontdekten dat verlies van Kif18A dodelijk is voor normale cellen, terwijl cellen zonder een mitotisch checkpoint kunnen leven zonder Kif18A. Dit bleek veroorzaakt te worden door onnodige activatie van het mitotische checkpoint. Door deze onnodige activatie gingen cellen zonder Kif18A dood in mitose. Door het mitotische checkpoint te verwijderen konden cellen zonder Kif18A weer normaal uit mitose gaan, en verdeelden deze cellen hun chromosomen eerlijk over twee dochtercellen. Maar, als de chromosomen eerlijk verdeelt kunnen worden, waarom leidt verlies van Kif18A dan tot activatie van het mitotische checkpoint? Wij vonden bewijs dat deze activatie op een onconventionele manier tot stand kwam. Normaal gesproken wordt het mitotische checkpoint geactiveerd door verlies van een connectie tussen het chromosoom (meer specifiek de kinetochoor) en de mitotische spoel. Maar na verlies van Kif18A bleek deze connectie nog aanwezig. Wij ontdekten dat de spanning die op deze connectie werd uitgeoefend door de mitotische spoel laag was, en dat dit leidde tot de (onnodige) activatie van het mitotische checkpoint. Deze data kan worden toegevoegd aan een lang bestaand debat in het mitose veld, of spanning op kinetochoren een rol kan spelen in mitotische checkpoint activiteit.

In **hoofdstuk 3** hebben we replicatie stress gebruikt om chromosomale instabiliteit te induceren. Het dupliceren van het genoom gebeurt tijdens de replicatie fase van de celdeling. Problemen die leiden tot een vertraging van replicatie vallen onder de noemer replicatie stress. Omdat alle kankercellen tekenen laten zien van replicatie stress, is dit een interessante eigenschap om uit te buiten. Met onze genetische screen vonden wij genen waarvan verlies niet lethaal was voor normale cellen, maar specifiek lethaal was voor cellen met replicatie stress. Wij identificeerden een groep genen met een rol in DNA-schade reparatie, passend bij het feit dat replicatie stress tot DNA-schade leidt. Daardoor zijn cellen met replicatie stress afhankelijk van factoren die DNA-schade repareren. Daarnaast vonden we genen met en tot nu toe niet bekende rol tijdens replicatie-stress of DNA-schade reparatie. Het begrijpen van de functie van deze genen kan ons nieuwe inzichten geven in replicatie-stress specifieke kwetsbaarheden.

In **hoofdstuk 4** maakten we cellen chromosomaal instabiel door een gen dat belangrijk voor condensatie, condensin II, te verwijderen. Condensatie van chromosomen is belangrijk, omdat compact DNA makkelijker eerlijk te verdelen is. Condensatie defecten worden soms gevonden in kankercellen, en kunnen leiden tot genetische instabiliteit in de vorm van DNA-bruggen in mitose. In onze genetische screen vonden we dat verlies van SRBD1 dodelijk is voor normale cellen, maar niet langer in cellen zonder condensin II. We ontdekten dat SRBD1 belangrijk is voor het eerlijk verdelen van DNA in mitose, aangezien verlies van SRBD1 grote defecten veroorzaakt in mitose. Hoewel de exacte functie van SRBD1 nog achterhaald moet worden, is onze hypothese dat SRBD1, in samenwerking met condensin II en topoisomerase II, voorkomt dat DNA hevig verstrengeld raakt.

Als laatste hebben wij in **hoofdstuk 5** alle verschillende chromosomale instabiele screens gecombineerd, om gemeenschappelijke factoren te identificeren die specifiek chromosomaal instabiele cellen doden. We vonden Bub1, condensin II, en CENPO als specifieke kwetsbaarheden voor al onze geïnduceerde vormen van chromosomale instabiliteit. Daarbij vonden wij dat alle gemeenschappelijke factoren ook geïdentificeerd waren in een screen waar cellen DNA-schade toegediend kregen via bestraling. Dit geeft aan dat chromosomale instabiele cellen gevoelig zijn voor verlies van DNA-schade reparatie mechanismen. Desalniettemin werd de grootste letaliteit met chromosomale instabiliteit gevonden in elke screen apart. Daarom geloven wij dat kankerpatiënten het meeste baat hebben bij het identificeren van de reden van de genetische instabiliteit in hun tumor, en om deze vervolgens specifiek aan te pakken.

CURRICULUM VITAE

Louise Janssen was born on the 24th of March 1993 in Muscat, Oman. In 2011 she graduated high school (VWO) at the Dr. Nassau College – Quintus in Assen. That same year, she started her Bsc in Biomedical Sciences at Leiden University. During this time, she was selected to take part in an exchange program with the Karolinska Institute (KI). Additionally, she did an internship at the Leiden University Medical Center in the lab of Prof. Dr. Henri Versteeg, where she investigated the role Tissue Factor in epithelial to mesenchymal transition. Moreover, she took part in several (educational) committees, where she guided students, improved the curriculum, and organized several social activities. After obtaining her Bsc degree in 2014, she continued her Msc degree in Biomedical Sciences at Leiden University. Due to her interest in cancer biology, she enrolled in the oncology track. Following that interest, she did an internship in the lab of Prof. Dr. René Medema at the Netherlands Cancer Institute (NKI) in Amsterdam, where she studied the role of novel genes in chromosome alignment. Next, she participated in a summer-school at the German Cancer Research Center (DKFZ) in Heidelberg, where she joined the lab of Prof. Dr. Bruno Kyewski to investigate the regenerative capacity of the thymus. Thereafter, she performed a seven-month internship in the lab of Dr. Willem Overwijk at the MD Anderson Cancer Center in Houston, where she investigated cancer vaccine resistance. During this time, she was selected to write a grant for the OOA Diamond program, where she ended up in the final five. After graduating her Msc *cum laude* in 2016, she started her PhD in the lab of Prof. Dr. René Medema, of which the results are presented in this thesis.

PUBLICATION LIST

Bempegaldesleukin selectively depletes intratumoral Tregs and potentiates T cell-mediated cancer therapy.

Meenu Sharma, Hiep Khong, Faisal Fa'ak, Salah E Bentebibel, [Louise ME Janssen](#), Brent C Chesson, Caitlin A Creasy, Marie-Andrée Forget, Laura Maria S Kahn, Barbara Pazdrak, Binisha Karki, Yared Hailemichael, Manisha Singh, Christina Vianden, Srinivas Vennam, Uddalak Bharadwaj, David J Twardy, Cara Haymaker, Chantale Bernatchez, Shixia Huang, Kimal Rajapakshe, Cristian Coarfa, Michael E Hurwitz, Mario Sznol, Patrick Hwu, Ute Hoch, Murali Addepalli, Deborah H Charych, Jonathan Zalevsky, Adi Diab, Willem W Overwijk.
Nat Commun. 2020 Jan 31;11(1):661. doi: 10.1038/s41467-020-14471-1.

Loss of Kif18A Results in Spindle Assembly Checkpoint Activation at Microtubule-Attached Kinetochores.

[Louise ME Janssen](#), Tessa V Averink, Vincent A Blomen, Thijn R Brummelkamp, René H Medema, Jonne A Raaijmakers.
Curr Biol. 2018 Sep 10;28(17):2685-2696.e4. doi: 10.1016/j.cub.2018.06.026.

BUB1 Is Essential for the Viability of Human Cells in which the Spindle Assembly Checkpoint Is Compromised.

Jonne A Raaijmakers, Roy GHP van Heesbeen, Vincent A Blomen, [Louise ME Janssen](#), Ferdy van Diemen, Thijn R Brummelkamp, René H Medema.
Cell Rep. 2018 Feb 6;22(6):1424-1438. doi: 10.1016/j.celrep.2018.01.034.

Intratumoral CD40 activation and checkpoint blockade induces T cell-mediated eradication of melanoma in the brain.

Manisha Singh, Christina Vianden, Mark J Cantwell, Zhimin Dai, Zhilan Xiao, Meenu Sharma, Hiep Khong, Ashvin R Jaiswal, Faisal Fa'ak, Yared Hailemichael, [Louise ME Janssen](#), Uddalak Bharadwaj, Michael A Curran, Adi Diab, Roland L Bassett, David J Twardy, Patrick Hwu, Willem W Overwijk.
Nat Commun. 2017 Nov 13;8(1):1447. doi: 10.1038/s41467-017-01572-7.

The immune system in cancer metastasis: friend or foe?

[Louise ME Janssen](#), Emma E Ramsay, Craig D Logsdon, Willem W Overwijk.
J Immunother Cancer. 2017 Oct 17;5(1):79. doi: 10.1186/s40425-017-0283-9.

ACKNOWLEDGMENTS

This thesis would not have been here without the unconditional support, guidance, and laughter of many. If you are reading this, thank you for being part of my (PhD) life!

First of all, I would like to thank you, **René**, for convincing me to not pursue a career in immunology, but rather to write a grant with you. Even though I did not end up working on epigenetic scars myself, doing my PhD in the Medema lab enabled me to see many diverse projects grow. I admire your broad scientific mind, and the fact that you always manage to have a great group of people around in your lab. My life would have never been the same without this opportunity you gave me, and for that I will be always grateful.

Extra special thank you to my co-promotor, **Jonne**. Your enthusiasm for science is infectious. Even though we sometimes do science in our own ways, it was great knowing you always had my back (even from the toilet with a beer in your hand). Thank you for many discussions (about science and life), for pushing me and my experiments to the next level every day, and for lots of laughter. I am sure you'll get to the bottom of our SRBD1 mystery, and we'll hugely celebrate it! I would never be where I am today without you.

I would also like to thank all the members of my reading committee (**Emile Voest, Geert Kops, Madelon Maurice, Marcel van Vugt, and Susanne Lens**) for taking the care and time to go through, and accept, this thesis. Moreover, I would like to thank my PhD committee, **René Bernardts, Thijn Brummelkamp, and Kees Jalink**, for their yearly input and advice on my, quite diverse, projects.

Next, I would like to thank the two most important people during my defense, my paranymphs **Anoek** and **Lisa**. You guys did not get this task randomly, let me tell you why! **Anoek**, akkefietje, FRISKIE!, thank you for your laugh, that vibrates through my whole soul (and the office walls of B5). With you around, every day is fun. We laugh, we sing, we dance, we drink, we swim (and sometimes complain) together. Your energy is unbreakable, your love for science radiates, and your support has helped me through a lot. I just know you will do great things! To doing many more koprollen in life together (where I watch while you do them). **Lisa**, from your internship until your PhD now, you have grown so much. You are such a dedicated friend, I hope you know how valued you are! Thank you for always listening to me, for waking up early to bike to the pool, for trusting me with your SCE assays, and sharing your cheese cake recipe with me. I am very happy we finally found you a

drinkable beer, and look forward to enjoy more borrels together! P.S. Thank your mom for all the pflaumenlikör.

Mar, thank you for convincing René to bring me back to the Medema lab after my internship. And thank you for convincing Ale to talk to me. But mostly, thank you for convincing me I was worth all this. You are the biggest fan anyone can wish for, and how cool is it that when your family grows, so does mine?! Looking forward to many more Christmases, cola + nugget nights, and code-name games (combination 3!) together. **Zeno**, thank you for always being interested, for showing me how to shuffle, and for making Mar happy. **Mateo**, you are a superstar. I love you all.

To the amazing Medema lab: everyone who was a part of it these past years really made this place a second home. Especially during the pandemic, it was great to have the comfort of a nice work-environment to escape to. **Anna**, from turning 24 on the 24th and 10 on the 10th, we started our PhD's together. Now you are not next to me, but on the other side of the world. Who would have thought? I am very grateful for all the happy crazy moments we spent together, inside and outside of the lab. Your determination makes you get what you want in life, and showed me how to get this thesis done myself too. See you soon! **Apostolos(t)**, once again you managed to stick around! Thank you for the nice conversations and for always stocking up the office with cookies. I am very happy you showed us the beauty and culture of Sifnos. **Dorrie**, I LOVE your positive attitude to life, and I will hate missing out on all the fun the lab will be having with you. Luckily I have the SKIENCE-playlist on Spotify to make up for that. You have been a sunny support in the office and my life, thank you for that! For sure we will have more special-beer and game nights. Stay true to yourself, you are great! **Lenno**, my bench-mate from the other side! Thank you for many chats through the hanging pipets. Whether about science or about life, it always felt easy to talk to you about anything. I am curious to see where the road is taking you. **Michael**, thank you for holding up in a lab surrounding you with wet-lab scientists, and for our interesting discussions during lunch and meetings. **Mila**, I am happy I got to know you better these last couple of months. I am excited to see where your projects will bring you, and hope you will enjoy the ride! **Rob**, the man that fixes the microscopes time and time again, but also my incubator, my chair, my pipets... The lab/B5 would fall apart without you. But you are also full of nice tips for Europe city trips, thanks! **Xabier**, how still waters can run deep. The tallest and kindest Spanish guy I know, but man can you turn fierce when playing any kind of game. Keep that fire, and please always beat René. **Marianne, Mariet, and Yvonne**, thank you for making space for us in

René's busy schedule, and thank you for organizing many other things (from lab-activities to PhD-defenses) throughout all these years. To the students I was lucky to supervise, **Raphaël, Nuria, Empar** and **Shiksha**, thank you for jumping on board of one of my projects and giving me the opportunity to teach. It was fun being part of your journeys and I am curious to see where you will go next!

Alberto, my Maine lobster buddy! I am happy I was one of the first to figure out you were going to propose at Disney world, and even happier to be part of such a nice wedding trip to Madrid. Thank you for always asking me how I am doing, and climbing lanterns together in Renesse. **Angela**, thank you for the stories, dinners and dances we shared together. **Benjamin**, the way you can communicate your science to any audience still baffles me. **Claire**, my condensin friend! Thank you for trying out some ChIPs for me. Your colorful outfits always made me cheerful! **Judith**, always kind and always thinking along, and she can even still dance and party! **Maryolo**, the last meerkat with her feet in B5. From students sleeping on the floor after a Christmas borrel, to PhD students competing in a triathlon together, and every other party/game-night/holiday trip in between: thank you. **Roel**, the smart guy that is always in for a party: let's get it started!

To all the other **B5 members**, the **Jalink, Rowland**, and **Sonnenberg** groups, thank you for the nice atmosphere on our floor, and the many cake-breaks. To former B5 members, **Jeroen, Femke, Rita, Chantal, Ahmed, Iraia, Roy, Andre, Ana, Daria**, thank you for making lab life a fun and inspiring place to work in! Thank you to **Jacqueline Jacobs** and her (former) group members for helpful input during one of the many Monday morning work discussions. Special thanks to **Aurora** and **Inés** who made DNA fiber assays fun. **Henri**, keeping everything in check at the NKI (including René), thank you for saving us from the possible impact of the window cleaner. Thank you **Vincent, Matthijs, Elmar, Joana, Abdel, Sarah, Martijn, Frank, Patrick** for helping my projects along various ways.

I am grateful for my extended international family: my NKI Mafia. **Antonio**, too many memories we have made together. The most special one might be singing on stage together in front of the whole NKI. Thank you for being positive and always in the mood for singing, dancing and partying. P.S. the gold is in the middle. **Clara**, your kindness is reflected in the sweet food you make. Thank you for being such a caring friend. **Eric**, the master of making life changes. I admire you for going after your own happiness. I hope you find it, you deserve the best. **Isa**, your laugh makes me want to laugh 100x more. Thank you for our talks and all the amazing memories we made together, including the

top 1 hit-song: I don't care about your old house – what you saady?! I love you loads. P.S. the gold is on the right. P.P.S. see you at 3 a.m. **Jeremy**, at some point you were texting my dad more than I was. Your crazy bikes are bringing you new adventures in Australia, and I can't wait to see it when I am there. Thank you for being the biker in our triathlon team, and for many other great memories together. **Mariana**, once I got up to your talking speed, it was impossible not to love you. Thank you for your pro-active (almost Dutch) attitude to life, and for making me laugh (either because you are funny, or clumsy...). **Ronak**, thank you for being my midnight Eminem rap-buddy! A party is never the same without you. **Simon**-tje, I still remember the first day I met you and Ale. Thank you for being a calm and steady friend, and for the worst hangovers of my life. P.S. the gold is on the left. **Theresa**, thank you for being sweet, humble, funny, and the best saboteur ever. P.S. You know where the gold is right? **Živa**, you're the type of friend everyone wishes to have. You would walk through fire for any one of us. Thank you for your support, advice, love, and all other memories throughout all these years. I am sure there will be many more to come. **Anniek, Bruno, Celia, João, Maria, Mathias, Miriam, Migurk, Ruben, Stefan, Soufiane**, thank you for making the Mafia parties unforgettable.

En dan mijn onmisbare support buiten het lab. **Sophia**, de vraag is, wat doen we in de tussentijd? Met jou is die tussentijd te veel om op te noemen. We staan altijd voor elkaar klaar, in the good and the bad, met veel vreten en filmpjes die jij quote terwijl ik ze niet ken, en vervolgens toch ook quote. Al mijn kronkels kan ik zonder oordeel bij je kwijt, en advies heb je altijd paraat. Thank you for being my bestie. Ik hou van jou! **Gido**, ik kan niet wachten om te komen logeren in het Soof en Gido bos! Als je iemand nodig hebt om te komen boren hoor ik het graag (ik neem mijn eigen boor mee!). **Marleen** en **Arnout**, bedankt voor de vele spelletjes avonden waarbij ik zoveel biertjes mocht drinken als ik zelf wilde. Extra liefde voor Marleen; het weekend-gevoel beginnen met een klets (en soms klaag) rondje om de Leidse grachten deed me vooral deze laatste maanden goed. Ly, ntb, wjnmk <3. **Madelaine, Simone** and **Juliette**, the moments spent together with you are always easy, lovely and tasty. Thank you for all the great conversations we had over the past years. Looking forward to our shared family skiing trips! Mijn BWertjes, **Annika, Coen, Eveline, Esmé, Kelsey, Lotte, Maarten, Sanne, Suzanne**, ook al zien we elkaar nu minder, ben ik blij dat het nog altijd goed voelt als we samen zijn. Bedankt voor jullie vriendschap! Mijn bitches, **Shanna, Marieke, Marit, Michelle** en **Sophia**, hoe leuk dat we na al die jaren, nu sommigen zelfs met kiddo's, nog steeds gesprekken kunnen hebben over dezelfde dingen als vroeger. **Iris**, mijn reismaatje, ik ben benieuwd waar onze volgende reis naar toe zal gaan. Het is alweer veel te lang geleden dat ik je de juiste weg gewezen heb!

Yazmin, bedankt voor de fysieke uitlaatklep tijdens bootycamp, voor je gezelligheid en je altijd luisterend oor voor iedereen. My Italian friends, **Georgia, Lorenzo, Francesca** (aka alligator), eh, che te devo di.. Meeting you in Houston has changed my life. I am happy my life then brought me Ale, since that makes a great excuse to come visit you so often! Grazie, e ci vediamo in Ancona/Bari.

Alla mia famiglia italiana, **Enzo, Tiziana, Francesco, Giacomo, Daniele, Nonna Elia, Soili + bambini, e Darko**: grazie per il calore, le battute e il cibo delizioso. Grazie per averci fatto visita e per aver supportato Ale nei Paesi Bassi.

Opa Ton, Oma Riet, het moment is eindelijk daar! Het onderzoek is natuurlijk nooit echt klaar, maar mijn PhD-onderzoek nu wel. Ik hoop dat jullie trots zijn, en kunnen meegenieten van deze mooie dag. Ik hou van jullie. **Caroline, Enno, Jasper, Michiel, Yvette, Sander, Marinette, Daniel, Daan** en de rest van de familie, tijd voor een feestje!

Papa en Mama, bedankt voor jullie onvoorwaardelijke steun en liefde. Niet alleen de afgelopen jaren, maar mijn hele leven. Onze koppige, doortastende genen hebben ons allemaal ver gebracht. Onze wekelijkse telefoontjes sleepten me door de laatste loodjes (een term die we nu hopelijk lang niet meer hoeven uit te spreken). Zij het in Gieten, of in Calpe, jullie zorgen altijd voor een warme plek om naar terug te keren. **Max**, mijn kleine grote broertje die steeds wijzer wordt. Bedankt dat je me hebt geleerd om af en toe mijn mond te houden (lukt bijna altijd nu). Ik had me geen grappiger, sterker, gezelliger, liever broertje kunnen wensen. Mijn lieve familie, ik hou van jullie.

Then to the best thing my PhD has brought me: **Ale**, AG, my wife. Thank you for making me smile the second you enter the room, to sing silly songs with me, and to feed me properly. You make my life more fun, and full of love. With you by my side I can do anything, from dancing on the street to jumping in a plane without worrying about not having a plan (for once in my life). I love you from here until the bedieland. Can't wait to discover the world, and your camping skills, together.

En om met de woorden van mijn **Oma Ada** af te sluiten: verder heb ik geen bal.

Lots of love,

Louise

